

The representation of cloud cover in atmospheric general circulation models

Dissertation
der Fakultät für Physik
der Ludwig-Maximilians-Universität München

vorgelegt von
Christian Jakob
aus Köthen

München, den 19. Oktober 2000

Gutachter der Dissertation:

Erster Gutachter Prof. Dr. R. Smith
Zweiter Gutachter Prof. Dr. U. Schumann

Tag der mündlichen Prüfung: 06. Februar 2001

Contents

Abstract	iii
Zusammenfassung	iv
1 Introduction	1
1.1 Motivation	1
1.2 Outline	5
2 Clouds in large-scale models	9
2.1 Clouds in the climate system	9
2.1.1 The global distribution of clouds	9
2.1.2 The effects of clouds in the climate system	12
2.2 Clouds and parametrization	18
2.3 A brief history of cloud parametrization	22
3 Cloud parametrization in the ECMWF model	31
3.1 The ECMWF model	31
3.2 The cloud parametrization scheme	33
3.3 The cloud parametrization in data assimilation	42
4 Cloud fraction in the ECMWF reanalysis	49
4.1 Introduction	49
4.2 Data	50
4.2.1 ISCCP	50
4.2.2 ERA	51
4.3 Results	51
4.3.1 Global mean	51
4.3.2 Zonal Means	52
4.3.3 Selected Areas	54
4.4 Summary and discussion	60
5 The parametrization of cloud generation	63
5.1 Introduction	63
5.2 The generation of convective clouds	63
5.2.1 The mass-flux concept	65
5.2.2 Cloud condensate	68
5.2.3 Cloud fraction	71
5.3 The generation of non-convective clouds	73

5.3.1	General remarks	74
5.3.2	Derivation of stratiform cloud source terms	76
5.3.3	Comparison to the T93 cloud scheme	80
5.3.4	Comparison with the distribution approach	84
5.3.5	Some thoughts on cloud decay	88
6	Cloud fraction and microphysics	91
6.1	Introduction	91
6.2	Cloud and precipitation overlap - The problem	93
6.2.1	A subgrid-scale precipitation model	95
6.2.2	Comparison of the subgrid-scale precipitation model with the original scheme	99
6.2.3	Summary and discussion	112
6.3	Cloud and precipitation overlap - A parametrization	114
6.3.1	Description of the stratiform precipitation parametrization	115
6.3.2	Comparison of the parametrization to the subgrid-scale model	121
6.3.3	The influence of the new parametrization on the model climate	125
6.3.4	Discussion	131
6.3.5	Conclusions	133
7	The evaluation of cloud parametrizations	135
7.1	Introduction	135
7.2	Model climate	136
7.2.1	Broadband radiative fluxes	136
7.2.2	Cloud radiative forcing	138
7.2.3	Cloud fraction	140
7.3	Single Column Modelling	142
7.4	NWP forecast evaluation	146
7.5	The verification of vertical cloud structure	148
7.6	The use of composite data sets	153
7.7	A strategy for cloud evaluation	159
8	Concluding remarks	163
A	List of acronyms	169
B	Mixed phase and saturation water vapour pressure	171
	References	173

Abstract

This dissertation describes various aspects of improvements made in the representation of clouds in the global forecast model of the European Centre of Medium-Range Weather Forecasts (ECMWF). Cloud parametrization has long been identified as one of the most crucial and uncertain aspects in General Circulation Models (GCMs) of the atmosphere, which are used for both Numerical Weather Prediction and the simulation of climate. It is therefore important to constantly monitor and improve the performance of cloud parametrizations in those models.

The first part of the work describes the implementation of an existing cloud parametrization into ECMWF's forecasting system with special attention to a new treatment of the prognostic cloud variables in data assimilation. This is followed by an analysis of the performance of the parametrization during a 15-year long data assimilation experiment carried out in the context of the ECMWF reanalysis project. It is shown that despite an overall good performance, several weaknesses in the simulation of clouds exist. Subtropical stratocumulus and extratropical cloudiness are underestimated, while the cloud fraction in the trade cumulus areas and in the Intertropical Convergence Zone is overestimated.

In the second part of the study detailed revisions of the parametrization of cloud generation by convective and non-convective processes are described. A consistent new description of cloud generation by convection is derived using the mass-flux approach. Furthermore an improved description of the generation of clouds by non-convective processes is introduced. The superiority of the new formulation compared to the existing one is demonstrated and links to other approaches to cloud parametrization are established.

The third part of the work studies the role of vertically varying cloud fraction for the description of microphysical processes. It is shown that the commonly used approach of representing precipitation in GCMs by means of grid-averaged quantities leads to serious errors in the parametrization of various physical processes such as the evaporation of precipitation, with severe consequences for the model's hydrological cycle. A new parametrization of the effects of vertically-varying cloud fraction based on a separation of cloudy and clear-sky precipitation fluxes is developed and its performance assessed. It is shown that this parametrization alleviates most of the identified problems and thereby more realistically describes the precipitation physics in the presence of cloud fraction variations.

The final part of the dissertation takes a critical look at the way the results of cloud parametrizations are evaluated today. A number of studies using a variety of data sources and modelling approaches are described and the need for a coordinated use of the various existing validation techniques is highlighted. A strategy to achieve such coordination is proposed.

This work provides contributions to virtually all facets of the development of cloud parametrizations. It combines theoretical aspects with the use of a variety of modelling approaches and data sources for the assessment of the performance of the parametrization. All model improvements described here are now part of the operational version of the ECMWF forecast model.

Zusammenfassung

Die vorliegende Dissertation beschreibt die Entwicklung einer Reihe von Verbesserungen in der Wolkenparametrisierung des globalen Vorhersagemodells des Europäischen Zentrums für Mittelfristige Wettervorhersage (EZMW). Die bedeutende Rolle, die der Parametrisierung von Wolken in globalen Zirkulationsmodellen, wie sie sowohl zur numerischen Wettervorhersage als auch zur Klimasimulation verwendet werden, zukommt, ist seit langem bekannt. Es ist daher unerlässlich das Verhalten solcher Parametrisierungen kontinuierlich zu analysieren und zu verbessern.

Im ersten Teil der Arbeit wird kurz die Einführung einer bereits existierenden Wolkenparametrisierung in das Vorhersagesystem des EZMW beschrieben. Besondere Aufmerksamkeit wird dabei der Entwicklung einer neuen Methode zur einfachen Bestimmung der notwendigen Anfangsbedingungen für die prognostischen Wolkenvariablen gewidmet. Anschließend wird das Verhalten der Parametrisierung in einem 15-jährigen Datenassimilationsexperiment, das innerhalb des EZMW-Reanalyseprojekts durchgeführt wurde, analysiert. Es wird gezeigt, dass trotz der allgemein guten Wiedergabe der beobachteten Wolkenklimatologie einige Probleme in der Simulation des Bedeckungsgrades auftreten. So ist der Bedeckungsgrad in subtropischem Stratocumulus und in extratropischen Breiten vom Modell unterschätzt, während in den Passat- und innertropischen Gebieten zu hohe Bedeckungsgrade simuliert werden.

Im zweiten Teil werden neue Ansätze zur Parametrisierung von Wolkenbildung durch sowohl konvektive als auch nichtkonvektive Prozesse beschrieben. Eine neue und konsistente Parametrisierung der konvektiven Wolkenbildung wird unter Zuhilfenahme der im Konvektionsschema verwendeten Massenflusstheorie hergeleitet. Desweiteren wird eine verbesserte Methode zur Bestimmung der Quellen nichtkonvektiver Wolken beschrieben. Die Vorteile dieser neuen Methode werden dargelegt und die Verbindung zu bekannten Herangehensweisen in der Wolkenparametrisierung wird aufgezeigt.

Der dritte Teil der Arbeit beschäftigt sich mit der Rolle, die Änderungen des Bedeckungsgrades mit der Höhe in der Beschreibung mikrophysikalischer Prozesse spielen. Es wird zunächst bewiesen, dass die weithin übliche Methode der Beschreibung des Niederschlags durch Gitterpunktmittelwerte zu erheblichen Fehlern in der Beschreibung verschiedener mikrophysikalischer Prozesse, wie zum Beispiel der Verdunstung von Niederschlag, führt. Dies hat weitreichende Konsequenzen für die realistische Beschreibung des hydrologischen Zyklus im Modell. Eine neue Parametrisierung der Effekte von Bedeckungsgradänderungen in der Vertikalen, die auf der getrennten Beschreibung von Niederschlag innerhalb und außerhalb von Wolken beruht, wird entwickelt und getestet. Es wird gezeigt, dass diese Parametrisierung viele der zuvor aufgezeigten Probleme behebt und damit eine realistischere Beschreibung der Niederschlagsentwicklung erlaubt.

Zum Abschluss der Dissertation wird ein kritischer Überblick über die derzeit verwendeten Methoden zur Validierung von Wolkenparametrisierung gegeben. Eine Reihe von am EZMW ausgeführten Studien, in denen viele der derzeit üblichen Validierungsmethoden und Datenquellen verwendet werden, werden kurz beschrieben. Es wird gezeigt, daß es für die zukünftige Verbesserung von Wolkenparametrisierungen notwendig sein wird, bekannte und neue Methoden in einer besser koordinierten Form anzuwenden. Eine mögliche Strategie hierfür wird beschrieben.

Der Inhalt dieser Arbeit berührt eine große Anzahl der Probleme in der Entwicklung von Wolkenparametrisierungen für globale Zirkulationsmodelle. Theoretische Aspekte werden

mit der Verwendung einer Vielzahl verschiedener Modellierungsmethoden und Datenquellen zur Validierung der Ergebnisse verknüpft. Alle hier beschriebenen Modellverbesserungen sind inzwischen integraler Bestandteil des operationellen Vorhersagemodells des EZMW.

Chapter 1

Introduction

1.1 Motivation

Clouds are a frequently observed natural phenomenon. They are estimated to cover between 60 and 70 % of the globe at any given time. At most locations on earth some clouds will occur on every single day. Clouds exist in a great variety of forms and on a large range of both temporal and spatial scales. Individual small cumulus clouds for instance cover a few hundred metres in the horizontal and vertical and normally have a lifetime of less than an hour. In contrast the vast, virtually ubiquitous stratocumulus decks covering the eastern parts of the subtropical oceans have a horizontal extent of several hundred kilometres, while being no more than a few hundred metres thick. The processes involved in the formation and dissipation of clouds span an even larger range of scales from micrometres for the condensation of individual droplets to thousands of kilometres for cloud formation in frontal systems associated with mid-latitude baroclinic systems.

Clouds are directly linked to a large variety of weather phenomena. Rain and snow are obviously produced in clouds, as are thunder and lightning. The latent heat release due to condensation processes is known to be one of the most important processes in the spinup and maintenance of tropical storms, which appear in their most violent form as hurricanes and typhoons. It is an everyday experience that clouds influence the radiative fluxes emitted both by the sun and the earth. If clouds form on an otherwise sunny day the maximum temperature near the surface will be lower than without them, a direct consequence of the reflection of sunlight by clouds. Likewise, if the sky is covered by low clouds at night the near-surface temperature will not drop as low as under clear sky conditions due to the trapping of terrestrial radiation by the clouds. Because of all these reasons it is obvious that it is desirable for any form of weather forecast to include a prediction of the occurrence

and type of clouds and precipitation. Just as importantly, the desire to estimate the future evolution of our planet's climate requires knowledge about clouds. This is due to their strong interaction with the radiative fluxes whose modification through changes in the atmospheric composition is of considerable concern.

The tools to predict the evolution of the weather (at least for more than 2 or 3 days in advance) and climate are numerical models of the global earth-atmosphere system. The atmospheric components of these models are often referred to as Atmospheric General Circulation Models (AGCMs) or just GCMs (since General Circulation Models of the ocean are not relevant for this work, the term "GCM" will be adopted for the rest of this thesis). For the reasons above these models require the description of the manifold influences clouds exert on the atmosphere. A GCM solves the partial differential equations governing the evolution of the atmospheric state variables in discrete form after partitioning the atmosphere into grid cells of finite extent both in the horizontal and in the vertical. One of the choices that need to be made is therefore that of the desired spatial resolution of the model. As outlined above, some cloud processes occur on very small scales, so that a detailed description of the intricate dynamics of individual clouds would require model resolutions of a few metres or less both in the horizontal and vertical. Current computing power does not allow the design of global models of such high resolution. Current GCMs are using horizontal resolutions of 50 to 100 km when used in global weather forecasting systems and larger than 200 km in the case of climate models. The use of those resolutions automatically restricts the way clouds can be described in GCMs. Just as in statistical thermodynamics, where the impossible description of the behaviour of individual molecules is replaced by the description of the statistical effects by introducing average (macroscopic) parameters, it is necessary to find parameters that describe the statistical behaviour of clouds given the resolved scales of the GCM. The technique of finding those parameters and representing them as a function of the resolved variables of the GCM is referred to as cloud parametrization. Parameters commonly chosen for the cloud description are the horizontal fractional area coverage of a model grid cell by clouds, or cloud fraction, and the average cloud condensate content in the grid cell. In 1975 A. Arakawa summarized the motivation for including cloud descriptions in GCMs and the state of research as follows (Arakawa, 1975):

"The importance of clouds in climate modelling cannot be overemphasized. Clouds, and their associated physical processes, influence the climate in the following ways:

1. By coupling dynamical and hydrological processes in the atmosphere through the heat

- of condensation and evaporation and redistributions of sensible and latent heat and momentum;
2. By coupling radiative and dynamical-hydrological processes in the atmosphere through the reflection, absorption, and emission of radiation;
 3. By coupling hydrological processes in the atmosphere and in the ground through precipitation; and
 4. By influencing the coupling between the atmosphere and the ground through modifications of the radiation and the turbulent transfers at the surface.

Although these cloud-dominated processes have long been known to be important in determining climate, clouds have been very poorly formulated in climate models.”

When confronted with this statement in November 1998, without knowing that it was made close to 25 years ago, almost all of the 100 participants in a workshop on “Cloud processes and cloud feedbacks in large-scale models” held at the European Centre for Medium-Range Weather Forecasts (ECMWF) supported it. This indicates that despite considerable efforts over the last 25 years, cloud parametrizations remain one of the most uncertain and yet crucial elements of global atmospheric models. Just how crucial cloud parametrization can be for the behaviour of GCMs in simulations of climate was demonstrated by Cess et al. (1990, 1996). They set out to investigate whether clouds potentially amplify or dampen a possible climate change induced by a changed composition of the atmosphere. For that purpose they carried out simulations with most of the existing GCMs worldwide and studied the model response to global modifications of the sea surface temperature from 2 K colder than observed to 2 K warmer than observed. This modelling strategy serves as a sufficiently simple surrogate for a possible climate change. Cess et al. (1990) then defined a cloud feedback parameter ($\Delta CRF/G$) as the change of the effects clouds exert on the radiative fluxes at the top of the atmosphere (TOA), ΔCRF , divided by an assumed direct radiative forcing, G , due to an increase in the concentration of atmospheric CO_2 . Given the value of G as $4 Wm^{-2}$, a cloud feedback factor of +1 then indicates a doubling of the direct effect while a negative cloud feedback factor represents a damping of the original perturbation. Figure 1.1 shows the cloud feedback parameter for all the models tested in 1990 and again in 1996.

It is evident from this figure that in the various models used in 1990 and in 1996 not even the sign of the cloud feedback parameter is consistent. Although the spread amongst the

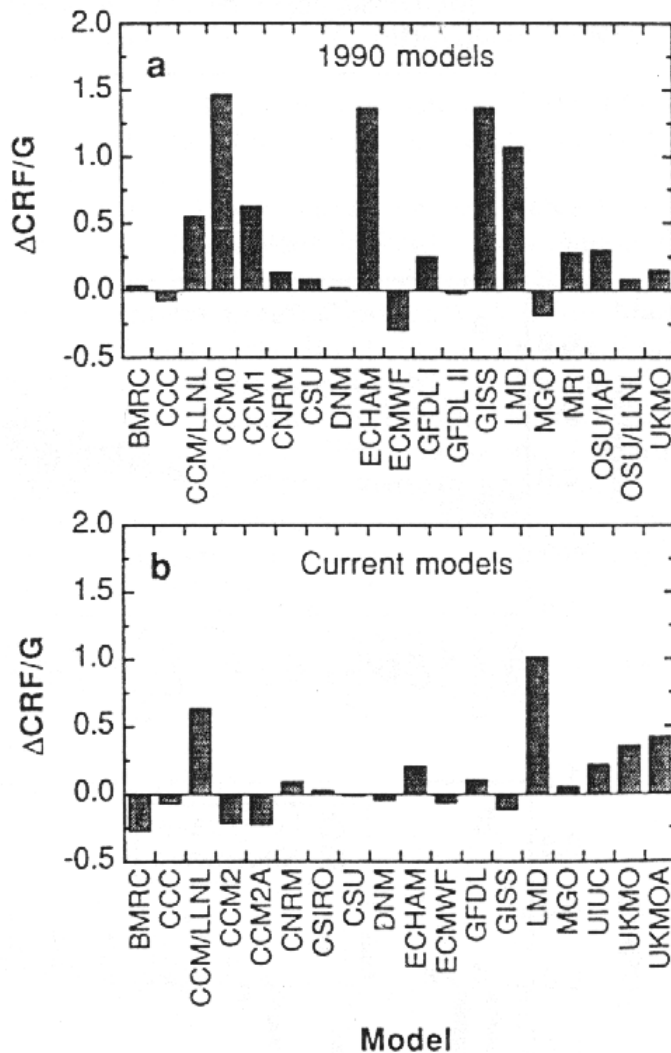


Figure 1.1: The cloud feedback parameter (see text for explanation) as produced by a number of GCMs in 1990 (top panel) and 1996 (bottom panel). From Cess et al., 1996.

models is smaller in 1996 than in 1990, it is still uncomfortably large. This can be taken as evidence for the large uncertainty in the current representation of clouds in climate models and the need for their improvement.

Besides their important role for climate, clouds and the precipitation generated in them are important everyday forecast products. It therefore appears adequate to require GCMs that are used for Numerical Weather Prediction (NWP) to provide cloud and precipitation information as direct model output with as high a quality as possible to give guidance for their forecasting. Needless to say, the representation of clouds will also influence forecasts of other weather elements such as near surface air-temperature and humidity. Not predicting observed stratus clouds on a winters night can for instance introduce forecast errors in low

level temperature easily in excess of several degrees.

For the reasons outlined above it is necessary to continuously improve the representation of clouds in GCMs, independent of their actual application. It can even be argued that if a GCM constitutes a good representation of the atmosphere it can be used for both NWP and the simulation of climate. In practice this approach is followed at a number of institutions, such as the United Kingdom Meteorological Office (UKMO). As will be shown in the following chapters there is a number of important aspects to be considered in the improvement of cloud parametrizations. This thesis summarizes the contributions of the author to cloud parametrization made through improving the parametrization in ECMWF's global NWP model and by evaluating its performance in a number of different ways. An outline of the thesis is provided in the next section.

1.2 Outline

The state of the art

Before describing improvements made to the ECMWF cloud parametrization it is necessary to establish the state-of-the-art at the time this research was initiated. Chapters 2, 3, and 4 are devoted to that purpose. **Chapter 2** provides a brief overview over the role of clouds in the climate system and the general techniques used to represent them in GCMs. This is followed by a short excursion into the historical development of cloud parametrizations. **Chapter 3** describes the general features of the ECMWF global forecasting model followed by a detailed description of its cloud parametrization developed by Tiedtke (1993, hereafter referred to as T93). The chapter concludes with a brief discussion of the implementation of this scheme into ECMWF's data assimilation system, a necessary requirement for its use in NWP. **Chapter 4** evaluates the performance of the scheme in the context of a 15 year long data assimilation carried out in the first ECMWF reanalysis project (ERA-15; Gibson et al., 1997). The cloud cover simulated during the reanalysis is compared with satellite data provided by the International Satellite Cloud Climatology Project (ISCCP; Rossow and Schiffer, 1983). This comparison serves two main purposes; i) the overall performance of the cloud parametrization is evaluated and problem areas uncovered and ii) guidance for users of the ERA-15 reference climatology data set is given.

The description of cloud generation

There are two major conceptual changes in cloud parametrization that were introduced with the T93 cloud scheme. First, the scheme is process-oriented and couples many of the model's physical processes directly to cloud generation and decay. This coupling, in particular to the convection parametrization, has been highlighted as one of the most important areas for necessary improvement in cloud parametrization (e.g., Randall, 1989). The second major new feature introduced in T93 is the treatment of cloud fraction with a prognostic equation. **Chapter 5** takes a critical look at the main cloud generation terms as proposed in the T93 parametrization. Consistent new formulations for both convective and stratiform cloud generation are derived and compared to previous approaches. Apart from deriving the specific cloud source terms for the parametrization at ECMWF the chapter tries to establish their theoretical background and their underlying assumptions so that future findings can be easily incorporated into the T93 and other cloud parametrizations.

Cloud fraction and microphysics

The improvement of the microphysical part of cloud parametrizations, i.e., the treatment of precipitation generation and decay has received much attention over the last few years. The main strategy used is to apply bulk microphysical models developed for cloud-resolving and meso-scale atmospheric models directly in GCMs. Unfortunately most of the recent studies either neglect or mistreat the role of cloud fraction in the microphysical parametrizations. Since modern cloud parametrizations predict cloud fraction at all model levels there can be large variations of cloud fraction with height. Therefore parts of the precipitation generated in a model cloud at one level can fall into cloudy sky below and parts into clear sky, leading to a very different evolution of the precipitation in the two parts. In the first part of **Chapter 6** a subgrid-scale precipitation model is developed and used to study the errors of the T93 parametrization arising from an improper treatment of cloud fraction in the microphysical parametrizations. This subgrid-scale precipitation model is then used in the second part of the chapter as a benchmark for the development of an entirely new treatment of precipitation and cloud overlap based on the separation of cloudy and clear-sky precipitation fluxes.

The evaluation of cloud parametrizations

One of the key aspects of developing new or improved parametrizations is how to measure success, or in other words how to validate (or invalidate) the cloud parametrizations. A

number of studies of this aspect of cloud parametrization work have been carried out in recent years by the author in collaboration with a number of research groups worldwide. **Chapter 7** provides an overview over the manifold aspects of the parametrization validation problem for clouds. The various results are put into the context of emerging new strategies for cloud parametrization evaluation. Considerable thought will be given to the use of only recently available new data sources such as cloud radar observation, which for the first time allow a systematic evaluation of the cloud vertical structure produced in model simulations.

Summary and outlook

Finally there is a summary of the author's contributions to the main lines of cloud parametrization development in recent years and an outlook for future developments in the light of increasing computing power and the availability of new global data sources for the evaluation of cloud parametrizations.

Chapter 2

Clouds in large-scale models

2.1 Clouds in the climate system

2.1.1 The global distribution of clouds

Before describing the effects of clouds on the earth-atmosphere system and how these effects are represented in GCMs, it seems appropriate to provide a brief description of the global distribution of clouds. Routine cloud observations are made in two different ways: from observers at the surface and from meteorological satellites. Recent estimates based on both these observation types estimate the global mean cloud cover at around 60 to 70 % (Warren et al., 1986, 1988, Rossow and Schiffer, 1999). There is a huge regional diversity in both the overall cloud coverage and the prevalent cloud type. Figure 2.1 shows the annual mean cloud cover for the years 1983 to 1990 as estimated from satellite observations as part of the International Satellite Cloud Climatology Project (ISCCP, Rossow and Schiffer, 1983, 1991) for all latitudes from $60^{\circ}N$ to $60^{\circ}S$. Higher latitudes are excluded from the figure because of the difficulties of estimating cloud cover over ice and snow-covered surfaces. To first order the global cloud cover distribution is a reflection of two main influences: the location of the main circulation systems covering the earth as well as the differences in the availability of moisture from the surface between ocean and land areas.

The equatorial tropics, which are dominated by the ascending branch of the thermally direct Hadley circulation in the Inter-Tropical Convergence Zone (ITCZ), exhibit a maximum of cloud cover of more than 65 %. The dominant cloud types in this region are clouds formed by moist convection. Those include cumuliform clouds, as defined in the World Meteorological Organization (WMO) International Cloud Atlas (1987) such as cumulonimbus, cumulus congestus and large organized complexes of clouds generated by a number of convective cells, often referred to as mesoscale convective systems (see Houze, 1993 and references therein),

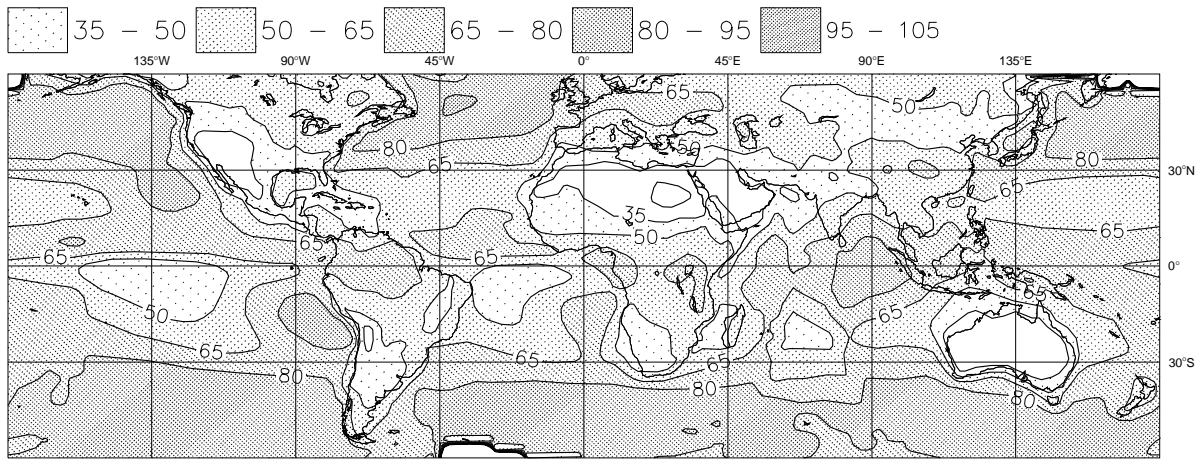


Figure 2.1: Mean geographical distribution of total cloud cover as estimated by ISCCP for July 1983 to December 1990

as well as various types of cirrus clouds that form in the upper-tropospheric outflow regions of the deep convective systems or in regions of ascending motion. It is the latter cloud types that are generally thought to contribute to the high values of cloud cover in this region. Although present to some extent, the land-sea contrast in cloud cover at tropical latitudes is small, since the relatively wet surfaces over tropical land areas can support significant amounts of convection.

In the descending branches of the Hadley circulation on both sides of the ITCZ, strong meridional gradients in cloud cover are apparent over the oceans, with large cloud cover on the eastern side of the large ocean basins and relative minima further west. The predominantly downward motion here generally suppresses cloud formation in the upper and middle troposphere. However, due to the abundance of water vapour near the ocean surface, clouds do form at the top of convective planetary boundary layers (PBL). Due to upwelling of cold ocean water at the west coasts of the subtropical continents the sea-surface temperatures (SSTs) there are fairly low (around 15°C) and increase to values of about 25°C in the most western parts of the subtropical ocean basins. Following a westward trajectory along the trade winds from cold to warm SSTs, the depth of the PBL increases accompanied by a reduction in the strength of the inversion at the PBL top. Over the cold SSTs the predominant cloud type is stratocumulus (Klein and Hartmann, 1993). As the SST increases and the subsidence decreases, more and more cumuliform clouds are encountered, which leads to a reduction in mean cloud cover from more than 80 % to less than 50%. The exact mecha-

nisms that achieve this transition in cloud cover are still unclear. In recent cloud-resolving model simulations (Krueger et al., 1995a,b; Wyant and Bretherton, 1997) the SST gradient alone has been shown to be able to cause a transition from stratocumulus clouds over the cold water to cumulus clouds over the warmer ocean surface. A schematic of the observed transition in cloudiness from the subtropics to the deep tropics is shown in Figure 2.2.

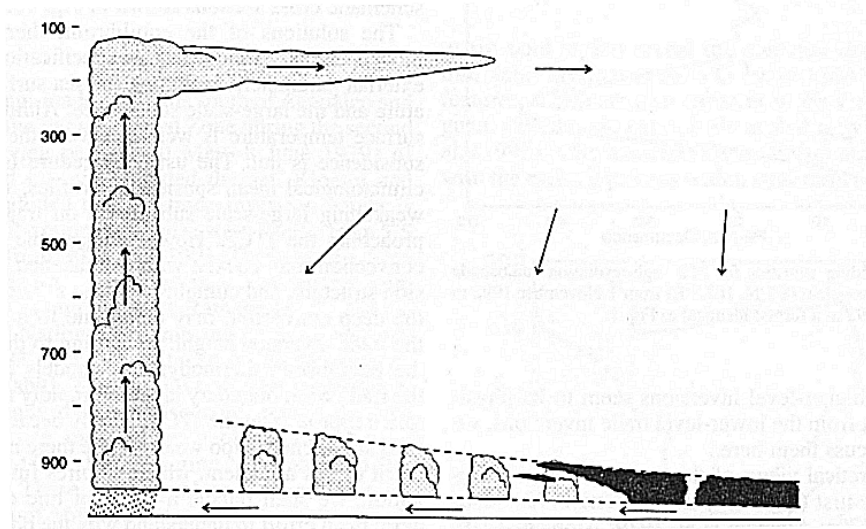


Figure 2.2: An idealized depiction of the transition from stratocumulus clouds to deep convection along a line from the west coast of the subtropical continents along the trade winds towards the ITCZ (from Schubert et al., 1995).

The sub-tropical land areas contain the absolute minima in cloud cover over the desert regions of the planet. Here, the humidity to generate clouds at the PBL top is not available from the surface and the drying effect of the subsiding motion leads to the most arid regions observed.

The extratropical oceans are the regions of maximum cloud cover across the globe. Here a mean cloud cover in excess of 80 % is measured. Different types of clouds such as those produced in and around midlatitude cyclones (Lau and Crane, 1995), and low-level stratus, which is the predominant cloud type in summer (Klein and Hartmann, 1993), contribute to this large overall coverage with cloud. The maximum cloud cover over land in extratropical regions can be found over Western and Central Europe where the absence of large North-South oriented mountain ranges allows clouds and humidity associated with eastward moving baroclinic systems to penetrate well inland. The rest of the extratropical continental areas show cloud covers around 50 %. In most areas cloud cover peaks in summer and is associated with deep and shallow convective clouds.

2.1.2 The effects of clouds in the climate system

The mere presence of clouds does not make them an object of interest for global modelling. However clouds influence the earth-atmosphere system in a variety of ways. These influences are often termed “cloud forcing”, a misleading classification, since a forcing normally refers to an external influence on a system. Since clouds form an intrinsic part of the climate systems, their effects will alter their own characteristics through feedback mechanisms, so that they cannot be considered a forcing mechanism in the classical sense. Nevertheless, the term forcing will be used throughout this chapter when necessary to be consistent with previously published studies.

Radiative effects

The main incentive for introducing a representation of clouds into global numerical models was and is that they modulate the radiative energy exchange between the atmosphere and its upper and lower boundaries. They interact with both the solar radiation in the shortwave part of the spectrum, and the thermal radiation emitted by the earth and the atmosphere in the longwave part of the spectrum. For shortwave radiation, clouds increase the albedo of the planet, thereby reducing the amount of radiation absorbed by the earth-atmosphere system as a whole. The emission of terrestrial radiation to space is decreased by their presence through a lowering of the effective brightness temperature of the earth. The details of the physics of the radiative transfer in clouds are far beyond the scope of this thesis and the reader is referred to the appropriate textbooks (e.g., Liou, 1992).

The parameters that directly affect the radiation field in and around clouds can be grouped into three main classes (Arking, 1991): i) the environment above and below the cloud, including temperature, humidity and aerosol distribution as well as surface albedo and emissivity; ii) the macrophysical structure of clouds such as their horizontal and vertical extent and spacing as well as their overall condensate content; and iii) the microphysical structure, e.g., cloud particle size, phase and shape. It is obvious that all these parameters need to be described in some form in a GCM in order to describe the cloud radiative effects. The main aim of cloud parametrization in this context is an accurate description of the cloud macrophysical structure. This is where the emphasis of this thesis will lie.

The overall impact of clouds on the radiation budget can be measured by comparing the radiative fluxes in cloudy to those in clear-sky conditions. The difference between the two has been termed cloud radiative forcing (Ellis, 1978) and can be defined separately for the

solar and terrestrial parts of the spectrum:

$$SWCRF = S_{clear} - S, \quad (2.1)$$

and

$$LWCRF = L - L_{clear}, \quad (2.2)$$

where $SWCRF$ and $LWCRF$ stand for shortwave cloud radiative forcing and longwave cloud radiative forcing respectively. L and S are the longwave and shortwave radiative fluxes and L_{clear} and S_{clear} their respective clear-sky values. Although these two quantities are theoretically defined at any level in the atmosphere, the major global data source for radiative fluxes are satellites which measure radiation at the top of the atmosphere (TOA). Even then the definition of clear-sky and cloudy scenes is far from trivial. There have been numerous studies (e.g., Ramanathan, 1987; Ramanathan et al., 1989; Hartmann and Doelling, 1991; Weaver and Ramanathan, 1996; Weare, 1997; Bony et al. 1997) to establish the effect clouds have on the TOA radiation budget many of which are based on data from the Earth Radiation Budget Experiment (ERBE; Barkstrom and Smith, 1986).

Figure 2.3 shows the TOA LWCRF (top) and SWCRF (middle) as measured by ERBE for the months of June/July/August 1987. The bottom panel of the same figure shows the sum of the two CRFs which represents the net effect of clouds on TOA radiation. Fluxes are taken negative upwards so that positive values indicate decreased and negative values increased upward fluxes. It is evident that in the longwave part of the spectrum clouds enhance the greenhouse effect of the earth-atmosphere system which leads to an additional warming of the system. The main areas of strong LWCRF are the tropical and extratropical latitudes with virtually no LWCRF in the subtropics. This can be explained by the fact that both tropical and extratropical cloud systems have high cloud tops, which significantly reduce the outgoing longwave radiation compared to clear-sky conditions. In contrast, the subtropics are dominated by clouds with relatively low tops which are often situated near temperature inversions at the top of convective boundary layers. Therefore the radiation emitted from the cloud tops does not differ very much from that emitted by the surface in those regions. In the shortwave part of the spectrum clouds significantly enhance the reflection of radiation received from the sun and therefore cool the planet. The most pronounced effects can be found in the tropics and the summer hemisphere (Northern hemisphere in Figure 2.3), which is partly due to the fact that the absolute values of solar radiation are largest there.

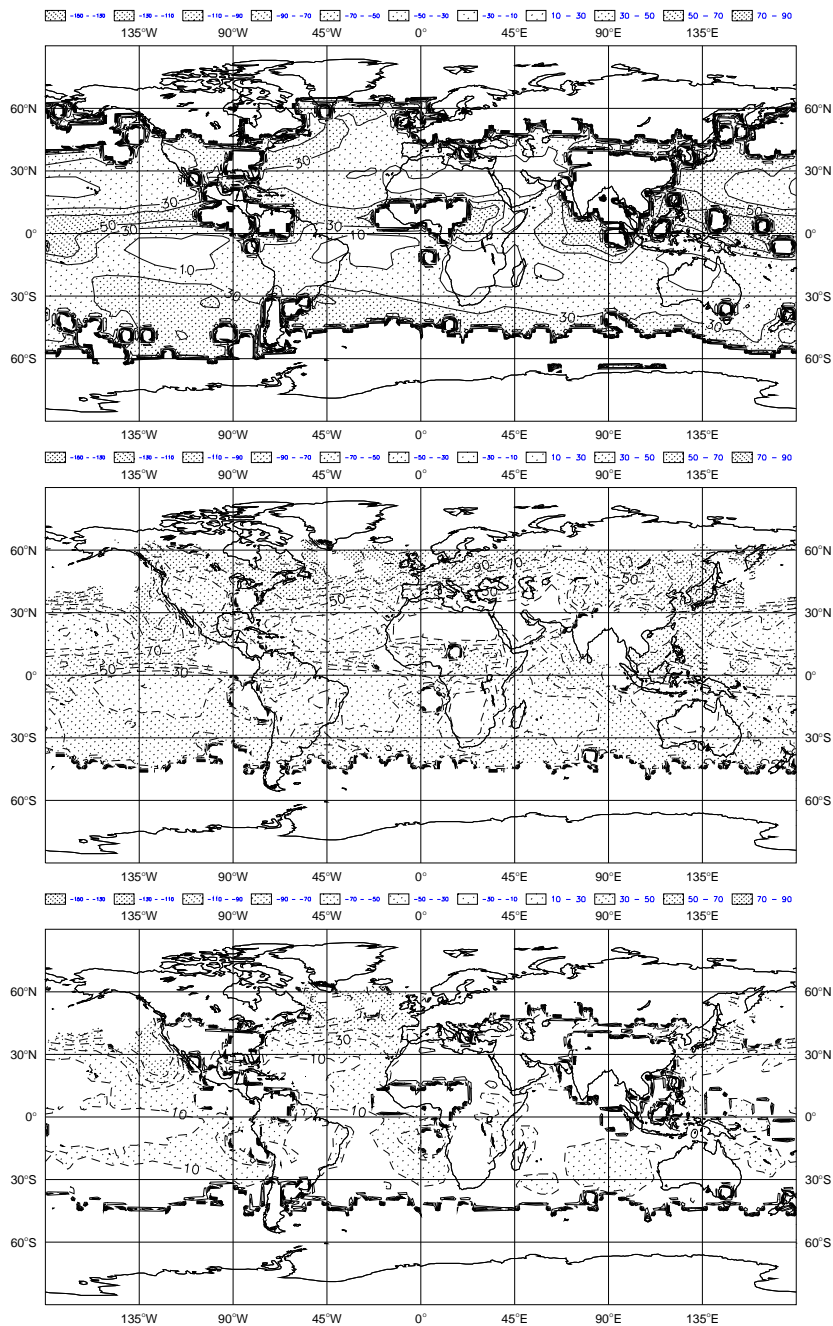


Figure 2.3: Mean geographical distribution of longwave (top), shortwave (middle) and net (bottom) cloud radiative forcing as estimated by ERBE for June/July/August 1987

As evident in the bottom panel, the net effect of clouds is to cool the earth-atmosphere system and is concentrated in subtropical latitudes and the summer hemisphere extratropics. Interestingly in the deep tropics, the longwave and shortwave effects of clouds almost cancel leading to only a small net cloud radiative forcing. It is important to note that all the

described effects are measured at the top of the atmosphere and do not allow conclusions about the heating/cooling profiles within the atmosphere, which would require measurements of CRF at various other levels in the atmosphere as well as at the surface. The lack of such data is one of the major caveats in progressing the understanding of the effects clouds have on the climate system. The only source to further our understanding of how clouds affect the general circulation is global modelling of which a few examples will be highlighted below.

Latent heat effects and precipitation

Phase changes of water are connected with the release of latent heat. Their occurrence in the atmosphere will therefore change its thermodynamic structure and ultimately affect the atmospheric flow. Atmospheric processes leading to the release or consumption of latent heat occur i) directly inside clouds and ii) in precipitation that has formed in clouds and is falling into clear sky under the influence of gravity. Hence the description of latent heat effects brought about by clouds requires the description of the formation and evaporation of cloud droplets or cloud ice particles as well as the processes that lead to the generation and decay of precipitation. This class of physical processes is normally referred to as cloud microphysics. A comprehensive review of cloud microphysics is beyond the scope of this work and textbooks by Cotton and Anthes (1989), Houze (1993), and Pruppacher and Klett (1997) provide further details. For the purpose of this work it is sufficient to be aware that a crucial part of describing the effects of clouds on the atmosphere lies in the description of cloud microphysical processes.

Besides the description of the latent heat effects, the parametrization of microphysical processes in clouds is a requirement for successful predictions of precipitation. This is of importance not only because precipitation is an obvious forecast product of an NWP model but more so because it constitutes a crucial component of the earth' hydrological cycle. As highlighted in Chapter 1, precipitation couples the atmospheric hydrological processes to those in the ground and influences surface processes through the modification of turbulent transfers. It is therefore obvious that any description of cloud effects in atmospheric models must include the release and fallout of precipitation together with a description of possible phase changes in the precipitating water species.

Clouds and the general circulation of the atmosphere

Of the cloud effects described above it is only the TOA cloud radiative forcing that is reasonably well observed. Knowledge of this forcing alone is obviously not sufficient to understand the role clouds play in the general circulation of the atmosphere. For this purpose measurements of radiative fluxes and latent heating throughout the atmosphere would be required to establish the vertical structure of cloud induced heating. Since such observations are not available, one has to rely entirely on modelling with the intrinsic difficulty that the representation of clouds in the model used to establish their effect might be inaccurate and the conclusions drawn from the results flawed. Nevertheless a number of useful modelling studies that establish the role of clouds in the context of the general circulation have been carried out in the past, two of which will be highlighted here.

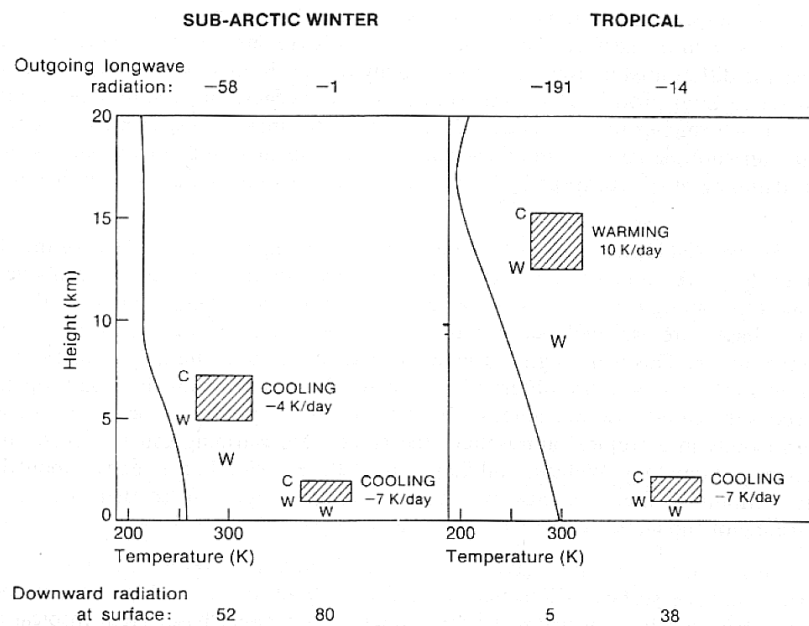


Figure 2.4: The influence of overcast high and low clouds on atmospheric heating and longwave radiative fluxes at the TOA and the surface in tropical and sub-arctic conditions (from Slingo and Slingo, 1988).

Slingo and Slingo (1988) investigated the role that the longwave cloud radiative forcing plays in the general circulation. They first established the direct effects of clouds due to longwave radiation by inserting high and low clouds into standard atmospheric profiles and calculating atmospheric heating and cooling rates using a radiation parametrization scheme. The results are summarized in Figure 2.4. From this figure it is evident that clouds warm both the earth-atmosphere system and the surface in the longwave spectral region. Cloud bases warm and

cloud tops cool. The net local effect is a cooling except in tropical latitudes where high cloud tops are sufficiently cold to lead to a net local warming. Hence, the atmosphere itself is generally cooled by clouds except in the tropics. The surface is warmed by clouds (in the longwave spectral region) with the largest effects in dry atmospheres being found mainly in high latitudes. High clouds significantly reduce the outgoing longwave radiation at the TOA, indicated by the numbers at the top of the figure, which represent differences between the assumed cloudy with clear-sky conditions. At the surface clouds, in particular those at low levels, lead to an increase in downward longwave radiation. The latter effect is more pronounced in the sub-arctic atmosphere, because of the less abundant water vapour, itself a strong absorber/emitter at infrared wavelengths.

After establishing the basic physical interactions between clouds and the atmosphere, Slingo and Slingo (1988) used a GCM and replaced the atmospheric longwave heating rates calculated in an integration with fully interactive clouds by clear-sky values retaining the influence clouds have on the longwave flux at the surface. They then compared the results of the two integrations in order to study the differences in circulation. They found that one of the major cloud effects is a heating of the upper tropical troposphere which leads to an acceleration of both subtropical jets. Due to the cooling by clouds at lower levels the lower troposphere becomes more unstable leading to an increase in the triggering of convection. This enhanced diabatic forcing leads to an intensification of the Hadley circulation in their model.

Randall et al. (1989) also performed a set of numerical experiments to investigate the role of clouds in the general circulation. They confirmed that it is the interaction of clouds and radiation with the convection that exerts the major influence on the general circulation, although the mechanism in their model was different from that in Slingo and Slingo (1988). In Randall et al.'s experiments thick upper-tropospheric anvil clouds actually lead to a cooling of the atmosphere in that region, contrary to the heating Slingo and Slingo (1988) found. The main reason was that the clouds produced by Randall et al.'s model were optically and geometrically much thicker with lower cloud bases, so that their cooling effect dominates. They draw the conclusion that "the upper tropospheric cloudiness associated with cumulus convection has a powerful influence on both the convection and the large-scale circulation" and call for a closer link of convection and cloud parametrization. Numerous studies since then have confirmed the role of upper tropospheric tropical cloudiness for both convection and general circulation (e.g., Lohmann and Roeckner, 1995; Donner et al., 1997; Jakob, 2000) and addressing the parametrization of the crucial link of convection to cloud formation will

form part of this thesis.

2.2 Clouds and parametrization

Independent of the numerical technique applied, the numerical solution of the hydrodynamic equations governing atmospheric motions at some stage involves approximating these continuous differential equations by finite difference equations applied to a grid with cells of finite volume. Even models that apply the spectral technique (e.g., Machenhauer, 1979), such as the ECMWF global model, evaluate parts of the numerical solution in this so-called grid-point space. The size of the finite volumes chosen depends to first order on the size of the domain of the numerical model and the available computational power. While the continuous differential equations describe the whole spectrum of atmospheric motions, their discrete form can only describe processes on scales of the order of twice the grid length. Typical horizontal grid lengths in contemporary global models range from around 50 km in NWP applications to more than 250 km in climate modelling. Models using this kind of horizontal grid size will from now on be referred to as large-scale models. Processes that act on scales smaller than these grid sizes are, *per sé*, not represented in the solution of the finite difference equations. However, they can affect the mean flow considerably since, for instance, large amounts of water vapour, heat and momentum are transported by turbulent and convective motions. Since an explicit treatment of the so-called subgrid-scale processes is prohibited, only their statistical effects on the mean state (in the grid-box sense) can be taken into account. The model variables are only known on the resolved scales, so that the description of these statistical effects has to be expressed in terms of the resolved scale. The general technique involved is referred to as parametrization.

As outlined above, the representation of clouds in numerical models of the atmosphere involves representing their effects on radiation as well as latent heat effects, the generation of precipitation, and the transports within convective clouds. All but the radiative effects of convective clouds are normally dealt with in a separate parametrization of cumulus convection. A comprehensive review of these parametrizations schemes is beyond the scope of this work. The reader is referred to textbooks such as Emanuel (1994) and reviews elsewhere in the literature (e.g., Emanuel and Raymond, 1993). There exists, however, a strong link between the latent heat and transport effects of convection and the cloud fields it produces and which affect the radiation field. The representation of that link is a subject of cloud

parametrization and is further explored in Chapter 5. For reasons outlined in the previous subsections, the representation of the radiative effects of all clouds and the latent heat effects of non-convective clouds require the description of at least the following quantities for each grid volume of a large-scale numerical model

- the horizontal coverage of cloud normally referred to as cloud fraction;
- the vertical extent of the clouds;
- the sources and sinks of cloud condensate including
 - condensation rate,
 - evaporation/sublimation rate,
 - conversion rate into precipitation and fallout;
- the phase of the condensate;
- the particle size and shape;
- the in-cloud distribution of condensate.

It is obvious from this list that the description of many of its items will imply scales much smaller than the typical resolution of large-scale models, ranging from micrometres for microphysical processes to several kilometres for updraughts in deep cumulus towers. The problem of representing clouds in large-scale models is therefore one of parametrizing their overall effects on the resolved scales.

From the preceding discussion it is obvious that there are a number of problems to overcome in the parametrization of clouds. First of all there exists a variety of cloud types, such as stratocumulus clouds at the top of convective boundary layers, vast cloud systems associated with extratropical disturbances, deep convective systems that might or might not be organized, and upper-tropospheric cirrus clouds. These different cloud types are formed, maintained and decay by a large number of different physical processes, such as convection, small-scale turbulence, large-scale ascent or descent and cloud microphysical processes that lead to the generation of precipitation. Many of these processes are only poorly understood and act on scales smaller than those resolved in a large-scale model requiring them to be parametrized themselves. Furthermore, as outlined above, the radiative effects of clouds, one of the main purposes for cloud parametrization, depend on a large number of different cloud

parameters that all need to be determined accurately to ensure their correct treatment in the radiation parametrization. Similar arguments hold for the microphysical processes that lead to the release of precipitation, whose description is another important task for cloud parametrizations.

Before providing a brief overview of how the problem of cloud parametrization has been addressed in GCMs, some general concepts for any cloud parametrization will be outlined.

One of the microphysical processes to be described in any cloud parametrization is the condensation process. Theoretically this involves the description of two distinct processes: the nucleation of cloud particles and their initial growth by diffusion of water vapour towards the nucleated particles. It is a well known fact that the main nucleation process in the atmosphere is that of heterogeneous nucleation of cloud particles on small aerosol particles usually referred to as Cloud Condensation Nuclei (CCN) (e.g., Pruppacher and Klett (1997)). In the presence of CCN, condensation occurs whenever the relative humidity exceeds its saturation value of 100%, while in the absence of CCN, large values of supersaturation must exist to allow the nucleation of sufficiently large droplets. In order to avoid the complex treatment of nucleation processes, all GCMs to date assume that CCN are always available in sufficient numbers, and the condensation problem reduces to removing any supersaturation. Although this assumption is reasonable throughout most of the atmosphere, recent observations and model studies (Heymsfield et al., 1998; Khvorostyanov and Sassen, 1998a,b; Gierens et al., 1999; Jensen et al., 2000; Gierens et al., 2000; Schumann et al., 2000) suggest that in the upper troposphere, significant supersaturations with respect to ice do occur. This is thought to be a consequence of the scarcity of CCN and the low water diffusivity at low temperatures. These findings present a challenge to cloud parametrizations and will require their modification in the near future.

A second important general concept in cloud parametrization is that of the fractional coverage of a model grid box with cloud, which is used in almost all current cloud parametrizations. Assuming that clouds form whenever the specific humidity locally exceeds its saturation value, which is true if sufficient CCN are available, fractional cloud cover implies that certain parts of a model grid box become supersaturated before others. This has several implications. One of them is that clouds exist in the model grid box before the grid-mean relative humidity reaches the saturation value of 100 %. This basic feature has been used in many cloud parametrizations to determine the cloud fraction by defining a critical relative humidity, RH_{crit} above which clouds exist in a grid box and a functional relationship that

increases cloud cover from zero below RH_{crit} to one when the entire grid box is saturated. It is immediately obvious that the definition of both RH_{crit} and the functional relationship are far from unique and for many years cloud parametrization was focussed on refining such definitions. Another consequence of considering cloud fraction is that there must exist a non-uniform statistical distribution of the distance from the local saturation point within the model grid box. This implies some variation of humidity and temperature around their mean value. The knowledge of these variations would in fact be sufficient to describe the cloud field within a grid box.

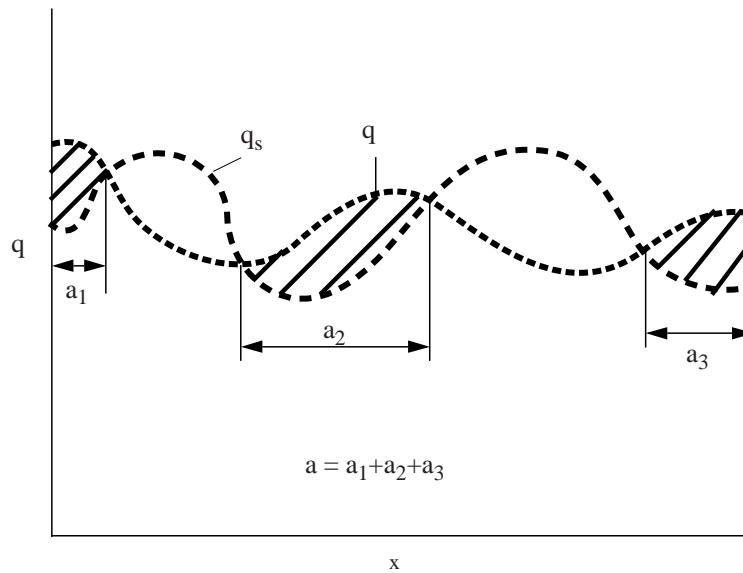


Figure 2.5: Schematic of the existence of clouds in the supersaturated areas of a one-dimensional model grid box. The x-axis represents space. The short-dashed line (q) shows the value of specific humidity as a function of location within the grid-box. The long-dashed line (q_s) shows the saturation value of specific humidity. Areas in which $q > q_s$ represent clouds, indicated by the hatched areas.

Figure 2.5 provides an illustration of this idea. In a one-dimensional model “grid box”, both specific humidity, q , and its saturation value, q_s , are non-uniform. In those areas where $q > q_s$ clouds are assumed to exist and the sum of the cloud areas divided by the size of the grid box is the total cloud fraction. The mathematical technique to describe these variations is to describe joint probability distribution functions for a temperature and a humidity variable. Unfortunately the distribution functions are neither known nor expected to be unique and will depend on many different physical processes. Nevertheless the introduction of the idea of distributions provides a conceptual framework for the development of cloud parametrizations. Chapter 5 will make use of this concept.

2.3 A brief history of cloud parametrization

The previous section has established the reasons why cloud processes need to be parametrized in global GCMs. The main effects of clouds were found to be their influence on the radiative fluxes, their latent heat effects and, in case of convective clouds, the ability to transport heat, moisture and momentum. It was also established that all but the radiative effects of convective clouds are treated in a separate convection parametrization, which is not the subject of this thesis. The role of clouds for GCMs has been recognized right from the beginning of global modelling, although in the first GCMs it was mainly the latent heat effects that were considered to be important. This section gives a brief overview of the major steps in the history of cloud parametrization. The various approaches will be considered in the context of the major effects that need to be described in the models. Each of the periods of development in cloud parametrization can be assessed using the following four questions:

- 1) How are non-convective condensation processes on subgrid scales described?
- 2) How are the radiation effects of the clouds derived after answering 1)?
- 3) How are the convection and cloud parametrizations linked?
- 4) How are the microphysical processes that lead to precipitation generation described?

Figure 2.6 provides an overview over the timeline of key aspects of the treatment of cloud-related processes in GCMs.

Early condensation schemes

In the early development of GCMs (e.g., Manabe et al., 1965) the latent heat effects of both convective and non-convective condensation processes were considered important enough to warrant some treatment. Furthermore, since the model included an evolution equation for a humidity variable, unphysical states of supersaturation needed to be avoided in the evolution of the model variables. Therefore a simple but effective condensation scheme was introduced in the models. Its basic idea was to carry out all model calculation, such as advection, radiation, boundary layer processes etc., and then readjust any possible supersaturated states occurring on the grid scale (i.e., in the grid-averaged variables) back to saturation. The condensate thus formed was removed instantaneously as precipitation. Hence, although condensation processes and therefore their latent heat effects were described, it was not clouds but precipitation that was formed during the condensation.

Cloud related Processes in GCMs

	60/70's	70/80's	80/90's	now and beyond
Condensation (non-convective)	$\bar{q} > \bar{q}_s$	$\bar{q} > \bar{q}_s$	l prognostic function of outcome of processes	l prognostic function of the processes themselves
Radiation effects	prescribed zonal mean albedo and emissivity of clouds	$a = f(RH)$ l prescribed	$a = f(RH)$ l prognostic	a prognostic l prognostic
Convection	no cloud interaction	$a_{cu} = f(CP)$ l_{cu} prescribed	$a_{cu} = f(CP)$ l_{cu} prescribed	condensate and mass as sources for a and l
Microphysics	none	none	simple bulk microphysics	complex bulk microphysics

Figure 2.6: An overview over the historic evolution of key aspects of cloud parametrization. For a detailed discussion see text. The symbols are defined as follows: \bar{q} is the grid-mean specific humidity, \bar{q}_s the grid mean of its saturation value. a represents cloud cover with a_{cu} describing the contribution from convectively generated clouds to that value. l represents the condensate content, with l_{cu} again describing that in convective clouds. RH is the grid-mean relative humidity and CP the rate of convective precipitation.

A similarly simple description of convection was used in which the temperature lapse rate for saturated grid columns was not allowed to exceed that of a moist adiabat. Any condensate formed in this “moist convective adjustment” process was also removed as precipitation.

The role that radiation effects of clouds play in the general circulation was considered small, so that most early GCMs used prescribed zonally-averaged cloud albedos and emissivities as input for their radiation calculations. Since all condensate was removed as precipitation, no description of microphysical processes was necessary, hence, early GCMs only described condensation processes with no cloud interaction whatsoever.

Diagnostic schemes

It was soon recognized that the radiative effects of clouds might play a crucial role in the general circulation of the atmosphere. The next generation of cloud parametrizations was therefore aimed at providing some interaction of cloudiness and the other model variables. This was usually achieved by parametrizing the cloud fraction as a function of relative humidity. This type of parametrization had already been proposed by Smagorinsky (1960),

but it wasn't before the early to mid 1980's that it was used in GCMs (e.g., Geleyn, 1980). The reasons for this are not entirely obvious, but might lie in i) the difficulties of validating the model predictions of cloud fraction and ii) the rather limited computing power available at the time.

The basic idea behind relative humidity schemes is that if the grid-mean relative humidity exceeds a threshold value, usually on the order of 80%, it is likely that some part of the grid volume has already reached saturation and therefore clouds have begun to form. If the grid-mean relative humidity reaches 100% the entire grid box is assumed to be covered with clouds. Since all models using this approach still used the model for condensation as before, the radiative and latent heat effects of clouds were entirely decoupled. Furthermore, since condensation occurred only for grid-mean values of relative humidity above 100%, but clouds existed before that, the amount of condensate needed for the description of the radiative effects of the model clouds was simply prescribed.

The development of more complex convection parametrizations allowed convectively generated clouds to be described as a function of the outcome of the convection parametrization. This was often achieved by linking the cloud fraction to the precipitation produced in the convection scheme and again prescribing the condensate content (e.g., Slingo, 1980).

Due to the simple removal of any moisture in excess of the saturation humidity as precipitation, the description of microphysical processes was still not necessary. This type of cloud parametrization is usually referred to as the "diagnostic" approach, since the main cloud parameters (cloud fraction and condensate amount) are diagnosed using the grid-averaged quantities. This approach was developed further by Slingo (1987) who introduced additional predictors, such as vertical motion and inversion strength at the top of convective boundary layers, into the cloud fraction description. It is worthwhile noting that this approach provides reasonable estimates of many of the main observed cloud patterns and can be made to work well by adjusting the many free parameters in the parametrization. It is this and the low computational cost that made it a widely used approach right up to the mid 1990's.

Prognostic condensate

One of the major drawbacks of the diagnostic approach described above is the obvious disconnection of the cloud latent heat effects from their radiative effects. This link was established in large-scale models in a parametrization by Sundqvist (1978) who introduced an additional prognostic model equation for cloud condensate, previously only applied in

cloud-scale modelling. By explicitly predicting the condensate amount formed, a link to the radiative impact of the clouds could be established through the direct use of the predicted condensate in the radiation calculations. A consistent diagnostic treatment of cloud fraction was also introduced. Cloud fraction simply remains a function of the grid-mean relative humidity. However, the latter is now directly influenced by the condensation processes, which are allowed to occur before grid-mean saturation is reached. The description of convective clouds remained unaltered by Sundqvist's approach.

One immediate consequence of carrying cloud condensate as a model variable, that should play a major role in the further development of cloud parametrizations, is that the conversion of some of the condensate to precipitation needs to be represented. Sundqvist (1978, 1988) used very simple models of the autoconversion process based on the work of Kessler (1969) and introduced some intuitive parametrization of the precipitation-enhancing collection processes as well as the Bergeron-Findeisen mechanism (see, e.g., Pruppacher and Klett, 1997), which leads to an acceleration of the conversion process from cloud condensate to precipitation in clouds when both the ice and water phase coexist.

Distribution schemes

In parallel to the introduction of what is now usually known as “the Sundqvist parametrization”, another approach emerged. It is based on ideas originally applied by Sommeria and Deardoff (1977) and Bougeault (1981) in much higher resolution cloud models and that was adapted to GCMs in various forms by LeTreut and Li (1988), Smith (1990) and Ricard and Royer (1993). Their parametrizations are all based on the idea outlined above, that the existence of clouds on the subgrid scale requires that the humidity and its saturation value or both are somehow distributed around their grid-mean value. The knowledge of their probability distribution functions (pdfs) is therefore sufficient to describe both cloud fraction and condensate content within a grid box. Sommeria and Deardoff (1977) suggested the use of a joint pdf for a temperature and a humidity variable. Since they were concerned with the description of non-precipitating boundary layer clouds they proposed the use of conservative thermodynamic variables, such as liquid water potential temperature, Θ_l and total mixing ratio, q_w .

Figure 2.7 illustrates the general idea of this approach. Both Θ_l and q_w are assumed to be distributed with a Gaussian joint pdf. A saturation curve for a given grid-mean temperature and pressure is then drawn. All the values of the pdf that lie above this saturation curve

culations. A major problem in both approaches is that they do not include clouds produced by convective processes as an integral part of their formulation. In models using either of these two cloud parametrization approaches, convective clouds are usually still treated as they were in diagnostic cloud parametrizations. This problem was identified by Randall (1989) as “the most serious deficiency of the cloud parametrizations in current GCMs”.

A variety of approaches to tackle this problem has been devised since then. The most common approach used in the schemes solving a prognostic equation for the condensate is to treat water substance detrained from convective updraughts as a source of cloud condensate for the ‘stratiform’ clouds. The exact nature of the link depends on the definition of ‘detrainment’ and can vary for different schemes. Examples for those treatments of convective clouds can be found in e.g., Ose (1993), Tiedtke (1993), Roeckner (1995), Del Genio et al. (1996), Fowler et al. (1996). Although using “detrained” condensate from convection as a source for cloud condensate has become a standard way of linking convection and radiation through cloud formation, the variety of different ad-hoc techniques used points to a lack of understanding of how exactly this link should work. A further major problem is how to represent the cloud fraction resulting from the detrainment process. Only Tiedtke (1993) and Randall (1995) have attempted to derive consistent treatments of both condensate and cloud fraction from convection. Chapter 5 of this work will discuss this issue at length and propose a new consistent set of source terms for clouds formed by convective processes.

Major conceptual changes in cloud parametrization have recently been introduced in a parametrization scheme developed by Tiedtke (1993, T93). This parametrization forms the background of the work described in this thesis and is described in detail in Chapter 3. There are two major conceptual changes introduced in T93. Firstly, cloud fraction is described by a prognostic equation, based on the mass budget for cloudy air. Secondly, and probably most importantly, a process-oriented approach to cloud parametrization has been introduced. This is illustrated in Figure 2.8. Conceptually all previous cloud parametrizations can be summarized by the top panel of Figure 2.8. Various physical processes, such as resolved scale ascent, convection, turbulence etc., modify one or several resolved variables and/or their tendency. Those resolved quantities (e.g., relative humidity or its tendency) are then used to evaluate the evolution of the model clouds. A major drawback of this approach is that the effects of parametrized processes, such as convection, which contribute directly to cloud formation and dissipation, are first “integrated” onto the grid scale only to be reinterpreted for subgrid-scale cloud processes.

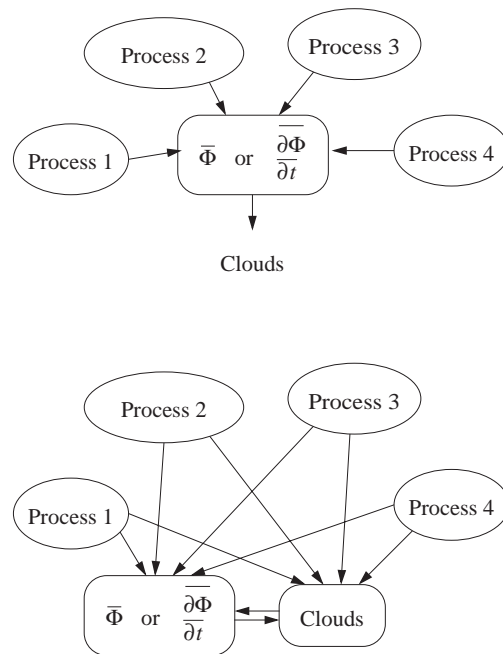


Figure 2.8: Schematic of the different approaches to cloud parametrization. The top panel shows the principles of “integrating” cloud schemes, while the bottom panel illustrates the process-oriented approach.

In contrast, in the T93 approach, each potentially cloud-modifying process, resolved (e.g., large-scale ascent) or parametrized (e.g., convection), directly alters the model’s cloud variables as well as other resolved-scale model variables. This way information available at the level of other physical parametrizations can be directly used in the cloud scheme and the clouds become a more integral part of the parametrization package. This “process-oriented” approach is illustrated in the bottom panel of Figure 2.8.

Most recently the attention in cloud parametrization has shifted significantly towards the treatment of cloud microphysics. This has been facilitated by increased computing power and the availability of sophisticated microphysics parametrizations from cloud-resolving and mesoscale numerical models. Recent examples for improved microphysical schemes in GCMs can be found in Fowler et al. (1996), Lohmann and Roeckner (1996), and Rotstayn (1997). Although increased sophistication in representing precipitation processes in GCMs is certainly justified, the transplant of a microphysics scheme from a cloud-resolving model to a GCM is not without problems. This is mainly due to the scales on which the input variables of the microphysical scheme are available and to the difference in time steps used by the different models. Microphysical processes are highly non-linear and their parametrization has to rely on the knowledge of the local amount of condensate. In GCMs only the grid-mean (or cloud-mean if cloud fraction is a model variable) value for condensate is known. This has led

to the need for significant modifications to microphysical constants in the parametrizations in order to achieve reasonable cloud condensate and precipitation amounts. The situation can be further complicated in the presence of vertically varying cloud fraction, and this will be subject of Chapter 6. The detailed treatment of microphysical process would also require the use of very short model time steps. Since GCMs are either used at high resolution in NWP or for long integrations in climate research, the use of such short time steps might be prohibitive and alternative solutions need to be found.

Summary of the current main lines of research

The current main lines of research which motivated much of the contents of this thesis are summarized in the list below. They encompass

- the link of convection (and other) parametrizations to cloud production and dissipation;
- the treatment of cloud fraction by using a prognostic evolution equation;
- improvements to the representation of microphysical processes;
- the use of new data sources and new approaches for cloud parametrization evaluation.
- the consistent treatment of cloud inhomogeneities in cloud and radiation parametrizations;

The following chapters will summarize the author's contribution to the progress made in those research areas in recent years at ECMWF.

Chapter 3

Cloud parametrization in the ECMWF model

The previous chapters have established the need to parametrize clouds in order to describe the various impacts they exert on the atmosphere, both through the alteration of the radiation field and through latent heat effects. In the rest of this thesis the emphasis will be on an improved representation of cloud fraction and its validation using the European Centre for Medium-Range Weather Forecasts (ECMWF) model and the cloud scheme embedded therein. The scheme was originally developed by Tiedtke (1993) and was implemented into the ECMWF operational system in 1995 (Jakob, 1994). In this chapter the main characteristics of the ECMWF model and its cloud scheme are described, followed by a brief overview over the technique developed to provide initial conditions for the scheme in the context of ECMWF's data assimilation system.

3.1 The ECMWF model

The ECMWF routinely produces numerical forecasts of the state of the global atmosphere. The Centre's Integrated Forecasting System (IFS) comprises a four-dimensional variational data assimilation system (4DVAR; Rabier et al., 2000; Mahfouf and Rabier, 2000; Klinker et al., 2000), a global atmospheric model, an ensemble prediction system (Molteni et al., 1996; Buizza et al., 1998; Buizza et al., 1999), and a suite of ocean wave models (The WAMDI group, 1988; Komen et al., 1994; Janssen et al., 1997).

The main emphasis of this study will be on the use of ECMWF's atmospheric model. Its main overall features can be summarized as follows:

- global spectral model with varying spectral resolution (T_L319 in operational version,

where the T indicates the use of triangular truncation with a truncation limit of 319 spectral coefficients; the subscript L indicates the use of a linear grid (see below));

- equivalent reduced linear grid (Hortal and Simmons, 1991; Hortal, 1999) for advection and physical parametrization (≈ 60 km horizontal resolution in the operational version);
- hybrid (η) vertical coordinate (Simmons and Struving, 1981; 60 model levels in the operational version);
- two-time level semi-Lagrangian advection scheme (Ritchie et al., 1995; Temperton et al., 1999; Hortal, 1999);
- model timestep, Δt , of 1200 s to 3600 s depending on horizontal resolution;
- seven prognostic model variables, namely

relative vorticity,

divergence,

logarithm of surface pressure,

temperature,

specific humidity,

cloud liquid water/ice content,

cloud fraction.

As explained in Chapter 2, the representation of the large-scale effects of processes acting on scales smaller than the grid size have to be included through so-called physical parametrizations. Typically these parametrizations are applied at individual grid points without direct interaction with neighbouring points. This interaction is achieved through altering the values of the resolved-scale variables in the grid-averaged equations. The physical parametrizations included in the ECMWF model are

- a radiation scheme (Morcrette 1990, 1991);
- a planetary boundary layer scheme (Louis et al., 1982; Beljaars and Holstlag, 1991; Beljaars and Betts, 1993; Beljaars, 1995a,b);
- a four-layer land surface scheme (Viterbo and Beljaars, 1995);

- a subgrid-scale orography scheme (Lott and Miller, 1997);
- a mass-flux convection scheme with CAPE closure (Tiedtke, 1989; Gregory et al., 2000);
- a fully prognostic cloud scheme (Tiedtke, 1993; Jakob, 1994).

3.2 The cloud parametrization scheme

In this section the ECMWF cloud parametrization as originally formulated by Tiedtke (1993) will be briefly summarized. The purpose is to provide sufficient background for the work presented in later chapters, which is aimed at evaluating and improving the original parametrization presented here. As before, the parametrization scheme in its original form will be referred to as the T93 scheme. The basic foundation of the T93 scheme are two prognostic equations for both condensate (cloud liquid water and cloud ice) and cloud fraction. The determination of the phase of the condensate is based solely on temperature, and the exact formulation for this, and the calculation of saturation water vapour pressure for the different water phases can be found in Appendix B. Rain and snow are treated as separate diagnostic quantities. The prognostic equations can be written as

$$\frac{\partial l}{\partial t} = A(l) + S_{cv} + S_{bl} + C - E - G_P - \frac{1}{\rho} \frac{\partial}{\partial z} (\rho \overline{w'l'})_{entr}, \quad (3.1)$$

and

$$\frac{\partial a}{\partial t} = A(a) + S(a)_{cv} + S(a)_{bl} + S(a)_C - D(a). \quad (3.2)$$

Here, l represents the grid-mean cloud condensate content and a the cloud fraction. $A(l)$ and $A(a)$ denote the advection of both prognostic variables. Sources of l and a are assumed to exist due to convection (S_{cv} and $S(a)_{cv}$), boundary layer turbulence at the top of mixed layers (S_{bl} and $S(a)_{bl}$) and due to non-convective condensation processes (C and $S(a)_C$). The decay of clouds occurs through evaporation for both variables (E and $D(a)$) and through the generation of precipitation (G_P) for condensate only. The flux term on the right hand side describes the possibility of cloud destruction near cloud tops through cloud top entrainment, for which no change of cloud fraction is assumed. The corresponding grid-scale equations for specific humidity, q , and dry static energy, $s = c_P T + gz$, can be written as

$$\frac{\partial q}{\partial t} = A(q) - S_{bl} - C + E + E_P - \frac{1}{\rho} \frac{\partial}{\partial z} (\overline{\rho w' q'})_{entr}, \quad (3.3)$$

and

$$\frac{\partial s}{\partial t} = A(s) + L(S_{bl} + C - E - E_P) - L_f M + c_p [(1 - a)R^{clr} + aR^{cld}] - \frac{1}{\rho} \frac{\partial}{\partial z} (\overline{\rho w' s'})_{entr}, \quad (3.4)$$

where additional to the symbols already used above L and L_f are the latent heat of condensation/sublimation and freezing respectively, E_P is the evaporation of precipitation, M is the rate of snowmelt, and R^{clr} and R^{cld} are the clear and cloudy-sky radiative heating rates. Note that here, in addition to advection, $A(q)$ and $A(s)$ contain contributions of all physical processes except cloud generation/dissipation and radiation. Therefore the convective cloud source does not appear in equations (3.3) and (3.4) since the description of the temperature and moisture effects has already been accounted for as part of the convection parametrization. Finally, the equation for the precipitation flux can be written as

$$P(z) = \int_z^{top} (G_P - E_P) dz. \quad (3.5)$$

The following paragraphs will describe the parametrization of the individual source and sink terms as originally proposed by Tiedtke (1993).

Convective clouds

Cumulus convection can produce clouds of various types, such as precipitating and non-precipitating cumulus, cumulonimbus clouds, anvils and cirrus “debris”. Here, information generated in the cumulus parametrization scheme is directly used for the formation of both cloud fraction and condensate. The cumulus parametrization used in the ECMWF model is a mass-flux type parametrization (Tiedtke, 1989; Gregory et al., 2000). Condensate formed in parametrized cumulus updraughts is assumed to be a direct source of cloud condensate through the detrainment process due to the deceleration of updraughts as well as turbulent mixing at their sides. The updraught mass is assumed to be cloudy and therefore forms a source for cloud mass in the model grid box. By using the additional assumption that clouds always fill a model layer entirely in the vertical, the amount of cloudy mass in a grid box can be used to estimate horizontal cloud cover. With these assumptions T93 defines the convective cloud sources as

$$S_{cv} = \frac{D_u}{\rho} l_u, \quad (3.6)$$

and

$$S(a)_{cv} = (1 - a) \frac{D_u}{\rho}, \quad (3.7)$$

where D_u is the detrainment of mass from convective updraughts, and l_u is the specific cloud water content in the updraughts. Note that the factor $(1 - a)$ appears since updraughts detrain cloud air simultaneously into clear sky and already existing clouds. It is evident that this factor ensures realistic physical limits at cloud fraction zero and one. An extensive discussion of the source terms represented by equations (3.6) and (3.7) as well as a more rigorous derivation can be found in Section 5.2.

Stratocumulus clouds

Stratocumulus clouds formed at the top of convective boundary layers require special treatment in the scheme, since they are not dealt with by the cumulus parametrization. Following the ideas for convective clouds, T93 attempts to use the mass-flux concept to derive source terms for these clouds. Defining the moisture transport in mass flux terms at cloud base as

$$F_{q,base} = \rho w_* (q_u - q_d), \quad (3.8)$$

one can evaluate the cloud base mass flux as

$$\rho w_* = \frac{F_{q,base}}{q_0 - [a(q_s + l_c)_t + (1 - a)q_t]}, \quad (3.9)$$

where ρw_* is the mass flux, q_u the specific humidity in the updraught part of the boundary layer thermals, and q_d the specific humidity in the downdraughts. The flux of specific humidity at cloud base, $F_{q,base}$, is produced by the boundary layer parametrization, and the subscripts 0 and t refer to a model level close to the surface and close to cloud top respectively. l_c is the in-cloud condensate content, i.e., $l_c = l/a$. With the additional assumptions that the distance between cloud base and cloud top is less than one model layer and that the mass-flux within the cloud reduces linearly from its cloud base value to zero at cloud top, cloud source terms similar to those for convection can be written as

$$S_{bl} = -\frac{1}{\rho} \frac{\partial(\rho w_*)}{\partial z} (l_u - a l_d) \quad (3.10)$$

and

$$S(a)_{bl} = -\frac{1}{\rho} \frac{\partial(\rho w_*)}{\partial z} (1 - a). \quad (3.11)$$

Stratiform clouds

The basic principle used in the parametrization of cloud formation by non-convective processes is that condensation is caused by the lowering of the saturation specific humidity, q_s , due to, e.g., large-scale lifting and/or diabatic cooling by radiation or other physical processes. The condensation rate in saturated air is then equal to the negative of the rate of change of the saturation specific humidity, i.e.,

$$C^* = -\frac{dq_s}{dt}, \quad \frac{dq_s}{dt} < 0. \quad (3.12)$$

The effects of large-scale lifting and diabatic cooling on the saturation specific humidity can be expressed as

$$\frac{dq_s}{dt} = \left(\frac{dq_s}{dp} \right)_{ma} (\omega + gM_c) + \frac{dq_s}{dT} \left(\frac{dT}{dt} \right)_{diab}, \quad (3.13)$$

where $\omega = dp/dt$ is the area-averaged generalized vertical velocity, $(dq_s/dp)_{ma}$ is the change of q_s along a moist adiabat, and $(dT/dt)_{diab}$ is the net tendency of temperature due to all diabatic processes except convection. The effects of convection on dq_s/dt are expressed through a compensating subsidence term, represented by the term gM_c in (3.13).

The cloud source for stratiform clouds can now be written as the sum of two contributions

$$C = C_1 + C_2. \quad (3.14)$$

C_1 represents condensation processes in already existing clouds and is easily derived from (3.12) as

$$C_1 = aC^* = -a \frac{dq_s}{dt}, \quad \frac{dq_s}{dt} < 0. \quad (3.15)$$

C_2 represents the generation of new clouds in the clear-sky part of the grid volume and requires additional assumptions. As discussed in Section 2.2 the existence of clouds on the subgrid scale i) requires some parts of the grid box to be saturated before the grid-mean relative humidity reaches 100 % and therefore ii) implies a distribution of temperature and/or humidity around the grid-mean value. Because of i), a decision needs to be made

when to allow subgrid cloud formation to take place. Here, similar to assumptions in previous cloud parametrizations (e.g., Slingo, 1987), T93 assumes a critical value of relative humidity, below which cloud formation is prohibited. The value used is 80% at 650 mb increasing to 100% when approaching boundary layer and stratosphere. Note, that unlike in previous cloud parametrizations, this threshold does not define the existence of clouds, but only the existence of **one** generation mechanism. Above the critical value of relative humidity the formation of new clouds is assumed to be proportional to the rate of change of saturation specific humidity divided by the grid-mean saturation deficit so that

$$S(a)_C = -(1 - a) \frac{dq_s/dt}{q_s - q}, \quad \frac{dq_s}{dt} < 0. \quad (3.16)$$

Using (3.16) the condensation in the newly formed clouds can be written as

$$C_2 = -\Delta a_c \frac{dq_s}{dt}, \quad \frac{dq_s}{dt} < 0. \quad (3.17)$$

T93 neither provides a thorough derivation of (3.16) nor does he provide a justification of retaining what appears to be a second order term in (3.17) when solving the prognostic condensate equation. Both these issues will be discussed at length in Section 5.3 and physically more consistent source terms will be derived there.

Evaporation of clouds

Evaporation of clouds is assumed to occur by several different processes: i) subsiding motion and diabatic heating, and ii) turbulent mixing of cloud air with unsaturated environment air. Hence,

$$E = E_1 + E_2. \quad (3.18)$$

The first process is an exact reversal of the condensation in already existing cloud for the case of increasing saturation specific humidity and can therefore be described by

$$E_1 = a \frac{dq_s}{dt}, \quad \frac{dq_s}{dt} > 0. \quad (3.19)$$

For simplicity it is assumed throughout the parametrization that the cloud condensate is uniformly distributed in the cloud. With the additional assumption that subsidence and diabatic heating are also uniformly distributed within a model grid box it follows that the

evaporation processes described by E_1 cannot alter the cloud fraction so that the only sink of cloud fraction for these processes is the total dissipation of cloud, whereupon

$$D(a)_1 = \frac{a}{\Delta t}, \quad l \rightarrow 0. \quad (3.20)$$

For the uncertain part of cloud erosion due to turbulent mixing it is assumed that the evaporation is proportional to the saturation deficit of the environment, so that

$$E_2 = aK(q_s - q), \quad (3.21)$$

where K represents an inverse timescale, whose value is chosen to be $10^{-6} s^{-1}$. Requiring that turbulent mixing leaves the in-cloud condensate content, $l_c = l/a$, unaltered one easily derives

$$D(a)_2 = \frac{E_2}{l_c}. \quad (3.22)$$

Precipitation processes

There are two different precipitation generation mechanisms considered in the scheme, i.e.,

$$G_P = G_{P,1} + G_{P,2}. \quad (3.23)$$

In pure ice clouds the generation of precipitation is treated as a sedimentation process of cloud ice:

$$G_{P,1} = \frac{1}{\rho} \frac{\partial}{\partial z} (\rho v_{ice} l). \quad (3.24)$$

The settling velocity v_{ice} is parametrized following Heymsfield and Donner (1990) as

$$v_{ice} = 3.29(\rho l_c^{0.16}). \quad (3.25)$$

Ice falling into cloud in the layer underneath is considered a source of cloud ice for that layer, while ice falling into clear sky is considered to be snow.

In mixed-phase and water clouds the parametrization of generation of precipitation follows Sundqvist (1978) and is written as

$$G_{P,2} = ac_0 l_c \left[1 - e^{-\left(\frac{l_c}{l_{crit}}\right)^2} \right], \quad (3.26)$$

where c_0^{-1} represents a characteristic timescale for the conversion of cloud droplets into rain drops and l_{crit} is a typical cloud water content at which the release of precipitation begins to be efficient. These parameters are adjusted as

$$c_0 = c_0^* F_{col} F_{Berg}, \quad (3.27)$$

and

$$l_{crit} = \frac{l_{crit}^*}{F_{col} F_{Berg}}, \quad (3.28)$$

to crudely take into account the collection of cloud droplets by raindrops falling through clouds (F_{col}) and the Bergeron-Findeisen mechanism (F_{Berg}). F_{col} and F_{Berg} are defined as

$$F_{col} = 1 + b_1 \sqrt{P_{loc}} \quad (3.29)$$

and

$$F_{Berg} = 1 + b_2 \sqrt{T_{BF} - T} \quad \text{if } 253K < T < T_{BF}, \quad (3.30)$$

where P_{loc} is the local precipitation rate and T_{BF} is the temperature at which the Bergeron-Findeisen mechanism is thought to begin enhancing precipitation. The values of the constants are chosen as in Sundqvist (1978) as $T_{BF} = 268K$, $b_1 = 100$, $b_2 = 0.5$, $c_0^* = 10^{-4} s^{-1}$, and $l_{crit}^* = 0.3g \cdot kg^{-1}$.

The evaporation of precipitation is described as

$$E_P = \left[\max(a_P - a, 0) \times 5.44 \times 10^{-4} \right] (q_s - q) \times \left[(\sigma)^{1/2} \frac{1}{5.9 \times 10^{-3}} P_{loc} \right]^{0.577}, \quad (3.31)$$

where $a_P - a$ is the cloud free area in which precipitation can evaporate, and $\sigma = p/p_s$ with p_s representing the surface pressure. The fraction of the grid box covered by precipitation is parametrized as

$$a_{P,k} = \max \left[a_{P,k-1}, \left(\frac{a_k \Delta P_k + a_{P,k-1} P_{k-1}}{P_{k-1} + \Delta P_k} \right) \right], \quad (3.32)$$

where P_{k-1} is the precipitation flux entering model level k from the level above and ΔP_k is the change in precipitation flux due to the generation of precipitation in model level k itself. The role of this parametrization is investigated further in Chapter 6, which discusses in great detail an approach to parametrize cloud and precipitation overlap.

Numerical integration

Cloud processes are rapidly varying in space and time. Since equations (3.1) and (3.2) need to be solved with the normal model timesteps of up to 3600 s (see Section 3.1) care has to be taken in their integration. T93 opted for the analytical integration of both equations. After rewriting the equation for cloud condensate as

$$\frac{\partial l}{\partial t} = A_l - B_l l, \quad (3.33)$$

and that for cloud fraction as

$$\frac{\partial a}{\partial t} = (1 - a)A_a - aB_a \quad (3.34)$$

the solutions to the equations become

$$l(t + \Delta t) = l(t)e^{-B_l \Delta t} + \frac{A_l}{B_l}(1 - e^{-B_l \Delta t}), \quad (3.35)$$

and

$$a(t + \Delta t) = a(t)e^{-(A_a + B_a)\Delta t} + \frac{A_a}{A_a + B_a} [1 - e^{-(A_a + B_a)\Delta t}]. \quad (3.36)$$

Cloud overlap

Both equation (3.1) and (3.2) are solved for each of the discrete model levels (sixty in the currently operational model version). This evidently allows for the variation of both cloud variables with height. Measurements of cloud fraction made from either the surface or at the TOA by satellites often only report the total coverage with cloud for a given area. It is therefore necessary to vertically integrate the cloud fraction information available at each model level assuming a certain form of cloud overlap between model levels to arrive at a total cloud cover that can be compared to observations. More importantly, the calculation of fluxes whose values are affected by the presence of cloud, in particular radiative and precipitation fluxes, also crucially depends on what is commonly known as the ‘‘cloud overlap assumption’’. There are various ways one can overlap the clouds produced at each model level. The three methods commonly used in GCMs are maximum, random, and maximum-random cloud overlap (e.g., Morcrette and Fouquart, 1986; Morcrette and Jakob, 2000). Let TCC_K be the total cloud cover between the model top and model level K , and a_k the cloud fraction at each model level k . The different cloud overlap assumptions can then be expressed as

$$TCC_K = \max_{k=1,K} a_k, \quad (3.37)$$

for maximum overlap;

$$TCC_K = 1 - \prod_{k=1,K} (1 - a_k), \quad (3.38)$$

for random overlap; and

$$TCC_K = 1 - \prod_{k=1,K} \frac{1 - \max(a_k, a_{k-1})}{1 - a_{k-1}}, \quad (3.39)$$

for maximum-random overlap.

Examples for all three overlap assumptions are illustrated in Figure 3.1.

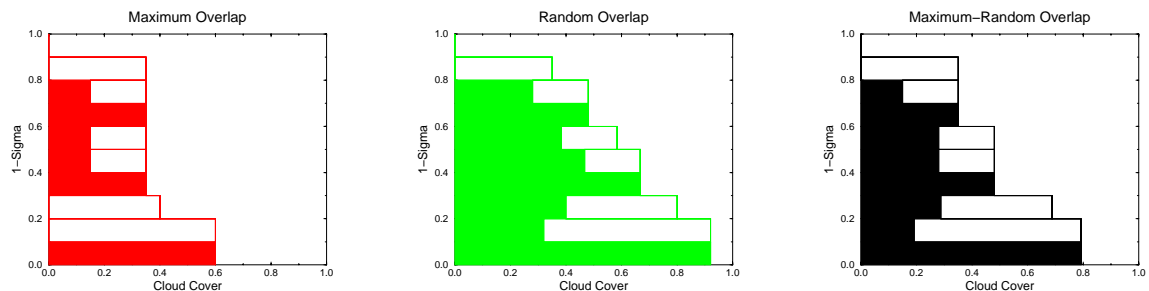


Figure 3.1: Illustration of the maximum (left), random (middle) and maximum-random (right) overlap assumption. White blocks indicate clouds at individual model layers whereas shaded areas indicate the total cloud cover at each layer. This is identical to the area over which any vertical fluxes are affected by cloud.

The figures show a number of model levels covered by clouds (white boxes). In each level the clouds are positioned according to the respective cloud overlap assumption. The shaded areas indicate the total cloud cover, or in other words the total area affected by clouds, at each model level. It is evident that the maximum overlap assumptions minimizes the area affected by clouds, while the random overlap assumption maximizes it. The maximum-random overlap assumption is a blend of the two, assuming maximum overlap for consecutive cloudy levels and random overlap for cloud layers separated by an entirely clear-sky model level. Not surprisingly, this overlap assumption yields areas influenced by clouds whose size is between that of maximum and random overlap. It is the maximum-random overlap assumption that is currently used in the ECMWF model. The effects of the cloud overlap assumption on various aspects of the ECMWF model results have recently been investigated

by Morcrette and Jakob (2000). The role of cloud overlap for precipitation processes will be investigated here in considerable detail in Chapter 6.

3.3 The cloud parametrization in data assimilation

As outlined in the previous section, at the core of the T93 parametrization there are two prognostic equations describing the time evolution of cloud fraction and cloud condensate. Since NWP is an initial value problem, as for any prognostic variable, it is necessary to prescribe initial conditions for the cloud fields. Tiedtke (1993) used the simplest of approaches by initializing the cloud fields to zero everywhere and let the clouds evolve during the course of the model simulation. It is immediately obvious, that this technique will lead to a gradual increase of clouds from zero to their equilibrium value early in the forecast. Note that this “cloud spin up” is a relatively new problem, since for a long time clouds in GCMs (including the ECMWF model) were parametrized diagnostically, implying that their state can always be instantaneously inferred from other atmospheric variables. One of the interesting questions with a prognostic parametrization is how long a time it takes within the forecast to reach the model’s equilibrium cloud fraction.

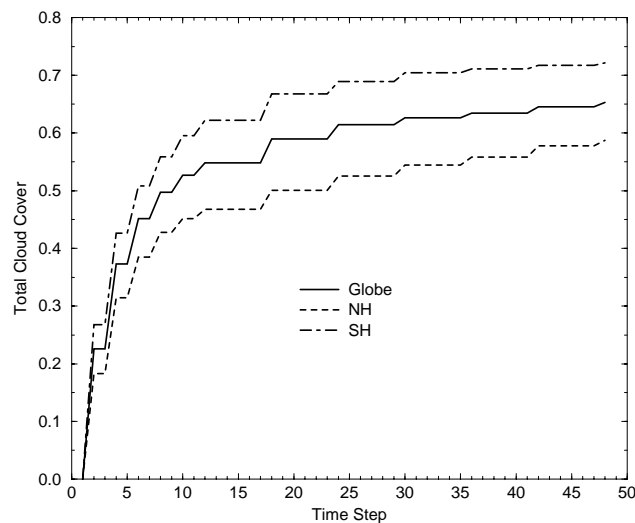


Figure 3.2: Development of global (solid), Northern hemisphere (dashed) and Southern hemisphere (dot-dashed) mean total cloud cover in a 24-hour forecast when starting with zero initial cloud. The length of one timestep is 30 min.

Figure 3.2 shows the time evolution of total cloud cover in a 24-hour forecast (T106L31,

$\Delta t = 30\text{min}$) initialized with zero cloud fields. It is evident that in this example the full development of the global cloud fields requires ten to twelve hours of forecast time. Note that the apparent “jumps” in total cloud cover are due to the fact that the model’s radiation parametrization is only executed hourly in the first 6 hours of the forecasts, and three-hourly thereafter. Since the calculation of total cloud cover (see Equation (3.39)) is linked to that parametrization, the values of this field are only updated in those time intervals. The prognostic cloud equations are still solved for every model timestep to yield new values of cloud fraction and cloud condensate at each model level.

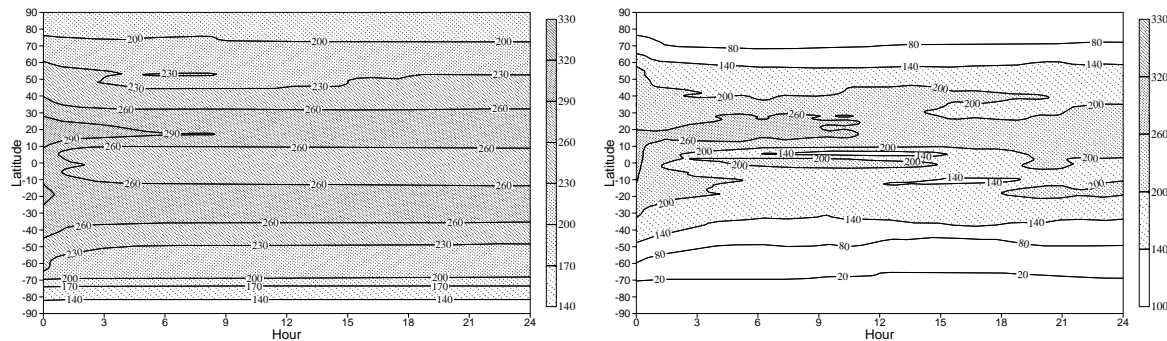


Figure 3.3: Development of zonal mean OLR (left) and TOA shortwave radiation (right) in a 24-hour forecast when starting with zero initial cloud.

One of the main reasons to parametrize clouds is their strong interaction with radiation. It is therefore reasonable to expect that the cloud spin up will lead to a spin up in the radiative fluxes of the model. This is illustrated in Figure 3.3, which shows the time evolution of zonal mean outgoing longwave radiation and net solar radiation at the top of the atmosphere for a forecast that was initialized with zero clouds. The spin up period in the radiative fields is on the order of six to nine hours in some areas. It is worthwhile noting that while only TOA quantities are shown here, the lack of clouds in the early forecast ranges will affect radiation fields at the surface just as strongly, and thereby modify the low-level temperature structure in particular over the land areas. Although the spin up effects outlined above might be acceptable for medium-range (five to ten days) forecasts, shorter forecast ranges (up to 24 hours) will certainly be affected by the “cloud spin up”. This is particularly critical for the data assimilation systems used to provide the model initial states.

Various data assimilation techniques have been in use at ECMWF over the past five years. They include an Optimum Interpolation (OI) system as used for ECMWF’s reanalysis project (Gibson et al., 1997), a three-dimensional variational data assimilation system (3DVAR,

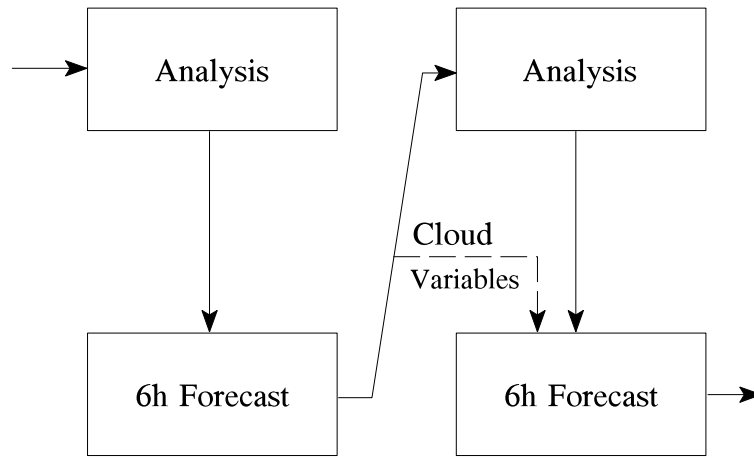


Figure 3.4: Treatment of the prognostic cloud variables in the data assimilation system.

Courtier et al., 1998; Rabier et al., 1998; Andersson et al., 1998) and the currently operational four-dimensional variational data assimilation system (4DVAR, Rabier et al., 2000; Mahfouf and Rabier, 2000; Klinker et al., 2000). The details of the different systems can be found in the appropriate references and a general overview over data assimilation techniques is given in the textbook of Daley (1991). The important feature that all techniques have in common is that they perform a very short-range forecast (typically six hours), which is usually referred to as the “first-guess” forecast, and then use a variety of observations to correct the results of this forecast in a statistically optimal way. The result of this correction is referred to as analysis and provides the initial conditions for the next first guess or in fact the medium-range forecast. This basic idea of “cycling” in data assimilation systems is illustrated in Figure 3.4. Note that the flow diagram in this figure is strictly only valid for OI and 3DVAR systems, the following discussion on the inclusion of clouds does however also hold for the more recent 4DVAR system.

Because of the very short forecast range of six hours and therefore the frequent re-initialization of the forecast model, it is the data assimilation system that is most vulnerable to cloud spin up effects as described above. As shown in Figures 3.2 and 3.3 the model clouds never reach their full extent in a six-hour forecast. Only few methods to initialize cloud variables within data assimilation systems have been proposed (e.g., Huang and Sundqvist 1993), and none of them has been applied in a global system. The method proposed here and adopted by ECMWF is indicated in Figure 3.4. At the end of a first guess forecast the two cloud variables are separated from the other prognostic model variables. Then the analysis is performed and all prognostic model variables except the cloud variables are adjusted using

observations. The unchanged cloud variables are then joined with the other, now modified, model variables and reintroduced into the system as initial conditions for the next first guess forecast.

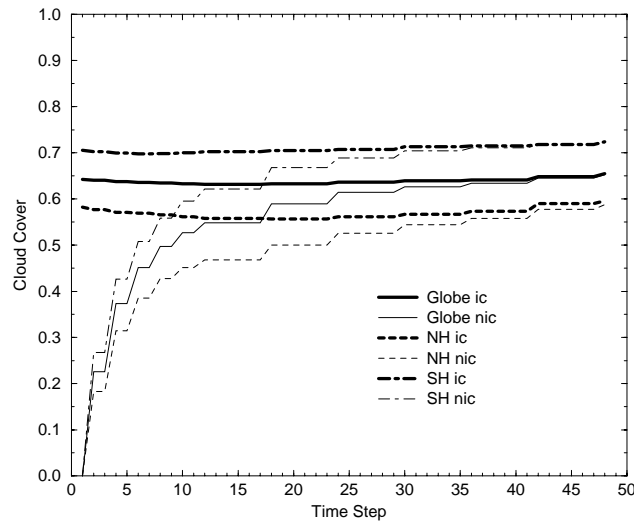


Figure 3.5: Development of global (solid), Northern hemisphere (dashed) and Southern hemisphere (dot-dashed) mean total cloud cover in a 24-hour forecast when starting with (thick lines, ic) and without (thin lines, nic) initial cloud. The length of one timestep is 30 min.

Although extremely simple, this method has proved sufficient to remove the spin up problems identified above. This is evident in Figures 3.5 and 3.6. Figure 3.5 shows the evolution of total cloud cover for the same areas as in Figure 3.2. No obvious spin up in those variables is detectable. For reference the plot also contains the curves from Figure 3.2 for the forecast started with zero initial clouds. Figure 3.6 shows the results for OLR and TOA shortwave radiation from the same forecast as in Figure 3.3, but this time started using initial clouds derived by the technique explained above. Also here, no spin up is evident.

One of the interesting questions when studying the cloud spin up is in what way the entire forecast system would be affected if no initial cloud information was available at the beginning of each first guess forecast. This has recently been studied by Mahfouf et al. (1999). They performed a week long data assimilation experiment with no initial cloud (Nocli) and carried out ten-day forecasts for each of the seven analyzed days. The results of this experiment were then compared to a control experiment in which the technique described here is used to determine non-zero initial conditions for the cloud variables.

Figure 3.7 shows the mean temperature error in the tropics (defined as the latitude belt

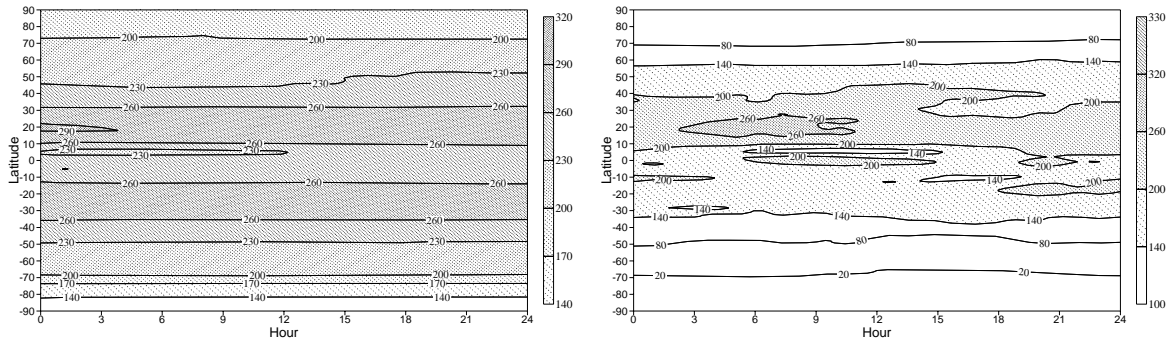


Figure 3.6: Development of zonal mean OLR and TOA shortwave radiation in a 24-hour forecast when starting with initial cloud determined as described in the text.

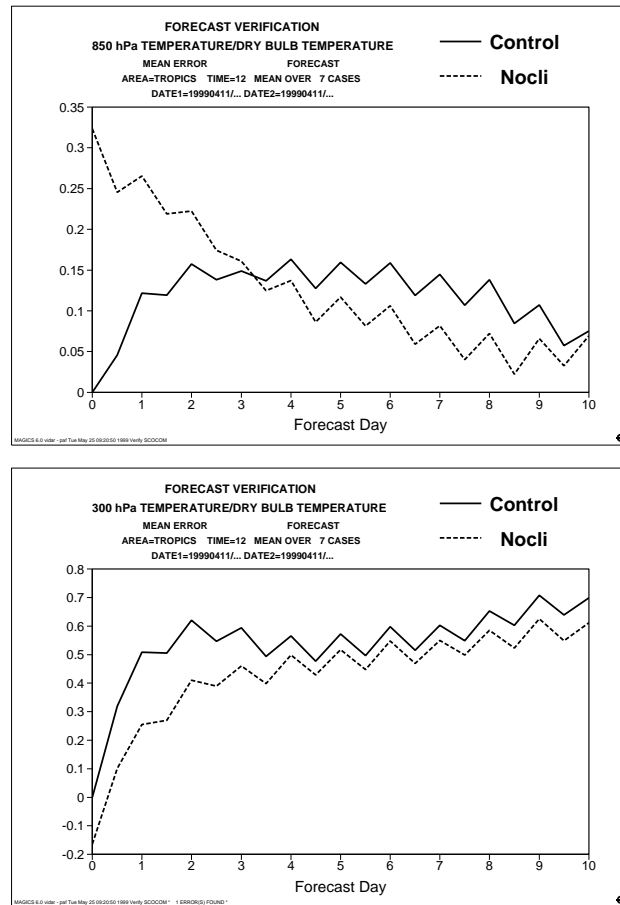


Figure 3.7: Mean tropical temperature error at 850 hPa (top) and 300 hPa (bottom) averaged over seven forecasts carried out with an assimilation and forecasting system that uses non-zero (Control) and zero (Nocli) initial cloud values.

from $20^{\circ}N$ to $20^{\circ}S$) at 850 hPa (top) and 300 hPa (bottom) as a function of forecast day. The results are averaged over the seven forecasts performed with the control system, i.e. with initial clouds (solid), and the Nocli system (dashed). Both systems are compared to

the analysis performed with the Control system. The initial temperature “error” of the Nocli system is therefore indicative of the temperature difference between the two analysis systems that has evolved purely from not using initial cloud information in one system. It is worthwhile noting that the existence of a difference in temperature error near the end of the forecasts, although small, indicates that even the model results far away from the initial conditions remain affected by them, an indication for the complexity of the model response to the changed initial conditions. The sign of the differences in temperature error is consistent with the radiative cloud effects described in Chapter 2. In the lower troposphere the absence of clouds leads to a reduction in atmospheric cooling and hence higher temperatures whereas in the upper troposphere the warming by clouds is reduced and hence lower temperatures occur in the Nocli system.

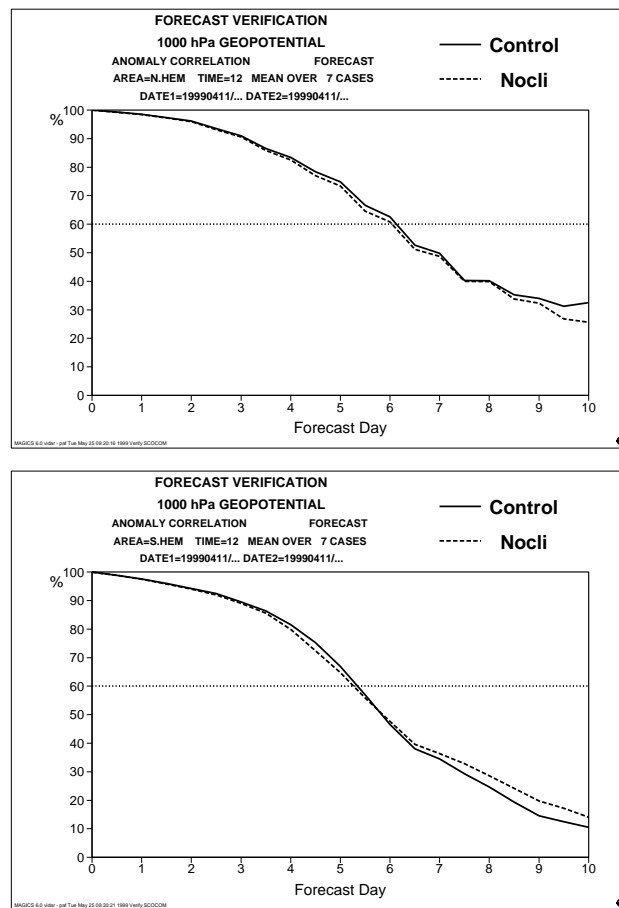


Figure 3.8: Anomaly correlation at 1000 hPa in the Northern (top) and Southern (bottom) hemisphere averaged over seven forecasts carried out with an assimilation and forecasting system that uses non-zero (Control) and zero (Nocli) initial cloud values.

More traditional forecast scores, such as the 1000 hPa anomaly correlation, show smaller, but still visible impacts of the treatment of initial cloudiness. Figure 3.8 shows this score for

both Northern (top) and Southern (bottom) hemisphere. A slight deterioration in forecast skill in the Noctis system is evident, although it would require a much longer data assimilation experiment to establish the statistical significance of this result.

It is worthwhile noting, that by applying the technique described here, ECMWF is the only forecasting centre that includes a method for the determination of initial clouds for a global forecast model. The ultimate aim is of course to fully include clouds into the data assimilation, i.e., to use cloud observations to modify the model clouds as is done for any other model variable now. Work in this area has only begun (e.g., Mahfouf et al., 1999) but it is an exciting prospect to combine a-priori information in form of a short-range forecast with measurements sensitive to clouds such as satellite radiances, to produce a full three-dimensional analysis of the state of global cloudiness. The currently used variational data assimilation techniques provide a useful framework for studies of this kind.

Chapter 4

Cloud fraction in the ECMWF reanalysis

4.1 Introduction

The cloud scheme described in the previous chapter constitutes a novel approach to the problem of cloud parametrization in large-scale models. In particular the use of a prognostic equation for cloud fraction has never been attempted before. It is therefore natural to evaluate the performance of the cloud fraction scheme, in particular, in as many ways as possible. This chapter together with Chapter 7 will demonstrate the use of different data sources and forecast products for this purpose.

Data assimilation systems run at operational NWP centres can be considered an ideal testbed for cloud parametrizations. As described in the previous chapter, short-range forecasts performed with the numerical model are corrected by introducing observations in a statistically optimal way. Therefore, in contrast to long-term climate simulations, the general circulation of the model atmosphere is to a large extent controlled by observations. As a consequence the model cloud parametrization is forced by the “best possible” large-scale flow and errors found in the cloud parameters can more readily be ascribed to shortcomings in the parametrization. A prerequisite for a successful comparison using short-range forecasts is however a negligible model spin up in the cloud variables. A technique to ensure small spin up has been described in Chapter 3 and has been applied in the data assimilation system used here.

Several Climate and NWP centres have carried out projects to reanalyse the state of the atmosphere for a considerable period of time with a data assimilation system that remains fixed over the whole analysis period (Schubert et al., 1993; Kalnay et al., 1996; Gibson et al., 1997). The main advantage over analyses produced operationally is the consistency in

the analysis system when creating a long-term data set.

ECMWF has carried out a reanalysis for the period 1979-1993 (Gibson et al., 1997) using an analysis and forecasting system similar to the one that was operational for most of 1995. The T93 prognostic cloud scheme was an integral part of that system. Since no observational data is used in the analysis to directly alter the cloud, a comparison of the cloud fraction simulated in the analysis system to those observed is a stringent test of the realism of the cloud parametrization.

This chapter provides a general overview over the quality of the representation of cloud cover in the ECMWF reanalysis (ERA) by comparing the ERA results with satellite observations provided by the International Satellite Cloud Climatology Project (ISCCP) (Rossow and Schiffer, 1983). The main emphasis is on time scales of longer than a month. The main goal of the comparison is to identify major problem areas for the cloud representation. Because of the chosen time scales the comparison cannot reveal erroneous details of the parameterization which need to be investigated in detailed process studies. With the method adopted in Section 3.3 to determine the initial values for the cloud parameters, spin-up problems have been shown to be negligible, so that short-range forecasts of cloud cover can be used in the comparison.

After providing an overview over the data used the main results of the comparison are presented in section 4.3 followed by a discussion. The main content of this chapter has been published in an article by Jakob (1999) in the Journal of Climate.

4.2 Data

4.2.1 ISCCP

ISCCP uses radiances measured by operational weather satellites to deduce a variety of cloud properties. Two channels, $0.6 \mu m$ and $11 \mu m$, common to both the geostationary and polar-orbiting satellites are used. A detailed description of the algorithms is given in Rossow and Garder (1993a). From the initial interpretation of the instantaneous radiance fields a variety of different products with varying spatial and temporal resolution are derived (Rossow and Schiffer, 1991). In this study the monthly mean cloud cover as provided in the ISCCP-C2 data set for the months from July 1983 to December 1990 at a horizontal resolution of 2.5° by 2.5° is used.

4.2.2 ERA

For the comparison to the satellite data a monthly mean data set of total cloud cover has been created from the ERA at the same horizontal resolution as ISCCP. Total cloud cover is calculated from the cloud cover predicted for each of the model levels by integrating from the model top using the maximum-random overlap assumption (see Section 3.2; Morcrette and Fouquart, 1986). As shown in Section 3.3 there is no noticeable spin-up in total cloud cover in the assimilation system. Therefore results of the six hour first guess forecasts have been used for the comparison, in order to have the best possible representation of the large-scale flow.

4.3 Results

4.3.1 Global mean

Table 4.1 shows the average cloud cover for July 1983 to December 1990 for the whole globe and separated into Northern hemisphere (NH) ($90^{\circ}N$ to $20^{\circ}N$), Southern hemisphere (SH) ($20^{\circ}S$ to $90^{\circ}S$), and tropics ($20^{\circ}N$ to $20^{\circ}S$). The data sets included are the ISCCP-C2 data, ERA and the operational analysis for which the averaging period is from 1987 to 1990.

	ISCCP	ERA	OPS
Globe	63.1	62.3	53.4
NH	59.3	57.3	52.6
SH	68.7	66.4	53.9
Tropics	61.2	63.2	53.8

Table 4.1: Area and time-averaged cloud cover for ISCCP, ERA and OPS. (*Note that the averaging period for OPS is only from 1987 to 1990*).

The ERA shows very good agreement with the observations with a slight underestimation of global cloudiness mainly resulting from an underestimation of cloud cover in the extratropics; the tropical cloud cover is slightly overestimated. The difference in cloud cover between Northern and Southern hemisphere is also very well simulated. As a reference the values as given by the operational 24-hour forecasts (OPS) from 1987 to 1990 are included in the table. The then operational diagnostic cloud scheme (Slingo, 1987) strongly underestimated cloud cover in all areas and showed no large hemispheric difference.

Figure 4.1 shows the temporal evolution of the global cloud cover. Again the correspondence between ERA and ISCCP is striking. The interannual variability in cloud cover is well

simulated with maxima in 1984 and 1985. However, the ERA cloudiness exhibits a strong annual cycle which is not supported by the observations. The cloudiness in the 1987-1990 operational system shows an even larger annual signal and a strong underestimation of cloudiness. There is a marked increase in cloudiness in the end of the period, which is related to a change to the cloud parametrization in the operational model in 1990. One of the purposes of the reanalysis projects was to eliminate such discontinuities arising from model/assimilation system changes.

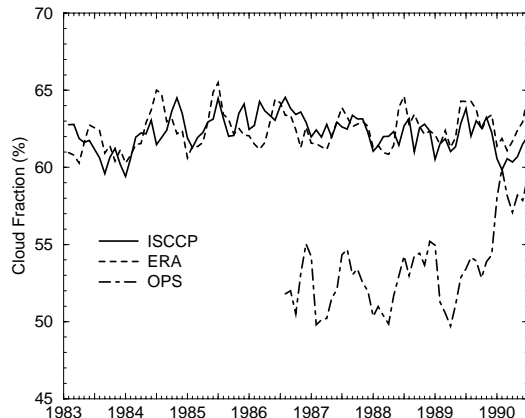


Figure 4.1: Time series of global mean cloud cover from July 1983 to December 1990 for ERA (solid), ISCCP C2 (dashed) and ECMWF operational 24h-forecasts (dot-dashed).

4.3.2 Zonal Means

Figure 4.2 shows the zonal distribution of cloudiness averaged over the entire period. The first three panels show the annual, July and January averages. There is fairly good agreement in the tropics and subtropics, but the extratropical cloud cover between 30° and 60° is underestimated in both hemispheres with an overestimation poleward of 60° . The significance of the differences poleward of 60° is difficult to assess due to difficulties in the ISCCP cloud detection over snow and ice (Rossow and Garder 1993b). Further discussion is therefore concentrated on the areas between $60^\circ N$ and $60^\circ S$.

The fourth panel of Figure 4.2 shows the difference in zonal mean cloud cover between July and January as an estimate of the annual cycle of cloudiness. There is good agreement between ERA and observations except for the NH extratropics, where a summer maximum in cloud cover is not simulated by the analysis. This will be investigated in the next subsection.

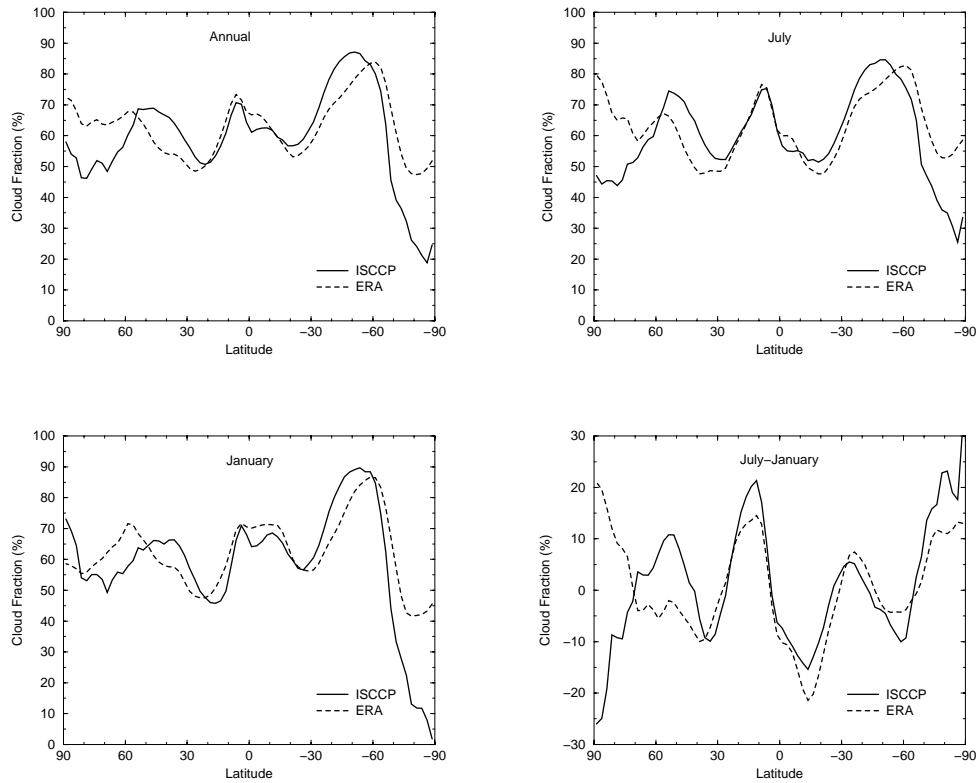


Figure 4.2: Zonal mean cloud cover for ISCCP and ERA averaged from 1983 to 1990 - Annual (top left) , July (top right), January (bottom left), and July minus January (bottom right).

Figure 4.3 shows the time evolution of zonal mean cloud cover for both ISCCP and ERA. The general distribution of clouds, with high cloud cover in both the tropical and extratropical belts and low cloud cover in the subtropics is well captured in the ERA. The month by month variation in cloud cover in the tropics which is governed by variations in the location of the Intertropical Convergence Zone (ITCZ) is very well represented, although the overall level of cloud cover is higher than observed. Some interannual variations such as the maximum in cloud cover around $10^{\circ}S$ in winter 1986/1987, are well captured, although the ERA shows a similar maximum in 1989/1990 which is not present in the observations. Subtropical cloudiness appears to be underestimated; seasonal variations are however well described with minima in the respective winter season. Extratropical cloudiness is strongly underestimated especially in the bands between 40° and $50^{\circ}N/S$. The annual migration of maximum values of cloudiness from $40^{\circ}N$ in late winter to $50^{\circ}N$ in summer, which is an annually recurring feature in the Northern hemisphere is not captured at all in the ERA which instead shows cloud cover maxima at around $55^{\circ}N$ in autumn.

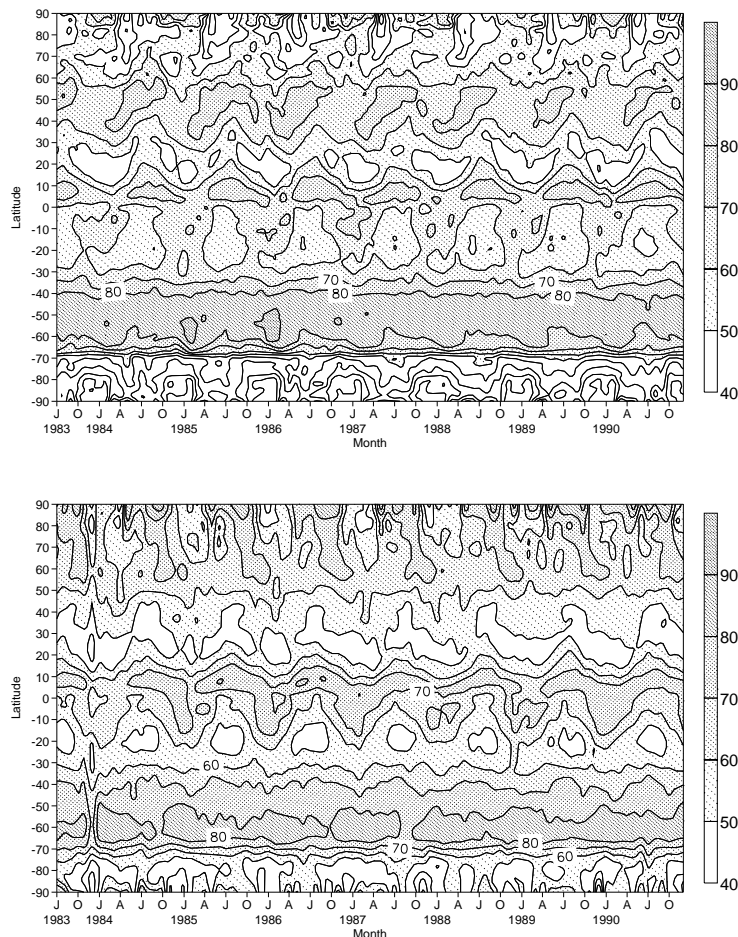


Figure 4.3: Time evolution of monthly averaged zonal mean cloud cover for ISCCP (top panel) and ERA (bottom panel).

4.3.3 Selected Areas

To assess the geographic distribution of the cloud cover differences the spatial distribution of cloud cover averaged over the entire period of the study is shown in Figure 4.4. The top two panels show the average cloud cover for ISCCP and ERA respectively whereas the bottom panel shows the difference of ERA minus ISCCP. The general spatial patterns agree reasonably well. The underestimation of extratropical cloud cover noted already in the zonal mean figures is quite evident with the largest errors occurring over the oceans. The good agreement of zonal mean cloud cover in the subtropics is due to a cancellation of errors, with an underestimation of the cloudiness in the stratocumulus areas off the west coasts of the subtropical continents and an overestimation in the trade cumulus areas. Tropical cloudiness is generally well represented with a slight overestimation over Africa and the Maritime continent.

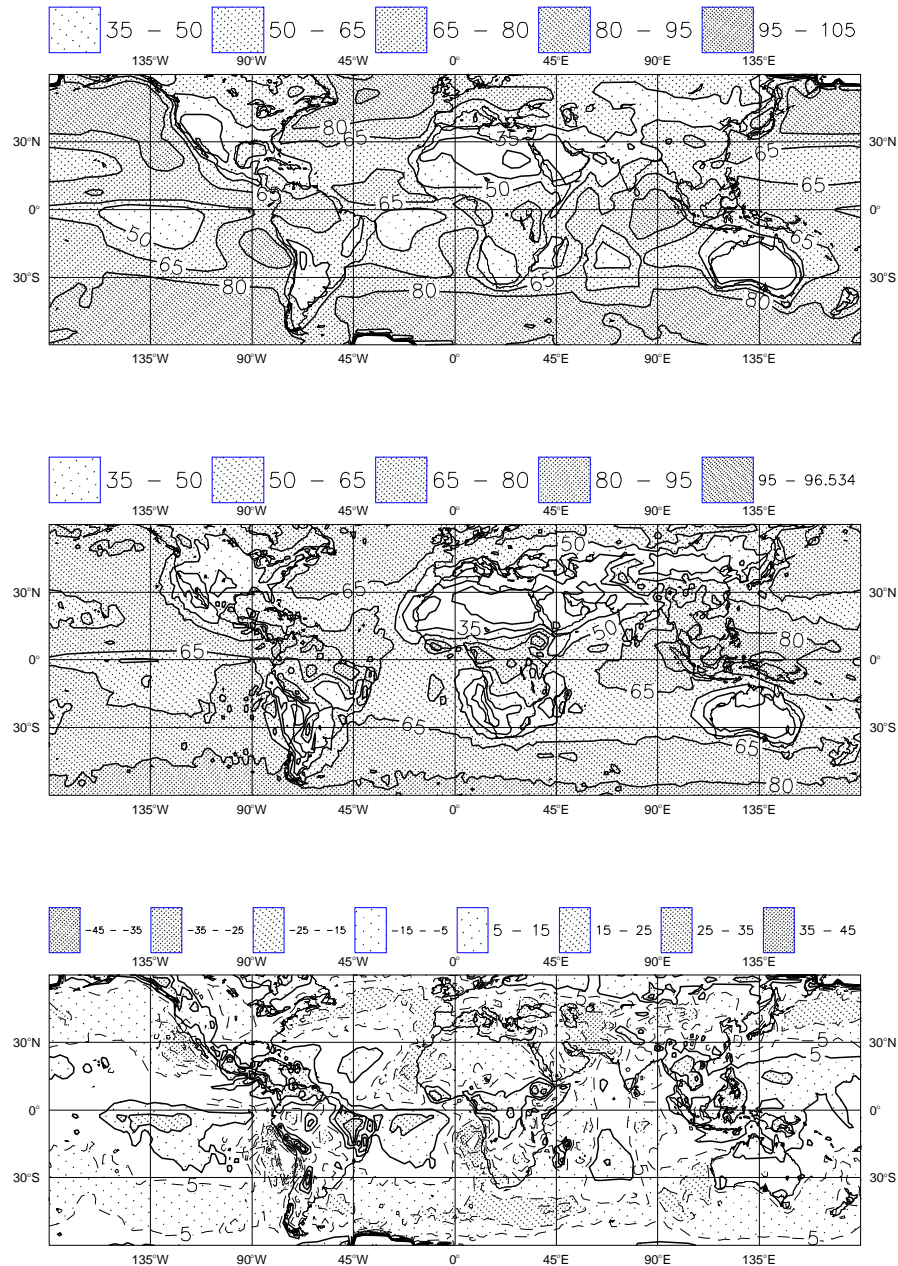


Figure 4.4: Annual mean of total cloud cover averaged from July 1983 to December 1990 for ISCCP (top), ERA (middle) and ERA minus ISCCP (bottom). Positive differences are depicted by thick solid lines and negative by thin dashed lines.

To investigate the spatial and temporal evolution of different climatological cloud regimes Hovmoeller diagrams of the mean annual cycle of cloud cover for selected latitude bands are presented. The averaging period is 1984 to 1990. Cloud cover is averaged over a 10° latitude band and the annual cycle is plotted as a function of longitude. The areas chosen are $50^\circ N$ to $40^\circ N$ representing extratropical cloudiness, $30^\circ N$ to $20^\circ N$ as an example for subtropical

cloud regimes and $10^{\circ}N$ to $0^{\circ}N$ as a tropical area.

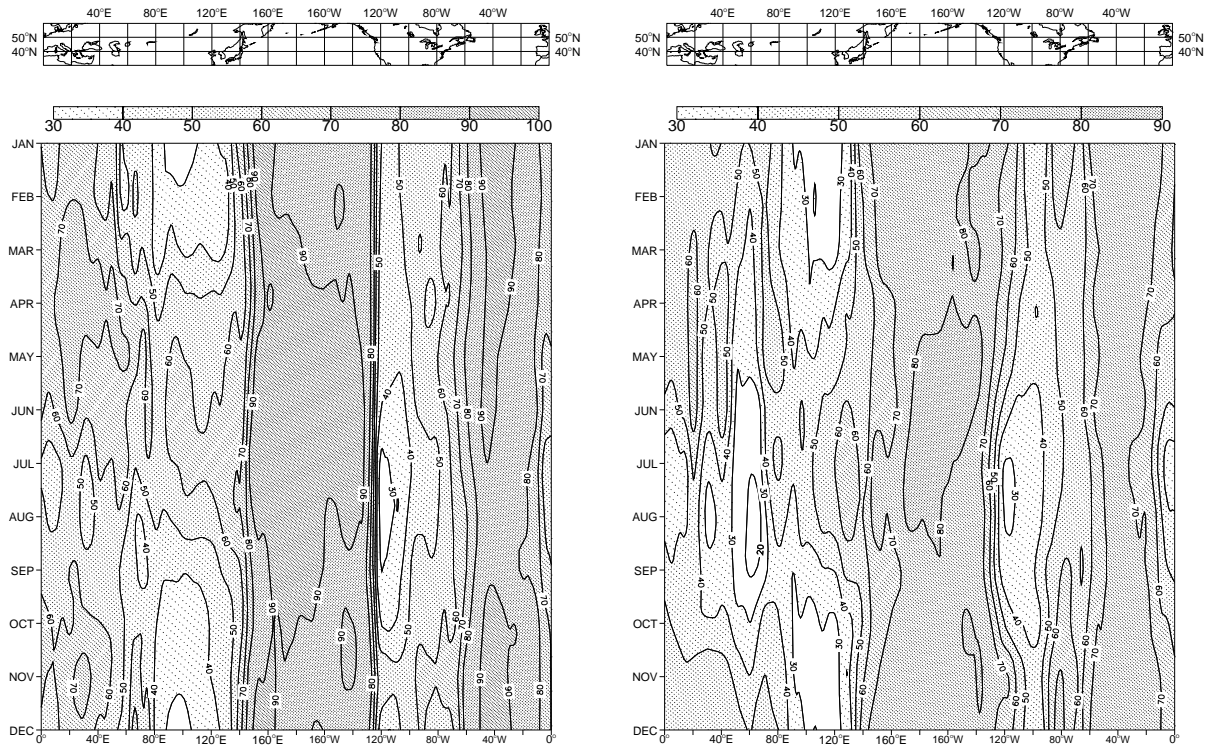


Figure 4.5: Mean annual cycle of cloud cover for ISCCP (left) and ERA (right) averaged over 40° to $50^{\circ}N$ for the years 1984 to 1990.

Extratropics

Figure 4.5 shows the evolution of cloud cover in the latitude band $50^{\circ}N$ to $40^{\circ}N$ for both ISCCP and ERA. The most pronounced feature of the cloudiness at those latitudes is the strong land-sea contrast with continuous cloud cover above 70 % over the oceans and considerably lower values over land. There are particularly sharp gradients on the west coast of North America and on the west coast of the Eurasian continent, especially in summer. The land-sea contrast in general is well captured by the ERA although the gradients appear to be weaker mainly due to a general underestimation of cloud cover over the oceans by more than 10 % which is further enhanced off the coast of North America in summer and autumn. In the ISCCP there is a pronounced annual cycle in cloudiness over the Pacific with a maximum in summer. This is mainly due to the annual cycle of low stratus clouds (Klein and Hartmann 1993) and is well captured by the ERA. Over the Atlantic the maximum cloud cover occurs in winter. In this region the low stratiform clouds exhibit their summer maximum further north (Klein and Hartmann 1993) so the influence of baroclinic

developments, which peak in winter, dominates the annual cycle. Over Western Europe the ERA generally underestimates cloud cover by more than 15%, but reproduces well the pronounced annual cycle with a cloud cover minimum in late summer. Over central Eurasia there exists a very strong annual cycle with a distinct summer maximum in the observations. Although ERA captures the low winter cloud amounts in this region very well, the summer maximum is underestimated by up to 20%. This behaviour could be explained by a lack of convective clouds over land in summer, which form the bulk of the cloudiness for those regions. This may include both fair-weather shallow cumuli and deep convective systems. Over the North American continent the predicted cloud cover matches the observed better although the winter maximum over the eastern part of the region is stronger in the ERA than in ISCCP. Care has to be taken in the interpretation of these differences because of the difficulties in the detection of clouds over snow covered areas in ISCCP. Revised ISCCP data sets that are currently being produced (Rossow et al. 1996; Rossow and Schiffer, 1999) will include better estimates of cloudiness over snow.

Subtropics

Figure 4.6 shows the same quantities as Figure 4.5 but for the latitude band $30^{\circ}N$ to $20^{\circ}N$. Those latitudes are dominated by stratocumulus and trade wind cumulus regimes over the oceans, but features like the Indian summer monsoon are also apparent in the observations. Two major deficiencies in the ERA cloudiness are immediately evident. First of all the trade cumulus regime cloud cover that dominates in summer over both the Pacific and the Atlantic ocean is overestimated by about 10 to 15 %. However, the very pronounced continuously large cloud cover off the North American continent, representing mainly stratocumulus clouds, is underestimated in the ERA by about 15 %. The cloudiness connected to the Indian summer monsoon is very well simulated with a 10 % overestimation of the peak values.

Tropics

Figure 4.7 shows the tropical cloud cover evolution averaged over 0° to $10^{\circ}N$ latitude. This region is dominated by the ITCZ for most of the year. Regions of special interest are the Western Pacific warm pool, the Eastern Pacific and the African Continent. The Western Pacific region is characterized by large cloud amounts throughout the year which ERA generally overestimates by 10 to 15 %.

The Eastern Pacific off the coast of South America is characterized by a strong annual

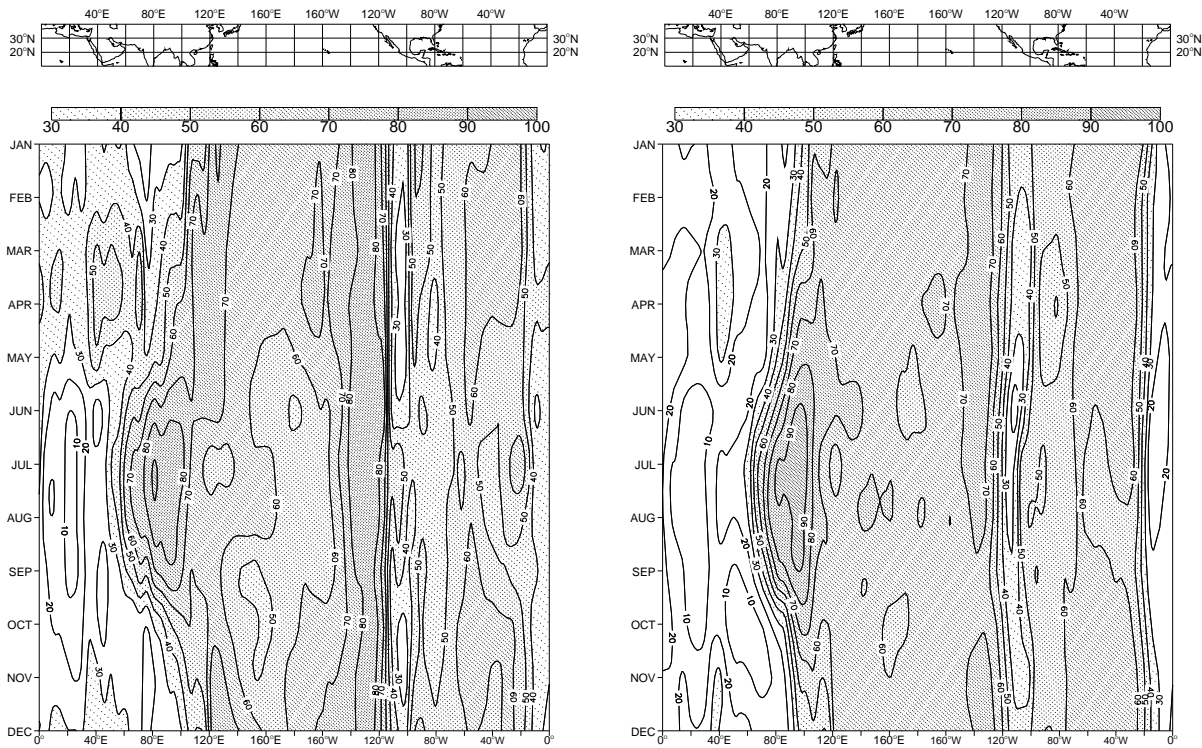


Figure 4.6: Mean annual cycle of cloud cover for ISCCP (left) and ERA (right) averaged over 20° to 30° N for the years 1984 to 1990.

cycle with a marked late summer maximum. Over the continent the annual cycle is of opposite phase with the cloudiness maximum occurring in winter and spring. This leads to a pronounced dipole structure of cloudiness between land and sea which is most likely caused by annually recurring changes in the Walker circulation. ERA generally captures this dipole structure and the phase of the annual cycles both over land and sea. There is however a general overestimation by 10 % of the cloudiness minima.

Over the African continent the signal is dominated by the movement of the ITCZ in and out of the region. In Summer there is a pronounced maximum in the observations which is reasonably well captured. Cloud cover over the central part of the continent is however overestimated, pointing to too intense convection over land. This is confirmed by a study by Stendel and Arpe (1997) who found an overestimation of precipitation in the ERA over tropical land.

Interannual variability

It has been shown so far that the ERA system captures many of the important annual variations in cloud cover. In order to investigate whether the system is also able to capture

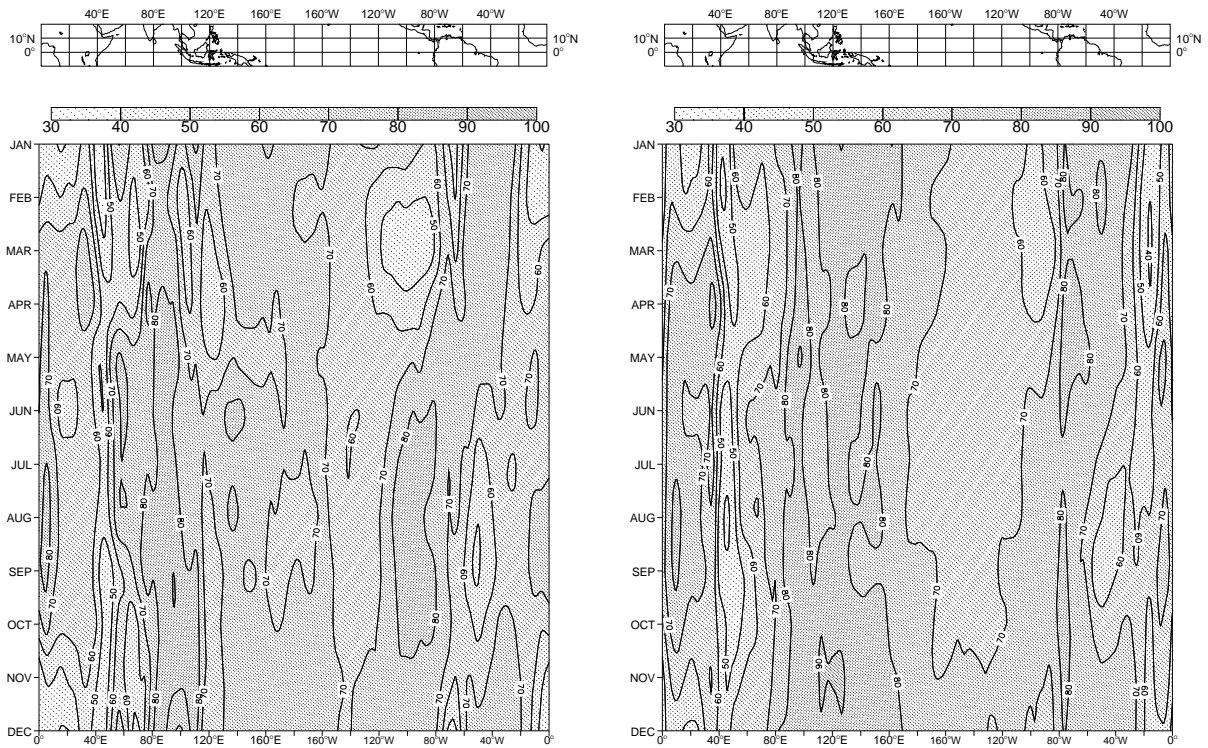


Figure 4.7: Mean annual cycle of cloud cover for ISCCP (left) and ERA (right) averaged over 0° to $10^{\circ}N$ for the years 1984 to 1990.

some of the observed interannual variability Figure 4.8 shows the evolution of the annual mean cloud cover in the latitude band $0^{\circ}N$ to $10^{\circ}N$ from 1984 to 1990. The strongest interannual signal in the tropics is that of the El Niño phenomenon. A moderate El Niño event occurred in 1987 and is clearly visible in the ISCCP observations. The cloud cover maximum normally located in the Western Pacific ocean follows the eastward shift in maximum sea surface temperature (SST) to the dateline. The cloud cover in the Eastern Pacific is enhanced. This is followed by a cloud cover minimum near the dateline in the following year characterized by cold SST's in the region. Although generally overestimating cloud cover over the Western Pacific the ERA captures both the shift of the cloud cover maximum and the minimum in 1988 indicating that the parametrization schemes that influence the simulation of cloud cover, most prominently the cloud and convection parametrizations, are able to respond reasonably to the SST forcing.

An interesting feature in Figure 4.8 is the continuous reduction in cloud cover over the African continent in ERA. This trend has also been noticed in precipitation by Stendel and Arpe (1997). Its reason is unknown since there are no obvious trends in data availability in that region.

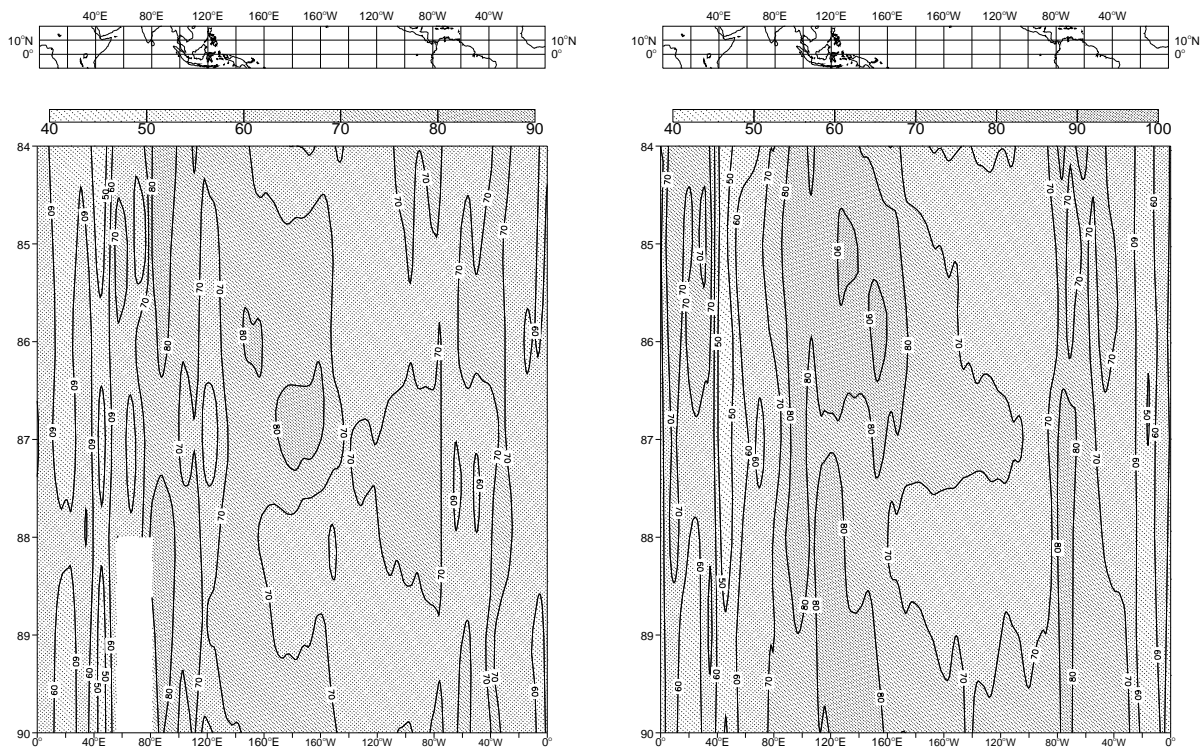


Figure 4.8: Time evolution of annual mean cloud cover for ISCCP (left) and ERA (right) averaged over 0° to $10^{\circ}N$ for the years 1984 to 1990.

4.4 Summary and discussion

The chapter compared the representation of cloud cover in the ECMWF reanalysis on time scales of months and longer against data from ISCCP for the years 1983 to 1990. The main purpose was to identify general areas of deficiencies in the cloud cover parametrization. The use of a data assimilation system in the assessment of a parametrization scheme is clearly superior to a long climate simulation because of the better representation of the large-scale conditions.

The representation of cloud cover in the prognostic cloud scheme used in the ERA is a great improvement compared to the diagnostic scheme that was still operationally used when the reanalysis project went into its production phase. There are however several areas of erroneous simulation of cloud cover even on long time scales. The major deficiencies are:

- an underestimation of extratropical cloud cover over the oceans by 10 to 15 %
- an overestimation of trade wind cumulus cover by about 10 to 15 %
- an underestimation of stratocumulus off the west coasts of the subtropical continents

by 15 %

- an underestimation of the summer maximum in cloud cover over the Eurasian continent

The comparison presented here cannot reveal the detailed reasons for the problems identified. However, it points strongly to the cloud regimes that require further research with detailed process studies (e.g., single column simulations).

One of the most likely applications of a reanalysis is the use of its surface winds and fluxes to drive ocean models. Of major importance hereby are the radiative fluxes. Although cloud cover is not the only influence, its erroneous representation will contribute strongly to errors in surface radiation. This has been confirmed by Kållberg (personal communication) for the ERA who found a strong underestimation of the solar radiation at the surface in the trade wind regions and an overestimation in the stratocumulus areas, in line with the cloud cover errors found here. Furthermore the trend in cloud cover over continental Africa pointed out in section 4.3 has also been identified in the precipitation fields by Stendel and Arpe (1997). These are examples of studies for which the results presented here can be of importance when interpreting the findings.

Chapter 5

The parametrization of cloud generation

5.1 Introduction

One of the main weaknesses of the parametrization of Tiedtke (1993) is the ad hoc way of formulating some of the source terms, in particular in the equation that describes the time evolution of cloud fraction. The main purpose of this chapter is to more rigorously derive source terms for cloud production, both from convective and non-convective processes, and thereby to give some insight in the working of the cloud parametrization with a view to future improvements. Section 5.2 will deal with the coupling of cloud and convection scheme, while Section 5.3 will look into ways to derive terms for non-convective cloud sources. The chapter closes with a brief discussion on the use of the concepts derived here for the parametrization of cloud decay.

5.2 The generation of convective clouds

One of the most important mechanisms of cloud formation is that of moist convection. Convective clouds appear in several forms such as precipitating and non-precipitating cumuli, cumulonimbi and anvil clouds. Together these clouds cover large parts of the globe (Warren et al., 1986; Warren et al., 1988). It has been recognized that the treatment of these cloud types has to form an important part of any cloud parametrization. Del Genio and Yao (1990) for instance found that treating cloud water produced in convective updraughts as source for stratiform clouds increases the cloud liquid water path in the Tropics by a factor of 3 to 4. In the experiments performed by Tiedtke (1993) about two thirds of the generation of cloud condensate is achieved by convective processes.

Most cloud schemes include a special treatment of convective clouds in some way. This treatment is complicated by the fact that the convective processes themselves are not resolved in GCMs and therefore need to be parametrized. The task of representing convective clouds is therefore that of finding a link between the convection parametrization and that of cloud processes. In diagnostic schemes (e.g., Slingo, 1987) this link is frequently achieved by diagnosing cloud fraction as a function of convective precipitation or the condensation rate in convective updraughts. A more recent approach taken in the schemes solving a prognostic equation for the condensate is to treat water substance detrained from convective updraughts as a source of liquid water for the 'stratiform' clouds. The exact nature of the link depends on the definition of 'detrainment' and can vary for different schemes. Del Genio et al. (1996) for instance treat all water that is condensed above 550 hPa in convective updraughts as source for cloud water. Other schemes (e.g., Ose, 1993; Tiedtke, 1993; Roeckner, 1995; Fowler et al., 1996) use the detrainment of water that is explicitly calculated by the convection schemes applied in the respective GCMs, which are all based on the representation of convection by so called mass-flux schemes (e.g., Arakawa and Schubert, 1974; Tiedtke, 1989). In those cloud schemes any detrained water is just added to the already existing cloud water in the grid box. In the fully prognostic scheme of Tiedtke (1993) the cloud fraction is also linked to the convection scheme through the detrainment of mass whereas all the other schemes treat cloud fraction in a diagnostic way. With the exception of Tiedtke (1993) the actual source terms used in the schemes are only mentioned verbally and no derivation is given even in Tiedtke (1993). Randall (1995) for the first time attempts to actually derive convective source terms of cloud water/ice and cloud fraction based on mass and water conservation arguments for a single model layer. The terms derived by him appear to be very similar to those of Tiedtke (1993).

It is the purpose of this section to derive source terms for both cloud condensate and cloud fraction that can be used in cloud schemes that treat one or both of these quantities with prognostic equations. A prerequisite for the derivation is that the convection parametrization is based on the mass-flux concept. The mass-flux convection scheme developed by Tiedtke (1989) will serve as an example here. However, the derivations made are easily applicable to other mass-flux schemes. After briefly introducing the main ideas of the mass-flux treatment of convection, source terms for both cloud condensate and cloud fraction will be derived. It will be shown that there is a unique and unambiguous way of to achieve the link between mass-flux convection and cloud scheme.

5.2.1 The mass-flux concept

Before deriving the source terms from convection for cloud condensate and cloud fraction it is necessary to review the basic ideas of the mass-flux concept as they are applied in many convection parametrization schemes today (e.g., Arakawa and Schubert, 1974; Tiedtke, 1989; Gregory and Rowntree, 1990).

A generic conservation equation for a scalar Ψ in an incompressible fluid averaged over a model grid volume can be written as (e.g. Stull, 1988, Tiedtke, 1989)

$$\frac{\partial \overline{\Psi}}{\partial t} + \overline{\mathbf{V}_h} \nabla_h \overline{\Psi} + \overline{w} \frac{\partial \overline{\Psi}}{\partial z} = -\frac{1}{\overline{\rho}} \frac{\partial}{\partial z} \overline{\rho w' \Psi'} + S_\Psi, \quad (5.1)$$

where \mathbf{V}_h is the horizontal wind speed, w is the vertical velocity, and S_Ψ is the body source term for Ψ respectively. The overbar denotes the grid-box average and the prime denotes the deviation from that average such that at any point in the grid volume

$$\Psi = \overline{\Psi} + \Psi'.$$

When interpreted as a grid-box average equation for a large-scale model the left-hand side of (5.1) represents the terms resolved by the model while the right hand side contains terms acting on the subgrid scale which need to be parametrized (see section 2.2).

In an atmosphere with active convection the large-scale (grid-scale in a model) vertical motion, \overline{w} , is the average of the mean ascent in active cumulus clouds and the mean motion, which can be ascending or descending, in the environment. With the assumption that active convection occupies a fraction σ of the horizontal area, the mass-fluxes in cumulus clouds, M_c , and in the environment, M_e , can be defined as

$$\begin{aligned} M_c &= \sigma \rho w_c \\ M_e &= (1 - \sigma) \rho w_e. \end{aligned}$$

Here, both w_c and w_e are defined as the perturbation vertical velocities with respect to the area-averaged motion, i.e.,

$$\begin{aligned} w_c &= w_{c,tot} - \overline{w} \\ w_e &= w_{e,tot} - \overline{w}. \end{aligned}$$

Furthermore with the definition of an active convection area and its environment the average value of Ψ can be written as

$$\bar{\Psi} = \sigma\Psi_c + (1 - \sigma)\Psi_e. \quad (5.2)$$

If it is now assumed that above cloud base the vertical eddy transport is entirely achieved by active cumulus convection; then after some algebra

$$\rho\overline{\Psi'w'} = \rho(\overline{\Psi w} - \bar{\Psi}\bar{w}) = \rho\sigma(1 - \sigma)(\Psi_c - \Psi_e)(w_c - w_e). \quad (5.3)$$

With the above definition of w_c and w_e and the usual assumption that $\bar{w}' = 0$ it easily follows that

$$\sigma w_c + (1 - \sigma)w_e = 0,$$

and hence,

$$w_e = -\frac{\sigma w_c}{1 - \sigma}.$$

Equation (5.3) can now be rewritten as

$$\rho\overline{\Psi'w'} = \rho\sigma w_c(\Psi_c - \Psi_e) = M_c(\Psi_c - \Psi_e).$$

Substituting Ψ_e from (5.2) yields

$$\rho\overline{\Psi'w'} = \frac{M_c}{1 - \sigma}(\Psi_c - \bar{\Psi}). \quad (5.4)$$

If the averaging area is much larger than the scale of individual convective draughts, which normally are not much larger than a few kilometers, it is reasonable to assume that $\sigma \ll 1$. Using this assumption in (5.4) leads to the final approximate form of (5.3) as

$$\rho\overline{\Psi'w'} = M_c(\Psi_c - \bar{\Psi}). \quad (5.5)$$

With (5.5) the subgrid-scale flux of the quantity Ψ has been expressed as the product of the cloud-scale mass flux and the difference of the values of Ψ inside and outside the cumulus elements. When reintroducing (5.5) into (5.1) it becomes obvious that in order to close the system of equations it is necessary to derive expressions for the convective mass flux, M_c , and the flux of Ψ inside the convective elements, $M_c\Psi_c$. This requires a model for the

ensemble of cumulus elements. Examples for such models are given by Arakawa (1969), Ooyama (1971), Yanai et al. (1973), Arakawa and Schubert (1974) and Tiedtke (1989) and only a brief summary will be provided here. For simplicity it will be assumed that there are no convective-scale downdraughts present in the averaging area, so that the net convective mass flux is achieved only by updraughts, i.e., $M_c = M_u$ and $\Psi_c = \Psi_u$, where subscript u stands for updraught quantities.

The balance equation for mass and quantity Ψ in a steady state for an individual convective updraught can be written as

$$\frac{1}{\rho} \frac{\partial M_i}{\partial z} = \epsilon_i - \delta_i$$

and

$$\frac{1}{\rho} \frac{\partial M_i \Psi_{u,i}}{\partial z} = \epsilon_i \bar{\Psi} - \delta_i \Psi_{u,i} + S(\Psi_{u,i}) - D(\Psi_{u,i}),$$

where ϵ_i and δ_i represent the rates of mass entrainment into and detrainment out of the convective updraught. $S(\Psi_{u,i})$ and $D(\Psi_{u,i})$ represent sources and sinks of $\Psi_{u,i}$ within the updraught, such as condensation in the case of Ψ representing heat or humidity, or the generation of precipitation if Ψ represents cloud condensate carried inside the updraughts. A further simplification of the problem often used in cumulus parametrization can be achieved by summing over all convective elements. This leads to the so-called bulk cumulus model equations as

$$\frac{\partial M_u}{\partial z} = E - D \tag{5.6}$$

and

$$\frac{\partial M_u \Psi_u}{\partial z} = E \bar{\Psi} - D \Psi_u + \rho S(\Psi_u) - \rho D(\Psi_u), \tag{5.7}$$

where $E = \rho \epsilon$ and $D = \rho \delta$. Introducing (5.5), (5.6) and (5.7) into (5.1) and making the additional assumption that sources and sinks for Ψ can only occur in convective updraughts (i.e., $S_\Psi = S(\Psi_u)$ and $D_\Psi = D(\Psi_u)$), (5.1) simplifies to

$$\frac{\partial \bar{\Psi}}{\partial t} + \overline{\mathbf{V}_h \nabla_h \Psi} + \bar{w} \frac{\partial \bar{\Psi}}{\partial z} = \frac{D}{\rho} (\Psi_u - \bar{\Psi}) + \frac{M_u}{\rho} \frac{\partial \Psi}{\partial z}. \tag{5.8}$$

This form of the large-scale evolution equation for $\bar{\Psi}$ in a convective atmosphere is usually interpreted as describing the influence of convection on the large-scale atmosphere through

the detrainment of the updraught values of Ψ into the environment and through advection of Ψ due to compensating downward motion between convective updraughts. The concept and the equations outlined here will be used in the subsequent sections to show that if the convection process is expressed using the mass-flux concept, there exists a unique and unambiguous coupling to cloud formation.

5.2.2 Cloud condensate

The mass-flux concept as described in the previous section will be used to find an expression for the contribution of convection to the grid-mean condensate content, \bar{l} . The starting point for the derivation is the grid-mean equation for the time evolution of \bar{l} in the presence of convection, which can be written as

$$\frac{\partial \bar{l}}{\partial t} = A(\bar{l}) + \bar{c} - \bar{e} - \overline{G_P} - \frac{1}{\bar{\rho}} \frac{\partial}{\partial z} (\overline{\rho w' l'})_{cv} \quad (5.9)$$

where \bar{l} is the grid-mean condensate content, $A(\bar{l})$ represents all transport processes of \bar{l} except for the convective flux which is represented by the last term on the right hand side. \bar{c} , \bar{e} , and $\overline{G_P}$ are the grid average of condensation, evaporation and generation of precipitation. Making use of the mass-flux concept (see section 5.2.1 and equation (5.5)), the convective flux of cloud condensate can be rewritten (omitting downdraughts for the moment) as,

$$(\overline{\rho w' l'})_{cv} = M_u (l_u - \bar{l}), \quad (5.10)$$

with M_u as the updraught mass-flux, l_u the updraught condensate content and \bar{l} the grid-mean condensate content.

Since the aim is to derive cloud source/sink terms due to convection, it is assumed that convection is the only active process in the grid box. Hence the only contribution to the grid-mean condensation \bar{c} is condensation in convective updraughts and therefore $\bar{c} = c_u$. Furthermore it is assumed that precipitation is only generated in convective updraughts so that $\overline{G_P} = G_{P,u}$. There are several ways of including the evaporation effects of convection on the grid-mean condensate. T93 identifies the compensating subsiding motion as the major influence on evaporation and hence defines

$$\bar{e} = e_{cv} = -\frac{M_u}{\bar{\rho}} a \left(\frac{d\bar{q}_s}{dz} \right)_{ma},$$

where a is the cloud fraction and \bar{q}_s the grid-mean saturation specific humidity; the subscript ma represents a moist adiabat. It will be shown below that it is not necessary to specify the

details of the evaporation term for the further derivation of the equations in the context of this chapter. Introducing the assumptions made and substituting (5.10) into (5.9) results in

$$\left(\frac{\partial \bar{l}}{\partial t}\right)_{cv} = c_u - G_{P,u} - \frac{1}{\bar{\rho}} \frac{\partial}{\partial z} [M_u(l_u - \bar{l})] - e_{cv}. \quad (5.11)$$

The steady state equation for the updraught condensate flux can be written as (e.g., Tiedtke, 1989; section 5.2.1)

$$\frac{\partial}{\partial z}(M_u l_u) = E_u \bar{l} - D_u l_u + \bar{\rho} c_u - \bar{\rho} G_{P,u}, \quad (5.12)$$

where E_u and D_u are the entrainment and detrainment rates, c_u represents the condensation and $G_{P,u}$ describes the generation of precipitation in the updraughts. Note, that (5.12) forms part of most mass-flux convection parametrization schemes, so that the values of the variables above are known after this parametrization is applied in the GCM. Historically the first term on the right hand side, which describes the entrainment of condensate, is neglected in convection parametrizations. However, it is obvious that it has to be taken into account when applying a mass-flux scheme for convection together with a cloud scheme describing condensate as a prognostic variable, because of the possibility of updraughts penetrating already cloudy areas. The entrainment of the grid-mean value of condensate \bar{l} implies that it is equally likely for the updraughts to occur in the cloudy area a as it is for them to occur in the cloud-free area $(1 - a)$. Introducing (5.12) into (5.11) leads to

$$\left(\frac{\partial \bar{l}}{\partial t}\right)_{cv} = \frac{D_u}{\bar{\rho}} l_u - \frac{E_u}{\bar{\rho}} \bar{l} + \frac{1}{\bar{\rho}} \frac{\partial}{\partial z}(M_u \bar{l}) - e_{cv}. \quad (5.13)$$

This equation reveals the interaction of convection with the grid-mean condensate in an interesting way. The first three terms on the right hand side all represent transport terms whereas the fourth term describes the evaporation. Condensate is produced by condensation in the convective updraughts and enters the grid-mean cloud condensate budget when detrained into the environment. At the same time the condensate in already existing clouds is entrained into the updraughts. The assumption of mass continuity implies compensating downward motion between the updraughts, which will lead to a flux of the grid-mean condensate. The divergence of that flux contributes to the local change of cloud condensate. This process is described by the third term in (5.13).

Equation (5.13) can be further simplified by using the mass continuity equation for the updraughts (5.6). This leads to the final form of (5.9) for convective processes as

$$\left(\frac{\partial \bar{l}}{\partial t}\right)_{cv} = \frac{D_u}{\bar{\rho}}(l_u - \bar{l}) + \frac{M_u}{\bar{\rho}} \frac{\partial \bar{l}}{\partial z} - e_{cv}. \quad (5.14)$$

Equation (5.14) gives a very similar expression for the influence of convection on the large scales as for other variables, such as heat and specific humidity, through a detrainment and a subsidence term (see section 5.2.1). However, it differs from the other variables in that the detrainment term is the dominant one in the case of condensate. Together with a definition of the evaporation term, this equation describes unambiguously the connection between grid-mean condensate and its convective source.

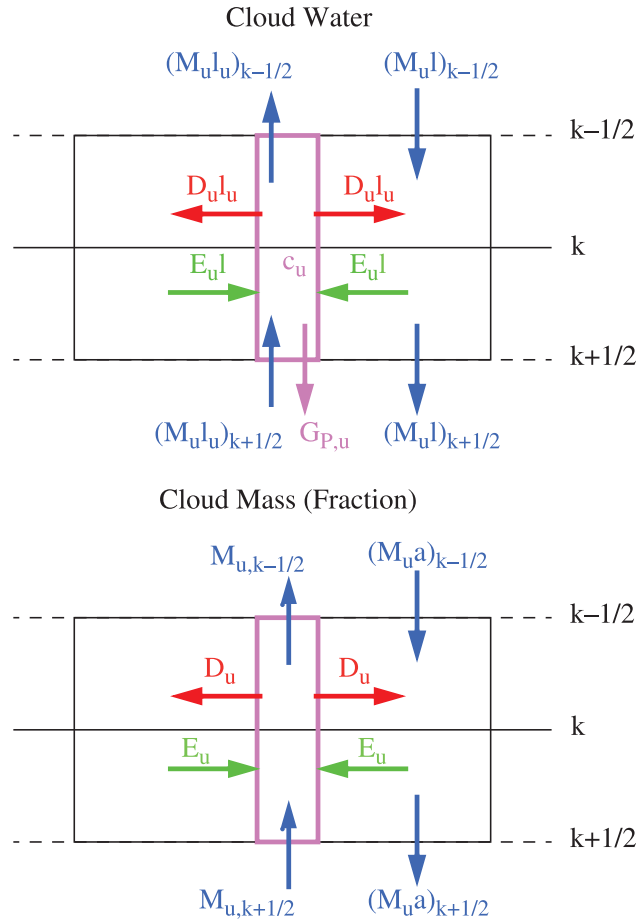


Figure 5.1: Schematic of the relevant quantities in the link between a mass-flux convection scheme and a prognostic cloud scheme for a given model level k . The “half-levels” $k - 1/2$ and $k + 1/2$ represent the boundaries of model level k , for which all fluxes are calculated. For the meaning of all other symbols the reader is referred to the text.

A schematic illustration of (5.14) can be found in Figure 5.1 (top panel). The condensate that is produced in the convective updraughts is detrained into the environment. Because of mass continuity, the injected mass (carrying l_u) replaces the same amount of mass present in the grid box before the convective event (carrying \bar{l}). Furthermore the upward motion

in the convective updraughts induces a downward motion in the environment, which itself advects grid-mean condensate and whose adiabatic heating effect leads to evaporation of cloud water.

5.2.3 Cloud fraction

To derive an equation similar to (5.14) for cloud fraction the following quantity is defined for a given volume:

$$\beta = \frac{m_{s,l}}{m_{tot}}. \quad (5.15)$$

β is the ratio of the mass in the saturated, cloudy part of a given volume to the total mass in that volume. If the volume under consideration is a GCM grid box and it is assumed that the density in the saturated part is approximately the same as in the unsaturated part, then

$$\beta_{GB} = \left(\frac{m_{s,l}}{m_{tot}} \right)_{GB} = \left(\frac{\rho_{s,l} V_{s,l}}{\rho_{s,l} V_{s,l} + \rho_{unsat} V_{unsat}} \right)_{GB} \approx \left(\frac{V_{s,l}}{V_{tot}} \right)_{GB} \equiv a,$$

which is the definition of cloud fraction, assuming that cloud air fills the grid box entirely in the vertical.

The aim now is to consider the influence of convection on the time evolution of β in a GCM grid box. There are generally two ways in which convection will influence β_{GB} ; i) through the transport of saturated mass due to convective fluxes and ii) through possible sources of saturated mass. Hence, a general expression for the change of β_{GB} due to convection can be written as

$$\left(\frac{\partial \beta_{GB}}{\partial t} \right)_{cv} = S_{\beta,cv} - \frac{1}{\bar{\rho}} \frac{\partial}{\partial z} (\overline{\rho w' \beta'})_{cv}. \quad (5.16)$$

First the flux term on the right hand side of (5.16) is considered. Inside the updraught the entire mass is assumed to remain cloudy during the ascent. In the environment however, only a parts of the mass are cloud. Hence, the flux of β for the entire grid volume can be approximated using the mass flux concept as

$$(\overline{\rho w' \beta'})_{cv} = M_u (1 - a). \quad (5.17)$$

Comparison of (5.17) with (5.5) reveals that the intensive quantity transported by the convective circulation is the cloudy mass per unit mass, just as defined in (5.15).

Now possible sources of cloud mass due to convection need to be defined. To do so all convective exchanges of mass that are taking place in the grid box are considered (see Figure 5.1, bottom panel). The air inside the updraught is always cloudy so that vertical transports inside the updraught do not change the mass of cloud air in the grid box. Furthermore it is assumed that the adiabatic heating due to compensating motion in the environment, e_{cv} , which constitutes a sink term for condensate according to (5.14), does not change the cloud fraction unless the whole of the condensate evaporates. In the latter case the cloud fraction will approach zero in one timestep. The underlying assumptions for this treatment are that both cloud water and compensating subsidence are assumed to be evenly distributed in the grid box. Hence, at each point in the box the same amount of water evaporates so that a change of cloud fraction is not possible. This assumption is also made in T93. A relaxation of this assumption will lead to source terms in equation (5.16) the exact form of which, like the evaporation term in equation (5.14), is not relevant in the context of this derivation.

A horizontal exchange of air between updraught and environment takes place through entrainment and detrainment. Detrainment transports saturated updraught air into the environment without changing its mass. However in the presence of cloudy mass of fraction a in the environment the entrained air will be a mixture of saturated air and unsaturated air. Hence,

$$E_u = (aE_u)_{s,l} + [(1-a)E_u]_{unsat}.$$

Note that the E_u is the same in both parts. The subscripts s,l and $unsat$ just flag the air as being saturated or not. The entrained saturated air will stay saturated inside the updraught and hence does not form a source of β for the grid box. Note, that even if the entrained air is subsaturated with respect to the updraught quantities and evaporation processes have to take place inside the updraught to re-saturate the entrained air, this will not change the mass of the saturated air. However, the entrained mass that is unsaturated before entrainment takes place will be immediately transformed into saturated air inside the updraught by definition of an always saturated updraught and therefore forms a source term for the saturated mass in the grid box. Hence,

$$S_{\beta,cv} = \frac{E_u}{\bar{\rho}}(1-a). \quad (5.18)$$

Introducing both the flux and the source term into (5.16) leads to

$$\left(\frac{\partial\beta_{GB}}{\partial t}\right)_{cv} \equiv \left(\frac{\partial a}{\partial t}\right)_{cv} = -\frac{1}{\bar{\rho}}\frac{\partial M_u}{\partial z} + \frac{1}{\bar{\rho}}\frac{\partial}{\partial z}(M_u a) + \frac{E_u}{\bar{\rho}}(1-a). \quad (5.19)$$

Now (5.6) can be used to replace the first term on the right hand side of (5.19) so that

$$\left(\frac{\partial a}{\partial t}\right)_{cv} = \frac{D_u}{\bar{\rho}} - \frac{E_u}{\bar{\rho}}a + \frac{1}{\bar{\rho}}\frac{\partial}{\partial z}(M_u a) \quad (5.20)$$

Similar to the first three terms in (5.13) for condensate this equation describes the change of cloud fraction as the result of horizontal and vertical transport terms. Further simplification of (5.20) by using (5.6) again leads to the final equation for a as follows

$$\left(\frac{\partial a}{\partial t}\right)_{cv} = (1-a)\frac{D_u}{\bar{\rho}} + \frac{M_u}{\bar{\rho}}\frac{\partial a}{\partial z} \quad (5.21)$$

Similar to (5.14) the effect of convection on the “large scale” in terms of cloud fraction can be described by a detrainment and a subsidence term. Equations (5.14) and (5.21), together with the cloud model equations of the convection parametrization, form a closed set of equations, which are derived under assumptions commonly made in mass-flux convection schemes and which describe the influence of convection on grid-mean condensate and cloud fraction.

To complete the scheme the influence of convective scale downdrafts on both equation (5.14) and (5.21) needs to be considered. Current mass-flux convection schemes do not consider the presence of cloud condensate in downdrafts. Hence there is no direct interaction between the convective scale downdrafts and the grid-mean condensate. However, downdrafts do lead to a change in the net cloud mass flux and therefore influence the compensating motion outside the convective area. This effect can easily be included into above equations by replacing the updraught mass flux M_u by the net cloud mass flux $M_c = M_u + M_d$ where M_d denotes the downdraught mass flux.

5.3 The generation of non-convective clouds

The formation of clouds due to non-convective processes, often labeled as “stratiform” clouds, is classically at the heart of cloud parametrization. As outlined in Chapter 2, most cloud parametrization schemes deal with this type of cloud exclusively and treat convective clouds as some kind of add-on. It is only since Tiedtke (1993) that cloud parametrizations try to incorporate cloud generation and dissipation processes of all types in a coherent scheme.

Many different methods have been proposed to describe non-convective cloud formation on the subgrid scale. In this section source terms for the T93 parametrization will be derived. This requires both sources of cloud condensate and cloud fraction to be described in a consistent way. An attempt will be made to show the obvious link to other approaches such as the statistical distribution schemes (e.g., Sommeria and Deardoff, 1977; Bougeault, 1981; Smith, 1990; Ricard and Royer 1993). Before going into the detailed derivation, some general features of non-convective subgrid-scale cloud formation will be discussed. Then the actual source terms will be derived followed by an extensive comparison of the terms derived here to those used in the original T93 parametrization. The link between the methods applied here and other parametrization approaches, in particular distribution schemes, will be highlighted. The section will close by exploring the possibility of deriving a sink term for cloud fraction using a similar approach to the source derivation.

5.3.1 General remarks

Before deriving the actual source terms for use in the context of Tiedtke's (1993) cloud parametrization some general concepts of cloud formation by non-convective processes and their numerical implementation need to be discussed.

It is worthwhile recalling from section 2.2 that the existence of stratiform clouds on subgrid scales has two major implications, i) clouds occur before the grid-mean value of relative humidity has reached 100 % and ii) temperature and/or specific humidity are somehow distributed around their respective grid-mean values, so that parts of the grid volume become saturated before others. These statements relate to the existence of clouds in a grid box and require some modification when the actual formation process, i.e., the cloud tendency, are to be parametrized for use in a prognostic cloud scheme as described here. In this case, apart from knowledge of the initial distributions of temperature and humidity, the distributions of their respective tendencies need to be known also. Thus the general case of parametrizing stratiform clouds requires four distribution functions (or two joint two-variable distribution functions) as well as their overlap to be described, based only on the knowledge of their mean value. Fortunately, there are several simplifying assumptions that can be made, of which the most important will be outlined here.

First, it will be assumed that the temperature inside and outside cloud are the same. This implies a (non-specified) physical process that redistributes latent heat released due to condensation processes between the cloudy and non-cloudy area on the time scale of a model

timestep. Although this assumption appears to be very artificial it is not different from the ever occurring problem of redistributing heat after partial advection of air from one grid volume to another, which constitutes an unavoidable numerical truncation error. Recent cloud parametrizations (Randall and Fowler, 1999) attempt to explicitly model the temperature adjustment between cloudy and clear air by assuming differences in the vertical motion in the two parts. Although intuitively attractive this remains an uncertain approach in the absence of knowledge of what maintains the apparently small temperature differences between clouds and environment which are observed in stratiform clouds.

The assumption of equal and homogeneous temperatures in cloudy and clear sky immediately simplifies the assumption about the distribution of specific humidity in the cloudy part, which can be assumed to be saturated at a value defined by the grid-mean temperature and pressure. The distribution of specific humidity in the cloud free part still needs to be specified.

In order to simplify the derivation further, it will be assumed that the main cloud production processes are those connected to changes in the temperature of an air parcel. Changes in the specific humidity content of the parcel alone are considered to be of no importance for cloud formation. It is immediately obvious that this assumption is valid for all processes considered in atmospheric models, except mixing. Stratiform cloud formation is therefore assumed to occur as a result of adiabatic cooling by vertical motion or due to diabatic cooling, e.g., by radiation (see equation (3.13)). Since the stratiform cloud formation only constitutes one source for cloud in the scheme described here, cloud formation due to mixing of air parcels can be described in separate terms.

With these assumptions the problem has been simplified to the description of a distribution of specific humidity in the cloud-free part of the grid box and the distribution of the change of temperature and therefore saturation specific humidity in time. The latter is equivalent to describing the horizontal distribution of vertical motion and diabatic heating.

A second interesting general issue is the accuracy that might be required in the numerical solution of prognostic equations for grid-mean condensate and cloud fraction. This problem can be illustrated by rewriting the grid-mean cloud condensate as

$$l = al_c,$$

where l_c is the “local” cloud water content and a the cloud fraction. Note that in this and the following equations of this section, the overbar has been omitted for brevity and variables

represent grid averages unless indicated otherwise.

The local time derivative of l then becomes

$$\frac{\partial l}{\partial t} = a \frac{\partial l_c}{\partial t} + l_c \frac{\partial a}{\partial t}. \quad (5.22)$$

If this equation is solved with a first-order accurate numerical scheme, such as

$$\Delta l = a^t \Delta l_c + l_c^t \Delta a, \quad (5.23)$$

a singularity exists for $a^t = 0$ and $l_c^t = 0$ which prevents the solution of (5.23). In practical terms this means that if one was to apply (5.23) to evaluate the change of grid-mean condensate, one would first have to solve an equation for Δa and create the condensate in the newly formed cloud area in the following timestep through the first term on the right hand side of (5.23). For small timesteps this might not constitute a significant problem, for timesteps employed in GCMs, however, the inconsistency between cloud fraction and grid-mean condensate introduced by the truncation error can become substantial. Therefore it appears appropriate to solve (5.22) with a more accurate scheme. One such scheme can be written as

$$\begin{aligned} \Delta l &= \frac{1}{2}(a^{t+1} + a^t)\Delta l_c + \frac{1}{2}(l_c^{t+1} + l_c^t)\Delta a \\ &= \frac{1}{2}(a^{t+1} - a^t + 2a^t)\Delta l_c + \frac{1}{2}(l_c^{t+1} - l_c^t + 2l_c^t)\Delta a \\ &= a^t \Delta l_c + l_c^t \Delta a + \Delta l_c \Delta a. \end{aligned} \quad (5.24)$$

It is obvious from (5.24) that the effect of the singularity for $a^t = 0$ and $l_c^t = 0$ is overcome in this numerical solution of (5.22) by retaining a second-order term. It is worthwhile noting that this term does increase the accuracy of the solution in any situation not just the singularity mentioned above. Because of the importance of the second-order term, all further derivations here will be made using finite differences. The differential forms of the derived equations can easily be derived by neglecting any second-order terms.

5.3.2 Derivation of stratiform cloud source terms

With the assumptions outlined above, stratiform cloud formation generally depends on the horizontal distributions of specific humidity in the clear sky area and the horizontal distribution of the tendency of the saturation specific humidity, Δq_s . Since for now, the emphasis

is on cloud formation, rather than decay, only cases with $\Delta q_s < 0$ will be considered. As already mentioned above, the processes changing q_s considered here are vertical motion and diabatic heating, but not mixing.

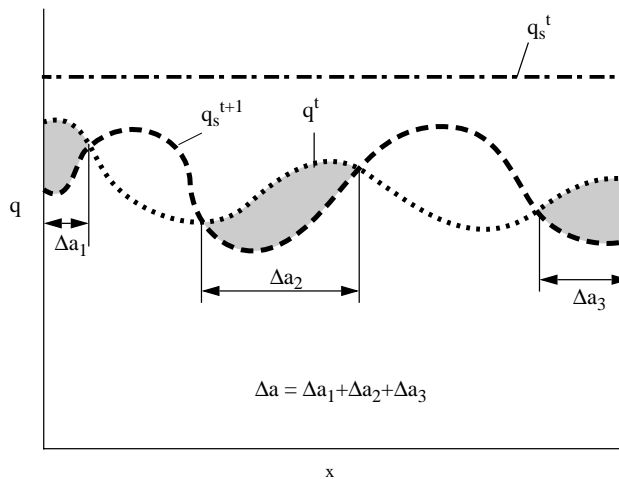


Figure 5.2: Schematic of cloud formation in a grid box with initially homogeneous temperature but inhomogeneous distributions of specific humidity, q and saturation specific humidity tendency, Δq_s .

Figure 5.2 shows a schematic of this conceptual idea. Shown is a one-dimensional “grid box”. At the initial time, t , a homogeneous temperature distribution, and hence a homogeneous distribution of saturation specific humidity q_s^t , exists in the grid box. The specific humidity at time t , q^t , is distributed around the grid-mean value. All values of q^t are lower than q_s^t and therefore the grid box is initially cloud free. Between time t and $t + 1$ the saturation specific humidity is lowered by varying amounts within the grid box. In all regions where the new saturation value falls below the specific humidity value condensation will occur and clouds will form. This results in an increase in cloud cover in the grid box by Δa . It is obvious from this figure that the change in cloud area not only depends on the unknown distribution functions for q^t and Δq_s , but also on how those distributions overlap. Therefore the application of the ideas outlined above must rely on heavy simplification of the picture in Figure 5.2 in order to be practical.

Figure 5.3 depicts such a simplified situation. Here a partly cloudy grid box is considered. The cloud fraction at time t is a^t , whereas the cloud-free area is $1 - a^t$. Since the temperature is again assumed to be uniform within the grid box, at all cloudy points within the grid box $q^t = q_s(T^t)$, denoted by the horizontal line. In order to be able to produce cloud in the still cloud-free part of the grid box, a distribution of specific humidity and/or tendency of saturation specific humidity needs to be assumed. Here, it is assumed that it is only the

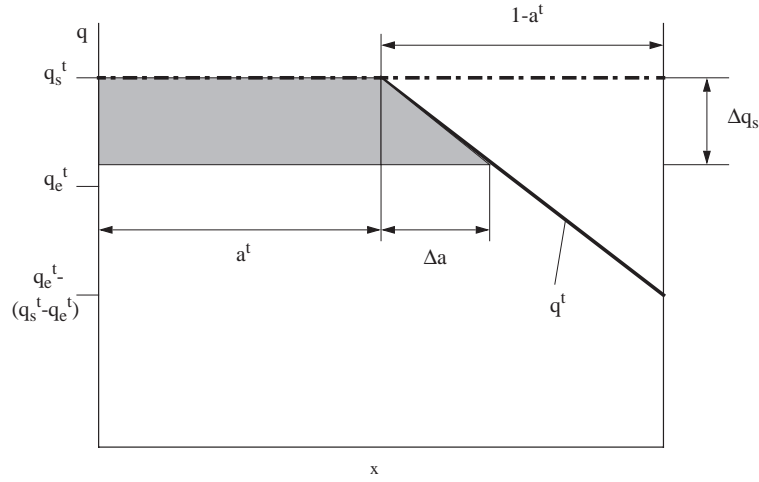


Figure 5.3: Schematic of cloud formation for the source terms derived here.

specific humidity that is non-uniform, while the change in saturation specific humidity is considered to be the same everywhere in the grid box. A very simple distribution of specific humidity is used. Since the cloud cover, a^t , and temperature, T^t , are known, one can evaluate mean value of specific humidity in the cloud-free environment using

$$q^t = a^t q_s^t + (1 - a^t) q_e^t \quad (5.25)$$

as

$$q_e^t = \frac{q^t - a^t q_s^t}{1 - a^t}. \quad (5.26)$$

It is then assumed that the specific humidity in the cloud free part of the grid box is uniformly distributed around this environment value, q_e^t . The boundaries of the distribution are chosen to be q_s^t and $q_e^t - (q_s^t - q_e^t)$ to make the distribution function symmetric around its mean. In Figure 5.3 such a distribution becomes a diagonal line as shown in the cloud-free area. Note that the "transformation" from distribution space into grid-point space merely requires plotting the cumulative distribution function. This is an important feature, which allows the use of more complex distribution functions of specific humidity if desired. This link between the derivation of cloud source terms performed here and a distribution-type cloud scheme will be explored in a later subsection. The change in saturation specific humidity, Δq_s , is assumed to be homogeneous throughout the entire grid box. Note that this is equivalent to assuming a homogeneous distribution of ascending motion and/or diabatic cooling. The former is probably justifiable since only grid-mean motions are resolved by the model. The

latter is doubtful in the presence of clouds that do not cover the entire grid box, since the radiative cooling at the top of these clouds will be much stronger than that in clear sky. It should be pointed out, however, that both assumptions are made in all cloud representations to date.

Figure 5.3 reveals one of the major advantages of a prognostic treatment of cloud fraction. Since it is already known that a fraction a^t of the grid box is cloudy, the generation of condensate in that part can be evaluated in a straightforward fashion as

$$\Delta l_{a,old} = -a^t \Delta q_s. \quad (5.27)$$

Note that the minus sign appears in (5.27) because condensation occurs if q_s is lowered, i.e., $\Delta q_s < 0$. In the cloud-free part of the grid box, simple triangle similarity yields a term for the change in cloud fraction, Δa , as

$$\frac{\Delta a}{-\Delta q_s} = \frac{1 - a^t}{2(q_s^t - q_e^t)},$$

and hence

$$\Delta a = -(1 - a^t) \frac{\Delta q_s}{2(q_s^t - q_e^t)}. \quad (5.28)$$

To write an equation that includes only grid-mean information, q_e^t can be substituted using (5.26) to give

$$\Delta a = -(1 - a^t)^2 \frac{\Delta q_s}{2(q_s^t - q^t)}. \quad (5.29)$$

The amount of condensate formed within the new cloud is

$$\Delta l_{a,new} = -\frac{1}{2} \Delta a \Delta q_s, \quad (5.30)$$

a second-order term that should be retained according to the discussion above. It is the simplicity of the distribution function chosen here that yields simple source terms for both cloud fraction and cloud condensate. This was a deliberate choice for various reasons. First, the real distribution of specific humidity is largely unknown for any given situation and therefore a simple description, although not necessarily correct, is for now as appropriate as any other more complex one. Second, the even simpler assumption of uniform Δq_s prohibits a large complexity in assumptions about q for consistency reasons. However, one of the main reason for the choice made here is the possibility to easily compare the derived source terms

to those proposed originally by Tiedtke (1993) and to derive some interesting features of the two sets of source terms. This will be the subject of the next subsection.

5.3.3 Comparison to the T93 cloud scheme

In this subsection the source terms for cloud fraction and condensate derived above will be compared to those used in T93 (see Chapter 3). First an analysis of the different behaviour of some crucial quantities related to the condensation/cloud formation process will be carried out. After that some simple examples of numerically explicit solutions will be presented to highlight shortcomings in the original parametrization and show the improved physical consistency of the terms derived here.

Prediction of cloud fraction

First the production terms of cloud fraction for the two schemes will be compared. The cloud fraction source term used in T93 is

$$\Delta a = -(1 - a^t) \frac{\Delta q_s}{q_s^t - q^t}. \quad (5.31)$$

The difference between this and (5.29) can be expressed by the ratio

$$\frac{(\Delta a)_{T93}}{(\Delta a)_{new}} = \frac{2}{(1 - a^t)} \quad (5.32)$$

It is immediately apparent, that the original scheme produces larger changes in a than the new one for a given change in q_s . The difference increases with initial cloud fraction. For the special case that $\Delta q_s = -(q_s^t - \overline{q^t})$, the original scheme would always predict cloud fraction one, whereas the scheme derived from the distribution would yield cloud fractions smaller than one, consistent with the fact that a part of the grid box has specific humidities lower than the grid average.

Environment humidity

Although never explicitly parametrized, the choice of source terms for a and l has implications for the evolution of specific humidity in the cloud-free part of the grid box, q_e . The behaviour of the two parametrizations compared here might provide some insight into the physical soundness of the schemes. The starting point of the investigation is the expression of grid-mean specific humidity as

$$q = aq_s + (1 - a)q_e, \quad (5.33)$$

as used before.

The change in q can then be written in finite difference form as

$$\Delta q = a\Delta q_s + (1 - a)\Delta q_e + \Delta a(q_s - q_e) + \Delta a(\Delta q_s - \Delta q_e). \quad (5.34)$$

Note that the last term on the right hand side of equation (5.34) is of second order and will be retained following accuracy arguments made above. Assuming the only change in specific humidity in the grid box is due to the condensation process itself, $\Delta q = -\Delta l$ and Δa can be replaced with the terms derived above for the two cloud schemes and (5.34) can be solved for Δq_e . For the T93 scheme this gives

$$a\Delta q_s + \Delta a\Delta q_s = a\Delta q_s + (1 - a)\Delta q_e - \Delta q_s + \Delta a\Delta q_s - \Delta a\Delta q_e,$$

which finally yields

$$\Delta q_e = \frac{\Delta q_s}{(1 - a - \Delta a)}. \quad (5.35)$$

Hence, in this scheme, the change in the specific humidity in the cloud-free environment is proportional to the change in saturation specific humidity, implying a reduction in q_e in the case of condensation ($\Delta q_s < 0$). The factor of proportionality is a function of the cloud fraction at the end of a timestep. As will be shown below, this has serious implication for the relative humidity of the cloud-free part. Since the cloud fraction is always positive and smaller than one the change in q_e is always larger than that in q_s implying a drying out of the cloud-free air in relative humidity terms, which will be particularly strong for large cloud fractions. It is worthwhile noting that the only effect of the second-order term is that Δa is retained in the denominator of (5.35), which does not change the general behaviour of the scheme in changing q_e .

The behaviour of the new scheme differs significantly from the original. Again Δq and Δa are substituted to give

$$a\Delta q_s + \frac{1}{2}\Delta a\Delta q_s = a\Delta q_s + (1 - a)\Delta q_e - (1 - a)\frac{\Delta q_s}{2} + \Delta a\Delta q_s - \Delta a\Delta q_e,$$

which can be rearranged as

$$\Delta q_e = \frac{\Delta q_s}{2}. \quad (5.36)$$

In this scheme the change in q_e is again proportional to that in q_s , implying a drying out of the environment in absolute humidity terms. However, the change in q_e is always half of that in q_s independent of cloud fraction, implying an increase in the relative humidity. The reason for the drying out is immediately apparent from Figure 5.3. By producing clouds in part of the grid box, the definition of q_e itself changes due to a change in the cloud-free area. The new q_e is now an average over the much drier area marked by $(1 - a)$ which contains those points of the distribution which are too dry to contribute to the condensation.

Simple explicit solutions

The prognostic equations for cloud fraction and cloud condensate, i.e., (3.1) and (3.2) for the original T93 scheme and (5.29) and (5.30) for the scheme derived here can be solved numerically in an idealized framework. It is assumed that in a given volume, the saturation specific humidity is reduced in every timestep by an amount sufficiently small to ensure stable and accurate numerical solutions. This forcing in q_s could be achieved for instance by some continuous uplift. The only process assumed to occur in the volume is cloud formation. The equations for cloud fraction and condensate will be solved together with the respective humidity equation, which in this idealized setup reduces to

$$\Delta q = -\Delta l,$$

Note that by imposing the change in q_s , $\Delta q_{s,forc}$, the need for an explicit temperature equation does not arise. However, the latent heat release due to condensation processes does counteract the imposed forcing and needs to be taken into account. This is achieved in the following way. The net change in q_s over one timestep can be written as

$$\Delta q_s = \Delta q_{s,forc} + \Delta q_{s,cond}, \quad (5.37)$$

where $\Delta q_{s,forc}$ is the prescribed forcing and $\Delta q_{s,cond}$ is the change in q_s due to condensation heating. Since the imposed changes in q_s , and hence in temperature, are assumed to be small, q_s at time $t + 1$ can be written with a high degree of accuracy as

$$q_s(T^{t+1}) \approx q_s(T^t) + \frac{dq_s}{dT}(T^{t+1} - T^t). \quad (5.38)$$

Using the first law of thermodynamics (5.38) can be rewritten for the condensation contribution as

$$\Delta q_{s,cond} = -\frac{L}{c_p} \frac{dq_s}{dT} \Delta q_{cond}. \quad (5.39)$$

Using

$$\Delta q_{cond} \approx a^t \Delta q_s,$$

which is true for both sets of equations used here, (5.39) can be substituted into (5.37) to give the final value for the forcing in q_s in the presence of condensation as

$$\Delta q_s \approx \frac{\Delta q_{s,forc}}{1 + a^t \frac{L}{c_p} \frac{dq_s}{dT}}. \quad (5.40)$$

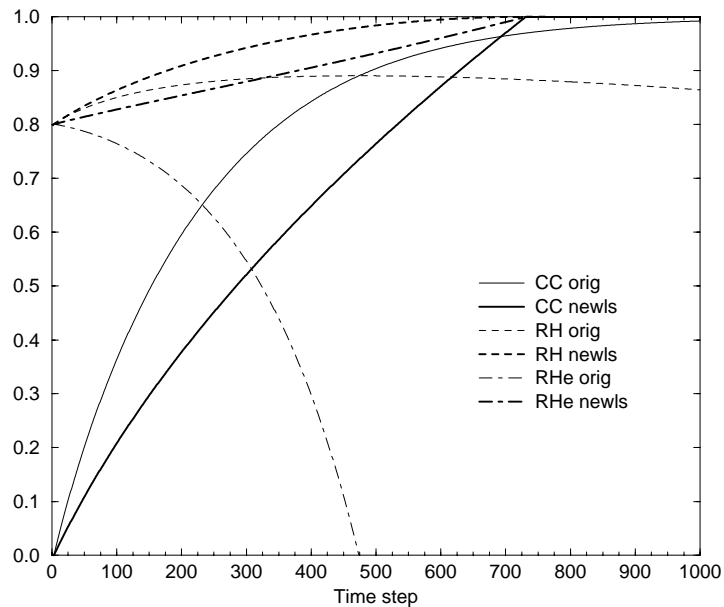


Figure 5.4: Time evolution of cloud cover (solid), grid-mean relative humidity (dashed), and relative humidity in the cloud free part of the grid box (dot-dashed) for the original T93 scheme (thin lines) and the source terms proposed here (thick lines). The solutions are for an idealized setup with initial conditions of $q_s = 10 \text{ g} \cdot \text{kg}^{-1}$, $q = 8 \text{ g} \cdot \text{kg}^{-1}$, $a = 0$, $l = 0$, and a forcing of $\Delta q_s = -0.01 \text{ g} \cdot \text{kg}^{-1}$. The latent heating effects of condensation are accounted for.

Figure 5.4 shows the evolution of cloud cover, grid-mean relative humidity, RH , and relative humidity in the cloud free part, RH_e , for integrations with the original scheme (thin lines) and the scheme derived above (thick lines). The initial conditions for the integrations are

$q_s = 10 \text{ g} \cdot \text{kg}^{-1}$, $q = 8 \text{ g} \cdot \text{kg}^{-1}$, $T = 285.65 \text{ K}$, $p = 900 \text{ hPa}$, $a = 0$, and $l = 0$. $\Delta q_{s,forc}$ is set to $-0.01 \text{ g} \cdot \text{kg}^{-1}$.

As expected from (5.32), the original scheme increases cloud fraction faster than the new formulation initially. However, as was obvious from (5.35) this occurs at the expense of an unphysical behaviour of the environmental value of specific and therefore relative humidity. This feature becomes obvious in a dramatic way around time step 450. Here, the cloud fraction as predicted by the original scheme becomes larger than the grid-mean relative humidity. Since

$$RH = a + (1 - a)RH_e,$$

this implies the impossible situation of negative values of relative humidity in the cloud-free part of the grid box. This is an example how ad-hoc choices for sources and sinks of cloud fraction and condensate can lead to an unphysical behaviour of the parametrization, if not checked for physical soundness. Note also that the original scheme would never give a cloud fraction equal to one. The new scheme does not show any of these problems. Although slower, cloud fraction evolves in balance with both the grid-mean and environmental values of relative humidity and all three reach the value of one within the same timestep.

5.3.4 Comparison with the distribution approach

In this subsection the link of the derivations made above to the “distribution scheme” approach used in various large-scale models (LeTreut and Li, 1988; Smith, 1990; Ricard and Royer, 1993) will be explored. One of the major differences is that in the schemes mentioned above, an assumption for the subgrid distribution of a temperature and a moisture related variable are used to describe the existence of clouds, whereas in the approach used here, distribution assumptions are used to describe the cloud formation process. Once some cloud has formed in the grid box, it is assumed that the specific humidity inside the cloud is equal to the saturation value at the grid-mean temperature. Hence, whatever distribution is used, it need only be defined for the clear-sky area.

A simple way to show the link between source terms and distributions is to derive equations (5.29) and (5.30) again, this time using the probability distribution function for specific humidity directly. In the derivation above, this distribution function, $f(q)$, is a uniform distribution around q_e^t between values of q_s^t and $q_e^t - (q_s^t - q_e^t)$ as illustrated in Figure 5.5. The superscript t signifies that the distribution is entirely defined by values known at the

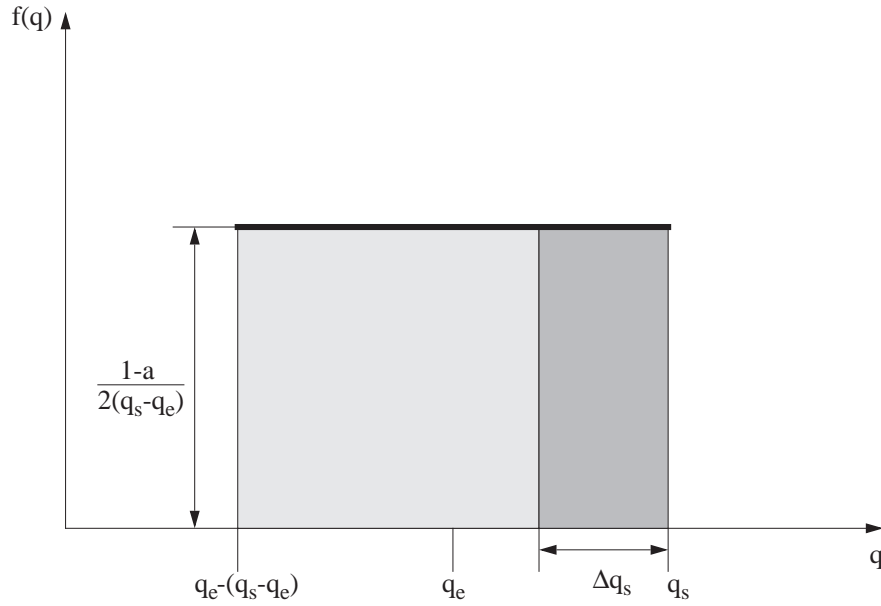


Figure 5.5: Probability distribution function of specific humidity in the cloud-free area of the grid box for a uniform distribution.

beginning of a model time step. The integral over the distribution has to be equal to the clear-sky fraction of the grid box, i.e.,

$$G(q) = \int_{q_e^t - (q_s^t - q_e^t)}^{q_s^t} f(q) dq = 1 - a^t. \quad (5.41)$$

Since in this simple example, $f(q) = \text{const.}$, $f(q)$ is entirely defined by (5.41) as

$$f(q) = \frac{1 - a^t}{2(q_s^t - q_e^t)}. \quad (5.42)$$

A change in saturation specific humidity as shown in Figure 5.5 will then change the cloud fraction, which is generally defined by

$$a = \int_{q_s}^{\infty} f(q_w) dq_w, \quad (5.43)$$

where q_w at any given point is the total water content, i.e. the sum of specific humidity and local cloud condensate, $q + l_c$, which in the cloud-free area reduces to specific humidity only.

Hence, within the boundaries of the integration, q_s^{t+1} and q_s^t , (5.42) is fully applicable.

The change in cloud fraction can be described as

$$\Delta a = \int_{q_s^{t+1}}^{\infty} f(q_w) dq_w - \int_{q_s^t}^{\infty} f(q_w) dq_w$$

$$\begin{aligned}
&= \int_{q_s^{t+1}}^{q_s^t} f(q_w) dq_w \\
&= -\frac{1-a^t}{2(q_s^t - q_e^t)} \Delta q_s,
\end{aligned} \tag{5.44}$$

with $\Delta q_s = q_s^{t+1} - q_s^t$. This is not surprisingly the same result as (5.28). The minus sign appears since Δq_s is defined as $q_s^{t+1} - q_s^t$. In the same way as cloud fraction, cloud condensate can be defined as the first moment of the distribution function $f(q_w)$, i.e.,

$$l = \int_{q_s}^{\infty} (q_w - q_s) f(q_w) dq_w. \tag{5.45}$$

In the clear-sky area again $q_w = q$ and hence, following the same arguments as above, the change of cloud condensate can be written as

$$\begin{aligned}
\Delta l &= \int_{q_s^{t+1}}^{q_s^t} (q - q_s^{t+1}) f(q) dq \\
&= \frac{1-a}{2(q_s - q_e)} \frac{\Delta q_s^2}{2} \\
&= -\frac{1}{2} \Delta a \Delta q_s,
\end{aligned} \tag{5.46}$$

equivalent to (5.30). Although mathematically straightforward, it is important to realize that it is possible to derive source terms for both cloud fraction and cloud condensate based on simple distribution assumptions. The importance lies in the fact that if knowledge about humidity distributions could be gathered from observations, more complex distribution functions can easily be introduced into the conceptual framework of the fully prognostic cloud scheme presented here. Unfortunately, a comprehensive data set covering a variety of cloud situations does not exist to date.

As an illustration for the use of more complex distribution functions the distribution shape as used by Smith (1990) will now be used to derive sources for cloud as above. Smith (1990) assumed a triangular distribution of a joint temperature and humidity variable to determine cloud fraction and cloud condensate content from prognostic equations for liquid water temperature and total water. Here, only the shape of this distribution will be used. It is assumed that in the clear-sky fraction of the grid box, the specific humidity is distributed as a symmetric triangular function around its mean value q_e , with the same boundaries as used above, i.e., q_s as the upper and $q_e - (q_s - q_e)$ as the lower boundary. Note, that these boundaries define the width of the distribution and are themselves defined by the initial cloud cover and the grid-mean specific humidity through (5.25). The change of q_s is again

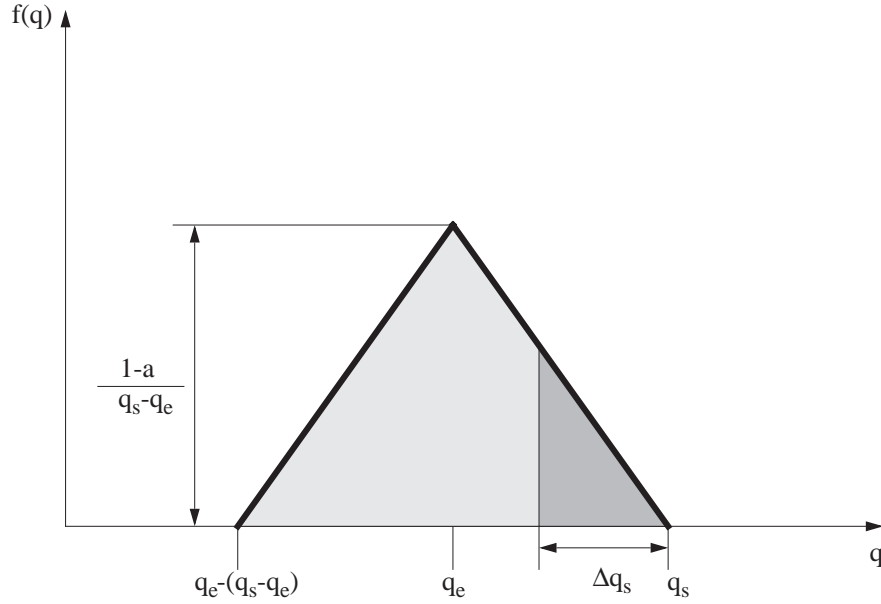


Figure 5.6: Probability distribution function of specific humidity in the cloud-free area of the grid box for a triangular distribution.

assumed to be homogeneously distributed within the grid box. A schematic picture of this situation is shown in Figure 5.6. The distribution function, $f(q)$, for this example can be written as

$$f(q) = \begin{cases} \frac{\alpha_{max}}{q_s^t - q_e^t} [q - (2q_e^t - q_s^t)] & \text{for } 2q_e^t - q_s^t \leq q \leq q_e^t \\ \frac{\alpha_{max}}{q_s^t - q_e^t} (q_s^t - q) & \text{for } q_e^t < q \leq q_s^t \end{cases} \quad (5.47)$$

where α_{max} is the maximum value of $f(q)$ which is reached at $q = q_e^t$. The value of α_{max} can be determined using (5.41). From this equation it follows that

$$\alpha_{max} = \frac{1 - a^t}{q_s^t - q_e^t}. \quad (5.48)$$

With this, the distribution function $f(q)$ is fully defined. All that is left now to determine source terms for cloud fraction and cloud condensate is to perform the integrations as in (5.44) and (5.46) using (5.47) as distribution function. The resulting source terms become

$$\Delta a = \frac{1 - a^t}{(q_s^t - q_e^t)^2} \left[\frac{\Delta q_s^2}{2} - H(q_e^t - q_s^{t+1})(q_e^t - q_s^{t+1})^2 \right], \quad (5.49)$$

and

$$\Delta l = -\frac{1}{3} \frac{1 - a^t}{(q_s^t - q_e^t)^2} \left[\frac{\Delta q_s^3}{2} - H(q_e^t - q_s^{t+1})(q_e^t - q_s^{t+1})^3 \right], \quad (5.50)$$

where $H(x)$ is the Heavyside function, defined as

$$H(x) = \begin{cases} 1 & x > 0 \\ 0 & x \leq 0 \end{cases}$$

It has been illustrated in this subsection, that consistent source terms for a cloud scheme that predicts both cloud fraction and cloud condensate using prognostic equations can be derived using assumptions about the distribution of specific humidity in the clear sky part of the grid box. The main question, whether it is this distribution that determines the cloud fraction evolution, remains unanswered. Intuitively it appears more likely that it is the subgrid-scale distribution of Δq_s , or in other words that of vertical velocity, that mainly determines which parts of the grid box experience cloud formation or decay. Work on converting this idea into the framework used here has not yet been carried out and should be pursued in the future.

5.3.5 Some thoughts on cloud decay

Before closing this chapter, it appears prudent to discuss the reverse problem of the above, namely the decay of clouds due to an increase in q_s brought about, e.g., by subsiding motion. In the cloud scheme originally proposed by Tiedtke (1993), it is assumed that the cloud condensate is homogeneous inside the cloudy area and that the change in q_s (i.e., the vertical motion and diabatic heating) are evenly distributed in the grid box. Those two assumptions automatically imply that processes that increase q_s change the cloud condensate in the same way at each point in the cloud, and therefore do not change the cloud fraction, until the entire cloud condensate has evaporated and the cloud disappears altogether. In other words, the processes mentioned lead to a thinning out of the cloud until its complete decay.

The issue of cloud inhomogeneity, i.e., the uneven distribution of condensate inside clouds, has received much attention recently, in particular by the radiation community (e.g., Cahalan, 1994; Barker, 1996; Barker et al., 1996; Tiedtke, 1996). This is so because the effects of those inhomogeneities on the radiative fluxes, in particular in the shortwave part of the spectrum, can be substantial. It needs to be pointed out here that if some form of distribution of cloud condensate was to be used in the radiative treatment of the model clouds, the assumptions made by Tiedtke (1993) about cloud dissipation can not hold anymore.

A simple example will be used here to illustrate the procedure that needs to be followed to derive sink terms for both cloud cover and cloud condensate in the presence of an inhomogeneous distribution of cloud condensate in the cloud. It is not surprising that this procedure is an almost exact copy of that for the cloud source terms used above. Again the simplest

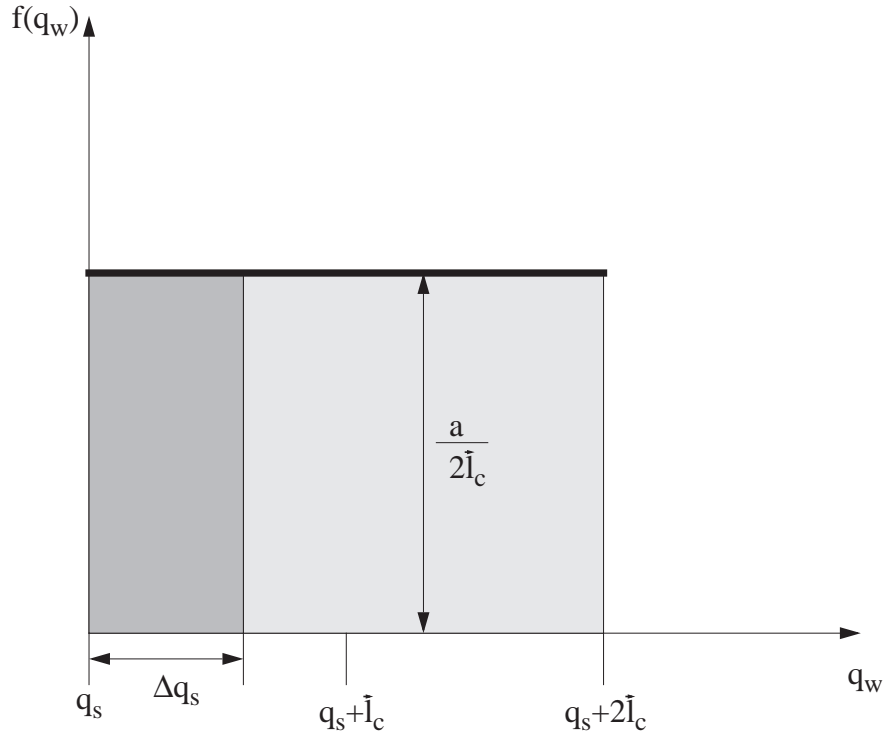


Figure 5.7: Probability distribution function of total water in the cloudy area of the grid box for a uniform distribution of cloud condensate.

distribution will be chosen to illustrate the method with minimum mathematical complexity. An extension to more complex distribution functions is straightforward. It is assumed that inside the cloud the cloud condensate is uniformly distributed between 0 and $2\bar{l}_c^t$ (Figure 5.7), where \bar{l}_c^t is again the in-cloud value for the condensate, i.e., $\bar{l}_c^t = l^t/a^t$. For the total water distribution, $f(q_w)$, this implies a uniform distribution of q_w inside the cloud between q_s^t and $q_s^t + 2\bar{l}_c^t$. Furthermore it is assumed that there is a homogeneous increase in q_s in the entire grid box. It is evident from Figure 5.7 that

$$a^t = \int_{q_s^t}^{q_s^t + 2\bar{l}_c^t} f(q_w) dq_w. \quad (5.51)$$

Since $f(q_w) = \text{const.}$ (5.51) can be used to evaluate $f(q_w)$ as

$$f(q_w) = \frac{a^t}{2\bar{l}_c^t}. \quad (5.52)$$

Furthermore from Figure 5.7 it can be seen that

$$a^{t+1} = \int_{q_s^{t+1}}^{q_s^{t+1} + 2\bar{l}_c^t} f(q_w) dq_w. \quad (5.53)$$

Subtracting (5.51) from (5.53) and substituting (5.52) gives the change in cloud fraction as a function of the change in q_s as

$$\Delta a = \int_{q_s^{t+1}}^{q_s^t} \frac{a^t}{2\bar{l}_c^t} dq_w = -\frac{a^t}{2\bar{l}_c^t} \Delta q_s, \quad (5.54)$$

with $\Delta q_s = q_s^{t+1} - q_s^t > 0$, which constitutes a sink term for cloud fraction given the above assumptions.

The derivation of the sink term for grid-mean condensate is slightly more complex. At time t the grid-mean condensate is defined by

$$l^t = \int_{q_s^t}^{q_s^t + 2\bar{l}_c^t} (q_w - q_s^t) f(q_w) dq_w, \quad (5.55)$$

which by using (5.52) reduces simply to $l^t = a^t \bar{l}_c^t$. The definition of l at time $t + 1$ can also be deduced from Figure 5.7 and is

$$l^{t+1} = \int_{q_s^{t+1}}^{q_s^{t+1} + 2\bar{l}_c^t} (q_w - q_s^{t+1}) f(q_w) dq_w, \quad (5.56)$$

which when solved for the given $f(q_w)$ is simplified to

$$l^{t+1} = a^t \bar{l}_c^t - a^t \Delta q_s - \frac{1}{2} \Delta a \Delta q_s. \quad (5.57)$$

The change in grid-mean condensate then becomes

$$\Delta l = l^{t+1} - l^t = -a^t \Delta q_s - \frac{1}{2} \Delta a \Delta q_s. \quad (5.58)$$

Note that (5.58) is exactly equivalent to the production term for grid-mean condensate derived in section 5.3.2. This does not come as a surprise, since exactly the same distributions for total water, q_w , have been used in the two derivations. The example shown here demonstrates that given a distribution function for condensate inside clouds, it is possible to derive consistent sink terms for cloud fraction and condensate. It is desirable that if such a distribution is assumed in certain parts of the model, such as in representing the radiative effects of clouds, it is also used in the source and sink derivation for the cloud equations, which can be more or less complex depending on the exact formulation of the distribution function itself.

Chapter 6

Cloud fraction and microphysics

6.1 Introduction

The development of cloud parametrizations that explicitly predict the amount of cloud condensate necessitates an increased sophistication in the description of microphysical processes. In diagnostic descriptions of clouds (e.g., Manabe et al., 1965) the generation of precipitation was simply achieved by precipitating out all condensate formed when removing supersaturation at the grid scale. The desire to “leave some condensate behind” as cloud demands at least a simple description of the manifold conversion processes from cloud to precipitation size particles, normally referred to as cloud microphysics. Many attempts to improve the description of these processes in GCMs have been reported on in the recent literature (e.g., Ghan and Easter, 1992; Bechthold et al., 1993; Fowler et al., 1996; Lohmann and Roeckner, 1996; Rotstayn, 1997).

One inherent difficulty in the description of cloud microphysics is that the processes take place on scales that are significantly smaller than GCM grid boxes. For many of the processes it is the local environment that determines parameters such as evaporation rates etc. An additional complication arises from the fact that most GCMs predict the occurrence of clouds over only part of their grid box using a cloud fraction parametrization of some form (e.g., Slingo, 1987; Sundqvist, 1988; Smith, 1990; Tiedtke, 1993; Rasch and Kristjansson, 1998). Cloud fraction parametrizations of this kind represent in a simple way the complex structure of cloud fields both in the horizontal and in the vertical. Figure 6.1 is a schematic of a distribution of clouds frequently encountered in tropical convective situations (e.g., Houze and Betts, 1981) where penetrating convective towers with their associated anvils and outflow cirrus coexist with shallow or medium convective clouds. One may ask if a cloud parametrization scheme should be able to resolve some of the variability shown in

Figure 6.1 by producing vertically varying cloud fraction and condensate.

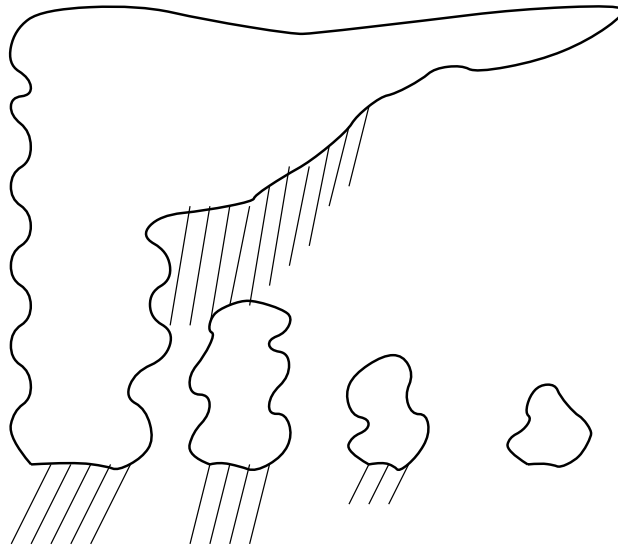


Figure 6.1: Schematic of a possible cloud distribution in the Tropics.

Vertical variations in cloud fraction and optical thickness influence the distribution of the radiative fluxes in the atmosphere. Radiation parametrization schemes account for this variability by introducing overlap assumptions (e.g., Geleyn and Hollingsworth, 1979; Morcrette and Fouquart, 1986), which determine the horizontal position of a 'cloud' at each model level relative to the clouds at other model levels. Yu et al. (1996) have used these overlap assumptions to divide model grid boxes into sub-columns when comparing model clouds to satellite observations. Stubenrauch et al. (1997) recently proposed an overlap scheme which creates blocks of cloud spanning several model levels in the vertical and then distributes the blocks in the horizontal following some overlap rules.

The effects of vertical variations of cloud fraction on the parametrization of microphysical processes have received far less attention than their radiative effects. For instance, if ice from a cirrus anvil falls into a cloud with supercooled liquid (as depicted in the leftmost low cloud in Figure 6.1), then the liquid may be converted to ice through the Bergeron process (e.g., Baker, 1997). Whether or not this occurs depends on whether the anvil ice falls into the lower cloud. Similarly evaporation of precipitation can only occur when precipitation falls into clear air. GCMs have shown a large sensitivity to the treatment of precipitation evaporation (e.g., Gregory, 1995) and it therefore appears to be desirable to treat the subgrid-scale nature of the evaporation process more carefully. Few studies have tried to account for such effects by determining a precipitation fraction (Rotstayn, 1997) or by adjusting microphysical parameters such as autoconversion rates and accretion rates in cases of vertically varying

cloud (Bechtold et al., 1993).

First in this chapter, the micro- and macrophysical impact of an explicit treatment of vertical variation of cloud fraction in the ECMWF cloud scheme (Tiedtke, 1993; Jakob, 1994; Chapter 3) is investigated. The technique applied is to divide each grid box horizontally at each level into a number, N , of smaller “sub-boxes”. Each of the sub-boxes is assigned to be either completely cloudy or completely clear depending on the cloud fraction predicted for the whole grid box by the cloud parametrization and on the cloud overlap assumption used by the radiation parametrization. This yields N vertical columns of sub-boxes with up to N different vertical distributions of cloud. The microphysics parametrization is then calculated separately for each column of sub-boxes. The relevant grid-mean quantities (e.g., precipitation fluxes, evaporation rates etc.) are computed by averaging over all sub-boxes. Comparison of the results to the original parametrization provides an indication of the subgrid-scale effects of cloud microphysics.

Having identified the major problem areas in the treatment of vertically-varying cloud fraction for microphysical calculations, the second part of the chapter will derive a simple parametrization to account for its effects. The basic idea is to divide the precipitation flux in each grid box into a cloudy and a clear-sky part and to describe the area coverage of each of the flux components and their overlap. Within the limits of current cloud overlap assumptions this approach solves the first-order problem of which part of the microphysical scheme to apply over which part of the grid box. It will be shown that the new parametrization captures most of the main features of the subgrid precipitation formulation derived in the first part of the chapter.

The main contents of this chapter is published in two articles in the Quarterly Journal of the Royal Meteorological Society (Jakob and Klein, 1999; Jakob and Klein, 2000) and the work has been carried out in collaboration with the co-author of these papers, Dr. S. A. Klein.

6.2 Cloud and precipitation overlap - The problem

As suggested by the schematic diagram in Figure 6.1, large vertical variations in cloud fraction can exist in nature over an area the size of a GCM grid box. Before investigating whether the representation of these effects in the ECMWF model is of importance, it is necessary to establish if the model produces significant vertical variations in cloud fraction. Figure 6.2 shows the zonal mean cloud distribution as a function of model level in the

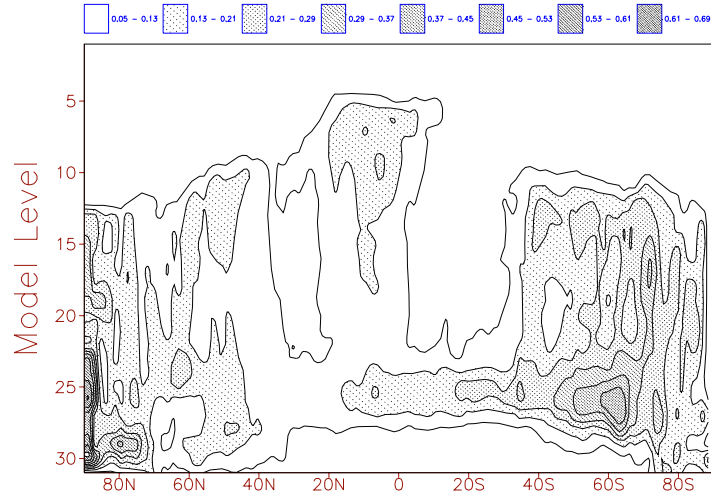


Figure 6.2: Zonal mean of cloud fraction in the ECMWF model for 1 July 1997, 12UTC. Altitude increases with decreasing model level number. The relation of the model levels to pressure is depicted in Figure 6.3.

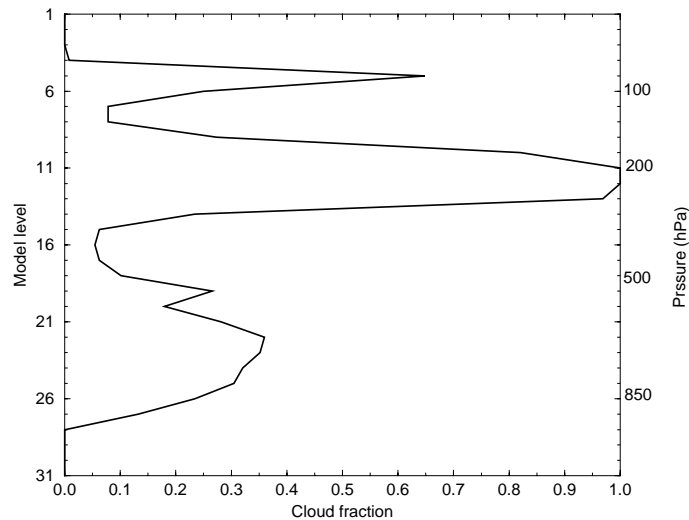


Figure 6.3: Vertical distribution of cloud fraction at a single point in the Tropics.

operational model for 1 July 1997, 12 UTC. Zonal mean cloud fraction varies substantially in the vertical in the model. However, in the zonal mean such a variation could be caused by the occurrence of clouds at different grid points in the horizontal and does not necessarily imply strong vertical variations at any given location. Figure 6.3 shows a cloud fraction

profile for a single point in the Tropics ($2^{\circ}N, 160^{\circ}E$) that was randomly chosen. It is evident that instantaneous local cloud fields produced by the ECMWF scheme can indeed have large vertical variations of cloud fraction. The cloud fields depicted in Figures 6.2 and 6.3 will form the basis of the investigations in the following subsections.

6.2.1 A subgrid-scale precipitation model

Bulk microphysical parametrizations (e.g., Hsie et al., 1980; Lin et al., 1983; Rutledge and Hobbs, 1983) describing the formation and evaporation of different precipitation species are typically formulated such that they are applicable on small scales in regions that are either totally clear or cloudy. Their application in large volumes such as a GCM grid box which can contain both cloudy and cloud free areas is therefore not straightforward. Several approaches to this problem have been proposed. The simplest approach is to ignore partial cloudiness and assume a cloud fraction of one whenever condensate occurs in a grid box (e.g., Fowler et al., 1996). Schemes that parametrize cloud fraction often use in microphysical calculations the in-cloud water content $l_c = l/a$ where l is the grid-mean water/ice content and a is the cloud fraction (Tiedtke, 1993). Until very recently (Bechthold et al., 1993; Tiedtke, 1993; Rotstayn, 1997), the rather obvious fact that partial cloud fraction yields precipitation that only covers a fraction of the grid box has been ignored.

In order to systematically assess the effects of partial cloudiness and partial precipitation coverage a subgrid-scale precipitation representation is developed. The basic idea is to subdivide each grid box into N sub-columns ($N = 20$ is used for most of this study) in which the cloud fraction is assigned to be zero or one at every model level. The microphysical parametrization is then applied to each of the sub-columns and the relevant grid-mean quantities (e.g., precipitation flux and evaporation rates) are calculated by summing up the values over all sub-columns. This is equivalent to an increased horizontal resolution for the microphysical calculations. A possible distribution of cloudy and clear sky sub-columns for the distribution of cloud fraction in Figure 6.3 is shown in Figure 6.4. To arrive at the distribution of cloudy and clear-sky sub-columns shown several assumptions were made, the details of which are explained below.

Firstly it is assumed that clouds completely fill the grid box in the vertical; i.e., the fraction of the grid volume that contains cloud is equal to the fraction of the horizontal area of a grid box that contains cloud. Although many clouds have thicknesses less than 500 meters (Wang and Rossow, 1995), this may not be too bad an approximation for the ECMWF model which

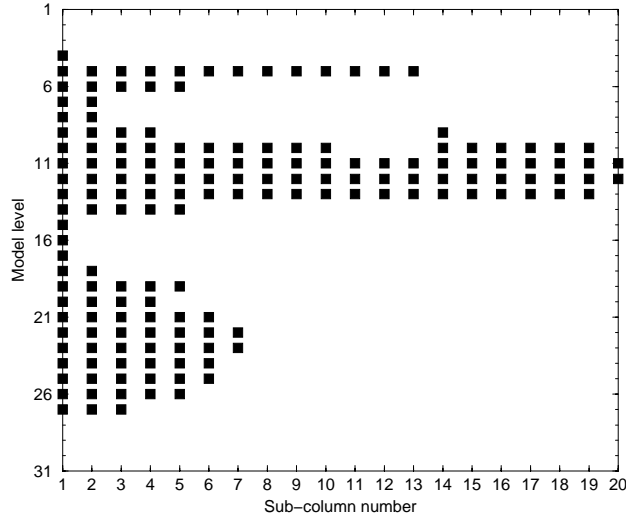


Figure 6.4: Arrangement of cloudy (black squares) and clear-sky columns for the cloud fraction profile in Figure 6.3 following the subgrid-scale algorithm.

has 31 to 60 levels in the vertical (see Chapter 3) with typical resolution of 40 hPa (about 400 to 700 m) in the troposphere.

Secondly, at each level the specification of which sub-columns contain cloud is entirely consistent with the cloud overlap assumption used for the subgrid-scale flux calculations in the radiation scheme. The overlap assumption currently used in the radiation scheme is that of maximum-random overlap (Geleyn and Hollingsworth, 1979; Morcrette and Fouquart, 1986; Section 3.2). It can be described using the following equation which specifies the total horizontal area, C^k , covered by clouds between the top of the atmosphere and a given model level k as :

$$\frac{1 - C^k}{1 - C^{k-1}} = \frac{1 - \max(a^{k-1}, a^k)}{1 - \min(a^{k-1}, 1 - \delta)}, \quad (6.1)$$

where a^k is the cloud fraction of level k , $\delta = 10^{-6}$, and $k = 1$ for the top model level. C^0 and a^0 are set to zero. This equation yields random overlap for clouds that do not occur in adjacent vertical levels but maximum overlap if clouds occur at adjacent levels with cloud fraction monotonically increasing or decreasing with height. This is broadly consistent with the data on cloud overlap of Tian and Curry (1989). At each level, the number of sub-columns that contain cloud is defined to be the nearest integer value of $20 \cdot a^k$.

The use of equation (6.1) provides a total cloud cover, C^k , by applying it from the model top to level k given the distribution of clouds layer by layer. However the knowledge of C^k and

a^k alone is not sufficient to unambiguously assign the distribution of cloudy sub-columns. In Figure 6.4 for instance it is obvious that C^k does not change below model level 11, where it reaches a value of 1. Hence, the five cloudy sub-columns in level 14, where $a^{14} \approx 0.25$, could be placed in any sub-box without violating (6.1). Therefore, two additional assumptions are made: i) in the spirit of maximum overlap for clouds in adjacent levels, clouds are assigned to those sub-columns, which contain cloud in the layer immediately above in preference to those sub-columns which do not contain cloud in the layer immediately above, but do have clouds higher in the same sub-column, and ii) the assignment of cloudy boxes begins from the sub-column furthest to the “left” that fulfills i). Since especially ii) is rather arbitrary, sensitivity tests to the placement of cloudy sub-columns will be carried out in a later subsection. The “left” assumption is used as the default assumption for the rest of this study because this is the cloud placement that is implicitly assumed in the current scheme (henceforth referred to as the T93 scheme as before).

The amount of liquid water and ice at each level is calculated over the mean cloudy area of the grid box as described in Tiedtke (1993). It must then be divided among the cloudy sub-columns at each level. For want of a better method, each cloudy sub-column is assigned the same amount of liquid water and ice assuming a constant in-cloud water/ice content defined as

$$l^k_{c,int} = \frac{l^k}{a^k_{int}}, \quad (6.2)$$

where l^k is the grid-mean liquid water/ice content and a^k_{int} is a rounded cloud fraction calculated as the fraction of sub-boxes at each level that contain cloud. It is necessary to use a rounded cloud fraction in the definition of $l^k_{c,int}$ in order to conserve water. After the allocation of the condensed water in the sub-columns, the same microphysical formulae used for the original model are applied to each sub-column separately. That is, for each sub-box, the generation and evaporation of precipitation is calculated at each level. Averaging over sub-columns yields grid-mean quantities (precipitation and evaporation rates) that can be compared to the T93 parametrization. In all calculations a homogeneous distribution of temperature at the beginning of the microphysical calculations is assumed, i.e. each sub-column has the same temperature initially. Through melting and evaporation of precipitation the temperature will change differently in each sub-column. The new grid-mean temperature is calculated from the grid-mean melting and evaporation rates that are calculated by averaging over their values in the individual sub-columns.

In applying the microphysical formulae to the sub-columns, two changes are necessary. The first change is to the melting of snow. In the current model, the amount of melting is limited such that the whole grid box would be cooled back to the freezing temperature over a time scale $\tau = 5h$, even if precipitation covers only a small fraction of the grid box. For the subgrid-scale precipitation model, the amount of melting is limited such that only the sub-column in which melting occurs can be cooled to the freezing temperature. This implies that if the fraction of the grid box covered by precipitation is less than unity, the energy available for melting is smaller in the subgrid-scale precipitation parametrization than in T93. The main effect of this difference is to spread melting further in the vertical.

The second change is to the evaporation of precipitation. The formula for evaporation of precipitation (Equation 3.31) depends in part on the humidity of the air into which the precipitation is evaporating. Instead of using the grid-mean humidity in the formula as is done in the current parametrization, an estimate of the humidity of the clear portion of the grid box is calculated using the cloud fraction and the grid-mean humidity. Assuming that the temperature inside the cloud is the same as the grid-mean temperature, the grid-mean specific humidity (q_v) is the sum of the saturation value at the grid-mean temperature (q_s) in the cloudy portion of the grid and a mean clear sky value humidity (q_v^{clr}):

$$q_v = a q_s + (1 - a) q_v^{clr} \quad (6.3)$$

To calculate the evaporation of precipitation in the subgrid-scale precipitation model it is assumed that each cloud-free sub-column has a value of specific humidity equal to the value of q_v^{clr} which satisfies (6.3).

In implementing the subgrid-scale precipitation model, special treatment was given to those grid boxes which have a cloud fraction less than one-half of the size of a sub-column (i.e., $a^k < 0.025$ for a model with 20 sub-columns). Normally, the rounding of cloud fraction to the nearest sub-column would assign all sub-columns as clear sky and no precipitation could be generated from clouds with these small cloud fractions. In order to avoid problems of that nature, it is required that if the cloud fraction is greater than zero then at least one sub-box in layer k must be filled with cloud. Water conservation in this case is ensured by redistributing the water quantities over the whole sub-box.

It is worthwhile pointing out that the distribution of the cloudy columns in Figure 6.4 should not be interpreted as a spatially contiguous distribution. Shifting all columns randomly, treating each one as a whole in the vertical, will by construction not change the results of

the simulation since each column is treated as an independent quantity. It is therefore better to think of the distribution of the cloudy columns as a probability state given the set of rules outlined above.

6.2.2 Comparison of the subgrid-scale precipitation model with the original scheme

Single grid point simulations

Both the subgrid-scale precipitation model and the current model are used to simulate the precipitation processes at a single grid point. To assess the direct effects of the subgrid model on precipitation related processes only the first timestep of the integration is considered, with all other physical processes switched off. Hence, the simulation is entirely governed by the initial profiles of cloud cover, cloud water/ice, humidity and the thermodynamic variables. The profiles used are those of the tropical case in Figure 6.3. The initial profile of grid-mean cloud water/ice is shown in Figure 6.5. The timestep used is 15 minutes which is a typical value used in ECMWF's T213L31 model.

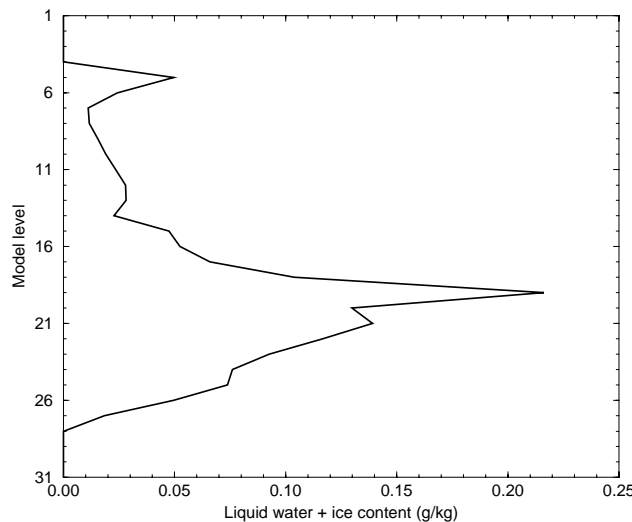


Figure 6.5: Vertical distribution of cloud liquid water plus ice in the single column model profile shown in Figure 6.3.

The aim of the study is to assess the impact of variations in cloud fraction on cloud microphysics. For this purpose the subgrid model can be regarded as a higher resolution model, which yields more accurate values of precipitation. The current parametrization should

approximate the subgrid model results if it were to properly account for the subgrid-scale variability of cloud and precipitation. Many factors, including a poor microphysical formulation itself, may cause the results of the subgrid model to be far from reality, but only the differences between the two simulations are of interest for the sensitivity study which is the purpose of this work.

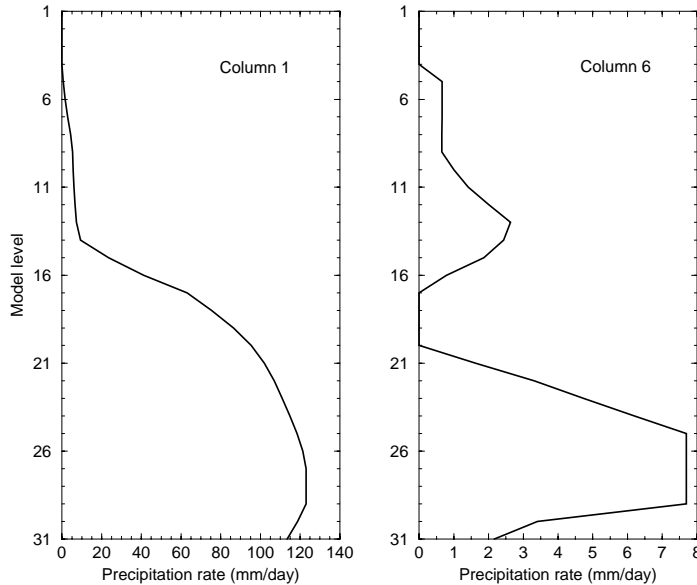


Figure 6.6: Vertical distribution of precipitation in sub-columns one (left panel) and six (right panel) of the subgrid precipitation model. The values refer to precipitation leaving the base of a given model level.

Using the distribution of cloudy and clear-sky sub-columns shown in Figure 6.4 the microphysical part of the cloud scheme is integrated separately for each of the sub-columns. A large variation is found in the precipitation fluxes between the different sub-columns. For example, Figure 6.6 shows the vertical distribution of precipitation for sub-columns one and six. Sub-column one, by construction, contains the maximum number of cloudy levels. Hence, precipitation falls through clouds from model level 5 down to model level 27, leading to large amounts of accretion and no evaporation above cloud base. As a consequence the precipitation rate reaches a maximum of more than 120 mm/day just above cloud base. In contrast sub-column six contains three cloud layers, extending over one, four and five model levels respectively, separated by layers of clear sky. Precipitation forms first in model level 5. Although levels 6 through 9 contain unsaturated air, the precipitation rate remains constant until the next cloudy layer (model level 10). No sublimation occurs between levels 6 and 9 because the T93 scheme assumes that precipitation cannot evaporate when the relative humidity exceeds a critical value of 80 %. After leaving the base of the second cloud layer

evaporation of precipitation results in the total depletion of the precipitation at level 17 so that no precipitation reaches the lowest cloud layer with its top at level 21. This is an example of the importance of the mechanism of collection of cloud condensate by precipitation. In this case no precipitation reaches the low cloud from above so that only the local warm-phase microphysics is important for the development of the lowest cloud layer. The precipitation reaching the surface in this sub-column (slightly more than 2 mm/day) is entirely due to conversion processes in the lowest cloud layer and has been reduced by evaporation in the sub-cloud layer.

By counting the sub-columns that contain precipitation at each level it is possible to derive the fraction of the grid box covered by precipitation (from now on referred to as precipitation fraction, a_P). This parameter is used in several ways in existing parametrization schemes (Bechthold et al., 1993; Tiedtke, 1993; Rotstayn, 1997). For example the evaporation of precipitation in model level k in the T93 parametrization is described as

$$E_P^k = \max(a_P^k - a^k, 0) \cdot 5.44 \cdot 10^{-4} (q_s^k - q^k) \left[(\sigma^k)^{\frac{1}{2}} \frac{1}{5.9 \cdot 10^{-3}} \frac{P^k}{a_P^k} \right]^{0.577}, \quad (6.4)$$

with $(a_P^k - a^k)$ representing the cloud-free area in which precipitation can evaporate and $\sigma^k = p^k/p_s$, where p_s is the surface pressure. The precipitation fraction, a_P^k , appears twice in this equation. Firstly it is used to calculate the area over which evaporation can occur as $a_P^k - a^k$ assuming maximum overlap between precipitation and cloud. Secondly it determines the ‘‘local’’ precipitation rate in the area that contains precipitation as P^k/a_P^k , where P^k is the grid-mean precipitation rate. The T93 parametrization contains a description of a_P^k which can be expressed as

$$a_P^k = \max \left\{ a_P^{k-1}, \left[\frac{a^k \Delta P + a_P^{k-1} P^{k-1}}{\Delta P + P^{k-1}} \right] \right\}, \quad (6.5)$$

where a_P^{k-1} is the area covered by precipitation leaving the level above and is thus the area covered by precipitation entering level k . P^{k-1} is the amount of precipitation leaving level $k-1$, ΔP is the amount of precipitation generated in level k , and a^k is the cloud fraction at level k . Evaporation of precipitation does not alter a_P , except when precipitation evaporates completely.

Figure 6.7 compares the precipitation fraction diagnosed from the subgrid model with that given by (6.5). The parametrization following (6.5) does not correctly capture the vertical distribution of a_P . There are two major differences; in the anvil region (model level 11 to

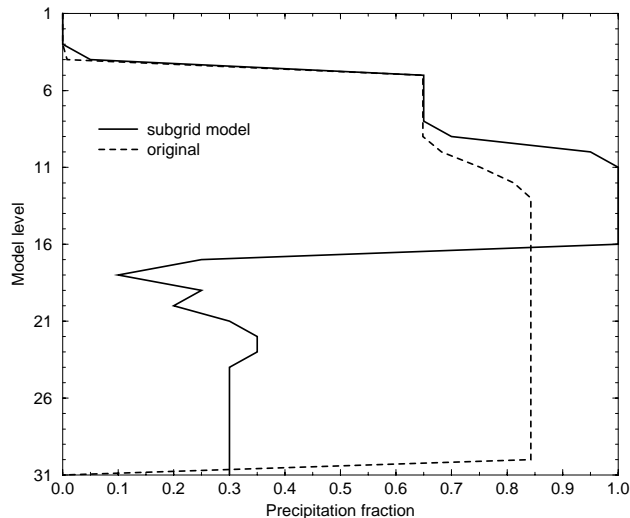


Figure 6.7: Precipitation fraction as simulated by the subgrid precipitation model (solid) and the T93 scheme (dashed). The values refer to the fraction covered by precipitation at the bottom of a given model level.

16), the precipitation fraction is underestimated by (6.5) whereas below those levels it is considerably overestimated. The reasons for these differences lie in the construction of (6.5). In this parametrization, a_P^k is determined as a weighted average of the precipitation fraction of level $k - 1$ and the cloud fraction in level k , where the weights are the precipitation flux in layer $k - 1$ and the change in precipitation flux due to microphysical processes in layer k . This weighting was introduced to prevent levels that do not contribute to precipitation from being contributors to a_P . In the example shown, this parametrization underestimates a_P in the anvil part since the precipitation added to the flux in that part (ΔP) is not large enough compared to the incoming flux from above (P) to increase the precipitation fraction to the correct value of 1. However, as is shown below, a more important difference is the overestimation of a_P below level 16. This difference results from the maximum statement in (6.5), which prevents a reduction in a_P unless all precipitation evaporates. This impacts the evaporation of precipitation, since the area over which precipitation is allowed to evaporate is defined as $a_P^k - a^k$.

Figure 6.8 compares the grid-mean evaporation rates of the subgrid and the T93 model. The grid-mean values for the sub-column model are calculated by averaging over the values of the individual sub-columns. As expected, large differences exist in the middle troposphere with a strong overestimation of evaporation by the original scheme. The most likely explanation

of this difference is that an overestimation of a_P overestimates the amount of precipitation available for evaporation. To test whether this is the major source of the difference, the simulation of the original scheme is repeated with the precipitation fraction prescribed to be that diagnosed from the subgrid precipitation model. The results are shown in Figure 6.8 (dot-dashed curve). At least in this case, the overestimation of a_P causes most of the large differences in evaporation of precipitation in the middle troposphere. However, there are still major differences such as that at model level 16.

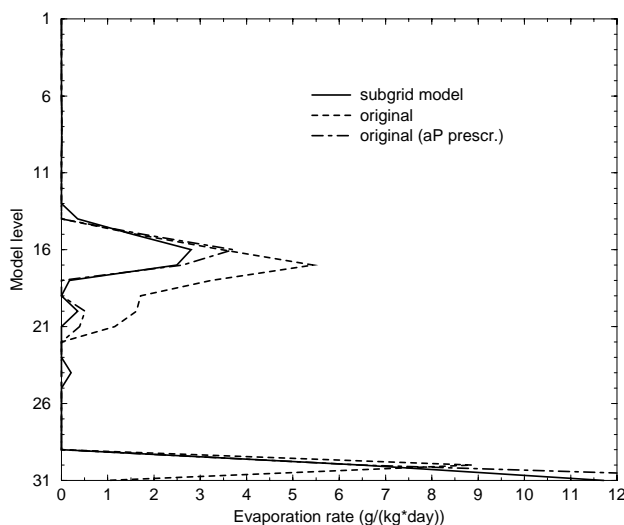


Figure 6.8: Evaporation rate as simulated by the subgrid precipitation model (solid), the T93 scheme (dashed), and the T93 scheme with prescribed a_P (dot-dashed).

It is worthwhile investigating the cause for this difference, since model level 16 is the only level where the “true” a_P is much larger than the cloud fraction, so that a significant area of the grid box is subject to evaporation of precipitation. Because the formula for evaporation depends on the local precipitation rate in the volume undergoing evaporation of precipitation, an overestimation of evaporation could result from an overestimation of the precipitation rate in this volume. Figure 6.9 shows the distribution of the precipitation rate in model level 16 for the subgrid model and the T93 scheme with prescribed a_P , just before the parametrization of evaporation is calculated. Since $a^{16} \approx 0.07$, only the first sub-column is assumed to be cloudy while $a_P^{16} = 1$. It is evident that for most of the sub-columns undergoing evaporation (columns 2 through 20) the precipitation rate before evaporation (solid curve) is lower than the mean precipitation rate given by the T93 scheme with prescribed a_P (dashed curve). In

fact, excluding the sub-column with the largest precipitation rate (column 1), which is not subject to evaporation since it is cloudy, the average precipitation rate of the subgrid model is 5.8 mm/day as compared to 7.9 mm/day for the T93 model. This difference directly contributes to the difference in evaporation rate at level 16. This suggests a very important error source in the T93 parametrization even with a perfect simulation of a_P^k , namely that the local precipitation rate in the region undergoing evaporation maybe significantly less than the grid-mean precipitation flux divided by the precipitation fraction. Using only a grid-averaged precipitation flux implies averaging the flux inside the cloud, where it increases downward due to conversion and accretion, with that outside the cloud which decreases downwards due to evaporation. This averaging leads to an artificial horizontal transport of precipitation from the generally larger values inside cloud to the generally smaller values outside cloud and thereby to the observed overestimation of evaporation. This problem will tend to occur at all cloudy levels with precipitation and $a_P^k > a^k$.

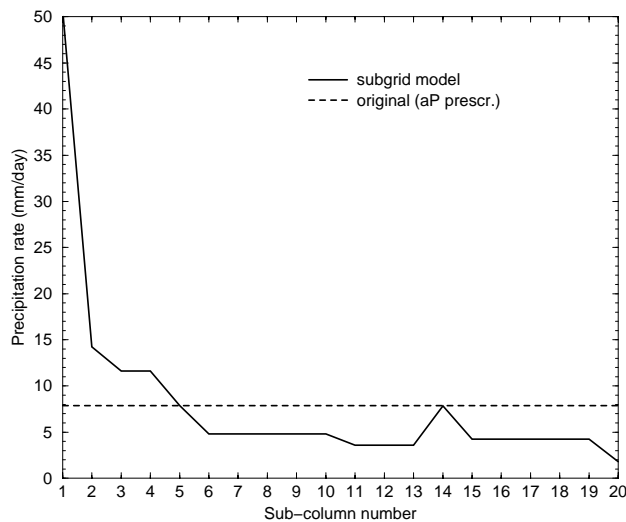


Figure 6.9: Precipitation rate at the top of model level 16 as simulated by the subgrid precipitation model (solid) and the T93 scheme with prescribed a_P (dashed).

Figure 6.10 compares the grid-mean precipitation flux for the same simulations as in Figure 6.8. Large differences between the subgrid and the T93 model begin at level 16 and increase downwards. The precipitation reaching the surface and hence the net latent heating of the column differ by more than 8 mm/day with no precipitation at all reaching the surface in the original scheme. Forcing the precipitation fraction to be that diagnosed from the subgrid model alleviates most of the discrepancies except near level 16.

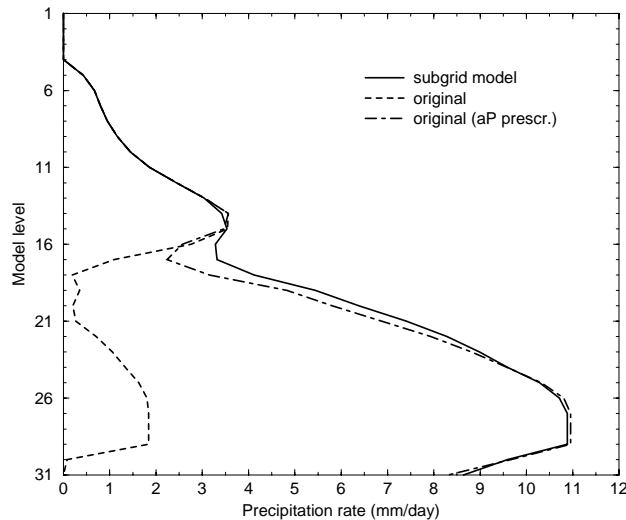


Figure 6.10: Precipitation rate as simulated by the subgrid precipitation model (solid), the T93 scheme (dashed), and the T93 scheme with prescribed a_P (dot-dashed).

Global model

Several errors in the parametrization of microphysical processes that result from improperly accounting for the subgrid-scale distribution of cloud and precipitation have been identified for a single case. To assess the generality of these results, the global ECMWF model is integrated for one timestep ($\Delta t = 60 \text{ min}$) at spectral resolution T63. The reason for using only one timestep is again to establish the direct effect of the subgrid model on the model physics without allowing feedbacks to occur. The precipitation fraction, evaporation rate, and precipitation rate are compared using the subgrid precipitation model and the current T93 for the initial conditions of the ECMWF operational model at 12UTC on 1 July 1997. The initial distribution of cloud fraction for this time was shown in Figure 6.2.

Figure 6.11 compares the zonal mean of the precipitation fraction as analysed from the simulation with the subgrid model to that of the T93 scheme. The differences between the two models are large with the most significant differences occurring in the Tropics. Similar to the single column case, the T93 scheme underestimates high level a_P , but largely overestimates midlevel a_P . The differences in the extratropical regions are smaller, although the subgrid model yields a smaller a_P in the middle troposphere. In the extratropics one could speculate that vertically varying cloud fraction plays a smaller role because cloud fraction is more uniform, e.g. in frontal cloud systems.

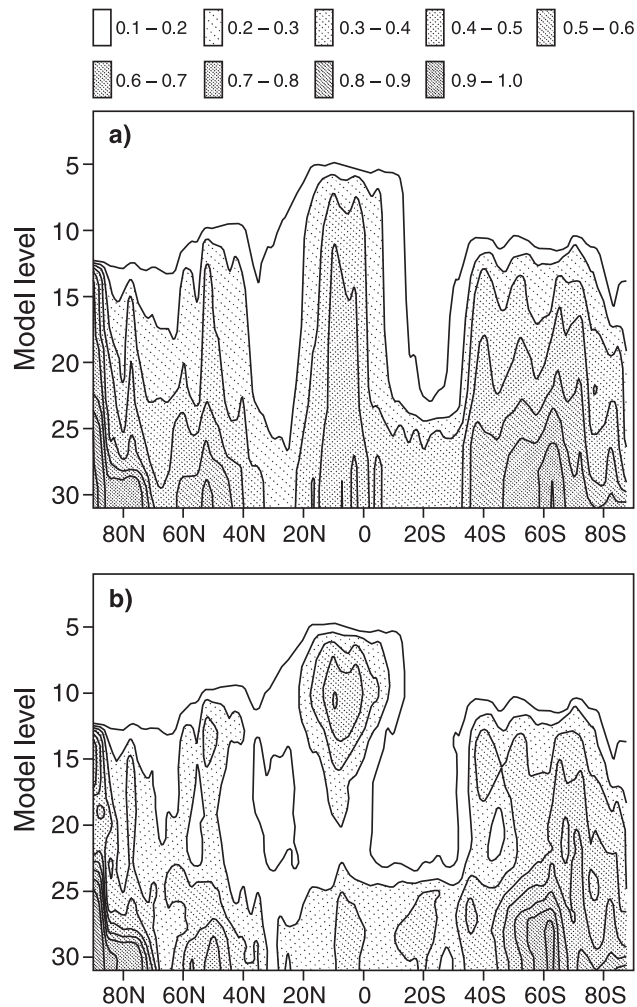


Figure 6.11: Zonal mean of precipitation fraction for the first timestep of a T63L31 integration with the global model for 1 July 1997, 12UTC. Top: T93, bottom: Subgrid model.

With errors in a_p similar to those in the single column simulation, similar errors in the grid-mean evaporation and precipitation rates can also be expected for the global model. Figure 6.12 shows the zonal mean of the grid-mean evaporation rate for both the T93 and the subgrid model, and Figure 6.13 the zonal mean surface large-scale precipitation. The strong overestimation of evaporation in the middle troposphere in the Tropics is evident and leads to a difference of up to 1.5 mm/day in zonal mean large-scale precipitation, equivalent to more than 40 W/m^2 of latent heat release.

Table 6.1 summarizes the global mean values for some of the components of the hydrological cycle for the first timestep. Starting from the same initial liquid water/ice content (0.126 mm) both models generate about the same amount of precipitation ($\approx 2.65 \text{ mm/day}$). However, the evaporation rate for the subgrid model is about 20 % smaller than that of the

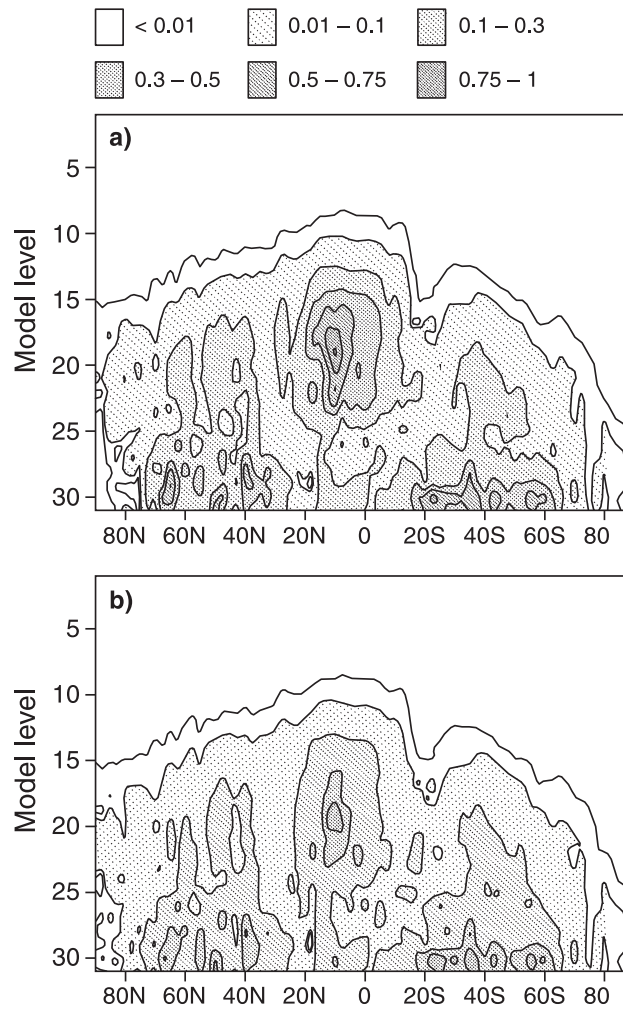


Figure 6.12: Zonal mean of evaporation rate in $g/(kg \cdot day)$ for the first timestep of a T63L31 integration with the global model for 1 July 1997, 12UTC. Top: T93, bottom: Subgrid model.

T93 model leading to about 0.2 mm/day more large-scale precipitation. Since the difference in the net latent heat release due to large-scale precipitation constitutes an extra forcing for the model it will certainly affect the full model simulation. As this study concentrates on the direct physical effects of vertically varying cloud fraction, a discussion of the effects on the model climate is beyond its scope and will be carried out elsewhere.

	T93	Subgrid
Liquid water/ice content (mm)	0.126	0.126
Formation of precipitation (mm/day)	2.67	2.65
Evaporation of precipitation (mm/day)	0.99	0.78
Surface precipitation (mm/day)	1.68	1.87

Table 6.1: Global means for components of the hydrological cycle (large-scale only) for the first timestep of a T63L31 integration with the subgrid precipitation model and the T93 scheme

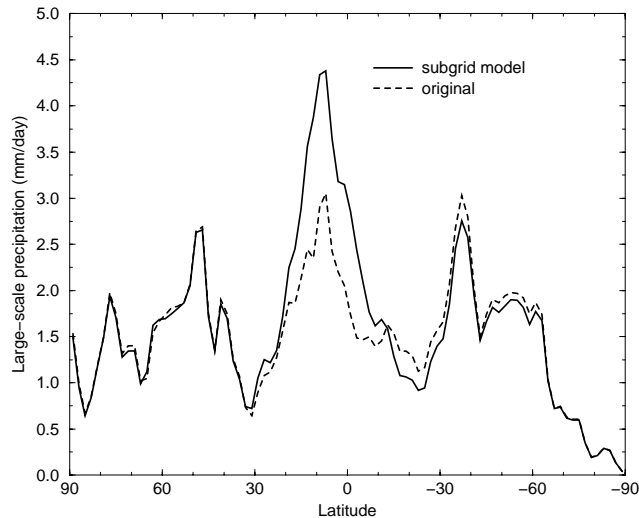


Figure 6.13: Zonal mean large-scale precipitation rate at the surface for the first timestep of a T63L31 integration with the subgrid precipitation model (solid) and the T93 scheme (dashed).

Sensitivities

Before ascribing differences between the T93 scheme and the subgrid model to "errors" in parametrization, it is necessary to establish that the results of the subgrid model are not sensitive to arbitrary assumptions in the construction of the model. The two main assumptions that might influence the results are the placement of cloudy boxes and the number of subgrid columns used.

As already mentioned in section 6.2.1 the horizontal distribution of the columns in Figure 6.4 should not be interpreted as a spatial distribution. In fact if all the columns were redistributed randomly the result of the precipitation calculations would not change at all. It is therefore more appropriate to consider the distribution of the columns as a probability distribution rather than a spatial one. One of the constraints for the distribution is the cloud overlap assumption for the grid box. This determines how many of the cloudy sub-boxes in a model level need to be placed in columns containing clouds in at least one of the higher levels in the column, and how many in columns that contain clear sky in all higher levels of the column. However, as explained above, the exact placement within each of these two groups (referred to as "cloud under cloud" and "cloud under clear sky") is ambiguous. The distribution shown in Figure 6.4 and used so far in the study is built by assigning higher probabilities to certain columns to be cloudy. For instance, in the case of cloud under cloud,

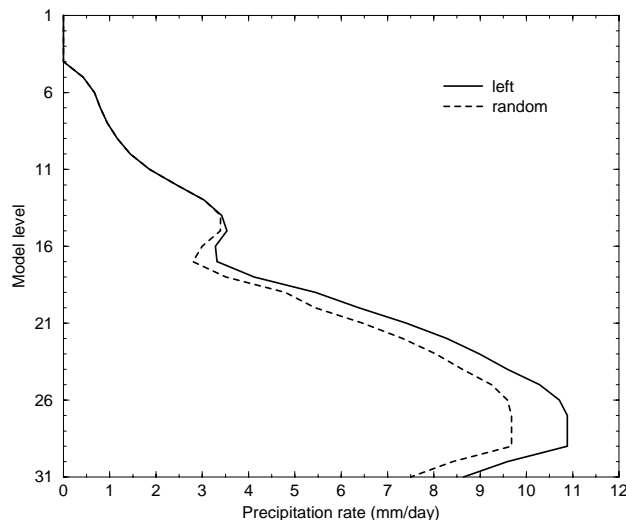


Figure 6.14: Precipitation rate as simulated by the subgrid precipitation model with “left” (solid) and “random” (dashed) cloud placement. Both simulations assume the same maximum-random cloud overlap assumption.

cloudy boxes are preferentially placed in columns that contain cloud in the layer immediately above. Furthermore for each of the two groups, the probability is artificially a function of the column index, because boxes are filled preferentially from the “left” (Figure 6.4). In order to study the impact of these assumptions on the grid-mean results, these preferences are removed and new clouds are placed randomly within each group. Note, however that the maximum-random cloud overlap assumption for the grid box as a whole as expressed in (6.1) is retained. The precipitation rate for the one-timestep integration in the tropics differs between these two column placement options (for convenience named left and random) by about 1 mm/day (Figure 6.14). The smaller precipitation rates in the random case result from smaller accretion rates caused by the removal of the “tower” of cloud that exists in the “left” placement case in column 1 (Figure 6.4). However, the differences are much smaller than those to the T93 parametrization (cf. Figure 6.10). The global model results (not shown) confirm the results of the single column simulation.

Another important sensitivity test is whether the results of the subgrid model depend on the number of sub-columns used. Since the subgrid model rounds the actual model cloud fraction to a multiple of the sub-column size, which is obviously a function of the number of columns used, it is desirable to use as many sub-columns as possible, to minimize rounding errors. However, if one expects the model cloud fraction to be accurate to not more than 0.05 than

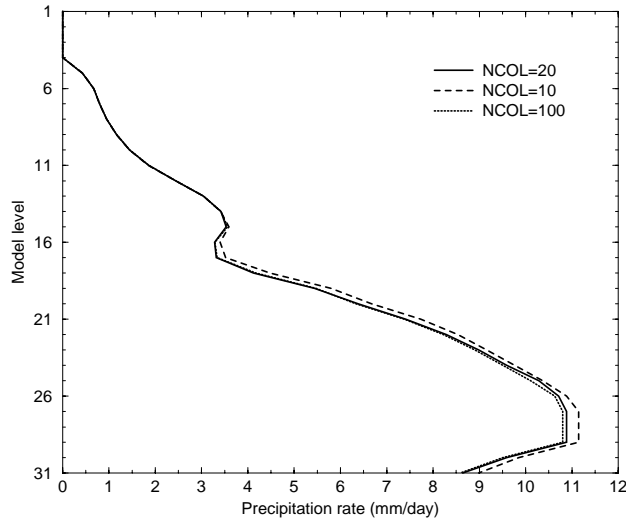


Figure 6.15: Precipitation rate as simulated by the subgrid precipitation model using 20 (solid), 10 (dashed) and 100 (dotted) sub-columns.

the use of say 100 sub-columns would not be sensible. Figure 6.15 shows the precipitation rate for the one-timestep integration in the Tropics using 10, 20 (default) and 100 sub-columns in the subgrid precipitation model. The differences between these simulations are smaller than the differences between simulations with different box placement (Figure 6.14) and certainly much smaller than the differences between the subgrid model and the T93 scheme (Figure 6.10). These results are confirmed by the global model experiment (not shown).

The use of different values for specific humidity in the calculations of precipitation evaporation (q_v in T93 and q_v^{clr} in the subgrid model) might also contribute to the differences shown. Therefore the single-column calculations were repeated using q_v in the subgrid model and q_v^{clr} in the T93 scheme. The results (not shown) indicate little sensitivity to the choice of specific humidity for the subgrid model and increased evaporation rates in the T93 parametrization leading to even larger discrepancies between the two simulations. The different behaviour of the two schemes can be explained by their very different simulation of precipitation fraction. In case of the subgrid model, the precipitation fraction decreases rapidly below the anvil so that evaporation of precipitation cannot occur at all or in only few sub-columns. Hence the small sensitivity of this scheme to the choice of specific humidity. In contrast the T93 parametrization creates large areas of evaporation below the anvil because of its overestimation of precipitation fraction. Hence changing the specific humidity used in the evaporation

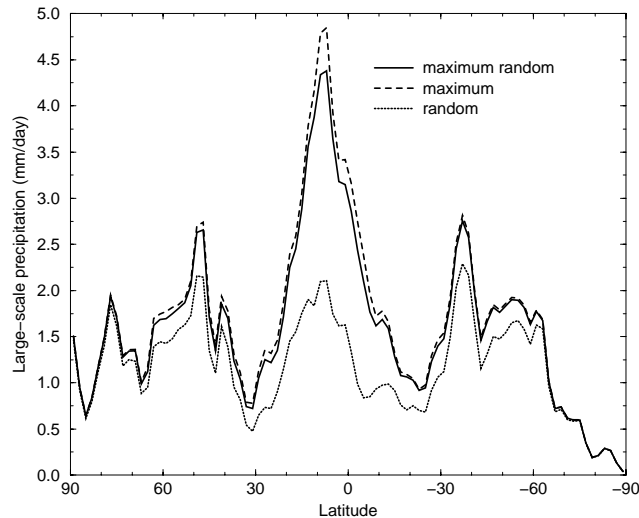


Figure 6.16: Zonal mean large-scale precipitation rate for the first timestep of a T63L31 integration with the subgrid precipitation model using maximum-random (solid), maximum (dashed), and random (dotted) cloud overlap.

calculations exerts a larger influence.

So far all sensitivity tests used the maximum-random overlap cloud overlap assumption of the current model. Altering this assumption will indicate what role the cloud overlap assumption will play when using a more complex treatment of vertically varying cloud fraction. It should be noted that since the T93 parametrization uses maximum-random overlap for clouds (and implicitly assumes a maximum overlap of cloud with precipitation), a comparison of the T93 scheme with the results of the subgrid model with a different overlap assumption is not appropriate. Hence, the main purpose of this test is to establish the sensitivity of the subgrid scheme (and hopefully parametrized cloud microphysics as well) to the cloud overlap assumption. Figure 6.16 shows the zonal mean precipitation of three one-timestep integrations of the global model using the subgrid precipitation scheme with maximum-random, maximum and random overlap. All integrations use the default method (“left”) to place cloudy boxes. It is evident, that a large difference exists between random overlap and the other two overlap assumptions. The reason for the large reduction in precipitation when using random overlap is the horizontal “spreading out” of the cloud, which leads to higher evaporation and lower accretion rates. The implications of this result are discussed below.

6.2.3 Summary and discussion

A subgrid precipitation model was developed to assess the performance of the 1993 ECMWF stratiform precipitation scheme in the presence of vertically varying cloud fraction. The basic idea of the subgrid scheme is to divide the model grid box into several sub-columns and, after distributing the parametrized cloud such that each column is either cloudy or clear sky, to solve the microphysics part of the parametrization for each column separately. Extensive comparisons between the sub-grid model and current parametrization have been carried out in the context of one-timestep experiments for both the single column model and the global model. The use of one-timestep simulations has been preferred to longer model integrations in order to understand the direct implications of the different treatment of cloudiness variations in the vertical.

The comparison revealed two important shortcomings of the T93 parametrization:

- There is an erroneous simulation of precipitation fraction.
- Large truncation errors are introduced by averaging the precipitation flux over the whole precipitation area. This average results from the assumption that the local precipitation rate equals the grid-mean precipitation rate divided by the precipitation fraction.

The main effect of these errors has been found to be an overestimate of evaporation, a process to which GCM parametrization are known to be very sensitive. A generalization of these results to other parametrization schemes is difficult, since little is revealed in the literature about the details of the treatment of cloud and precipitation overlap when parametrizing stratiform precipitation in connection with cloud fraction. An exception is the study of Rotstayn (1997), which addresses the first item on the list above. However, to the authors' knowledge, there is no parametrization that attempts to address the second item above, which can be equally important once a good parametrization of the precipitation fraction has been found.

Several sensitivity studies were carried out to estimate the impact of assumptions used in the construction of the subgrid model. Little sensitivity has been found to the number of sub-columns used as long as the number is large enough to avoid large rounding errors. A number greater than ten appears sufficient in the ECMWF model. A slightly larger sensitivity exists to the way the sub-columns are filled with cloud once the general cloud overlap assumption

has been enforced. Although larger than the sensitivity to the number of sub-columns the differences are small compared to those with the original parametrization introducing some confidence in the findings of the comparison.

However, a large sensitivity has been found to the general overlap assumption. A change from maximum-random to random overlap leads to a dramatic decrease of the stratiform precipitation rate over the whole globe. This is not surprising since the random overlap assumption maximizes the spreading out of the clouds in the grid box thereby reducing the accretion rate and increasing the evaporation rate. It is necessary to stress again that this large sensitivity does not invalidate the general results of the study, since the current parametrization uses a maximum-random overlap of clouds and therefore cannot be sensibly compared to a subgrid scheme that uses a different cloud overlap scheme. However, the large sensitivity stresses the need for improved knowledge on the best way of overlapping clouds when introducing a treatment of vertically varying cloud fraction, not only into the radiation, but also into the microphysics parametrization. It is also noteworthy that given the relatively high vertical resolution of the ECMWF model (around 40 hPa in the free troposphere) the random overlap assumption does not seem appropriate.

In the light of the current tendency to improve microphysical parametrizations in large-scale models by introducing more and more complex bulk microphysical schemes, the results here suggest that great care has to be taken when addressing the fact that modern cloud parametrizations can produce large variations in cloud fraction in the vertical. A balance between the sophistication of the cloud microphysics and the sophistication of the cloud macrophysics (e.g. cloud and precipitation fractions and their overlaps) would seem to be prudent.

A necessary step is, of course, the validation of the vertical cloud variation produced by the parametrization. Little is known about the performance of cloud schemes for GCMs in that respect although a recent first study by Mace et al. (1998a), which compares model clouds to radar observations at the model's vertical resolution on an hourly time scale, shows encouraging results for the ECMWF model. However, the study is limited to cloud occurrence statistics at one location and in one season and therefore does not cover the variety of cloud situations encountered globally.

There is a variety of possible applications of the subgrid model developed for this study. The most obvious is its direct implementation into a GCM, but this might not be practical because of the extra calculations introduced by the multiple integrations of the mi-

crophysics parametrization. Adding the subgrid model with 20 sub-columns to a T63L31 4 month integration of the ECMWF model increased the CPU time by about 10 %. One can speculate that this increase will be even larger when more sophisticated microphysical parametrizations are used. Nevertheless the subgrid model can provide guidance in the development of a parametrization of the effects discussed. The results above indicate that such a parametrization has to contain at least two components: a treatment of precipitation fraction and a treatment that avoids the averaging of the precipitation flux over the whole precipitation area, for instance by introducing separate clear-sky and cloudy precipitation fluxes. A parametrization using the results here will be described in the next section of this chapter.

Other applications of the subgrid model include the testing of the radiation parametrization in terms of its treatment of vertically varying cloud fraction, given a fixed overlap assumption (Liang and Wang, 1997). Developing suitable methods of treating cloud inhomogeneity (e.g., Tiedtke, 1996) using the subgrid model for guidance appears to be a potential application also. There is no doubt that with the improvements in cloud parametrization over the last decade, more thought has to and will be given to the role of variations of cloud within one grid column and the subgrid model presented here can be used in the development of appropriate parametrizations of their effects.

6.3 Cloud and precipitation overlap - A parametrization

The previous section has established the importance of a careful treatment of cloud fraction in the microphysical parametrization schemes in large-scale models. It has been shown that a minimum requirement for a successful introduction of the effects of vertically varying cloud fraction in such a parametrization is the description of the area fraction covered by precipitation within a model grid box and the relaxation of the assumption of a single grid-mean value for the precipitation flux. In the following subsections a simple parametrization scheme for the above overlap effects will be derived and tested. The basic idea of the scheme is the separation of clear and cloudy sky precipitation fluxes and the description of their respective area fraction. First the new scheme will be described and its design will be compared to the current formulation. This will be followed by an extensive comparison of the performance of the parametrization to the subgrid model described above. Having

established the superiority of the new parametrization over the current one the new scheme will be used in seasonal simulations with the ECMWF model to establish its effect on the model climate. A brief discussion will end the chapter.

6.3.1 Description of the stratiform precipitation parametrization

Within large-scale models, stratiform precipitation is usually treated diagnostically such that the vertical divergence of the downward flux of precipitation is balanced by the microphysical sources (e.g. precipitation formation) and sinks (e.g. precipitation evaporation) (e.g., Heymsfield and Donner, 1990; Ghan and Easter 1992):

$$g \frac{\partial}{\partial p} (\rho l_P V_P) = S_P, \quad (6.6)$$

In (6.6), l_P is the specific humidity of precipitation condensate, V_P is the mass-weighted fall speed of the precipitation mass, and S_P is the time rate of change of precipitation mass due to microphysical sources and sinks, with units of *kg condensate (kg air)⁻¹s⁻¹*. Other symbols have their traditional meaning. Equation (6.6) ignores the time tendency of precipitation condensate. This assumption is reasonable given that the time for precipitation to reach the surface is often considerably less than the timestep of the parametrized microphysics. From this equation, the downward flux of precipitation mass P at a given pressure p is the vertical integral of the sources and sinks of precipitation at all higher levels:

$$P(p) \equiv \rho l_P V_P = \frac{1}{g} \int_0^p S_P dp'. \quad (6.7)$$

Original parametrization

In T93, the downward precipitation flux is represented by a single mean value for the grid cell,

$$\bar{P} \equiv \frac{1}{A} \int P dA, \quad (6.8)$$

where A is the area covered by the grid cell. The fractional area of the grid cell in which the precipitation rate is greater than zero is denoted

$$a_P \equiv \frac{1}{A} \int H(P) dA, \quad (6.9)$$

where $H(x)$ is a unit step function defined to be 1 if $x > 0$, and zero otherwise. Within the area a_P , the parametrization implicitly assumes that the local value of the precipitation rate, P , is uniformly equal to \bar{P}/a_P .

The fractional area covered by precipitation at the bottom of a model level, k , is given by:

$$a_{P,k} = \max \left\{ a_{P,k-1}, \frac{a_k \Delta \bar{P}_k + a_{P,k-1} \bar{P}_{k-1}}{\Delta \bar{P}_k + \bar{P}_{k-1}} \right\}, \quad (6.10)$$

where

$$\Delta \bar{P}_k \equiv \frac{1}{A} \int \left(\frac{1}{g} \int_{p_t}^{p_b} S_P \cdot H(S_P) dp' \right) dA \quad (6.11)$$

is the increase in \bar{P} due to the microphysical sources of precipitation (e.g. autoconversion, accretion, ice-settling, etc.) from the pressure at the top of the grid cell, p_t , to the pressure at the base of the grid cell, p_b . The index of the model levels, k , is assumed to increase downwards. The second option of the maximum operator in (6.10) is a weighted average of the cloud fraction at level k , a_k , and the precipitation area at the top of the grid cell, $a_{P,k-1}$, where the weights are the fraction of the precipitation at the base of level k that originated from level k and the fraction of the precipitation at the base of level k that originated from higher levels, respectively. By weighting the precipitation source by a_k , T93 implicitly assumes that the whole area of the cloud contributes to the precipitation source. Note that T93 assumes that clouds fill the vertical extent of a grid cell completely such that the fraction of the volume which contains clouds is equal to the fraction of the area which contains clouds. As discussed in the previous section, the maximum operator prevents $a_{P,k}$ from decreasing when (6.10) is solved from the model top to the surface. Only in the case that all of the precipitation evaporates at a particular level does $a_{P,k}$ return to zero. In determining precipitation evaporation, the fractional area over which precipitation is evaporating is assumed to be $\max(0, a_{P,k} - a_k)$. This assumes a maximum overlap between the area containing stratiform precipitation and the cloudy area. The local value of the precipitation rate in the area where precipitation is evaporating is assumed to be $(\Delta \bar{P}_k + \bar{P}_{k-1})/a_{P,k}$. Note that precipitation generated at level k may evaporate at the same level if $a_{P,k-1} > a_k$; this is inconsistent with the assumption that where it occurs, cloudy air completely fills the vertical extent of the grid cell.

New parametrization

The main difference between the new and old parametrization is that the precipitation flux is represented by mean values for the cloudy and clear portions of the grid cell (see Figure 6.17). That is, the grid-mean precipitation flux in cloudy areas is defined by:

$$P^{cld} \equiv \frac{1}{A} \int P \cdot H(l) dA, \quad (6.12)$$

where the step function marks the portion of the grid cell containing cloud with a condensate specific humidity l . The fractional area which contains the cloudy precipitation flux is denoted by

$$a_P^{cld} \equiv \frac{1}{A} \int H(l) H(P) dA. \quad (6.13)$$

Within the area containing the cloudy precipitation flux, the local precipitation rate, P , is assumed to be uniform with the value P^{cld}/a_P^{cld} . Similarly the grid cell mean precipitation flux in clear areas and the fractional area containing precipitation flux in clear areas are:

$$P^{clr} \equiv \frac{1}{A} \int P \cdot (1 - H(l)) dA, \quad (6.14)$$

and

$$a_P^{clr} \equiv \frac{1}{A} \int (1 - H(l)) H(P) dA \quad (6.15)$$

respectively. Within the area containing the clear precipitation flux, the local precipitation rate, P , is assumed to be uniform with the value P^{clr}/a_P^{clr} . With these definitions, $\bar{P} = P^{cld} + P^{clr}$ and $a_P = a_P^{cld} + a_P^{clr}$.

The method to determine a_P^{cld} and a_P^{clr} is as follows. If precipitation is generated at a particular level through the processes of autoconversion or ice sedimentation, it is assumed to be generated in the cloud uniformly and thus at the base of level k , $a_{P,k}^{cld} = a_k$. The precipitation generated in this cloudy region is given by:

$$\Delta P_k^{cld} \equiv \frac{1}{A} \int \left(\frac{1}{g} \int_{p_t}^{p_b} S_P \cdot H(l) dp' \right) dA, \quad (6.16)$$

and the cloudy precipitation flux at the base of level k is given by $P_k^{cld} = \tilde{P}_k^{cld} + \Delta P_k^{cld}$, where the tilde symbol indicates the value of P^{cld} at the top of level k . Because the cloud is assumed to be internally homogenous, (6.16) simplifies to

$$\Delta P_k^{cl d} = a_k S_P^{cl d} \frac{(p_b - p_t)}{g}, \quad (6.17)$$

where $S_P^{cl d}$ is the generation rate of precipitation inside the cloud. If only accretion occurs in the clouds at level k , $a_{P,k}^{cl d}$ equals $\tilde{a}_{P,k}^{cl d}$, the fractional area that contains cloudy precipitation flux at the top of level k .

Because the clear-sky precipitation flux is assumed to be horizontally uniform, evaporation does not alter the area containing clear-sky precipitation flux such that $a_{P,k}^{cl r} = \tilde{a}_{P,k}^{cl r}$. Only in the case that all of the clear-sky precipitation flux evaporates in level k does $a_{P,k}^{cl r} = 0$. The clear-sky precipitation flux at the base of level k is given by $P_k^{cl r} = \tilde{P}_k^{cl r} + \Delta P_k^{cl r}$, where $\tilde{P}_k^{cl r}$ is the clear-sky precipitation flux at the top of level k , and

$$\Delta P_k^{cl r} = \frac{1}{A} \int \left(\frac{1}{g} \int_{p_t}^{p_b} S_P \cdot (1 - H(l)) dp' \right) dA = \tilde{a}_{P,k}^{cl r} S_P^{cl r} \frac{(p_b - p_t)}{g}, \quad (6.18)$$

where $S_P < 0$ indicates precipitation evaporation. Note that in the new parametrization, precipitation evaporation is a function of $\tilde{P}_k^{cl r}$ guaranteeing that precipitation generated at a level cannot evaporate in the same level. This will ensure consistency with the assumption that, where present, clouds fill the vertical extent of the grid cell and that horizontal transfer of precipitation mass from cloudy to clear regions of the grid cell is not possible.

At the interfaces between levels, precipitation mass that is in cloud at the upper level may fall into clear air at the lower level, or precipitation mass that is in clear air at the upper level may fall into cloud at the lower level. Thus at level interfaces an algorithm is needed to transfer precipitation and its area between the cloudy and clear portions of the grid box. The algorithm is constructed by determining the fractional area associated with each transfer and then transferring precipitation fluxes between clear and cloudy components according to the assumption that the precipitation flux is horizontally uniform, but with different values in the clear and cloudy regions containing precipitation.

At level interfaces, there are four possible areas to be defined (Figure 6.17): the area in which cloudy precipitation flux falls into cloud at the lower level, the area in which cloudy precipitation flux falls into clear air at the lower level, the area in which clear-sky precipitation flux falls into clear air at the lower level, and the area in which clear-sky precipitation flux falls into cloud at the lower level. To determine these areas, the cloud overlap assumption is applied to determine the relative horizontal location of clouds in the upper and lower levels. The cloud overlap assumption for the ECMWF model was introduced in equation

(6.1). This equation yields maximum overlap for clouds in adjacent levels and random overlap for clouds separated by clear levels. From this equation, one can determine the portion of clouds of the lower level that is not overlapped by clouds at all higher levels; this area, $\Delta C = C_k - C_{k-1}$, cannot have any precipitation falling into it. Using this assumption, the area for which cloudy precipitation flux falls into clear air at the level below is given by

$$\Delta a_{P,cl\rightarrow clr} = a_{P,k-1}^{cl} - \min(a_k - \Delta C, a_{P,k-1}^{cl}). \quad (6.19)$$

Equation (6.19) makes the further assumption that there is maximum overlap between the area covered by cloudy precipitation at the base of the upper level and the portion of the lower level cloud which lies beneath clouds in higher levels, $a_k - \Delta C$. With the assumption that the precipitation flux is horizontally uniform, the amount of cloudy precipitation flux at the upper level that falls into clear air at the level below is

$$\Delta P_{cl\rightarrow clr} = \frac{\Delta a_{P,cl\rightarrow clr}}{a_{P,k-1}^{cl}} \cdot P_{k-1}^{cl}. \quad (6.20)$$

The area in which clear-sky precipitation flux of the upper level falls into cloud at the level below is

$$\Delta a_{P,clr\rightarrow cl} = \max(0, \min(a_{P,k-1}^{clr}, a_k - \Delta C - a_{k-1})), \quad (6.21)$$

which assumes maximum overlap between the portion of the cloud at the lower level k which has cloud at some higher level other than $k - 1$, and the area covered by the clear precipitation flux. Again, with the assumption that the precipitation flux is horizontally uniform, the amount of clear-sky precipitation flux from the upper level that falls into cloud at the level below is

$$\Delta P_{clr\rightarrow cl} = \frac{\Delta a_{P,clr\rightarrow cl}}{a_{P,k-1}^{clr}} \cdot P_{k-1}^{clr}. \quad (6.22)$$

Finally, the areas and fluxes at the top of level k can be related to those at the base of level $k - 1$ by

$$\tilde{a}_{P,k}^{cl} = a_{P,k-1}^{cl} + \Delta a_{P,clr\rightarrow cl} - \Delta a_{P,cl\rightarrow clr}, \quad (6.23)$$

$$\tilde{a}_{P,k}^{clr} = a_{P,k-1}^{clr} - \Delta a_{P,clr\rightarrow cl} + \Delta a_{P,cl\rightarrow clr}, \quad (6.24)$$

$$\tilde{P}_k^{cld} = P_{k-1}^{cld} + \Delta P_{clr \rightarrow cld} - \Delta P_{cld \rightarrow clr}, \quad (6.25)$$

$$\tilde{P}_k^{clr} = P_{k-1}^{clr} - \Delta P_{clr \rightarrow cld} + \Delta P_{cld \rightarrow clr}. \quad (6.26)$$

From these equations it is clear that the total precipitation area, $a_P^{cld} + a_P^{clr}$, and the precipitation flux, $P^{cld} + P^{clr}$, are conserved at level interfaces.

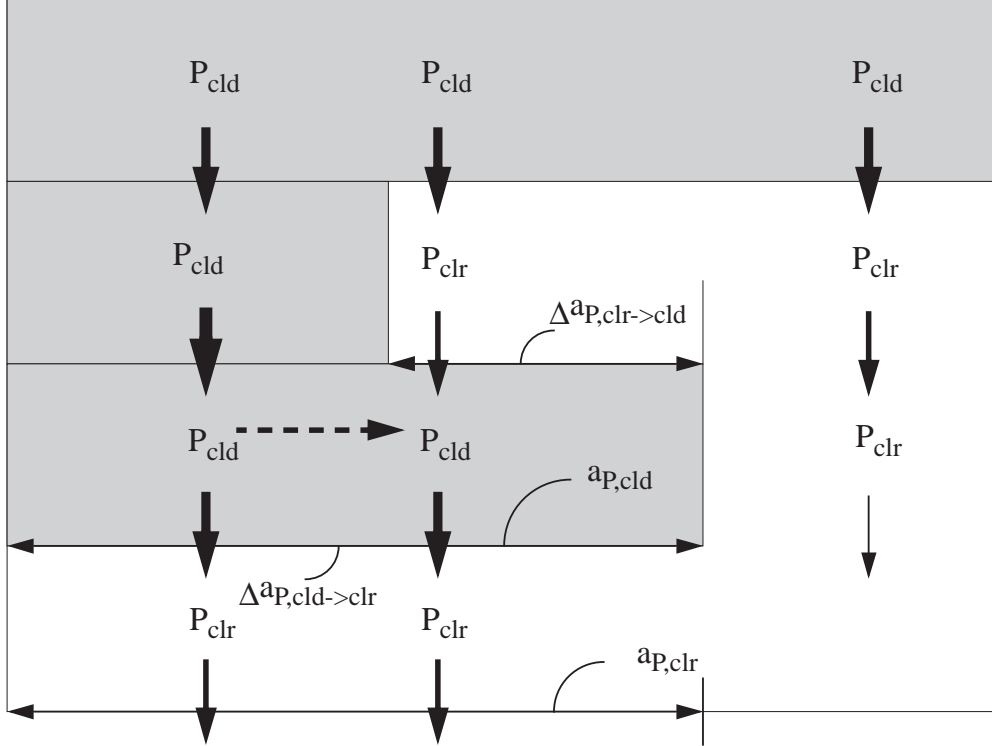


Figure 6.17: Schematic of the new parametrization scheme. For a detailed explanation see text.

Figure 6.17 shows a schematic of the new scheme with some examples of the areas and transitions outlined above. Shown are four model layers with the grey areas indicating clouds. The arrows represent the precipitation fluxes in clouds (P_{cld}) and clear sky (P_{clr}). The width of the arrows indicates the magnitude of the flux. All precipitation starts in clouds in the top layer. Part of it is then converted into clear-sky precipitation when falling into the next layer. The precipitation in cloud is enhanced whereas the clear-sky part is reduced by evaporation. Three distinct areas exist at the interface between the second and third layer. A cloud-to-cloud transition, a clear sky to cloud transition and a clear sky to clear sky transition. Since the precipitation in the cloudy part of the third layer originates partly in cloudy sky and partly in clear sky above, an implied horizontal flux (indicated by

the dashed arrow) exists due to the averaging of the two incoming contributions into one cloudy flux. This is one of the remaining shortcomings of the new scheme whose effect will be outlined in the next subsection. In the part of the grid box that is clear sky at all levels below the first, evaporation leads to the complete removal of precipitation when reaching the bottom of the lowest level, so that clear-sky precipitation only exists underneath the part of the grid box that has cloud in more than one layer. With this concept in mind the next section will evaluate the new parametrization using the subgrid precipitation model developed above (from hereon referred to as JK99 model for brevity) as a reference.

6.3.2 Comparison of the parametrization to the subgrid-scale model

The two main reasons for developing the above parametrization were i) the failure of the current parametrization to predict the correct area coverage of precipitation and ii) the inadequacy of the use of a single flux of precipitation to describe the microphysically different regimes inside and outside clouds. Both lead to an overestimation of evaporation of precipitation when compared to the subgrid precipitation model developed above. Although the results given by this model might be far from the truth due to inadequacies in the prediction of the cloud fields and in the actual microphysical formulations, the model has been used only to examine the effects of vertical cloud fraction variations on precipitation microphysics for a fixed set of cloud and microphysical parameterizations. As such, it is valid to test the behaviour of the new parametrization described above against this model which resolves the horizontal rates and area covered by stratiform precipitation. In this section the results of the current and the new parametrization of cloud and precipitation overlap will be compared against the subgrid model. The approach taken above to concentrate on single timestep experiments performed with both the single-column version and the full ECMWF model will be followed. This way feedback processes cannot occur and the results indicate the direct physical effect of the parameterizations. The initial conditions used for the experiments are identical to those in section 6.2 (see Figures 6.2 and 6.3).

Single column model

Figure 6.18 shows the fractional area of a grid box that is covered with precipitation as predicted by the JK99 subgrid model, by the T93 parametrization and by the new parametrization. It is evident that the new parametrization yields results that are very close to the

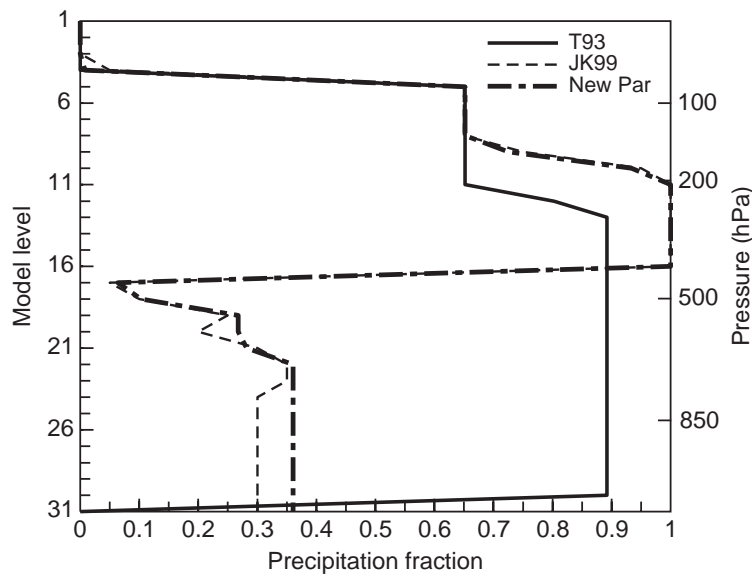


Figure 6.18: Precipitation fraction at a single tropical point as predicted in a single timestep by the T93 parametrization (solid), the JK99 subgrid model (dashed) and the new parametrization (dot-dashed).

subgrid model. In fact from model level 1 to 19 the differences are entirely due to the rounding applied in the JK99 model which assumes cloud cover to change in steps of 0.05. The discrepancies below that level are still very small, but are the result of the new formulation and will be discussed below.

As shown above the correct prediction of the precipitation fraction is a necessary, but not sufficient condition to correctly account for cloud overlap effects on microphysical processes. The key quantities that ultimately determine the latent heat release and its vertical distribution in the GCM grid box are the grid-mean evaporation and precipitation rate. These quantities are shown for the three precipitation schemes in Figure 6.19. The top panel shows the vertical distribution of evaporation rate. As for precipitation fraction, the agreement between the JK99 model and the new parametrization is excellent from the model top to model level 19, whereas the T93 scheme overestimates evaporation in model levels 16 and below. The main reasons for this overestimation have been identified in section 6.2.2 as the overestimation of precipitation fraction (see Figure 6.18) and the use of a single (grid-mean) flux in all microphysics calculations. The new parametrization, although distinguishing between clear-sky and cloudy precipitation flux, still averages at the bottom of each level within these two categories. This, as a consequence of the vertical distribution of cloud fraction (Figure 6.3), leads to the strong overestimation of evaporation evident in Figure 6.19 (top panel) in model level 20. A large cloudy precipitation flux builds up in the very small fraction that is

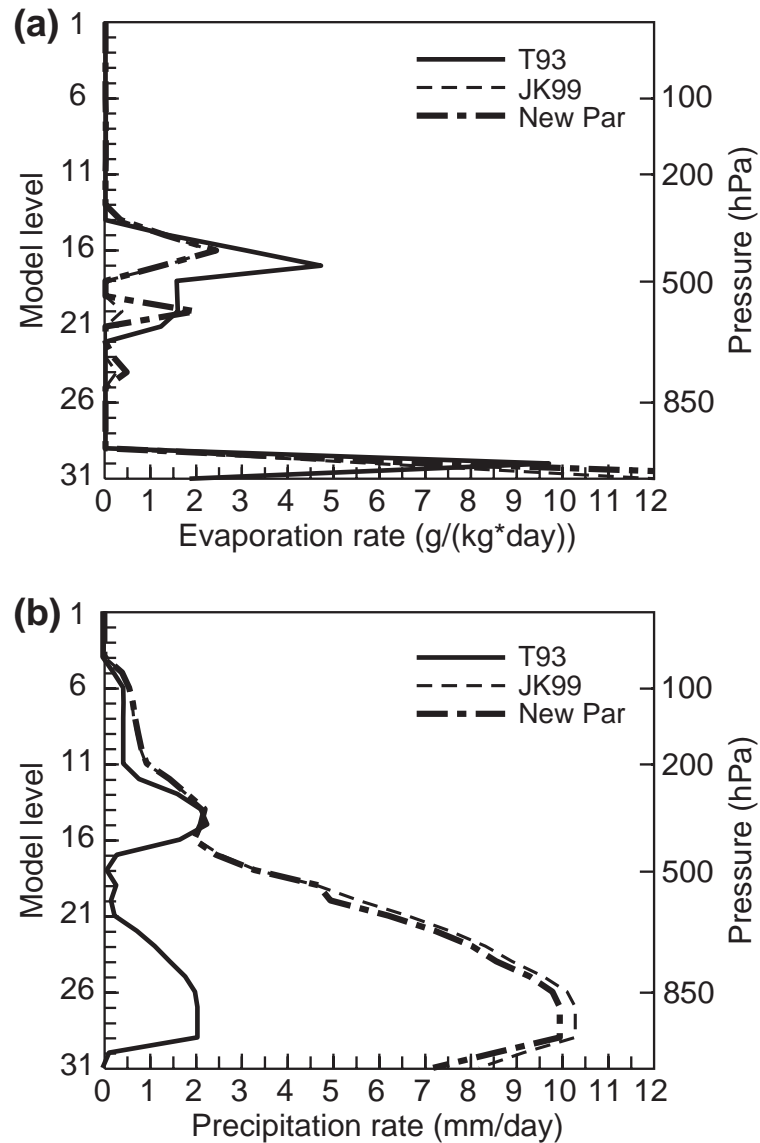


Figure 6.19: Grid-mean evaporation rate (top) and precipitation rate (bottom) as predicted in a single timestep by the T93 parametrization (solid), the JK99 subgrid model (dashed) and the new parametrization (dot-dashed).

cloudy from cloud top (model level 5) to the base of level 18. In model level 19, this large flux is (wrongly) spread out (averaged) over the larger cloud fraction in that level. Due to a reduction in cloud fraction in the next level below (model level 20) this large flux is partly made available for evaporation in that level. In the more accurate JK99 subgrid model this "spreading out" does not occur, so that here only the precipitation generated in model level 19 itself is available for evaporation leading to much smaller evaporation rates. Also note that the overestimation of precipitation evaporation in levels 23 and 24 results from the same error in parameterization.

The effect of the overestimated evaporation is also seen in the grid-mean precipitation flux (Figure 6.19, bottom panel), for which the new parametrization agrees extremely well with the JK99 model down to level 19. Below that the precipitation flux is underestimated. The differences are, however, considerably smaller than between the T93 parametrization and the JK99 model.

Despite the obvious limitations of the new parametrization as outlined above, the major shortcomings of the T93 scheme for the single column case are largely alleviated.

Global model

Although the single column model results give an indication of how a parametrization change affects the model results, the cases chosen may have a limited representativeness. It is therefore necessary to assess the performance of the schemes in the full global model. Figures 6.20 and 6.21 show the zonal mean distribution of precipitation fraction and evaporation rate as predicted by the three schemes for the first timestep of a T63L31 version of the ECMWF global model.

The largest difference in the prediction of precipitation fraction between the T93 (top panel) and the JK99 (middle panel) models occurs in the tropics. Here the T93 scheme shows a monotonic increase in precipitation fraction from the cloud top to the surface. The reasons for this increase are discussed above. In contrast the new parametrization (bottom panel) represents the "true" distribution of precipitation fraction as given by the JK99 model very well. There is a slight overestimation of precipitation fraction (about 10 %) in the upper tropical troposphere which is most probably caused by averaging problems similar to those described in the previous section, but this time for clear sky.

As expected from the single column results the T93 scheme overestimates the evaporation of precipitation in the tropical mid-troposphere (by up to a factor of two in the zonal mean). The new parametrization constitutes a major improvement. There is, however, a residual overestimate of evaporation of precipitation, indicating that the single column case and the problems therein are typical for the tropics.

In the extratropics the new parametrization improves the representation of precipitation fraction. However, there are only small effects on evaporation, which is already in good agreement for the T93 scheme. It can be speculated that this better agreement is due to much smaller vertical variations in cloud cover in these regions and hence a smaller influence of the new parametrization.

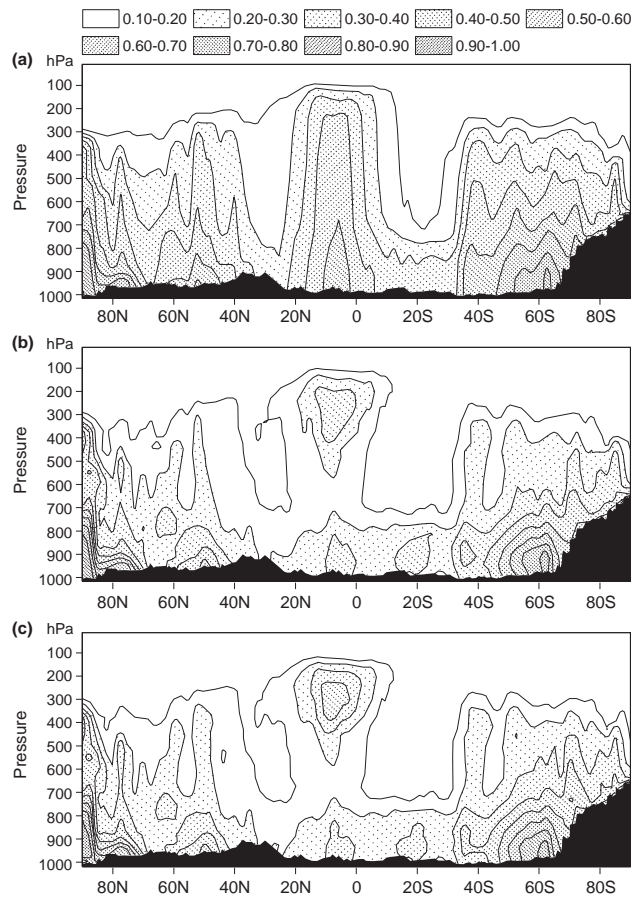


Figure 6.20: Precipitation fraction as predicted in a single timestep by the T93 parametrization (top), the JK99 subgrid model (middle) and the new parametrization (bottom).

Finally, Figure 6.22 presents the zonal mean distribution of large-scale precipitation (i.e., precipitation produced by the schemes discussed here). As expected from the previous figures the T93 scheme strongly underestimates precipitation at the surface in the tropics. This major problem of the T93 scheme is removed when applying the new precipitation scheme.

In summary the new parametrization, although still exhibiting some easily understandable problems, captures the main effects of the vertical variation of cloud fraction on the parametrized precipitation fluxes as identified by the subgrid model.

6.3.3 The influence of the new parametrization on the model climate

The previous section has demonstrated that the new parametrization significantly alters the behaviour of the large-scale precipitation generation and dissipation terms of the ECMWF model. In this section the influence of those changes on the model climate will be investi-

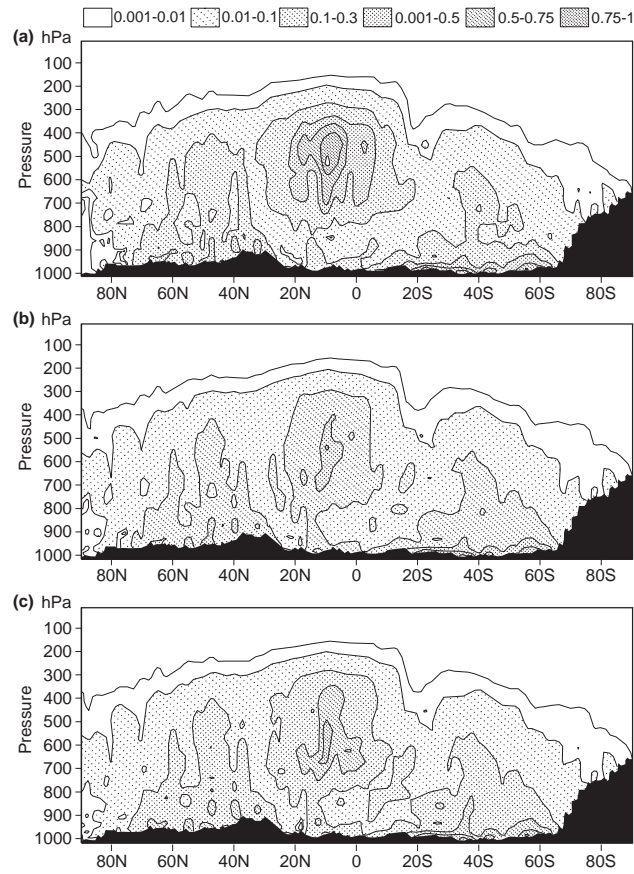


Figure 6.21: Evaporation rate ($\text{g}/(\text{kg} \cdot \text{day})$) as predicted in a single timestep by the T93 parametrization (top), the JK99 subgrid model (middle) and the new parametrization (bottom).

gated. For that purpose the model was integrated for 4 months at spectral resolution T63 using 31 model levels in the vertical. The initial dates chosen are 26 April 1987, 1 May 1987, 5 May 1987, 27 October 1987, 1 November 1987, and 6 November 1987. Initial conditions were taken from ECMWF reanalysis fields. The sea surface temperatures (SSTs) were prescribed. The spring initial dates were used to create ensemble average results for June/July/August 1987 (JJA87) and the autumn initial dates for average results for December/January/February 1987/88 (DJF87/88). The six integrations were carried out for both the current parametrization (Control) and the scheme described above (New Par). For detailed studies of individual components of the model's hydrological cycle, shorter (30 days) integrations were carried out for both parametrizations using data for 1 July 1998 as an initial condition.

One of the parameters that exhibited large differences between the schemes in the first timestep was the large-scale precipitation at the surface (Figure 6.22). Figure 6.23 shows the same quantity for the ensemble average of the three JJA87 integrations. The sign of

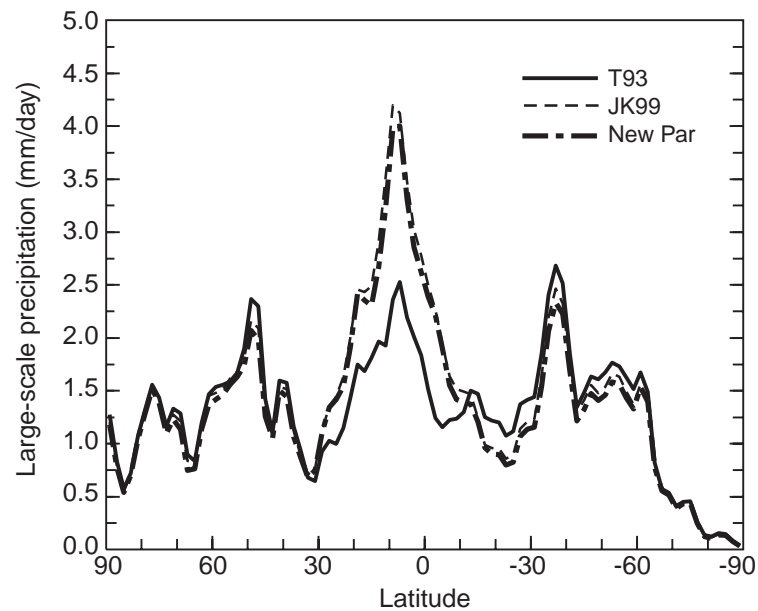


Figure 6.22: Zonal mean large-scale precipitation as predicted in a single timestep by the T93 parametrization (solid), the JK99 subgrid model (dashed) and the new parametrization (dot-dashed).

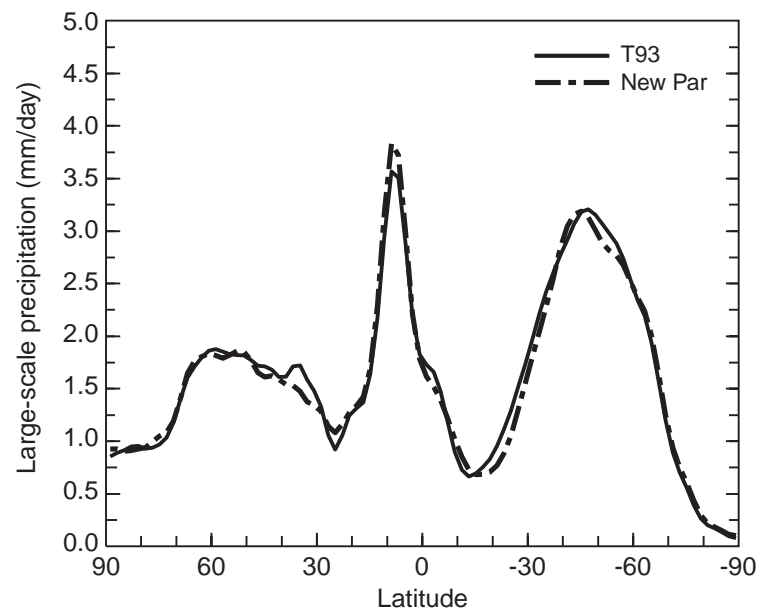


Figure 6.23: Zonal mean large-scale precipitation for JJA87 from an ensemble of three integrations using the current (solid) and new (dot-dashed) precipitation schemes.

the differences, with the new scheme predicting more precipitation in the tropics and less in most of the extratropical latitudes, is the same as in the initial timestep. The magnitude, however, is greatly reduced. The maximum difference in the tropics is now on the order of 8 % as compared to 60 % in the first timestep. This indicates an adjustment process that offsets the direct effect of the new parametrization to evaporate less precipitation in the

tropical mid-troposphere (see Figure 6.21).

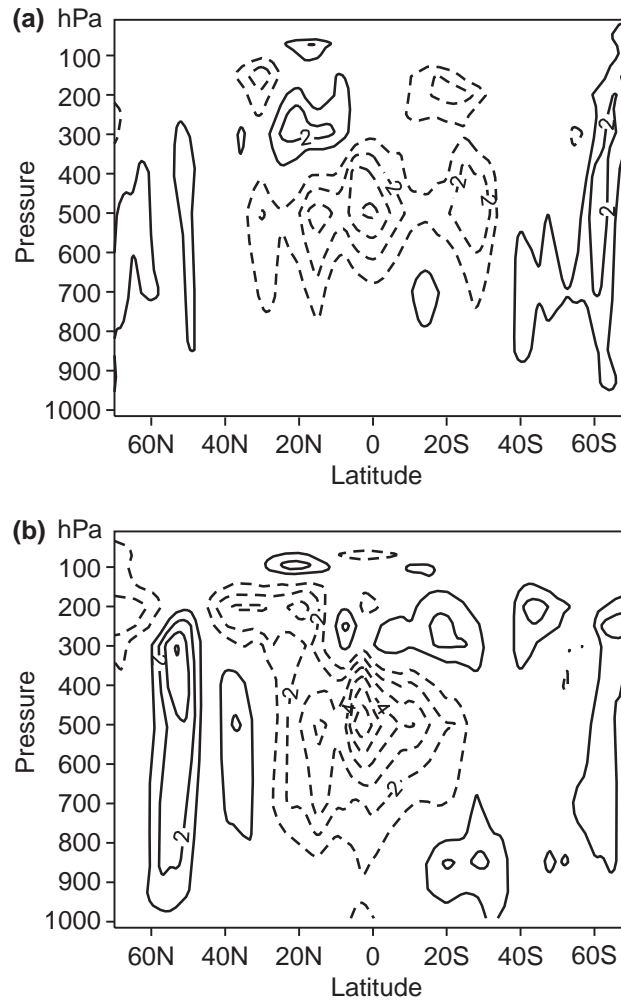


Figure 6.24: Zonal mean cross section of relative humidity difference (new minus current) for ensembles of three integrations for both JJA87 (top) and DJF87/88 (bottom). Contours are every 1 %.

A possible process contributing to the model adjustment is a drying of the tropical mid-troposphere due to the reduced evaporation of precipitation. This constitutes a negative feedback since more precipitation can evaporate in a drier environment. Figure 6.24 provides evidence for the occurrence of this feedback in the model. In both seasons the relative humidity of the mid-troposphere is reduced by about 4 to 6 %, with the larger reduction in winter. Changes in the zonal mean temperature field, however, are much less noticeable, being less than 0.2 K everywhere within the tropics (not shown).

Figure 6.25 provides a detailed schematic of the model's water reservoirs and conversion rates averaged over 30 days of a T63L31 integration in the tropics (20°N to 20°S). The figure shows the values for the integration using the new parametrization, with those for

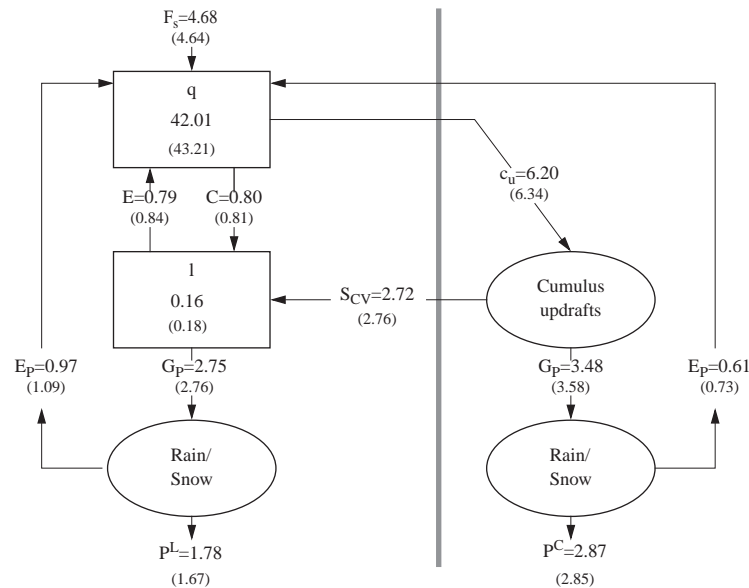


Figure 6.25: Hydrological cycle: Tropical average ($20^\circ N$ to $20^\circ S$) of atmospheric water vapour q , cloud liquid water/ice content l , and conversions between water vapour, cloud liquid water/ice and rain/snow in stratiform clouds (left) and cumulus updrafts (right). The results are averages over a 30-day integration at T63L31 initialized on 1 July 1998 with the new scheme with values for the control model shown in parentheses. Units are mm for water reservoirs and mm/day for conversion terms. The terms are: F_s - surface evaporation, C - large-scale condensation of cloud liquid water/ice, E - large-scale evaporation of cloud liquid water/ice, S_{CV} - source of cloud liquid water/ice from convection, G_P - generation of precipitation, E_P - evaporation of precipitation, c_u - condensation in cumulus updrafts, P^L - large-scale precipitation at the surface, P^C - convective precipitation at the surface.

the control model shown in parentheses. Several interesting details emerge. The increase in large-scale precipitation of about 0.1 mm/day that was already evident in Figure 6.23 is mainly due to a reduction in the evaporation of precipitation, which is of the same order. The cloud liquid water/ice content has been reduced by slightly more than 10 %. Despite this, the conversion to precipitation has not changed much in magnitude indicating a higher efficiency in that process, e.g. through higher accretion rates in the cloudy fluxes. The drying of the mid-troposphere is apparent in the vertically integrated water vapour (q), which is reduced by 1 kg/m^2 (i.e., mm water). The convective activity, as measured by the condensation in cumulus updrafts, has slightly decreased, possibly due to entrainment of drier midtropospheric air into the convective updrafts. This leads to a slight decrease in the convective source of cloud liquid water/ice, with the convective precipitation largely unaltered.

Figure 6.26 shows the time evolution over the first ten forecast days of the differences in some of the terms shown in Figure 6.25 between the new parametrization and the control model. Here day 0 represents the first model timestep. In the first timestep the new parametrization

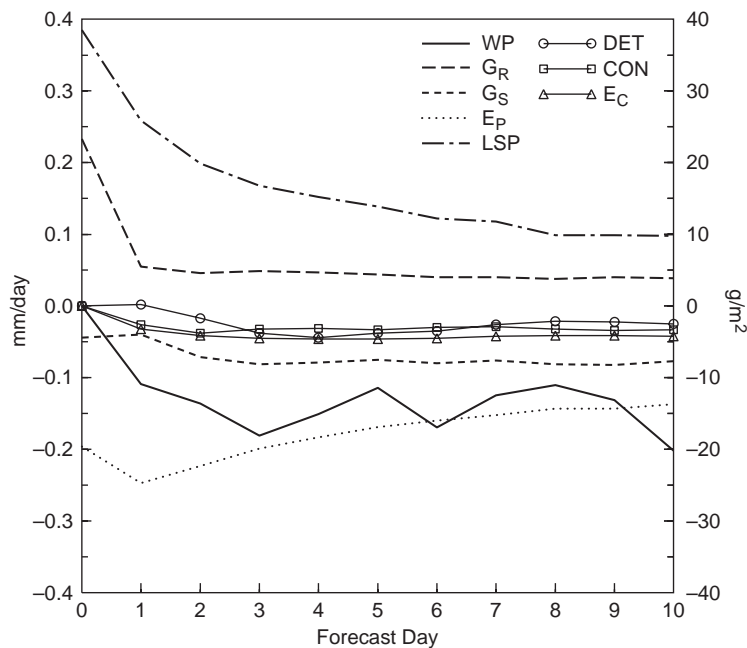


Figure 6.26: Hydrological cycle: Time series of the difference (New Par - T93) in the tropical average ($20^{\circ}N$ to $20^{\circ}S$) of some terms shown in Figure 6.25 for the first 10 forecast days. Day 0 represents the first model timestep. The terms are: WP - liquid+ice water path, G_R - generation of rain, G_S - generation of snow, E_P - evaporation of large-scale precipitation, LSP - large-scale precipitation at the surface, DET - source of cloud liquid water/ice from convective detrainment, CON - large-scale condensation of cloud liquid water/ice, E_C - large-scale evaporation of cloud liquid water/ice.

produces significantly more large-scale precipitation due to i) a decrease in evaporation and ii) an increase in the conversion to rain. The former has been extensively described in previous sections. The latter is due to the fact that the separate accounting of clear and cloudy precipitation fluxes in the new parameterization eliminates the "horizontal" transport of precipitation from cloud to clear sky which occurs in the original parametrization through averaging effects. Consequently, the new parameterization yields higher in-cloud precipitation rates and as a result warm phase accretion increases significantly. No accretion is assumed to occur in the pure ice phase ($T < -23^{\circ}C$), hence there is no increase in the generation of snow. A fairly fast adjustment (1 to 3 days) occurs in the precipitation conversion terms together with the reduction in cloud liquid water/ice described above. After day 3, apart from variations in the cloud liquid water/ice differences around a lower mean, the only significant changes occur in the differences of large-scale precipitation and evaporation. This is due to the much slower process of drying the tropical mid-troposphere (not shown) which occurs on the typical time scale for humidity changes in the tropics of about 10 days. At day 10 both large-scale precipitation and evaporation difference have almost reached their 30 day average value (see Figure 6.25).

6.3.4 Discussion

It was shown that the new parametrization of cloud and precipitation overlap introduced in section 6.3.1 provides a better description of the effects of this overlap on the microphysical processes. It was further demonstrated that, as a result of this, individual components of the hydrological cycle of the ECMWF global atmospheric model are significantly altered. The model climate is affected to a moderate extent. An obvious outstanding question in this investigation is whether the resulting changes constitute an improvement when compared to observations. There are two major caveats when attempting to answer this question. Firstly, the parameters that show the largest sensitivity, such as mid-tropospheric tropical humidity, stratiform precipitation fraction, and evaporation rate, are either difficult, or as in the case of evaporation rate, impossible to measure directly, especially on a global scale. Secondly, although it has been proven that the new parametrization captures overlap effects much better than the current one (see section 6.3.2) there is no reason that this alone should automatically lead to improved model results. This is due to uncertainties in other parts of the parametrization, most prominently perhaps the formulation of the microphysical parametrization itself. In the case of T93 for instance, artificial thresholds for relative humidity have been set above which evaporation of precipitation is suppressed. The values range from 70% in convective situations to 80% elsewhere. These low threshold values in the control model have compensated for the overprediction of evaporation which results from the insufficiently accurate description of overlap effects in T93. However, in order to study the impact of the new parametrization directly, these threshold values were retained in the simulations with the new parametrization presented here. Assessing the impact of changing the thresholds is beyond the scope of the work presented here.

A very important parameter of the new parametrization is the fractional coverage of precipitation in a grid box. This parameter determines the local values of the precipitation flux and hence the “intensity” with which various microphysical processes can act. Furthermore it is a parameter that is in principle measurable, for instance by using a scanning precipitation radar. One such set of measurements has been published by Sui et al. (1997) for an extended period of ship-borne radar measurements with a scan range of 150 km during the Tropical Ocean Global Atmosphere Coupled Ocean-Atmosphere Response Experiment (TOGA COARE). In order to assess the performance of both the T93 and the new parametrization in simulating precipitation fraction, a 30 day integration at T63L31 (about 200 km horizontal resolution) for December 1992 has been carried out. Figure 6.27

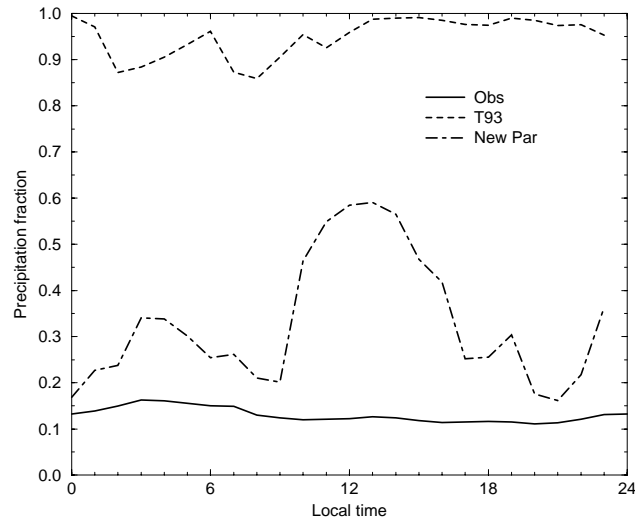


Figure 6.27: Monthly average stratiform (i.e. large-scale) precipitation fraction at the surface as a function of local time. Shown are observations by ship-borne radar during TOGA COARE (solid) and predictions for December 1992 at $2^{\circ}S$ and $155^{\circ}E$ by a T63L31 integration using the T93 scheme (dashed) and the new parametrization (dot-dashed).

shows the precipitation fraction derived from the observations and from the two model integrations at a grid point located at $2^{\circ}S$ and $155^{\circ}E$ as a function of local time of day. The averages for each hour exclude the no-precipitation events, i.e. the comparison will not be affected by possible discrepancies in the occurrence of precipitation in the model runs and in the observations. Note that because of the “climate” nature of the model integration, the comparison can only be qualitative and should be interpreted in that way. The observed values are typically between 0.1 and 0.15, whereas the T93 parametrization predicts values that are always larger than 0.85. The new parametrization yields values of 0.2 to 0.6 with an unrealistically large diurnal maximum around local noon. This is very likely due to sampling problems since averaging the model results over a larger area removes the peak (not shown). Although still higher than observed, the results of the new parametrization constitute a major improvement. It should again be emphasized that this comparison is only meant to highlight the possibility of comparing some of the crucial parameters of the new parametrization scheme to observations.

One of the biggest advantages of the new scheme is that it improves the knowledge about which microphysical parametrization to apply over which part of the grid box and that it produces better estimates of the local precipitation rates needed in those parametrizations.

Therefore it can be seen as a prerequisite for the successful application in GCMs of complex microphysical schemes, as they are applied in cloud resolving and/or mesoscale models.

6.3.5 Conclusions

A new parametrization for cloud and precipitation overlap for use in GCMs has been developed. It is based on distinguishing between cloudy and clear-sky precipitation fluxes during the descent of the precipitation through the model layers. The scheme has been introduced into ECMWF global forecast model. Extensive single timestep tests against a subgrid precipitation model developed by Jakob and Klein (1999) show the superiority of the new scheme over the current parametrization. The main change in the model physics is a reduction of precipitation evaporation in the tropical mid-troposphere and an increase in the conversion of cloud water to rain due to enhanced accretion. The scheme has a moderate effect on the model climate through a decrease of the tropical mid-tropospheric relative humidity by 4 to 8 % depending on season. The tropical large-scale precipitation is increased by about 8 %. By design the new parametrization produces better estimates of local precipitation fluxes involved in the microphysical processes and therefore paves the way for increased complexity in their parametrization.

Chapter 7

The evaluation of cloud parametrizations

7.1 Introduction

A crucial aspect when modelling a physical system, or parts of it, is the evaluation of the realism of the model results using observations of the phenomenon in question. With increasing complexity of the model the evaluation of specific components becomes increasingly difficult. Current GCMs can probably be considered as one of the most complex models of a physical system, not only because of the large number of processes described in them, but also because of the non-linear character of their interactions.

Clouds form an integral part of all current GCMs and, as described in the previous chapters, strongly affect the overall model results through their interaction with many processes. Modern GCMs, such as the ECMWF global model, predict a number of cloud parameters, in particular cloud fraction and the content and phase of condensate, for all their model layers, and thereby provide a huge amount of information. The current operational version of the ECMWF model for example, predicts two cloud variables at more than 10 million points in the atmosphere at each of the model's time-steps. This wealth of model results goes far beyond the capabilities of measuring clouds (in the broad sense) and will do so indefinitely. The question then arises, how the model's simulation of the multitude of different cloud systems that exist in nature at any given time can be evaluated.

It is not the intention of this chapter to provide a comprehensive review of all cloud validation studies ever carried out for GCMs. Instead the ECMWF model will be used to illustrate past and present methods of the evaluation of clouds. Strengths and weaknesses of the individual techniques will be highlighted. Special emphasis will be placed on recent efforts to improve the capabilities in cloud evaluation. The chapter will provide a review of some

of the evaluation techniques used up to today at ECMWF with focus on the most recent efforts. The use of some of the most promising new data sources, namely active remote sensing instruments, such as cloud radar, for cloud evaluation will be explored.

Given the fairly large number of GCMs in use worldwide in both NWP and climate simulation it is not surprising that a large number of studies have dealt with the problem of evaluating the simulation of clouds and their radiative effects in these models. Recent examples for such evaluation studies are referenced in previous chapters (in particular Chapter 4) and throughout the following sections. Despite the large variety of studies most of them can be placed in one of two main categories: the evaluation of the model climate and case studies. In the following sections recent work with the ECMWF model will be used to illustrate some of these techniques and to highlight their advantages and drawbacks. Section 7.6 will introduce a technique which has only recently been used for cloud parametrization evaluation, that of compositing by dynamical regime. Recent results of studies carried out at ECMWF will serve as examples to illustrate how this technique can bridge the gap between model climate and case study and thereby provide new insight into the workings of a particular cloud parametrization. The chapter will close by proposing a strategy for cloud evaluation in GCMs that integrates most of the current techniques into a coherent procedure.

7.2 Model climate

7.2.1 Broadband radiative fluxes

The main impetus for the inclusion of clouds into GCMs is their interaction with radiation. It is therefore not surprising that one of the most common techniques to evaluate cloud parametrizations is to compare radiative fluxes produced by the model to those observed by satellites at the top of the atmosphere. One of the most frequently used data set for such comparisons is the broadband flux measurements gathered during the Earth Radiation Budget Experiment (ERBE; Barkstrom and Smith, 1986).

Figure 7.1 shows the difference in TOA shortwave (top panel) and longwave (bottom panel) between simulations for June/July/August (JJA) 1987 made with the operational version of ECMWF model as used in most of 1998, but at lower horizontal resolution, and the ERBE observations. The model integrations start on 1 May 1987 at a resolution of T63L31 and use prescribed, time-varying sea surface temperatures (SSTs). Upward fluxes are taken as negative so that a negative difference indicates a too strong upward flux, i.e., too much

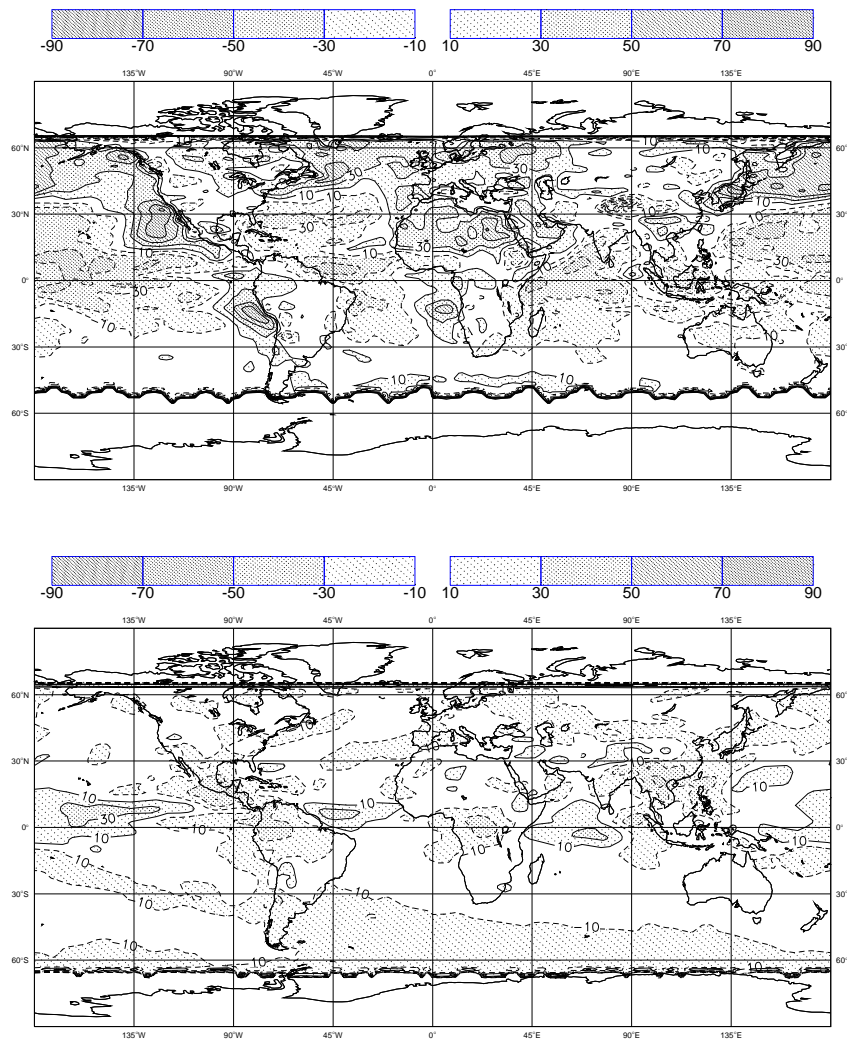


Figure 7.1: Difference in shortwave (top) and longwave (bottom) radiation at the top of the atmosphere between a model integration and ERBE observations for June/July/August 1987. Positive differences are shown as solid contours, negative differences as dashed. The contour interval is 20 W m^{-2} with shading starting at $\pm 10 \text{ W m}^{-2}$. The model integration is carried out with CY18R6 of the ECMWF model at T63L31 resolution. The initial date is 1 May 1987. SSTs are time varying and prescribed.

reflection in the shortwave case and too high emission in the longwave part of the spectrum. Several regions of erroneous TOA radiation emerge for both spectral regions. TOA shortwave radiation is overestimated (pointing to too little reflection) in the extratropics, predominantly over the oceans but also over land, over the eastern part of the sub-tropical oceans and over the Sahara region. It is underestimated over most of the deep tropics and over the western parts of the subtropical oceans. The outgoing longwave radiation (OLR) is underestimated (positive difference) over much of the ocean in the tropical belt, strongly overestimated over the tropical continents and overestimated to a lesser extent in the extratropics.

One of the advantages of evaluating broadband radiative fluxes is that they form part of the planet's energy balance and are therefore a key quantity to be accurately simulated in GCMs. The biggest drawback of the technique when applied to cloud evaluation is that information on the overall model radiative fluxes per sé does not deliver any information about the radiative effect of the model clouds. The errors seen could result not only from erroneous model clouds, but also from the wrong description of the surface albedo in case of the shortwave radiation or from wrong surface temperatures or poor simulations of the water vapour distribution in the longwave part of the spectrum. The coincidence of some of the error patterns with regions dominated by particular cloud types does however raise the suspicion of problems in the description of the radiative effect of these types of clouds. The strong overestimation of TOA shortwave radiation in what was identified as regions of extensive coverage with stratocumulus in Chapter 2 could well point to a problem in their representation. The introduction of more a priori information, e.g., the use of the relatively good knowledge of the albedo of the sea surface, also makes it more likely that the errors identified in Figure 7.1 are related to errors in the radiative behaviour of clouds. On the other hand, the large error in shortwave radiation identified over the Sahara, a region of almost zero cloud occurrence, probably indicates a problem in the description of surface albedo.

7.2.2 Cloud radiative forcing

In order to better understand which of the errors identified above are due to cloud radiative effects, a better variable to compare is the cloud radiative forcing as derived from satellite observations (see Chapter 2). This can easily be achieved in a model by storing the clear-sky radiative fluxes at each gridpoint and compare them to the all-sky fluxes as outlined in Chapter 2. Note that this procedure differs from the way the cloud radiative forcing is derived from data in that the clear-sky radiation in the model is calculated for cloudy columns by just ignoring the cloud variables, but still using the water vapour and temperature profiles of a cloudy column. In contrast, the cloud radiative forcing in the data is derived by comparing cloudy columns with neighbouring (both in space and time) true clear-sky columns. The difference introduced this way can amount to a few Wm^{-2} (Cess and Potter, 1987; Cess et al., 1992) and needs to be considered in cases of small model errors. As will be shown below, the errors of the ECMWF model in many regions are in excess of $10 Wm^{-2}$ so that this effect should not affect the conclusions drawn here.

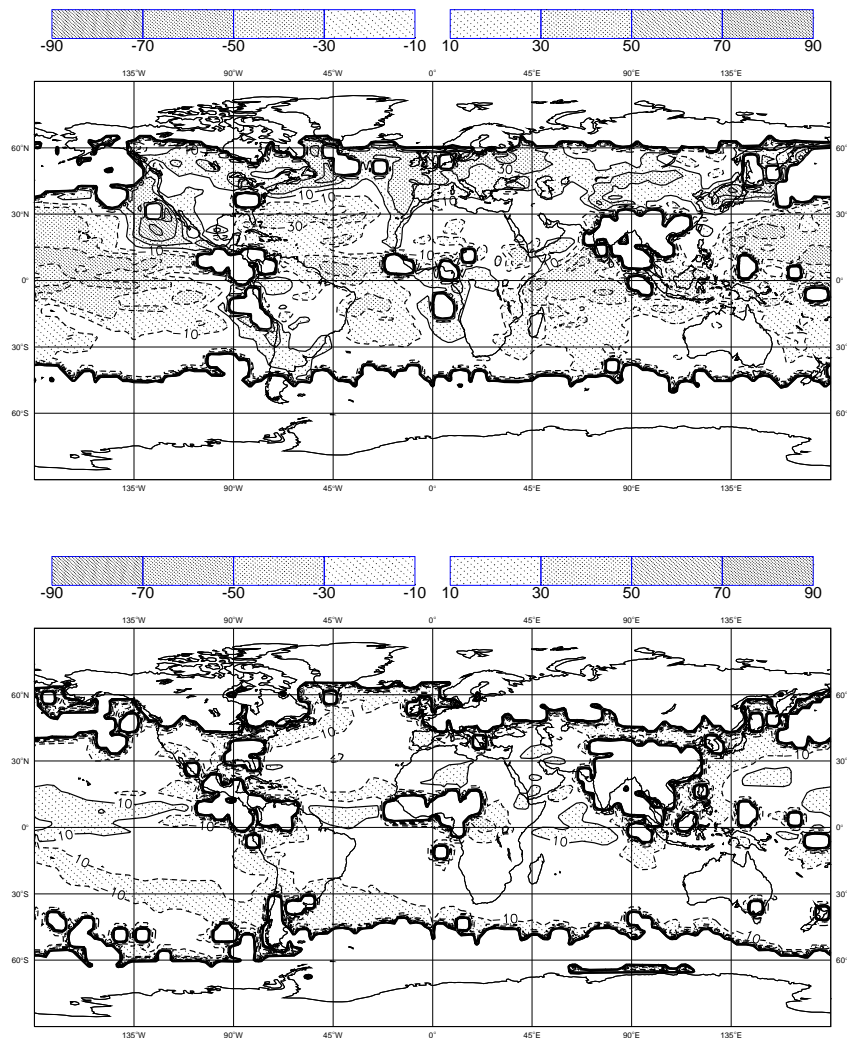


Figure 7.2: Difference in shortwave (top) and longwave (bottom) cloud radiative forcing at the top of the atmosphere between a model integration and ERBE observations for June/July/August 1987. The model integration is carried out with CY18R6 of the ECMWF model at T63L31 resolution. The initial date is 1 May 1987. SSTs are time varying and prescribed. White areas surrounded by heavy contouring denote missing data.

Figure 7.2 shows the difference in shortwave (top panel) and longwave (bottom panel) cloud radiative forcing for the same model simulation as above. It is obvious that most of the pattern and size of the errors for both spectral regions are very similar to those in the full radiative fluxes shown in Figure 7.1. This confirms the suspicions raised in the previous subsection and identifies clouds as the major source for error in the radiative fluxes at the top of the model atmosphere. This is not too surprising, since the knowledge about clear-sky radiative transfer is much further advanced than that of the representation of clouds and their interaction with radiative fluxes. The errors identified in the previous two Figures for

the ECMWF model can therefore be summarized as

- too reflective clouds (solar) over the deep tropical oceans and the western parts of the subtropical oceans
- too little reflection (solar) from clouds over the eastern part of the subtropical oceans and in the extratropics
- excessively large cloud effects in the longwave over ocean areas in the deep tropics

The advantage of using model climate comparisons to cloud radiative forcing observations is that it is possible to study the overall radiative effects that the clouds exert on the model atmosphere and thereby to assess whether the net effect model clouds have is properly represented. One of the major drawbacks of the technique is that this net effect is the result of many cloud parameters as discussed extensively in Chapter 2. The overestimated shortwave cloud radiative forcing in the trade cumulus regions described above can therefore be the result of too high cloud fraction, too large cloud liquid water contents, too small assumed particle sizes, the misrepresentation of broken cloud effects in the radiation parametrization or a combination of any of those. From the perspective of cloud parametrization this is an extremely dissatisfying result since it provides no guidance to where the emphasis for future development should be. All one can learn is where the general problem areas (in the geographic sense) are. One step to improving this situation is to try and evaluate the parameters predicted by the cloud parametrization, such as the model cloud fraction.

7.2.3 Cloud fraction

Figure 7.3 shows a difference between the mean total cloud fraction for JJA 1987 from the same model simulations as above and that derived from the ISCCP-C2 data set (see Chapter 4). The main model errors are

- an underestimation of cloud fraction in the stratocumulus regions off the west coast of the subtropical continents
- an underestimation of cloud fraction over the extratropical oceans
- an overestimation of cloud fraction over the ocean areas of the deep tropics

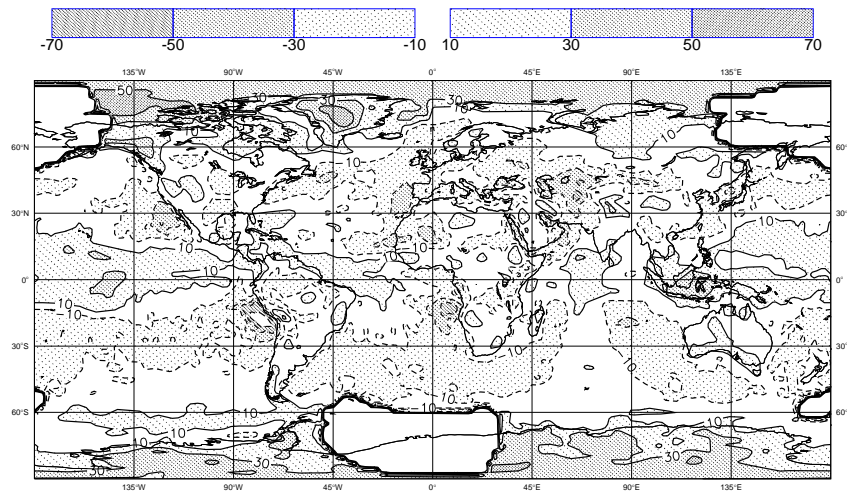


Figure 7.3: Difference in total cloud cover between a model integration and ISCCP observations for June/July/August 1987. The model integration is carried out with CY18R6 of the ECMWF model at T63L31 resolution. The initial date is 1 May 1987. SSTs are time varying and prescribed. White areas surrounded by heavy contouring denote missing data.

These errors are consistent with the errors found above in the cloud radiative forcing. There is however no obvious error in cloud fraction over the trade-cumulus areas that could explain the large errors in cloud radiative forcing there.

The comparison of mean cloud fraction at first glance reveals model errors that are more indicative for errors in the cloud parametrization itself. However, it has to be kept in mind, that the model results are taken from a four months long integration. A major drawback of the use of simulations of this type is that errors in any part of the model, including the cloud parametrization itself, will lead to feedback processes. Those can alter the model climate in such a way that the dynamical forcing becomes so unrealistic, that in certain parts of the globe a successful representation of clouds becomes impossible. The lack of stratocumulus over the eastern parts of the subtropical oceans might therefore well be due to flaws in the cloud parametrization, but it might also be a consequence of unrealistic dynamical forcing. This type of cloud exists in a subtle balance of boundary layer growth due to surface fluxes and large-scale subsidence. A slight over- or underestimation of subsidence can therefore have grave consequences for the simulation of clouds in this region. It is conceivable that such an error in subsidence rate can occur for instance due to an overestimate of the strength of the thermally direct Hadley circulation, that encompasses most of the tropics and subtropics. Even if the lack of clouds in these regions was due to errors in the cloud parametrization itself, the kind of diagnostics used so far cannot provide any insight into why the errors

occur.

Based on this discussion, two obvious modifications to the methods used so far are desirable. First one would like to evaluate the model clouds in the “best possible” dynamical environment, so that errors revealed in the evaluation study can be more easily ascribed to shortcomings in the cloud parametrization itself. Chapter 4 provided an approach to this problem through the use of an NWP system. This approach will be further explored below. Another desirable feature of an evaluation would be to find techniques that can reveal the details of the model cloud evolution. A common technique that addresses both of the problems mentioned is the use of so-called Single Column Models (SCMs).

7.3 Single Column Modelling

A computationally efficient way of performing evaluation studies using a physical parametrization package used in a GCM is to perform a so-called Single Column Model (SCM) simulation. Rather than using a full three-dimensional GCM a single column is “extracted” and the results of the model in only this column are considered. This is facilitated by the fact that all current physical parametrizations used in GCMs are assumed to be locally applicable and therefore only require information at a single grid point and no direct interaction between model grid-columns. The three-dimensionality of the GCM is only achieved through the model “dynamics” (i.e., the solution of the grid averaged hydrodynamic equations), for which the physical parametrizations represent a forcing term. Since this is so, it is obvious that the information from neighbouring grid-cells, such as advection terms, which in the full model are provided by the model “dynamics”, needs to be prescribed in an SCM. Various techniques for this have been developed and are summarized in Randall and Cripe (1999).

By design the SCM approach has the advantage to be relatively inexpensive and since only information in a single model column is generated the intricate details of a parametrization can be easily explored. Another great advantage of the technique is that through the prescription of the boundary conditions, errors created through feedback processes in the full GCM cannot occur and if the boundary conditions were perfect, all errors visible in the SCM would be solely due to errors in the parametrization. This advantage is unfortunately a disadvantage in itself since it might be the errors that are caused by those feedbacks that one wants to investigate. The major difficulty for the SCM approach, however, is to find suitable observational data sets which i) can provide enough information to derive the

boundary conditions for the SCM, such as the advection of all model variables and vertical motion, and ii) provide observations to evaluate the performance of the parametrization in question. Because of these high demands on a data set suitable for SCM studies only very few such data sets exist today. Those include a data set for modelling the Lagrangian evolution of the marine cloud-topped PBL gathered during the Atlantic Stratocumulus Transition Experiment (ASTEX; Albrecht et al., 1995), a number of data sets for the study of shallow cumulus clouds collected during the Barbados Oceanographic and Meteorological Experiment (BOMEX; Holland and Rasmusson, 1973; Nitta and Esbensen, 1974) and the Atlantic Trade-Wind Experiment (ATEX; Augstein et al., 1973), and a few data sets for the study of penetrative convection derived during the Global Atmospheric Research Program's (GARP) Atlantic Tropical Experiment (GATE; e.g., Houze and Betts, 1981), during TOGA COARE (Webster and Lukas, 1992) and more recently the Atmospheric Radiation Measurement Program (ARM; Stokes and Schwartz, 1994). Designing parametrizations using only a few cases like these carries the high risk of the nonrepresentativeness of the cases chosen and although SCM simulations are successful, the same parametrizations do not perform well once implemented into the full GCM.

Two major activities have been taking place over the last five to ten years to improve the usefulness of SCMs in parametrization development, in particular that of cloud and convection parametrizations. The first is to gather more observations for the use in case studies. At the forefront of this activity is the ARM program. The aim of this program is to collect quasi-continuous data sets related to clouds and cloud-radiation interaction at various locations distributed over the globe. To date ARM is collecting data at sites located in the Southern Great Plains (SGP) of the North American Continent, at Barrow (Alaska) and at two locations in the Tropical Western Pacific (Manus and Nauru island). Since the observations are by design Single Column Observations (SCO), their use in SCM studies is an obvious target. Several studies of this kind using mainly data from the SGP site have already been carried out (e.g., Randall and Cripe, 1999).

A second major activity aimed at the improved use of SCMs in cloud parametrization development is carried out by the World Climate Research Program's (WCRP) Global Energy and Water Cycle Experiment (GEWEX) Cloud System Study (GCSS) (Browning et al., 1993). The basic idea in this program is to increase the number and therefore representativeness of available SCM case studies through the use of high-resolution cloud models which enable a detailed simulation of cloud processes that need to be parametrized in GCMs. These models

are normally referred to as Cloud Resolving Models (CRM). Depending on the cloud type under study the spatial resolution of such models varies from several meters in the horizontal and vertical for boundary layer cloud studies using Large-Eddy Simulation Models (LES; see Mason (1994) for a review), to several hundred meters in case of Cumulus Ensemble Models (CEM; e.g., Moncrieff et al., 1997, and references therein) used for studies of deep convective systems. The GCSS strategy is to first use these models for the simulation of observed situations. Through the comparison of the model results to observations, the CRMs can be improved and confidence in their ability to accurately simulate cloud process can be gained. Having established this ability, the CRMs can be used in any kind of simulation, even idealized, to provide the "truth" against which an SCM can be evaluated. GCSS has undertaken a large number of model intercomparisons involving both CRMs and SCMs in order to achieve this goal (e.g., Bechthold et al., 1996; Moeng et al., 1996; Bretherton et al., 1999; Bechthold et al., 2000; Redelsperger et al., 2000; Ryan et al., 2000).

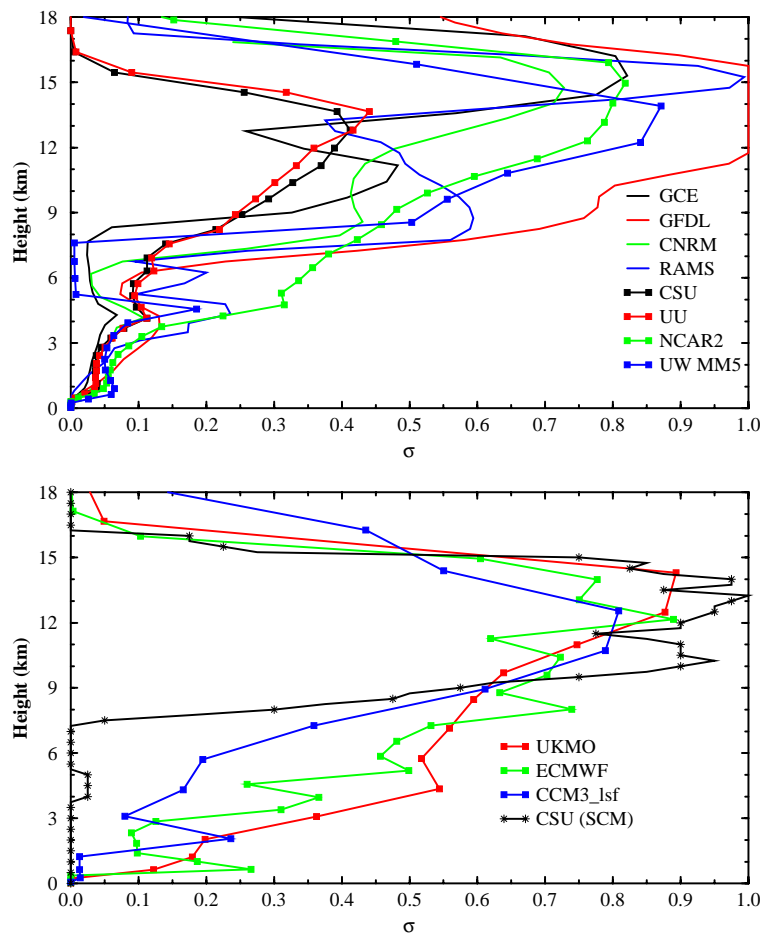


Figure 7.4: Six-day average of cloud fraction as a function of height from simulations for a period of TOGA COARE (20 to 25 December 1992) with a number of CRMs (top) and SCMs (bottom).

Figure 7.4 shows an example of the kind of results that have become available from GCSS studies for cloud parametrization. The figure shows a six-day average of the vertical profile of cloud fraction, one of the crucial results of a cloud parametrization, for a period in late December 1992 of the TOGA COARE field experiment. The top panel shows results from simulations using CRMs whereas the bottom panel depicts the results from SCM simulations. Note, that the external forcing was prescribed identically for all models. The figure highlights both the strength and the intrinsic difficulties of the GCSS approach so far. It is undoubtedly useful to use a variety of state-of-the-art CRMs (instead of just one) to carry out simulations as the above. That way, by assessing the spread in the results, one gains some confidence or, as in this case, one is cautioned on the direct use of the CRM results as a surrogate for observations. From Figure 7.4 it is difficult to argue that the SCMs perform considerably worse in simulating the vertical distribution of cloud cover, which, given the large spread in the CRM results and the absence of observations, should not necessarily be interpreted as an indication that the SCMs are correct.

The above figure also highlights another danger, the so-called “intercomparison trap”, into which the cloud parametrization community is sometimes in danger of falling. Just simulating various cases with a large number of models and comparing the results will not automatically lead to the improvement of any of them. A more useful approach would be to formulate ideas and hypotheses on how the various cloud processes should be included in parametrizations, and then assess and test those ideas using the full power of the GCSS framework. It also appears necessary to view the model intercomparison activities in the wider context of other tools available to assess the performance of cloud parametrizations. This will be discussed further in Section 7.7. The points raised here have been recognized by the GCSS and its strategy is currently under revision. Despite this criticism, one should not underestimate the achievements of programs like GCSS. Cloud and large-scale modelers have been brought together to address the issue of parametrizing clouds; a large library of case studies for various cloud types is now available to the scientific community and a protocol exists for their use. Furthermore more and more knowledge on the use of CRMs to investigate cloud parametrization issues is emerging.

Overall the SCM approach, in particular when seen in the context of programs like ARM and GCSS provides valuable information for cloud parametrization development. This is particularly true if the approach is seen as part of a wider strategy of evaluating cloud parametrizations, which will be outlined in a later section.

7.4 NWP forecast evaluation

The advantage of a case study, as already highlighted in the previous section, is that it is usually performed when detailed observational data is available for model evaluation. The procedure in SCM studies is then to find such well observed cases and execute dedicated model simulations. In the case of global NWP another approach is immediately obvious. Here, the full GCM is used to predict the state of the atmosphere globally on a daily basis for several days ahead. Therefore each day many “case studies” are available from such a forecast. It is now only a matter of finding suitable observations to compare the forecasts with. As in SCM studies it is desirable when evaluating the cloud parametrization to minimize the influence of errors in other parts of the model. Therefore it is common to choose forecasts in the range of less than three days, in which the numerical solutions are known to be most accurate, for the model evaluation.

The most obvious comparison possible is that to cloud observations routinely collected by observers on the ground and included in the reports that are distributed regularly via the Global Telecommunications System (GTS). This type of comparison is carried out on a daily basis at many NWP centres and is used mainly for monitoring forecast performance. One of the immediate benefits of this routine monitoring is that the effects of changes in the cloud parametrization should be reflected in the monitoring statistics. An example for this is shown in Figure 7.5. This figure shows the evolution of the mean (thick lines) and standard deviation (thin lines) of the forecast error in total cloud cover averaged over many meteorological stations in Europe. The time series shows monthly averages of 60-hour (dashed) and 72-hour (solid) operational forecasts from January 1988 to February 2000. There is a significant reduction in both mean error and standard deviation in April 1995. Not surprisingly, this can be traced back to a change in the model’s cloud parametrization, namely the introduction of the T93 parametrization into the operational model. Although mostly very general in nature, the results of routine monitoring of the forecast results do provide some guidance to the development of cloud parametrization by exposing general problem areas, similar to climate simulations. The big advantage over climate simulations is that, through the use of short-range forecasts, model errors can be more easily ascribed to the parametrization itself since the large-scale flow is expected to be more realistically captured.

The use of NWP for cloud parametrization evaluation is not restricted, of course, to the use

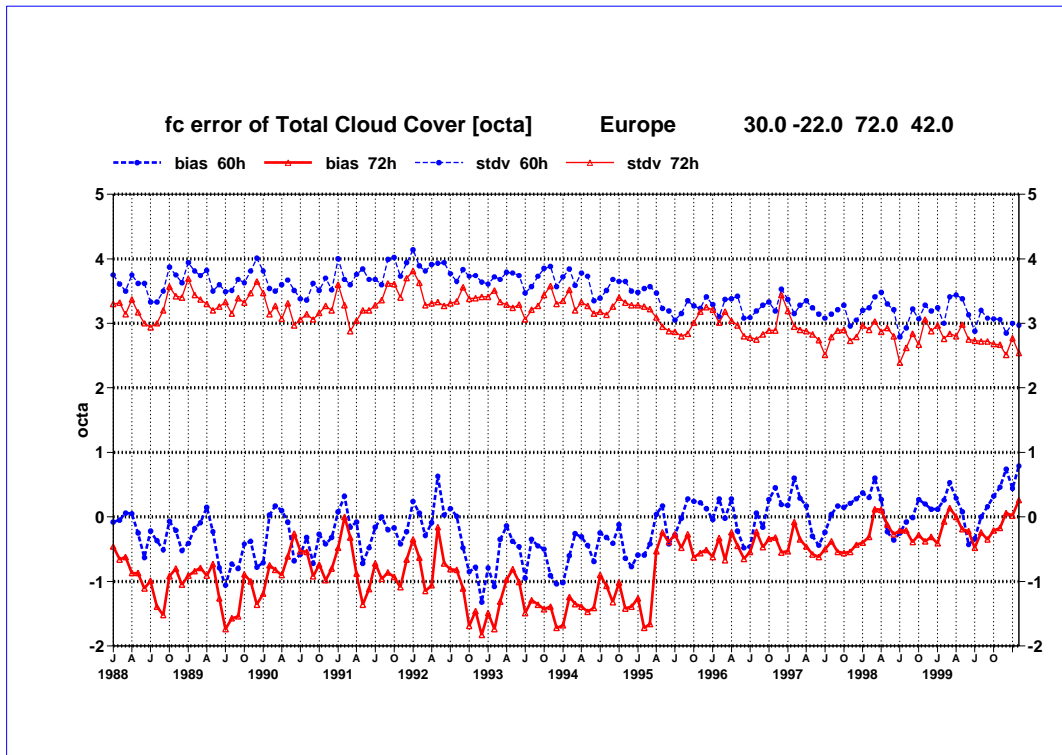


Figure 7.5: Time series of short-range forecast model errors in total cloud cover (in octa) for Europe (the exact averaging area is indicated in the top right corner) when compared to SYNOP observations. Shown are monthly means of the mean error (thick lines) and the standard deviation (thin lines) for all operational 60-hour forecasts (valid at 00 UTC; dashed) and 72-hour forecasts (valid at 12 UTC; solid).

of operational products. If there are dedicated observational campaigns, it is always possible to carry out dedicated model simulations covering the period of the observations. This is even desirable, since it allows the evaluation of several versions of a parametrization or even completely different sets of parametrizations. The use of NWP models in this context can provide a natural extension to the SCM approach described above. If data are available at a single point for a given period of time, it is of course feasible to extract the forecast model results at the same point for comparison with the observations. Using a sequence of short-range forecasts one can even build long data sets, such as done globally in Chapter 4. The advantage of using the full GCM for this purpose is twofold. First, there is no need to prescribe the boundary conditions for the model column used, since those are the result of the full three-dimensional model itself. Second, the parametrization under investigation is working in the environment it is designed for. The disadvantages of the method are first of all the huge cost (a full GCM needs to be integrated to extract information at a single point), and secondly the uncertainties in other model components, which might lead to errors in the

parametrization under study. The first problem can be overcome by again using products from operational forecasts, which are performed “anyway”, while the second problem is minimized by the use of short-range forecasts. ECMWF has been regularly providing data to several field experiments such as the various ARM sites and the Surface Heat and Energy Budget of the Arctic (SHEBA) experiment (Curry et al., 2000). A number of studies using this kind of data have been carried out (Mace et al., 1998a; Miller et al., 1999; Beesley et al., 2000; Bretherton et al., 2000; Hogan et al., 2000) and provide insight into the ECMWF model’s performance. An example will be highlighted in the following section.

7.5 The verification of vertical cloud structure

The use of forecast results as highlighted in the previous section together with the recent availability of data from active remote sensing instruments such as cloud radar and lidar, provides the possibility of beginning to evaluate not only the total cloud cover, as done so far, but the vertical cloud fraction structure. This was highlighted in Chapter 6 as an important necessary step for the more realistic simulation of precipitation and radiation in GCMs. A number of studies (Mace et al., 1998a; Miller et al., 1999; Hogan et al., 2000) have attempted to evaluate the vertical cloud structure of the ECMWF model for various locations. Since this can be considered as one of the most important developments in cloud parametrization evaluation in recent years, a brief summary, in particular of the study carried out by Mace et al. (1998a), will be provided here together with an outlook for possible extensions to these exciting new evaluation activities.

The aim of Mace et al. (1998a) was to evaluate the prediction of the vertical distribution of hydrometeor occurrence (clouds and precipitation) over the ARM Southern Great Plains (SGP) measuring site for the months of December 1996 to February 1997. The observations are provided by applying a statistical masking algorithm to generate a binary description of significant echo returns from the 35-GHz-millimeter cloud radar (MMCR), that operates in quasi-continuous mode at this site. The result of this algorithm is an hourly description of the boundaries of the areas assumed to be filled with hydrometeors with about 100m vertical resolution. To compare this with model output, the data were remapped onto the model grid.

The model results are taken from operational 12- to 35-hour forecasts. A long time-series of hourly data at the ARM SGP site is generated by aggregating consecutive model forecasts.

Both model cloud and precipitation of any phase are considered to determine the occurrence of hydrometeors. A summary of the comparison is shown in Figure 7.6. The Figure shows the vertical frequency distribution of hydrometeor occurrence averaged over the entire comparison period for both data (solid line) and model (dashed line). Model and data agree generally quite well, both showing maxima in the frequency of occurrence between 6 and 9 kilometres and in the PBL. The model tends to slightly overpredict hydrometeor occurrence except for the uppermost part of the troposphere and near the surface.

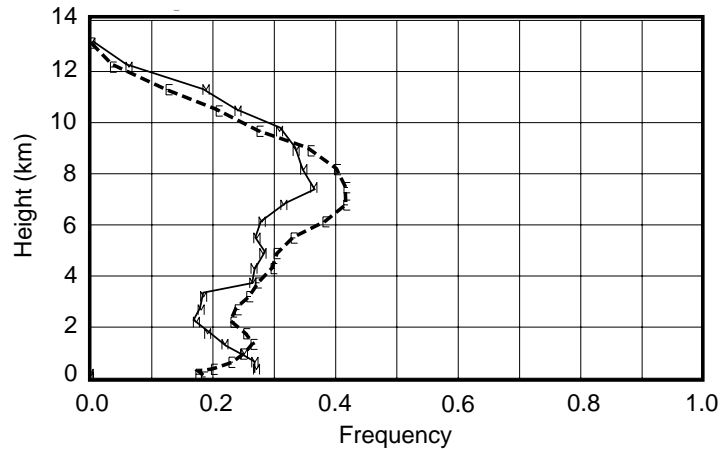


Figure 7.6: Comparison of the vertical frequency distribution of hydrometeor occurrence at the ARM SGP site during the winter season 1996/1997. The ECMWF model is depicted by the dashed line with the symbol “E” and the radar by the solid line with the symbol “M”. From Mace et al. (1998a).

One of the big advantages of the use of NWP models for cloud parametrization evaluation is that the model results are forecasts of an actually observed atmospheric state. This allows for a rigorous quantitative comparison of the model with the observations, while in climate models, if at all, only the statistical distributions of both model and observations could be compared. A quantitative evaluation of the model performance can be achieved by using statistical evaluation measures for categorical forecasts. At every model level and every hour an observation and a forecast of the existence of hydrometeors exist, leading to four possible outcomes of the model comparison which are summarized in Table 7.1.

	Radar - Yes	Radar - No
Model - Yes	A	B
Model - No	C	D

Table 7.1: Summary of the contingency table for the model-to-radar comparisons.

From this contingency table several objective performance measures can be calculated (e.g.,

Wilks, 1995). The measures used here are the hit rate (HR), the false alarm rate (FAR), the threat score (TS), and the probability of detection (POD), which are defined as

$$\begin{aligned}
 HR &= \frac{A+D}{A+B+C+D}, \\
 FAR &= \frac{B}{A+B}, \\
 TS &= \frac{A}{A+B+C}, \\
 POD &= \frac{A}{A+C}.
 \end{aligned}
 \tag{7.1}$$

The four values are calculated for the entire period and averaged over the entire troposphere. The results are shown in the top line of Table 7.2. Taken on their own it is very difficult to judge whether the objective measures calculated mean success or not. Of course, their ideal values are known (one for HR, TS, and POD, and zero for FAR), but just how serious are deviations from those numbers? In order to provide better judgement on the model performance, two alternative forecasts of the hourly hydrometeor occurrence are created. The first alternative forecast is a persistence forecast. Here, it is simply assumed that the hydrometeor occurrence observed at 12 UTC on a certain day (the initial time of a model forecast), is still true 12 to 35 hours later. The objective scores for this forecast are shown in the second line of Table 7.2 labeled ‘‘Persistence’’. Another alternative forecast is a random forecast, but bounded by the observed ‘‘climatology’’. Here the mean frequency of occurrence for each month is calculated as a function of height. Then random forecasts for each hour of the month are generated under the constraint that the mean frequency of occurrence of the forecasts equals that of the observations. The objective scores for this forecast are shown in the last line of Table 7.2. Both of these forecasts, although not ideal, can be considered viable options in the absence of an atmospheric model and therefore provide a minimum skill level that any model forecast should exceed to be termed useful.

	HR	TS	POD	FAR
Model	0.82	0.44	0.68	0.45
Persistence	0.76	0.23	0.37	0.61
Climatology	0.69	0.13	0.23	0.77

Table 7.2: Model-to-radar comparison results.

It is obvious from Table 7.2 that the model exceeds the performance of the two alternative forecasts in all measures, i.e., HR, TS and POD are higher and the FAR is lower. A good

overall measure of skill in a forecast is the difference of POD and FAR, sometimes termed the true skill score (TSS), $TSS = POD - FAR$, since it essentially measures the ability of a forecasting system to detect the event to be forecast against the number of false alarms. In this measure the model is the only of the three forecasting systems that shows any, if small, skill (positive TSS). Both persistence and climatology forecasts yield negative TSS, indicating that they cannot be used to predict the vertical cloud distribution at the ARM SGP site.

From the results of their study, Mace et al. (1998a) concluded that it is worthwhile pursuing a more in-depth comparison of the ECMWF model's vertical cloud structure to ground-based radar observations. The main weaknesses of the study were the very short period of time for which the comparison was carried out and the limitation of only considering hydrometeor occurrence. It was therefore recommended to try and extend the work to a longer data set (which was not available then) and to derive model parameters, such as cloud fraction and/or condensate content.

A number of other studies on the vertical cloud structure of the ECMWF model have been carried out since. Miller et al. (1999) compared the vertical distribution of cloud fraction derived from the Lidar In-space Technology Experiment (LITE; McCormick et al., 1993) with that produced by short-range forecasts of the ECMWF model, and found an overall excellent performance of the model. More recently, Hogan et al. (2000) investigated the vertical distribution of cloud (and precipitation) fraction as predicted by model forecasts for a location in the South of England for the months of October 1998 to January 1999, by comparing to ground-based cloud radar-derived values, and found the model to be in reasonable agreement. Most recently a two-year data set of radar derived cloud fraction has become available for the ARM SGP site, which for the first time enables a comparison over the entire annual cycle. First results indicate that the model performance in winter and spring is similar to the results in Mace et al. (1998a), while in summer, when clouds are predominantly of convective origin, the model performs less well.

Another recent development is attempts to retrieve cloud condensate content from using a suite of ground-based active and passive remote sensors, including the MMCR used above. Recently Mace et al. (1998b) have derived ice contents for isolated cirrus clouds from combined radar reflectivity and infrared interferometer data. Figure 7.7 shows an attempt to use this information for a first evaluation of the ECMWF model performance in simulating the ice content in those clouds. The figure shows the frequency distribution of ice content

for clouds at temperatures lower than 219 K and higher than 227 K (note that all clouds in this study need to be colder than 250 K to be ice clouds) derived from observations and two versions of the ECMWF model. The bounding temperatures were chosen because they represent the 33 % and 67 % percentiles of the observed cloud distribution with respect to temperature. The observations were gathered between November 1996 and December 1997. The model data represents the periods November 1996 to October 1997 (Mod97) and January to July 1998 (Mod98). Although the time periods over which the comparison is made are not identical, enough cases are used in all samples to allow at least a qualitative comparison.

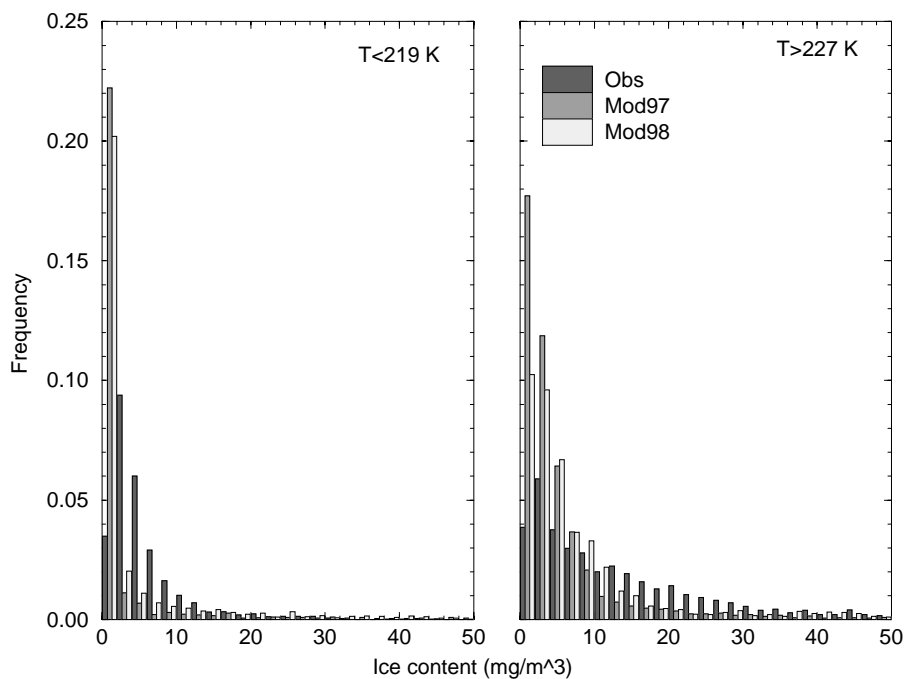


Figure 7.7: Frequency distributions of cloud ice in isolated cirrus (see Mace et al., 1998b, for definition) over the ARM SGP site for two different temperature ranges. Shown are values derived from a combination of radar reflectivity and infrared interferometer data and from two versions of the ECMWF model.

It is evident that a marked difference in the shape of the observed distributions exists for the two temperature regimes. At low temperatures the distribution is fairly narrow and exhibits a large peak at low ice contents. Although similar in shape the distribution at high temperatures is much broader and the peak at low ice contents is less pronounced. Large ice contents are encountered more frequently at high temperatures. The difference in the distributions is captured to a fair degree by the two model versions. However, both

severely overestimate the frequency of very low ice contents and underestimate the number of events with intermediate values. It is evident that despite those problems, the 1998-version of the model, which incorporates a change in the numerical treatment of falling cloud ice, constitutes an improvement over the 1997-version. Although only qualitative in nature the comparison shown is a major step forward in model evaluation. For the first time long time series of observations of cloud ice exist and can be compared to GCM results at least in a statistical way.

All the studies summarized in this section are far from comprehensive and should be considered as first attempts or feasibility studies for the use of data derived from active remote sensors. The prospect of the installation of such instruments on future satellites; the launch of CloudSat (Stephens et al., 1998a), carrying a cloud radar is planned for 2003; emphasises the need for more in-depth studies of this type in order to be able to optimally use the wealth of data the satellite will no doubt provide as soon as it becomes available. The possibility of evaluating both vertical cloud structure and cloud ice content on a global scale, which has been identified as a major gap in our understanding (Stephens et al., 1998b), will open a new era of cloud parametrization evaluation. First glimpses into this era have been taken.

7.6 The use of composite data sets

In the examples above, the evaluation of the cloud parametrization involved either highly averaged information or information from individual case studies. Both types of comparisons have some serious drawbacks. If the model climate of some cloud-related parameter is compared to observations, the reasons for agreement or disagreement can be completely unrelated to the quality of the cloud parametrization. A good example for this might be the simulation of the stratocumulus clouds off the west coasts of the subtropical continents. As shown in Figure 7.3 the ECMWF model strongly underestimates the cloud fraction in those regions. Although one would imagine the cloud parametrization being at fault, it is also entirely possible that the vertical velocity at the top of the PBL, which is a significant component in the equilibrium of many influences that lead to the existence of stratocumulus clouds, is in error. Since there are no observations of vertical velocity, although some comparisons of the ECMWF model subsidence rates in the subtropics have been carried out by Betts et al. (1995), it is difficult to assess whether this is really the case. In turn the possibly wrong subsidence can exist for many reasons, such as errors in the strength of the Hadley

circulation due to errors in cumulus parametrization. From this kind of argument, the details of which are not particularly relevant, it is obvious that comparisons based on the model climate alone can shed little light on what might be wrong with the cloud parametrization scheme.

In regions predominantly covered by one cloud type, such as the above quoted stratocumulus areas, the problems mentioned can partly be overcome by using averages of short-range forecasts to build up the "model climate". This has been demonstrated in Chapter 4 and some further examples have been highlighted above. As already mentioned the advantage of the use of short-range forecasts is that the factors influencing the cloud parametrization can be assumed to be reasonably close to observations, since the latter were used in the generation of the model's initial state. But what about regions of large variance in cloud amount and type, such as over the extratropical oceans. Here one is inclined to prefer case studies of some kind to investigate the performance of the cloud parametrization. This approach can provide substantial amounts of detail on the workings of the parametrization. However, there is one major drawback as well. The choice of the cases for study is far from trivial and is often forced upon the investigation by the limited amount of observations available. This might lead to the choice of interesting, but completely unrepresentative cases. If a cloud parametrization was made to work for such a case the majority of cases might still be poorly simulated. And even if the case is representative, success in simulating an individual case does not guarantee a good performance of the model and the cloud parametrization in general.

A possible way to reconcile the model climate and case study approaches is to find "more intelligent" ways of averaging the data, so that the general characteristics of certain cloud systems remain intact even when a large number of cases is included in the average. Two attempts of such an averaging approach to which the author has contributed will be highlighted here.

A survey of clouds over the North Atlantic and North Pacific

The first composite study outlined here follows an idea of Tselioudis et al. (2000) and is based on data products provided by ISCCP. Up to this point only monthly mean values of total cloud fraction derived in this project have been considered here for the use in model evaluation. ISCCP provides a much larger set of data than that (Rossow and Schiffer, 1991; Rossow and Schiffer, 1999). For each satellite pixel an attempt to derive cloud top pressure

and cloud optical thickness is made and the joint statistical distribution of both parameters over larger areas (roughly 2.5×2.5 degrees) is provided on a three-hourly basis. Tselioudis et al. (2000) use this data to survey the shape of the above distribution functions for the ocean area of the Northern Hemisphere extratropics (NHE, 30° to $60^\circ N$) as a function of dynamical regime. They use the simplest indicator for different "weather" situations, namely the surface pressure, to define three "dynamical" regimes as anomalously low, normal and anomalously high pressure. Even with this extremely simple classification they find remarkably different cloud distributions. An example is shown in the left panels of Figure 7.8. Shown are two-dimensional "histograms" of cloud top pressure versus optical thickness for the NHE in April 1992 when the local surface pressure is more than 5 hPa below (top) and 5 hPa above (bottom) its monthly average value.

The difference in the "cloud" distribution between the two chosen regimes is quite marked. In the below-average pressure regime three predominant types of cloud appear, thick high top clouds, very likely associated with frontal systems, as well as medium-high top thin clouds (most likely altostratus and altocumulus), and low clouds of medium optical thickness associated with cloudiness at the top of the PBL. In the above-average regime the latter become the predominant cloud type while the thick high-top clouds are virtually absent. This type of cloud distribution is what one would expect in the subsidence regions of high-pressure systems over the oceans and ahead of and behind extratropical cyclones (see below). Tselioudis et al. (1998) proposed to use this technique to evaluate the performance of GCMs in simulating not only the mean cloud properties but also the observed difference in cloud structure between the different dynamical regimes. The middle and right panels of Figure 7.8 shows the result of such a comparison using short-range forecasts from the ECMWF model for April 1992. The model is probed in exactly the same way as the data, i.e., local pressure anomalies based on the model results are calculated and the cloud top pressure vs. optical thickness distributions are derived. The technique to derive these distributions from the model cloud fields attempts to find the radiative cloud top (instead of the physical one) by taking into account that the cloud emissivity of thin cirrus layers can be well below one. The technique is described in detail in Klein and Jakob (1999).

A number of important differences between model and data are evident. First of all the total cloud cover, indicated by "TCC" at the top of each panel, is underestimated for both regimes, by about 15 % in the negative anomaly regime and by 20 % for positive pressure anomalies. For negative pressure anomalies, the clouds are, when present, too optically thick

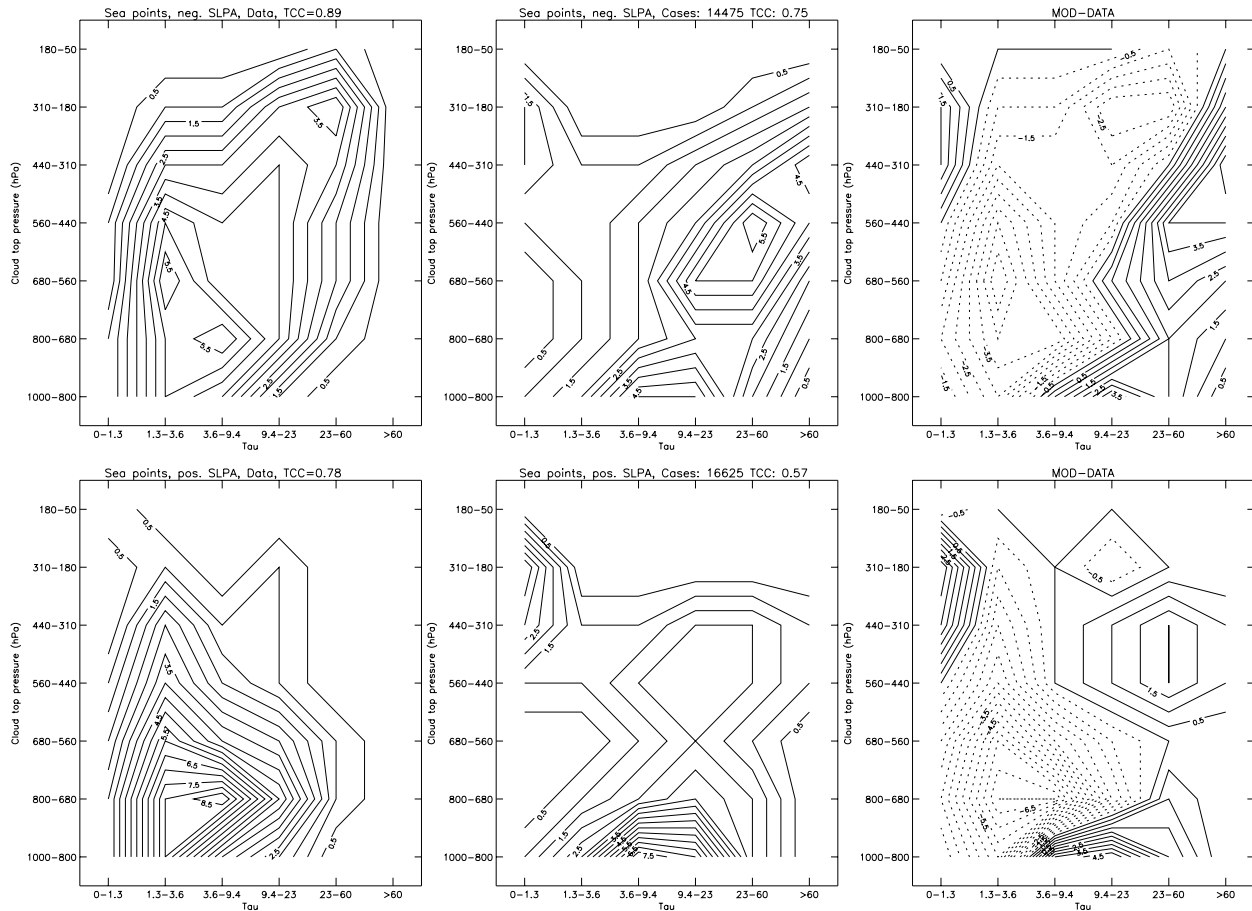


Figure 7.8: Distribution of cloud top pressure vs. cloud optical thickness for the ocean areas of $30^{\circ}N$ to $60^{\circ}N$ in the month of April 1992. The data is stratified into local negative sea level pressure anomalies (from the monthly mean) of more than -5 hPa (top panels) and positive sea level pressure anomalies of more than $+5$ hPa (bottom panels). Distributions are derived from ISCCP D1 data (left), and ECMWF T106L31 12- and 24-hour forecasts (middle). The right panels show the difference between model and data.

and their tops are too low when compared to the data. When repeating the model analysis using the physical instead of the radiative cloud top (not shown), the latter effect disappears, indicating that the model is producing cloud tops at the right height but that the top parts of the clouds are optically too thin, pointing to a deficiency in the ice water content. In the positive pressure anomaly regime the model cloud tops appear to be too low and the clouds are too optically thick. Also the model produces both optically thick mid-level to high-top clouds and thin high-top clouds that are not observed. It is well possible, that the cloud top pressure error for low clouds in this regime is due to the difficulty to determine the exact cloud top in the data for clouds at the top of PBL's capped by an inversion, which can lead to a misinterpretation of the height associated with the measured brightness temperature. However, the overestimation in optical thickness is most likely a true model problem.

It is intriguing that the model has a tendency to underestimate total cloud cover and seems to “compensate” for that by producing too thick clouds. The errors identified here, although for a different period, are nevertheless consistent with the underestimation of the reflection of solar radiation and shortwave cloud radiative forcing that was pointed out in Figures 7.1 and 7.2.

It is worthwhile stressing again, that the comparison carried out here is far from comprehensive and is only meant to illustrate a new technique to try and analyse model errors in the representation of clouds. The technique is currently being refined and other “dynamical” compositing criteria are being investigated. Although simple, the approach proves to provide very useful information on the cloud representation. First, it combines cloud fraction information with radiative effects of the clouds when present by studying the optical thickness. Second, by splitting the data set by using some “dynamic” criterion, regimes in which model errors are particularly large can be identified and investigated further using other tools, such as SCM studies. Furthermore, although short-range forecasts have been used here this is not a requirement of the method, since the dynamical criterion (pressure anomaly of a certain size in this case) can be, and is in the example above, entirely defined by model data. This makes this technique useful not only for NWP models but any GCM.

Validating clouds associated with extratropical cyclones

More complex compositing techniques, that reveal cloud parametrization problems in even greater detail can of course be applied. One such study is that of Klein and Jakob (1999, hereafter KJ99), which is based on an idea of Lau and Crane (1995, hereafter LC95). Here the cloud structure in extratropical cyclones over the North Atlantic is studied. For a given set of locations LC95 identify from data the optically thickest clouds occurring over a number of years and use those events as their compositing criterion. Each maximum-optical-thickness point (in time and space) is then considered the centre of a relative coordinate system and all occurrences (roughly 1200 in LC95) are overlaid using this coordinate system. The result is a composite of the spatial distribution of the observed cloud and other meteorological fields, as shown in the top panel of Figure 7.9.

Shown are the mean anomalies from a five-day average (taken for each individual case) of 1000-hPa horizontal wind (arrows) and geopotential height, as well as the occurrence of various cloud types. High-top clouds are depicted in red, mid-level top clouds in yellow and low top clouds in blue. The darkness of each colour indicates optical thickness. Note, that

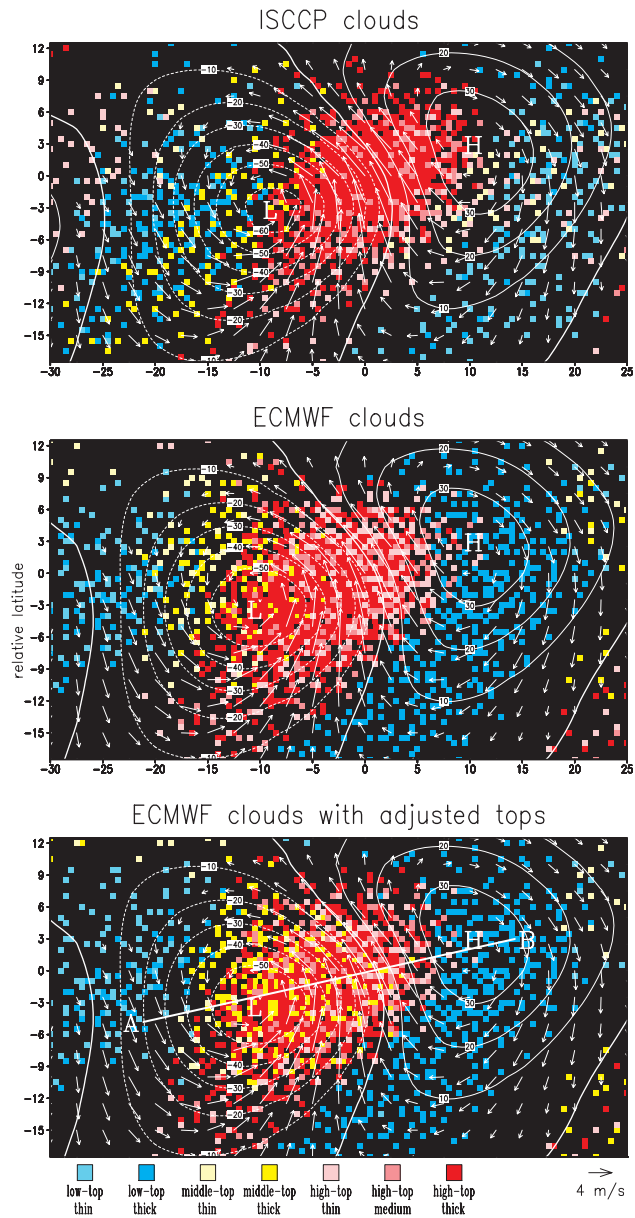


Figure 7.9: (a) Distributions of 1000 hPa horizontal wind (arrows, see scale at bottom right) and geopotential height (contours, interval 10 m) from ERA analyses, and various cloud types (colour pixels) from ISCCP observations as shown in LC95. The ordinate (abscissa) of the coordinate system corresponds to displacements in degrees from the reference location. Inside each $2.5^\circ \times 2.5^\circ$ the presence and abundance of a certain cloud type is indicated by plotting a number of randomly scattered pixels with the colour designated to the cloud type (see legend). Each pixel represents a 1 % positive deviation from the background field as estimated as the five-day average centered on the key dates. (b) as 1(a) but from 24h ERA forecasts using physical cloud top pressure, (c) as 1(b) but using emissivity-adjusted cloud top pressure.

the center of the plot contains the optically thickest clouds by construction. The 1000-hPa height field reveals the relative location of the low pressure center, which is positioned to the southwest of the clouds with maximum optical thickness. A large “shield” of high top thick clouds, as they are normally associated with warm fronts, is evident to the northeast

of the low pressure centre. Middle-top thick clouds extend out of the low-pressure region to the southwest. Ahead and behind the composite cyclone the cloud fields are dominated by low-top medium-thick clouds.

KJ99 have used short-range forecasts from ERA to generate the same picture of the cloud distribution around extratropical cyclones from the ECMWF model. The exact dates and locations of LC95 were used to position the cyclones and the same analysis techniques were applied. As above the cloud top pressure used to define clouds as high-, mid- and low-top can be derived using the physical or the radiative cloud top (see KJ99 for details). The middle panel of Figure 7.9 shows the model results when using the physical cloud top while the bottom panel contains the results for the radiative cloud top. It is evident from this Figure that the model is able to reproduce the overall distribution of cloudiness around the cyclone quite well, perhaps with the exception of the cloud band extending southwestward from the low-pressure centre. On closer inspection, however, similar errors to those identified above in the pressure anomaly composites appear. The high-top clouds are optically too thin, leading to large errors in cloud top height when using the radiative cloud top (which is what a satellite would most likely identify). The low-top clouds are optically too thick in particular in the regions ahead of the cyclone. KJ99 carried out a number of sensitivity studies and identified the microphysical assumptions for ice settling as one of the major sensitivities for the simulation of the high-top cloud optical thickness. None of their studies was able to reduce the error in low-top cloud optical thickness.

The two studies briefly summarized here demonstrate the usefulness of the idea of composite-averaging in the evaluation of cloud parametrizations. By averaging over a large number of cases in such a way that key dynamical and hence cloud structures remain intact, it is possible to identify not only the deficiencies of the model cloud representation but also the dynamic environment in which they occur. This provides first clues for possible model errors, which can then be investigated further. The next section proposes a new strategy for the evaluation of cloud parametrizations in which “compositing” will play a central role.

7.7 A strategy for cloud evaluation

In the previous sections various commonly applied methods for the evaluation of cloud parametrizations have been outlined. Although numerous studies using one or more of the outlined techniques have been published over the last few years, a lack of coherence

in the application of several techniques to the same model is clearly visible. Most likely this is because each of the techniques as such requires substantial resources. However, this apparent lack of a strategy when evaluating cloud parametrizations has led to a considerable dilution of efforts. In this short section a coherent strategy that relies mainly on the known techniques described above will be proposed. It is schematically outlined in Figure 7.10.

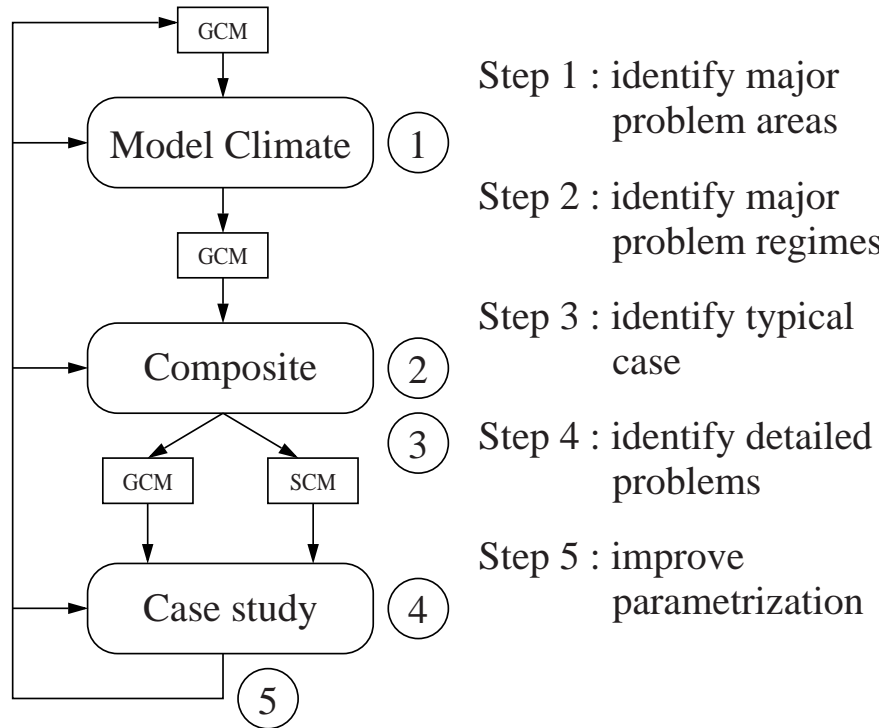


Figure 7.10: A strategy for the evaluation of cloud parametrizations in GCMs.

At the core of this strategy is the attempt to link the evaluation of the model climate to the selection of cases for case studies through the use of compositing techniques such as those described in the previous section. The evaluation of the model climate normally reveals areas (in the geographic sense) in which the clouds and/or their effects are not correctly represented. As pointed out in Section 7.2 it is virtually impossible to infer reasons for the observed errors from such studies. Those can normally only be discovered in detailed case studies. But how should a case be chosen, such that it is typical for the model error? This is where compositing observations and model results using some criterion that describes the main mechanisms in the cloud generation and/or maintenance should prove useful. By applying techniques similar to those highlighted in Section 7.6 not only is a first link to the possible causes for model problems established but also the typical model error is revealed. From the (hopefully) considerable number of cases entering each composite average, one can

then select those for which the model error is close to the mean error in the composite. That way it is ensured that the now following case study represents a typical model behaviour, rather than an extreme one. The case study can be carried out either with the full GCM, e.g., in an NWP environment, or with a corresponding SCM. After improving the parametrization it is of course necessary to repeat the entire validation process to i) test the performance of the new parametrization in all aspects of the model and ii) identify the next target for improvement.

One of the caveats of this strategy is of course the availability of the necessary observational data sets. These need to be fairly comprehensive to enable the use of either an NWP model or an SCM and to facilitate the validation of the results. With the availability of long term data sets such as those collected in the context of ARM program and through the combination of analyses produced by operational NWP centres and the vast amount of satellite data available, these problems appear soluble to a large extent.

Finally it is worthwhile pointing out that the real improvements of a cloud parametrization will not result from evaluation studies of any kind, with or without a strategy. They can only result from the knowledge of the model errors, gained from evaluation studies, and first and foremost from ideas of individuals or groups, which can then be put to the test using the strategy outlined above.

Chapter 8

Concluding remarks

This thesis discusses the cloud parametrization scheme in the global forecast model of ECMWF and the ways that it has been improved since its origin. A number of general key issues for an improved representation of clouds in GCMs have been identified in Chapter 2. Chapters 3 and 4 then established the state of the art when work started. Chapters 5 and 6 contain the author's main contributions to many of the key issues outlined before followed by a short excursion into the evaluation of cloud parametrizations in Chapter 7.

As outlined in chapter 2, modern cloud parametrizations have changed from an integrating to a more process-oriented approach. This transition requires a more detailed description of each individual cloud-generation or cloud-decay process within the limits of a parametrization. One of the most crucial processes of cloud generation is that of moist convection. Despite its importance, a coherent description of the link of convection to cloud parametrization has been elusive for many years (e.g., Randall, 1989). Only recently have attempts been made to introduce a more direct link through the use of detrained condensate as a source of cloud. Here it has been shown for the first time that the source of not only cloud condensate, but also cloud fraction from convection can be derived consistently if the convection parametrization is formulated using the mass-flux approach. It is worthwhile noting that in this derivation no assumptions besides those already made in the convection parametrization itself needed to be introduced. This is important for future improvements and will be discussed further below.

In the same context it was demonstrated that it is possible to derive source terms for the generation of stratiform clouds (both cloud fraction and condensate) using simple distribution assumptions for specific humidity in non-cloudy sky. It has been shown that a strong link exists in this part of the parametrization to the so-called "distribution"-approach to cloud parametrization as used in a variety of GCMs today. The strict derivation of the

source terms for both convective and non-convective processes using clearly stated assumptions has increased the credibility of the use of a prognostic equation for the description of the time-evolution of cloud fraction as introduced by Tiedtke (1993). It was made clear which assumptions were made to derive currently used source terms and how changes to those assumptions will affect the details of the parametrized cloud sources. A brief discussion of cloud decay along the lines of the cloud generation derivations demonstrates that the approaches developed here can be extended to this problem as well.

Another crucial area for necessary improvement as identified at the beginning of this work is that of the description of cloud-microphysical processes. These processes play a decisive role in the determination of the cloud condensate content, which in turn strongly affects the radiative behaviour of the clouds. Most current efforts in this area of research concentrate on the introduction of a higher level of sophistication in the description of the microphysical processes themselves. Here, it was shown that the presence of cloud fraction as a model variable requires careful consideration of the effects of cloud and precipitation overlap. A simple subgrid-scale precipitation model was developed and used to evaluate the performance of the original parametrization of Tiedtke (1993). It was demonstrated that the common treatment of precipitation with a single grid-averaged flux is insufficient and leads to large errors in precipitation evaporation with consequences for the model's hydrological cycle. A new parametrization that separates cloudy and clear-sky precipitation fluxes was developed. This parametrization was evaluated using the subgrid-scale model and successfully introduced into the ECMWF global model. Given the size of the errors found, it can be argued that the improved treatment of cloud fraction in the precipitation parametrization is a necessary prerequisite for the introduction of more sophisticated microphysical formulations. The work described here, although not improving the description of cloud microphysics itself, is therefore of utmost importance for the further development of GCMs in this area.

In order to measure improvement in cloud parametrization it is necessary to develop tools for its verification. A number of verification methods, some of them established, others newly developed, have been illustrated here and examples for their application to validate the ECMWF cloud parametrization have been presented. The use of new data sources that have only recently become available, such as ground-based cloud radar observations, as well as the introduction of new validation techniques, such as that of composite averaging, have played a major role in this description. It has been argued that despite the large variety of efforts in cloud parametrization validation, the results are often unsatisfactory. One possible

reason for this is the sporadic and non-systematic use of one or a few of the available techniques. Therefore a strategy for an improved and more coherent use of the techniques available today has been proposed.

From the summary provided here it is obvious that much of the work presented in this thesis would not have been possible without the support of the entire ECMWF team as well as colleagues from other institutions. Therefore it is valuable to summarize my original contributions.

The two introductory chapters constitute my literature overview and are based on a wide range of published research. The first part of Chapter 3 is based entirely on the work of Tiedtke (1993). The implementation of the cloud scheme into the data assimilation system described in the last section of that chapter has been proposed, carried out and tested by me, although the actual results presented here originate from Mahfouf et al. (1999) who repeated my earlier experiments with a more recent version of the forecasting system. The comparison of the cloud simulations in ERA-15 with satellite observations described in Chapter 4 was planned and carried out entirely by myself and resulted in the publication of the results in Jakob (1999).

The research on cloud source terms from convective sources in the first part of Chapter 5 was inspired by the work of Tiedtke (1993) and Randall (1995). The actual derivation in the form presented here was carried out by me and its results are original. The study of the the stratiform source terms resulted from comments of various colleagues about the original T93 formulation. Dr. S. A. Klein contributed the code for the simplified explicit model used to compare the new formulation to the original. The comparison to the distribution schemes as well as the extension of the method to cloud decay are my original work.

Both the development of the subgrid-scale precipitation model as well the new precipitation parametrization described in Chapter 6 follow my original ideas. The further development of those ideas to actually workable solutions as well as the implementation into the ECMWF model have been carried out equally by myself and Dr. S. A. Klein, who also co-authored the two publications (Jakob and Klein, 1999; Jakob and Klein, 2000), which form the basis of the chapter.

The first sections of Chapter 7, in particular Sections 7.2 and 7.4, rely on standard evaluation procedures followed at ECMWF. The particular examples used were chosen and analyzed by me. Section 7.5 is based on a study I carried out with Dr. G. G. Mace from the University of Utah. It was my idea to compare model forecasts of hydrometeors as categoric forecasts to

radar observations and to evaluate the model performance against some other hypothetical forecasts. I analyzed the model data in that respect and provided Dr. Mace with the results, which he included in the resulting joint publication (Mace et al., 1998a). The work on the use of composite data sets as described in the two parts of section 7.6 was mainly carried out by Drs. S. A. Klein (Klein and Jakob, 1999) and G. Tselioudis (Tselioudis et al., 1998). My role in this work was mainly in the support of the interpretation of the results and some technical assistance. The strategy proposed at the end of the chapter is based on my own ideas and is a result of trying to integrate the various approaches to cloud parametrization evaluation into a coherent methodology.

At the end of an extensive work such as this it is appropriate to briefly discuss the author's personal views on the future developments in the areas covered here.

Cloud parametrizations began as purely a statistical description of the main cloud parameters. More recently a transition to more physically-based, process-oriented approaches has taken place. It is likely that this development will continue over the next few years. This means that the emphasis has shifted from "statistically" describing the clouds themselves to describing the "statistics" of the processes that generate them and that lead to their decay. If one considers for instance vertical motion on various scales as a major cloud production and destruction mechanism, it is necessary to describe, amongst others, the probability distribution function of vertical motion within in a model grid box in order to describe the cloud evolution. It is obvious that the current assumptions used, for instance in Chapter 5, are severe oversimplifications of these pdf's. Very little work has been carried out in this area and the improved representation of statistics of this kind should lead to improved cloud representations.

A somewhat related issue is the description of the strong link between cloud and convection parametrization. It has been shown here that for a certain type of convection parametrization, namely mass-flux schemes, a direct and simple link of that kind can be established without additional assumptions. This means, that an improved representation of convective clouds will depend strongly on the progress made in the description of convection itself. It is rather obvious that the properties of the clouds produced by convection will depend crucially on the microphysical and mixing (entrainment/detrainment) assumptions made in the convection parametrization. Many questions in those areas remain unanswered so far, and progress in convection parametrization will be essential for a better cloud representation in GCMs.

In the area of cloud microphysics the use of more sophisticated bulk-cloud microphysical models has already started. An interesting question will be just how sophisticated these parametrizations need to be in order to capture the essence of the cloud evolution that is necessary to accurately simulate global weather and climate. The answer to these questions are unclear today. Simplified model assumptions, such as the constant presence of sufficient condensation nuclei, are challenged by data at least for ice clouds and need to be revisited. Another crucial question here, as in the treatment of microphysical processes in convection parametrizations, will be how to deal with the strong non-linearities in the behaviour of microphysical processes. An inhomogeneous distribution of condensate in a model grid box, which will undoubtedly result from the possible inhomogeneous distributions of vertical motion discussed above, will lead to very different microphysical evolutions. Work on the importance and the treatment of this in GCMs is only starting.

The area of cloud parametrization validation will be strongly influenced by the availability and use of new data sources, such as space-borne cloud radar and lidar instruments, which for the first time will deliver near-global information on cloud-vertical structure and, more importantly, cloud ice content. The usefulness of these new data sources will depend on the development of adequate techniques of comparison. Use of this data for assimilating cloud information into the data assimilation systems of NWP centres will provide new challenges to the cloud parametrizations applied in those systems and will thereby also contribute to their improvement.

Many important questions in the field of cloud parametrization remain unanswered and will provide challenges to our ability to represent clouds in large-scale models for many years to come.

Appendix A - List of acronyms

3DVAR	3-Dimensional VARIational data assimilation
4DVAR	4-Dimensional VARIational data assimilation
AGCM	Atmospheric General Circulation Model
ARM	Atmospheric Radiation Measurement program
ASTEX	Atlantic Stratocumulus Transition EXperiment
ATEX	Atlantic Trade-wind EXperiment
BOMEX	Barbados Oceanographic and Meteorological EXperiment
CAPE	Convective Available Potential Energy
CCN	Cloud Condensation Nucleus
CEM	Cumulus Ensemble Models
CRF	Cloud Radiative Forcing
CRM	Cloud Resolving Model
CY18R6	ECMWF model version CYcle 18 Release 6
DJF87/88	December/January/February 1987/1988
ECMWF	European Centre for Medium-Range Weather Forecasts
ERA	ECMWF Re-Analysis
ERBE	Earth Radiation Budget Experiment
EZMW	Europäisches Zentrum für Mittelfristige Wettervorhersage
FAR	False Alarm Rate
GARP	Global Atmospheric Research Program
GATE	GARP's Atlantic Tropical EXperiment
GCM	General Circulation Model
GCSS	GEWEX Cloud System Study
GEWEX	Global Energy and Water Cycle EXperiment
GTS	Global Telecommunications System
HR	Hit Rate
IFS	Integrated Forecasting System
ISCCP	International Satellite Cloud Climatology Project
ITCZ	InterTropical Convergence Zone
JJA87	June/July/August 1987
JK99	Reference to Jakob and Klein (1999)
KJ99	Reference to Klein and Jakob (1999)
LC95	Reference to Lau and Crane (1995)
LES	Large Eddy Simulation
LITE	Lidar In-space Technology Experiment
LWCRF	LongWave Cloud Radiative Forcing
MMCR	MilliMetre Cloud Radar

NH	Northern Hemisphere
NHE	Northern Hemisphere Extratropics
NWP	Numerical Weather Prediction
OI	Optimum Interpolation data assimilation
OLR	Outgoing Longwave Radiation
OPS	ECMWF's OPERational Suite
PBL	Planetary Boundary Layer
pdf	probability distribution function
POD	Probability of detection
SCM	Single Column Model
SCO	Single Column Observation
SGP	Southern Great Plains site of the ARM program
SH	Southern Hemisphere
SHEBA	Surface Heat and Energy Budget of the Arctic
SST	Sea Surface Temperature
SWCRF	ShortWave Cloud Radiative Forcing
T93	Reference to Tiedtke (1993)
TOA	Top Of Atmosphere
TOGA COARE	Tropical Ocean Global Atmosphere Coupled Ocean-Atmosphere Response Experiment
TCC	Total Cloud Cover
TS	Threat Score
TSS	True Skill Score
UTC	Universal Time Coordinated
WCRP	World Climate Research Program
WMO	World Meteorological Organization

Appendix B - Mixed phase and saturation water vapour pressure

As discussed in Chapter 3 the ECWMF cloud parametrization solves only one prognostic equation for cloud condensate. Hence, the distinction of the water and ice phase has to be parametrized diagnostically. Cloud water and ice are distinguished solely as a function of temperature by describing the fraction of water in the total condensate, α_w , as

$$\begin{aligned}\alpha_w &= 0 & T \leq T_{ice} \\ \alpha_w &= \left(\frac{T-T_{ice}}{T_0-T_{ice}}\right)^2 & T_{ice} < T < T_0 \\ \alpha_w &= 1 & T \geq T_0.\end{aligned}$$

T_{ice} and T_0 represent threshold temperatures between which a mixed water/ice phase is allowed to exist and are currently chosen as $T_{ice} = 250.16K$ and $T_0 = 273.16K$. Any condensate that is formed or destroyed will be divided into water and ice using α_w . In order to properly account for the thermodynamic effects in the mixed-phase regime the latent heat of phase changes is calculated as

$$L = \alpha_w L_v + (1 - \alpha_w) L_s,$$

where L_v and L_s are the latent heat of vaporisation and sublimation respectively. Furthermore the saturation specific humidity is calculated as

$$q_s = \alpha_w q_{s,wat} + (1 - \alpha_w) q_{s,ice},$$

where the subscripts *wat* and *ice* indicate the saturation values with respect to water and ice, and $q_{s,*}(T, p)$ is described by

$$q_{s,*} = \frac{\epsilon e_{s,*}(T)}{p - (1 - \epsilon) e_{s,*}(T)},$$

where ϵ is the ratio of the specific gas constants for dry air and water vapour, $\epsilon = R_d/R_v$, and the $*$ in the subscript stands for either the water or ice phase. The saturation water vapour pressure is expressed using Tetens formula

$$e_{s,*}(T) = a_1 e^{a_{3,*} \frac{T-T_0}{T-a_{4,*}}}.$$

The constants currently in use are $a_1 = 611.21 Pa$, $a_{3,wat} = 17.502$, $a_{3,ice} = 22.587$, $a_{4,wat} = 32.19 K$, and $a_{4,ice} = -0.7 K$. These values are chosen to provide a best fit to those published in the Smithsonian Meteorological Tables (1951) and the more modern ASHRAE values (Gueymard, 1993) over water (see Simmons et al. (1999) for further details).

References

- Albrecht, B. A., C. S. Bretherton, D. W. Johnson, W. H. Schubert and A. Shelby Frisch, 1995: The Atlantic Stratocumulus Transition Experiment – ASTEX. *Bull. Amer. Meteor. Soc.*, **76**, 889-904.
- Andersson, E., J. Haseler, P. Undén, P. Courtier, G. Kelly, D. Vasiljević, C. Branković, C. Cardinali, C. Gaffard, A. Hollingsworth, C. Jakob, P. Janssen, E. Klinker, A. Lanzinger, M. Miller, F. Rabier, A. Simmons, B. Strauss, J-N. Thépaut and P. Viterbo, 1998: The ECMWF implementation of three dimensional variational assimilation (3DVar). Part III: Experimental results. *Quart. J. Roy. Met. Soc.*, **124**, 1831-1860.
- Arakawa, A., 1969: Parameterization of cumulus convection. *Proc. WMO/IUGG Symp. Numerical Weather Prediction*, Tokyo, Japan. Meteor. Agency, 1-6.
- Arakawa, A., and W. H. Schubert, 1974: Interaction of a cumulus cloud ensemble with the large-scale Environment, Part I. *J. Atmos. Sci.*, **31**, 674-701.
- Arakawa, A., 1975: Modelling clouds and cloud processes for use in climate models. GARP publication series, No. 16: The physical basis of climate and climate modelling.
- Arking, A., 1991: The radiative effects of clouds and their impact on climate. *Bull. Amer. Meteor. Soc.*, **71**, 795-813.
- Augstein, E., H. Riehl, F. Ostapoff, V. Wagner, 1973: Mass and energy transports in an undisturbed Atlantic trade-wind flow. *Mon. Wea. Rev.*, **101**, 101-111.
- Baker, M.B., 1997: Cloud microphysics and climate. *Science*, **276**, 1072-1078.

- Barker, H.W., 1996: A parameterization for computing grid-averaged solar fluxes for inhomogeneous marine boundary layer clouds. Part I: Methodology and homogeneous biases. *J. Atmos. Sci.*, **53**, 2289-2303.
- Barker, H.W., B.A. Wielicki, and L. Parker, 1996: A parameterization for computing grid-averaged solar fluxes for inhomogeneous marine boundary layer clouds. Part II: Validation using satellite data. *J. Atmos. Sci.*, **53**, 2304-2316.
- Barkstrom, B. R., and G. L. Smith, 1986: The Earth Radiation Budget Experiment: Science and implementation. *J. Geophys. Res.*, **24**, 379-390.
- Bechthold, P., J.P. Pinty, and P. Mascart, 1993: The use of partial cloudiness in a warm-rain parameterization: A subgrid-scale precipitation scheme. *Mon. Wea. Rev.*, **121**, 3301- 3311.
- Bechthold, P., S.K. Krueger, W.S. Lewellen, E. van Meijgaard, C.-H. Moeng, D.A. Randall, A. van Ulden, and S. Wang, 1996: Modelling a stratocumulus-topped PBL: Intercomparison among different one- dimensional codes and with large eddy simulation. *Bull. Amer. Meteor. Soc.*, **77**, 2033-2042.
- Bechtold, P., J. L. Redelsperger, I. Beau, M. Blackburn, S. Brinkop, J. Y. Grandpeix, A. Grant, D. Gregory, F. Guichard, C. Hoff, and E. Ioannidou., 2000: A GCMSS model intercomparison for a tropical squall line observed during TOGA-COARE. Part II: Intercomparison of SCMs and with CRM. *Quart. J. Roy. Met. Soc.*, **126**, 865-888.
- Beesley, J. A., C. S. Bretherton, C. Jakob, E. Andreas, J. Intrieri, and T. Uttal, 1999: A comparison of ECMWF model output with observations at SHEBA. *J. Geophys. Res.*, in press.
- Beljaars, A. C. M. and Holtslag, A. A. M., 1991: Flux parametrization over land surfaces for atmospheric models. *J. Appl. Meteor.*, **30**, 327-341.
- Beljaars, A. C. M. and Betts, A. K., 1993: Validation of the boundary layer representation in the ECMWF model. *ECMWF Seminar proceedings on: Validation of models over Europe, 7-11 September 1992*, **Vol II**, 159-196.
- Beljaars, A. C. M., 1995a: The parametrization of surface fluxes in large scale models under

- free convection. *Quart. J. Roy. Met. Soc.*, **121**, 255-270.
- Beljaars, A. C. M., 1995b: The impact of some aspects of the boundary layer scheme in the ECMWF model. *ECMWF Seminar proceedings on: Parametrization of subgrid-scale physical processes, September 1994*.
- Betts, A. K., C. S. Bretherton, and E. Klinker, 1995: Relation between mean boundary layer structure and cloudiness at the R/V Valdivia during ASTEX. *J. Atmos. Sci.*, **52**, 2752-2762.
- Bony, S., Lau, K.-M., Sud, Y. C., 1997: Sea surface temperature and large-scale circulation influences on tropical greenhouse effect and cloud radiative forcing. *J. Clim.*, **10**, 2055-2077.
- Bougeault, P., 1981: Modelling the trade-wind cumulus boundary layer. Part I: Testing the ensemble cloud relations against numerical data. *J. Atmos. Sci.*, **38**, 2414-2428.
- Bretherton, C. S., S. K. Krueger, M. C. Wyant, P. Bechtold, E. van Meijgaard, B. Stevens, and J. Teixeira, 1999: A GCSS boundary layer model intercomparison study of the first ASTEX Lagrangian experiment. *Boundary-Layer Meteorol.*, **93**, 341-380.
- Bretherton, C. S., S. R. de Roode, and C. Jakob, E. L. Andreas, J. Intrieri, and R. E. Moritz, 2000: A comparison of the ECMWF forecast model with observations over the annual cycle at SHEBA. submitted to *J. Geophys. Res.*
- Browning, K. A., 1993: The GEWEX Cloud System Study (GCSS). *Bull. Amer. Meteor. Soc.*, **74**, 387-399.
- Buizza, R., T. Petroliagis, T. N. Palmer, J. Barkmeijer, M. Hamrud, A. Hollingsworth, A. Simmons and N. Wedi, 1998: Impact of model resolution and ensemble size on the performance of an ensemble prediction system. *Quart. J. Roy. Met. Soc.*, **124**, 1935-1960.
- Buizza, R., J. Barkmeijer, T. Palmer and D.S. Richardson, 1999: Current status and future developments of the ECMWF ensemble prediction system. In *Proceedings of the ECMWF Expert meeting on ensemble prediction system*, 15-16 June, 1998, ECMWF, Shinfield Park, Reading, RG2 9AX, UK.
- Cahalan, R.F. et al., 1994: The Albedo of Fractal Stratocumulus Clouds. *J. Atmos. Sci.*,

51, 2434-2455.

Cess, R.D., and G.L. Potter, 1987: Exploratory studies of cloud radiative forcing with a general circulation model. *Tellus*, **39A**, 460-473.

Cess, R.D., G.L. Potter, J.-P. Blanchet, G.J. Boer, M. Deque, W.L. Gates, S.J. Ghan, J.T. Kiehl, H. Le Treut, Z.X. Li, X.-Z. Liang, B.J. McAvaney, V.P. Meleshko, J.F.B. Mitchell, J.-J. Morcrette, D.A. Randall, L. Rikus, E. Roeckner, J.-F. Royer, U. Schlese, D.A. Sheinin, A. Slingo, A.P. Sokolov, K.E. Taylor, W.M. Washington, R.T. Wetherald, and I. Yagai, 1990: Intercomparison and interpretation of climate feedback processes in seventeen atmospheric general circulation models. *J. Geophys. Res.*, **95D**, 16601-16617.

Cess, R.D., G.L. Potter, W.L. Gates, J.J. Morcrette, and L. Corsetti, 1992: Comparison of general circulation models to Earth Radiation Budget Experiment data: Computation of clear-sky fluxes. *J. Geophys. Res.*, **97D**, 20421-20426.

Cess, R.D., M.H. Zhang, W.J. Ingram, G.L. Potter, V. Alekseev, H.W. Barker, E. Cohen-Solal, R.A. Colman, D.A. Dazlich, A.D. Del Genio, M.R. Dix, V. Dymnikov, M. Esch, L.D. Fowler, J.R. Fraser, V. Galin, W.L. Gates, J.J. Jack, J.T. Kiehl, H. Le Treut, K. K.-W. Lo, B.J. McAvaney, V.P. Meleshko, J.-J. Morcrette, D.A. Randall, E. Roeckner, J.-F. Royer, M.E. Schlesinger, P.V. Sporyshev, B. Timbal, E.M. Volodin, K.E. Taylor, W. Wang, and R.T. Wetherald, 1996: Cloud feedback in atmospheric general circulation models: An update. *J. Geophys. Res.*, **101D**, 12791-12794.

Cotton, W. R., and R. A. Anthes, 1989: Storm and cloud dynamics. Academic Press, 880 pp.

Courtier, P., E. Andersson, W. Heckley, J. Pailleux, D. Vasiljević, M. Hamrud, A. Hollingsworth, F. Rabier and M. Fisher, 1998: The ECMWF implementation of three dimensional variational assimilation (3DVar). Part I: Formulation. *Quart. J. Roy. Met. Soc.*, **124**, 1783-1808.

Curry, J. A., P. V. Hobbs, M. D. King, D. A. Randall, P. Minnis, G. A. Isaac, J. O. Pinto, T. Uttal, A. Bucholtz, D. G. Cripe, H. Gerber, C. W. Fairall, T. J. Garrett, J. Hudson, J. M. Intrieri, C. Jakob, T. Jensen, P. Lawson, D. Marcotte, L. Nguyen, P. Pielewski, A. Rangno,

- D. C. Rogers, K. B. Strawbridge, F. P. J. Valero, A. G. Williams, D. Wylie, 2000: FIRE Arctic clouds experiment. *Bull. Amer. Meteor. Soc.*, **81**, 5-29.
- Daley, R., 1991: Atmospheric data analysis. *Cambridge University Press*, 457pp.
- Del Genio, A. D., and M.-S. Yao, 1990: Predicting cloud water variations in the GISS GCM. *Preprints of Conf. on Cloud Physics*, San Francisco, Amer. Meteor. Soc., 497-504.
- Del Genio, A.D., M.-S. Yao, W. Kovari, and K.K.-W. Lo, 1996: A prognostic cloud water parametrization for global climate models. *J. Clim.*, **9**, 270-304.
- Donner, L. J., C. J. Seman, B. J. Soden, R. S. Hemler, J. C. Warren, J. Stroehm, and K.-N. Liou, 1997: Large-scale ice clouds in the GFDL SKYHI general circulation model. *J. Geophys. Res.*, **102D**, 21745-21768.
- Ellis, J. S., 1978: Cloudiness, the planetary radiation budget and climate. Ph.D. thesis, Colorado State University, Fort Collins, 129 pp.
- Emanuel, K. A., and D. J. Raymond, 1993: The representation of cumulus convection in numerical models. *Meteorol. Monographs of the Amer. Meteorol. Soc.*, **46**, 246 pp.
- Emanuel, K. A., 1994: Atmospheric convection. *Oxford University Press*, 580 pp.
- Fowler, L.D., D.A. Randall, and S.A. Rutledge, 1996: Liquid and ice cloud microphysics in the CSU general circulation model. Part I: Model description and simulated microphysical processes. *J. Clim.*, **9**, 489-529.
- Geleyn, J.-F., and A. Hollingsworth, 1979: An economical analytical method for the computation of the interaction between scattering and line absorption of radiation. *Beitr. Phys. Atmos.*, **52**, 1-16.
- Geleyn, J.-F., 1980: Some diagnostics of the cloud/radiation interaction in the ECMWF forecasting model. *ECMWF Workshop on 'Radiation and cloud-radiation interaction in numerical modelling.'*, 135-162.
- Ghan, S. J. and R. C. Easter, 1992: Computationally efficient approximations to stratiform

cloud microphysics parameterization. *Mon. Wea. Rev.*, **120**, 1572-1582.

Gibson, J.K., P. Kållberg, S. Uppala, A. Hernandez, A. Nomura, and E. Serrano, 1997: ECMWF Re-Analysis Project Report Series: 1. ERA description. *ECMWF 1997*, 72 pp.

Gierens, K., U. Schumann, M. Helten, H. Smit, A. Marengo, 1999: A distribution law for relative humidity in the upper troposphere and lower stratosphere derived from three years of MOZAIC measurements. *Annales Geophysicae*, **17**, 1218-1226.

Gierens, K., U. Schumann, M. Helten, H. Smit, and Pi-H. Wang, 2000: Ice-supersaturated regions and sub visible cirrus in the northern midlatitude upper troposphere, *J. Geophys. Res.*, in press.

Gregory, D., and P. R. Rowntree, 1990: A mass flux convection scheme with representation of cloud ensemble characteristics and stability- dependent closure. *Mon. Wea. Rev.*, **118**, 1483-1506.

Gregory, D., 1995: A consistent treatment of evaporation of rain and snow for use in large-scale models. *Mon. Wea. Rev.*, **123**, 2716-2732.

Gregory, D., J.-J. Morcrette, C. Jakob, A. C. M. Beljaars, and T. Stockdale, 2000: Revision of convection, radiation and cloud schemes in the ECMWF Integrated Forecasting System. *Quart. J. Roy. Met. Soc.*, **126**, 1685-1710.

Gueymard, C., 1993: Assessment of the accuracy and computing speed of simplified saturation vapor equations using a new reference data set. *J. Appl. Meteor.*, **32**, 1294-1300.

Hartmann, D. L., and D. Doelling, 1991: On the net radiative effectiveness of clouds. *J. Geophys. Res.*, **96D**, 869-891.

Heymsfield, A.J., and L.J. Donner, 1990: A Scheme for Parameterizing Ice-Cloud Water Content in General Circulation Models. *J. Atmos. Sci.*, **47**, 1865-1877.

Heymsfield, A. J., L. M. Miloshevich, C. Twohy, G. Sachse, and S. Oltmans, 1998: Upper-tropospheric relative humidity observations and implications for cirrus ice nucleation. *Geophys. Res. Letters*, **25**, 1343-1346.

- Hogan, R. J., C. Jakob, A. J. Illingworth, 2000: Comparison of ECMWF cloud fraction with radar derived values. submitted to *J. Appl. Meteor.*
- Holland, J. Z., and E. M. Rasmusson, 1973: Measurements of atmospheric mass, energy and momentum budgets over a 500-kilometer square of tropical ocean. *Mon. Wea. Rev.*, **101**, 44-55.
- Hortal, M., and A.J. Simmons, 1991: Use of reduced Gaussian grids in spectral models. *Mon. Wea. Rev.*, **119**, 1057-1074.
- Hortal, M.; The development and testing of a new two-time-level semi-Lagrangian scheme (SETTLS) in the ECMWF forecast model. *ECMWF Technical Memorandum*, **292**, 17 pp.
- Houze jr., R. A. and A. K. Betts, 1981: Convection in GATE. *Rev. Geophys. Space Phys.*, **19**, 541-576.
- Houze jr., R. A., 1993: Cloud Dynamics. *Academic Press*, 573 pp.
- Huang, X.-Y., and H. Sundqvist, 1993: Initialization of Cloud Water Content and Cloud Cover for Numerical Prediction Models. *Mon. Wea. Rev.*, **121**, 2719-2726.
- Hsie, E. Y., R. D. Farley, and H. D. Orville, 1980: Numerical simulation of ice phase convective cloud seeding. *J. Appl. Meteor.*, **19**, 950-977.
- Jakob, C., 1994: The Impact of the New Cloud Scheme on ECMWF's Integrated Forecasting System (IFS), *Proceedings of ECMWF/GEWEX Workshop on Modelling, Validation and Assimilation of Clouds*, ECMWF, November 1994.
- Jakob, C., 1999: Cloud cover in the ECMWF reanalysis. *J. Clim.*, **12**, 947-959.
- Jakob, C., and S. A. Klein, 1999: The role of vertically varying cloud fraction in the parametrization of microphysical processes in the ECMWF model. *Quart. J. Roy. Met. Soc.*, **125**, 941-965.
- Jakob, C., and S. A. Klein, 2000: A parametrization of the effects of cloud and precipitation overlap for use in General Circulation Models. *Quart. J. Roy. Met. Soc.*, **126**, 2525-2544.

- Jakob, C., 2000: Ice clouds in Numerical Weather Prediction models - progress, problems, and prospects. in Lynch, D. (ed.) "Cirrus", Oxford University Press, in press.
- Janssen, P. A. E. M., B. Hansen, and J.-R. Bidlot, 1997. Verification of the ECMWF Wave Forecasting system against Buoy and Altimeter Data. *Weather and Forecasting*, **12**, 763-784.
- Jensen, E. J., O. B. Toon, S. A. Vay, J. Ovarlez, R. May, P. Bui, C. H. Twohy, B. Gandrud, R. F. Pueschel, and U. Schumann, 2000: Prevalence of ice supersaturated regions in the upper troposphere: Implications for optically thin ice cloud formation. *J. Geophys. Res.*, in press.
- Kalnay, E., M. Kanamitsu, R. Kistler, W. Collins, D. Deaven, L. Gandin, M. Iredell, S. Saha, G. White, J. Woollen, Y. Zhu, M. Chelliah, W. Ebisuzaki, W. Higgins, J. Janowiak, K.C. Mo, C. Ropelewski, J. Wang, A. Leetmaa, R. Reynolds, R. Jenne, and D. Joseph, 1996: The NCEP/NCAR 40-year reanalysis project. *Bull. Amer. Meteor. Soc.*, **77**, 437-471.
- Kessler, E., 1969: On the distribution and continuity of water substance in atmospheric circulations. *Meteor. Monogr.*, **10**, No. 32, Amer. Met. Soc., 84 pp.
- Khvorostyanov, V. I., and K. Sassen, 1998a: Cirrus cloud simulation using explicit microphysics and radiation. Part I: Model description. *J. Atmos. Sci.*, **55**, 1808-1821.
- Khvorostyanov, V. I., and K. Sassen, 1998b: Cirrus cloud simulation using explicit microphysics and radiation. Part II: Microphysics, vapor and ice mass budgets, and optical and radiative properties. *J. Atmos. Sci.*, **55**, 1822-1845.
- Klein, S. A., and D. L. Hartmann, 1993: The seasonal cycle of low stratiform clouds. *J. Clim.*, **6**, 1587-1606
- Klein, S. A., and C. Jakob, 1999: Validation and sensitivities of frontal clouds simulated by the ECMWF model. *Mon. Wea. Rev.*, **127**, 2514-2531.
- Klinker, E., F. Rabier, G. Kelly, and J.-F. Mahfouf, 2000: The ECMWF operational implementation of four dimensional variational data assimilation. Part III: Experimental results and diagnostics with the operational configuration. *Quart. J. Roy. Met. Soc.*, **126**, 1191-1215.

- Komen, G. J., L. Cavaleri, M. Donelan, K. Hasselmann, S. Hasselmann and P.A.E.M. Janssen, 1994: Dynamics and modelling of ocean waves. *Cambridge University Press*, 532pp.
- Krueger, S. K., G. T. McLean, and Q. Fu, 1995a: Numerical simulation of the stratus-to-cumulus transition in the subtropical marine boundary layer. Part I: Boundary-layer structure. *J. Atmos. Sci.*, **52**, 2839-2850.
- Krueger, S. K., G. T. McLean, and Q. Fu, 1995b: Numerical simulation of the stratus-to-cumulus transition in the subtropical marine boundary layer. Part II: Boundary-layer circulation. *J. Atmos. Sci.*, **52**, 2851-2868.
- Lau, N.-C., and M.W. Crane, 1995: A satellite view of the synoptic- scale organization of cloud properties in Midlatitude and Tropical circulation systems. *Mon. Wea. Rev.*, **7**, 1984-2006.
- Le Treut, H., and Z.-X. Li, 1988: Using Meteosat data to validate a prognostic cloud generation scheme. *Atm. Res.*, **21**, 273-292.
- Liang, X.-Z., and W.-C. Wang, 1997: Cloud overlap effects on general circulation model climate simulations. *J. Geophys. Res.*, **102**, 11039-11047.
- Lin, Y.-L., R. D. Farley, and H. D. Orville, 1983: Bulk-parameterization of the snow field in a cloud model. *J. Clim. Appl. Meteor.*, **22**, 1065-1092.
- Liou, K. N., 1992: Radiation and cloud processes in the atmosphere. *Oxford University Press*, 487 pp.
- Lohmann, U., and E. Roeckner, 1995: Influence of cirrus cloud radiative forcing on climate and climate sensitivity in a general circulation model. *J. Geophys. Res.*, **100**, 16305-16323.
- Lohmann, U. and E. Roeckner, 1996: Design and performance of a new cloud microphysics scheme developed for the ECHAM general circulation model. *Clim. Dyn.*, **12**, 557-572.
- Lott, F. and Miller, M.J., 1997: A new subgrid-scale orography parametrization: Its formulation and testing, *Quart. J. Roy. Met. Soc.*, **123**, 101-127.

- Louis, J.F., Tiedtke, M. and Geleyn, J.F., 1982: A short history of the operational PBL-parameterization at ECMWF. *Workshop on boundary layer parameterization, November 1981*
- Mace, G.G., C. Jakob, and K. P. Moran, 1998a: Validation of hydrometeor occurrence predicted by the ECMWF model using millimeter wave radar data. *Geophys. Res. Letters*, **25**, 1645-1648.
- Mace G. G., T. P. Ackerman, P. Minnis and D. F. Young, 1998b: Cirrus layer microphysics properties derived from surface-based millimeter radar and infrared interferometer data. *J. Geophys. Res.*, **103**, 23207-23216.
- Machenhauer, B., 1979: The spectral method. in *Numerical Methods used in atmospheric models.*, GARP publication series No. 17, 121-275.
- Mahfouf, J.-F., A. C. M. Beljaars, F. Chevallier, D. Gregory, C. Jakob, M. Janisková, J.-J. Morcrette, and P. Viterbo, 1999: The importance of the Earth Radiation Mission for numerical weather prediction. *ECMWF Technical Memorandum*, **288**, 77 pp.
- Mahfouf, J.-F., and F. Rabier, 2000: The ECMWF operational implementation of four dimensional variational data assimilation. Part II: Experimental results with improved physics. *Quart. J. Roy. Met. Soc.*, **126**, 1171-1190.
- Manabe, S., J. Smagorinsky, and R. F. Strickler, 1965: Simulated climatology of a general circulation model with a hydrological cycle. *Mon. Wea. Rev.*, **93**, 769-798.
- Mason, P. J., 1994: Large-eddy simulation: A critical review of the technique. *Quart. J. Roy. Met. Soc.*, **120**, 1-26.
- McCormick, M. P., D. M. Winker, E. V. Browell, J. A. Coakley, C. S. Gardner, R. M. Hoff, G. S. Kent, S. H. Melfi, R. T. Menzies, C. M. R. Platt, D. A. Randall, and J. A. Reagan, 1993: Scientific investigations planned for the Lidar In-space Technology Experiment (LITE). *Bull. Amer. Meteor. Soc.*, **74**, 205-214.
- Miller, S. D., G. L. Stephens, and A. C. M. Beljaars, 1999: A validation survey of the ECMWF prognostic cloud scheme using LITE. *Geophys. Res. Letters*, **26**, 1417-1420.

- Moeng, C.-H., W. R. Cotton, C. S. Bretherton, A. Chlond, M. Khairoutdinov, S. Krueger, W. S. Lewellen, M. K. MacVean, J. R. M. Pasquier, H. A. Rand, A. P. Siebesma, R. I. Sykes, and B. Stevens, 1996: Simulation of a stratocumulus-topped PBL: Intercomparison among different numerical codes. *Bull. Amer. Meteor. Soc.*, **77**, 261-278.
- Molteni, F. R. Buizza, T.N. Palmer and T. Petroliagis, 1996: The ECMWF ensemble prediction system: methodology and validation. *Quart. J. Roy. Met. Soc.*, **119**, 269-298.
- Moncrieff, M.W., S.K. Krueger, D. Gregory, J.-L. Redelsperger, and W.-K. Tao, 1997: GEWEX Cloud System Study (GCSS) working group 4: Precipitating convective cloud systems. *Bull. Amer. Meteor. Soc.*, **78**, 831-845.
- Morcrette, J.-J., and Y. Fouquart, 1986: The overlapping of cloud layers in shortwave radiation parameterizations. *J. Atmos. Sci.*, **43**, 321-328.
- Morcrette, J.-J., 1990: Impact of changes in the radiation transfer parametrization plus cloud optical properties in the ECMWF model. *Mon. Wea. Rev.*, **118**, 847-873
- Morcrette, J.-J., 1991: Radiation and cloud radiative properties in the European Centre for Medium-Range Weather Forecasts forecasting system. *J. Geophys. Res.*, **96**, 9121-9132
- Morcrette, J.-J., and C. Jakob, 2000: The response of the ECMWF model to changes in cloud overlap assumption. *Mon. Wea. Rev.*, **128**, 1707-1732..
- Nitta, T., and S. Esbensen, 1974: Heat and moisture budget analyses using BOMEX data. *Mon. Wea. Rev.*, **102**, 17-28.
- Ooyama, V. K., 1971: A theory on parametrization of cumulus convection. *J. Meteor. Soc. Japan*, **49**, 744-756.
- Ose, T., 1993: An examination of the effects of explicit cloud water in the UCLA GCM. *J. Meteor. Soc. Japan*, **71**, 93-109.
- Pruppacher, H. R., and J. D. Klett, 1997: Microphysics of clouds and precipitation. Kluwer Academic Publishers, 954 pp.

- Rabier, F., A. McNally, E. Andersson, P. Courtier, P. Undén, J. Eyre, A. Hollingsworth and F. Bouttier, 1998: The ECMWF implementation of three dimensional variational assimilation (3DVar). Part II: Structure functions. *Quart. J. Roy. Met. Soc.*, **124**, 1809-1829.
- Rabier, F., H. Järvinen, E. Klinker, J.-F. Mahfouf, and A. Simmons, 2000: The ECMWF operational implementation of four dimensional variational data assimilation. Part I: Experimental results with simplified physics. *Quart. J. Roy. Met. Soc.*, **126**, 1143-1170.
- Ramanathan, V., 1987: The role of Earth radiation budget studies in climate and general circulation research. *J. Geophys. Res.*, **92**, 4075-4094.
- Ramanathan, V., R. D. Cess, E. F. Harrison, P. Minnis, B. R. Barkstrom, E. Ahmad, and D. Hartmann, 1989: Cloud radiative forcing and climate: Results from the Earth Radiation Budget Experiment. *Science*, **243**, 57-63.
- Randall, D.A., 1989: Cloud parameterization for climate modeling: Status and prospects. *Atm. Res.*, **23**, 245-361.
- Randall, D. A., Harshvardhan, D. A. Dazlich, and T. G. Corsetti, 1989: Interactions among radiation, convection and large-scale dynamics in a General Circulation Model. *J. Atmos. Sci.*, **46**, 1943-1970.
- Randall, D. A., 1995: Parameterizing fractional cloudiness produced by cumulus detrainment. In *Cloud Microphysics Parameterizations in Global Atmospheric Circulation Models*, **WMO/TD-No. 713**, 1-16.
- Randall, D. A., and L. D. Fowler, 1999: EAULIQ: The next generation. *Colorado State University Atmospheric Science Paper*, **673**, 65 pp.
- Randall, D. A., and D. G. Cripe, 1999: Alternative methods for specification of observed forcing in single-column models and cloud system models. *J. Geophys. Res.*, **104**, 24527-24546.
- Rasch, P. J., and J. E. Kristjansson, 1998: A comparison of the CCM3 model climate using diagnosed and predicted condensate parameterizations. *J. Clim.*, **11**, 1587-1614.

- Redelsperger, J. L., P. R. A. Brown, F. Guichard, C. Hoff, M. Kawasima, S. Lang, Th. Montmerle, K. Nakamura, K. Saito, C. Seman, W. K. Tao, and L.J. Donner., 2000: A GCMSS model intercomparison for a tropical squall line observed during TOGA-COARE. Part I: Cloud-Resolving Models. *Quart. J. Roy. Met. Soc.*, **126**, 823-863.
- Ricard, J. L., and J. F. Royer, 1993: A statistical cloud scheme for use in an AGCM. *Annales Geophysicae*, **11**, 1095-1115.
- Ritchie, H., C. Temperton, A.J. Simmons, M. Hortal, T. Davies, D. Dent, and M. Hamrud, 1995: Implementation of the Semi-Lagrangian method in a high resolution version of the ECMWF forecast model. *Mon. Wea. Rev.*, **123**, 489-514.
- Roeckner, E., 1995: Parameterization of cloud radiative properties in the ECHAM4 model. 'Cloud microphysics parameterizations in global atmospheric circulation models', **WMO-TD-No. 713**, 105-116.
- Rossow, W.B., and R.A. Schiffer, 1983: The International Satellite Cloud Climatology Project (ISCCP): The first project of the World Climate Research Program. *Bull. Amer. Meteor. Soc.*, **64**, 779-784.
- Rossow, W.B., and R.A. Schiffer, 1991: ISCCP cloud data products. *Bull. Amer. Meteor. Soc.*, **72**, 2-20.
- Rossow, W.B., and L.C. Garder, 1993a: Cloud detection using satellite measurement of infrared and visible radiances for ISCCP. *J. Clim.*, **6**, 2341-2369.
- Rossow, W.B., and L.C. Garder, 1993b: Validation of ISCCP cloud cloud detections. *J. Clim.*, **6**, 2370-2393.
- Rossow, W.B., A.W. Walker, D.E. Beuschel, and M.D. Roiter, 1996: International Satellite Cloud Climatology Project (ISCCP) Documentation of New Cloud Datasets. WMO/TD-No. 737, World Meteorological Organization, 115 pp.
- Rossow, W. B., and R. A. Schiffer, 1999: Advances in understanding clouds from ISCCP. *Bull. Amer. Meteor. Soc.*, **80**, 2261-2287.

- Rotstayn, L.D., 1997: A physically based scheme for the treatment of stratiform clouds and precipitation in large-scale models. I: Description and evaluation of the microphysical processes. *Quart. J. Roy. Met. Soc.*, **123**, 1227-1282.
- Rutledge, S.A., and P.V. Hobbs, 1983: The mesoscale and microscale structure and organization of clouds and precipitation in midlatitude cyclones. VIII: A model for the "seeder-feeder" process in warm-frontal rainbands. *J. Atmos. Sci.*, **40**, 1185-1206.
- Ryan, B. F., J. J. Katzfey, D. J. Abbs, C. Jakob, U. Lohmann, B. Rockel, L. D. Rotstayn, R. E. Stewart, K. K. Szeto, G. Tselioudis, and M. K. Yau, 2000: Simulation of a cold front using cloud-resolving, limited-area, and large-scale models. *Mon. Wea. Rev.*, in press.
- Schubert, S.D., J. Pfaendtner, and R. Rood, 1993: An assimilated data set for Earth science applications. *Bull. Amer. Meteor. Soc.*, **74**, 2331-2342.
- Schubert, W. H., P. E. Ciesielski, C. Lu, and R. H. Johnson, 1995: Dynamical adjustment of the trade wind inversion layer. *J. Atmos. Sci.*, **52**, 2941-2952.
- Schumann, U., H. Schlager, F. Arnold, J. Ovarlez, H. Kelder, . Hov, G. Hayman, I. S. A. Isaksen, J. Staehelin, and P. D. Whitefield, 2000: Pollution from aircraft emissions in the North Atlantic flight corridor: Overview on the POLINAT projects, *J. Geophys. Res.*, **105**, 3605-3631.
- Simmons, A.J., and R. Strufing, 1981: An energy and angular-momentum conserving scheme, hybrid coordinates and medium-range weather prediction, *ECMWF Tech. Rep.*, **No. 28**.
- Simmons, A. J., A. Untch, C. Jakob, P. Källberg, and P. Undén, 1999: Stratospheric water vapour and tropical tropopause temperatures in the ECMWF analyses and multi-year simulations. *Quart. J. Roy. Met. Soc.*, **125**, 353-386.
- Slingo, J. M., 1980: A cloud parametrization scheme derived from GATE data for use with a numerical model. *Quart. J. Roy. Met. Soc.*, **106**, 747-770.
- Slingo, J.M., 1987: The development and verification of a cloud prediction scheme for the ECMWF model. *Quart. J. Roy. Met. Soc.*, **113**, 899-927.

Slingo, A., and J. M. Slingo, 1988: The response of a general circulation model to cloud longwave radiative forcing. I: Introduction and initial experiments. *Quart. J. Roy. Met. Soc.*, **114**, 1027-1062.

Smagorinsky J., 1960: On the dynamical prediction of large-scale condensation by numerical methods. *Geophys. Monogr.*, **5**, 71-78.

Smith, R.N.B., 1990: A scheme for predicting layer clouds and their water content in a general circulation model. *Quart. J. Roy. Met. Soc.*, **116**, 435-460.

Smithsonian Meteorological Tables, 1951, prepared by R. J. List. Smithsonian Institute Press, Washington, USA.

Sommeria, G., and J. W. Deardoff, 1977: Subgrid-scale condensation in models of non-precipitating clouds. *J. Atmos. Sci.*, **34**, 344-355.

Stendel, M., and K. Arpe, 1997: ECMWF Reanalysis Project Report Series: 6. Evaluation of the hydrological cycle in reanalyses and observations. *ECMWF 1997*, 52 pp.

Stephens, G. L., D. G. Vane, and S. J. Walter, 1998a: The CloudSat mission: A new dimension to space-based observations of cloud in the coming millenium. *Proceedings of GCSS-WGNE Workshop on cloud processes and feedbacks in large-scale models*, ECMWF, 9-13 November 1998.

Stephens, G. L., C. Jakob, and M. Miller, 1998b: Atmospheric ice - a major gap in understanding the effects of clouds on climate. *GEWEX Newsletter*, **8**, no. 1.

Stokes, G.M., and S.E. Schwartz, 1994: The Atmospheric Radiation Measurement (ARM) Program: Programmatic background and design of the Cloud and Radiation Test Bed, *Bull. Amer. Meteor. Soc.*, **75**, 1201-1221.

Stubenrauch, C.J., A.D. Del Genio, and W.B. Rossow, 1997: Implementation of subgrid cloud vertical structure inside a GCM and its effect on the radiation budget. *J. Clim.*, **10**, 273-287.

Stull, R. B., 1988: An introduction to boundary layer meteorology. *Kluwer Academic Pub-*

lishers, 666 pp.

Sui, C.-H., K.-M. Lau, Y.N. Takayabu, and D.A. Short, 1997: Diurnal variations in Tropical oceanic cumulus convection during TOGA COARE. *J. Atmos. Sci.*, **54**, 639-655.

Sundqvist, H., 1978: A parameterization scheme for non-convective condensation including prediction of cloud water content, *Quart. J. Roy. Met. Soc.*, **104**, 677-690.

Sundqvist, H., 1988: Parameterization of condensation and associated clouds in models for weather prediction and general circulation simulation, *Physically-Based Modelling and Simulation of Climate and Climate Change*, M.E. Schlesinger, Ed., Kluwer, 433-461.

Temperton, C., M. Hortal, and A. Simmons, 1999: A two time-level semi-Lagrangian global spectral model. *ECMWF Technical Memorandum*, **283**, 18pp.

Tian, L., and J.A. Curry, 1989: Cloud overlap statistics. *J. Geophys. Res.*, **94**, 9925-9935.

Tiedtke, M., 1989: A comprehensive mass flux scheme for cumulus parametrization in large-scale models. *Mon. Wea. Rev.*, **117**, 1779-1800.

Tiedtke, M., 1993: Representation of Clouds in Large-Scale Models, *Mon. Wea. Rev.*, **121**, 3040-3061.

Tiedtke, M., 1996: An extension of cloud-radiation parameterization in the ECMWF model: The representation of subgrid-scale variations of optical depth. *Mon. Wea. Rev.*, **124**, 745-750.

Tselioudis, G., C. Jakob, and U. Lohmann, 1998: A methodology to construct survey cloud datasets for climate model validation. *Report of GCSS Working Group 3 to the GCSS Science Panel*, Hawaii, 1998.

Tselioudis, G., Y. Zhang, and W. B. Rossow, 2000: Cloud and radiation variations associated with northern midlatitude low and high sea level pressure regimes. *J. Clim.*, **13**, 312-327.

Viterbo, P. and Beljaars, A.C.M., 1995: An improved land surface parametrization scheme in the ECMWF model and its validation. *J. Clim.* **8**, 2716-2748.

- The WAMDI-group: Hasselmann S., Hasselmann K., Bauer E., Janssen P.A.E.M., Komen G.J., Bertotti L., Lionello P., Guillaume A., Cardone V.C., Greenwood J.A., Reistad M., Zambresky L. and Ewing J.A., 1988. The WAM model-a third generation ocean wave prediction model., *J. Phy. Oc.*, **18**, 1775-1810.
- Wang, J., and W.B. Rossow, 1995: Determination of cloud vertical structure from upper-air observations. *J. Appl. Meteor.*, **34**, 2243-2258.
- Warren, S.G., C.J. Hahn, J. London, R.M. Chervin, and R.L. Jenne, 1986: Global distribution of total cloud cover and cloud type amounts over land. *NCAR Tech. Note NCAR/TN-273+STR*, 29pp.
- Warren, S.G., C.J. Hahn, J. London, R.M. Chervin, and R.L. Jenne, 1988: Global distribution of total cloud cover and cloud type amounts over the oceans. *NCAR Tech. Note NCAR/TN-317+STR*, 42pp.
- Weare, B. C., 1997: Comparison of NCEP-NCAR cloud radiative forcing reanalyses with observations. *J. Clim.*, **10**, 2200-2209.
- Weaver, C.P., and V. Ramanathan, 1996: The link between summertime cloud radiative forcing and extratropical cyclones in the North Pacific. *J. Clim.*, **9**, 2093-2109.
- Webster, P. J., and R. Lukas, 1992: TOGA COARE: The Coupled Ocean-Atmosphere Response Experiment. *Bull. Amer. Meteor. Soc.*, **73**, 1377-1416.
- Wilks, D.S., 1995: Statistical Methods in the Atmospheric Sciences. *Academic Press*, 467 pp.
- World Meteorological Organization, 1987: International Cloud Atlas. WMO, Geneva, 212pp.
- Wyant, M. C., C. S. Bretherton, H. A. Rand, and D. E. Stevens, 1997: Numerical Simulations and a conceptual model of the stratocumulus to trade cumulus transition. *J. Atmos. Sci.*, **54**, 168-192.
- Xu, K.-M., and D.A. Randall, 1996: Evaluation of statistically based cloudiness parameterizations used in climate models. *J. Atmos. Sci.*, **53**, 3103-3119.

Yanai, M. et al., 1973: Determination of Bulk Properties of Tropical Cloud Clusters from Large-Scale Heat and Moisture Budgets, *J. Atmos. Sci.*, **30**, 611-627.

Yu, W., Doutriaux, M., Sèze, G., LeTreut, H. and M. Desbois, 1996: A methodology study of the validation of clouds in GCMs using ISCCP satellite observations. *Clim. Dyn.*, **12**, 389-401.

Acknowledgements

There is a large number of people without whom this thesis would never have been written and to whom I wish to express my sincere gratitude.

First of all I would like to thank my supervisors Prof. Roger Smith and Dr. Martin Miller for their constant support and encouragement during the course of this study. I would also like to thank Prof. Ulrich Schumann for acting as a referee and for his helpful comments on an early version of the manuscript.

I would like to thank the management of ECMWF for allowing me to carry out this work while being employed in the Research Department of ECMWF. I am also indebted to the entire ECMWF team for providing the unique working conditions without which a lot of this work would not have been possible. I am especially grateful to Dr. Michael Tiedtke who got me started in the world of Numerical Weather Prediction. It was the many discussions with him that got me hooked to the problems involved in cloud parametrization and his early guidance is highly appreciated. Discussions with my colleagues of the Physical Aspects Section of ECMWF, in particular Drs. Anton Beljaars and Joao Teixeira, provided new ideas, insights and encouragement.

A stay of Dr. Stephen Klein at ECMWF has led to some of the most enjoyable and productive months of my working life. I enjoyed every minute of the many discussions and the joint work on several projects whose results I was able to use in this thesis. I thank Stephen for that and his friendship.

A number of people outside ECMWF supported this work in many different ways. It is impossible to name them all, but I would like to express special thanks to Dr. Gerald Mace for giving me the chance to work with him on the first ever use of cloud radar data for model evaluation and to Dr. George Tselioudis for his ideas and support in the cloud survey study using ISCCP data. I would also like to express my gratitude to Drs. David Randall and Chris Bretherton who over the years inspired the work on cloud generation carried out in

this thesis.

Finally I would like to thank my wife and my son for putting up with an either absent or very tired husband and father for the last 12 months. Without their support the completion of this thesis would not have been possible.

Lebenslauf

Persönliche Daten

Name Christian Jakob
geboren am 8. Februar 1967
in Köthen, Sachsen-Anhalt
Familienstand verheiratet
Kinder 1 Sohn
Anschrift 55 Rookery Close, Shippon, OX13 6LZ, England

Schulausbildung

in Dessau
Grundschule 1973-1981 an der 1. Polytechnischen Oberschule
Gymnasium 1981-1985 an der Erweiterten Oberschule "Philantropinum"
1985 Abitur

Wehrdienst

1985-1987 in Falkensee und Kleinmachnow

Studium

Meteorologie 1987-1992 an der Humboldt-Universität zu Berlin
Diplomarbeit zum Thema: *Methodische Untersuchungen zur Regionalisierung von Ergebnissen Globaler Zirkulationsmodellrechnungen mit Hilfe statistischer Verfahren*
August 1992 Diplom in Meteorologie
seit November 1998 Promotionsstudent an der Ludwig-Maximilians Universität München

Beruflicher Werdegang

1992-1993 Wissenschaftlicher Mitarbeiter am Meteorologischen Institut der Humboldt-Universität zu Berlin
seit 1993 Wissenschaftlicher Mitarbeiter am Europäischen Zentrum für Mittelfristige Wettervorhersage in Reading (England)
Januar 2000 Beförderung zum Senior Scientist